PRACA DOKTORSKA

Institute of Physical Chemistry
Polish Academy of Sciences
Kasprzaka 44/52
01-224 Warszawa, Poland

SELF-ASSEMBLY OF SELECTED AMPHIPHILIC

CALIX[4]ARENES AND CALIX[6]ARENES

IN SOLID STATE – SINGLE CRYSTAL

X-RAY DIFFRACTION STUDIES

Aleksander Shkurenko

PhD thesis

This dissertation was prepared within the International Ph.D. Studies
at the Institute of Physical Chemistry Polish Academy of Sciences

Supervisor: Professor Kinga Suwińska
Department of Physical Chemistry of Supramolecular Complexes

Warsaw, March 2014

Acknowledgements

I wish to express my sincere appreciation, first and foremost, to my advisor Prof. Dr. Kinga Suwińska for her guidance, support, patience and for motivating me to complete this thesis. Moreover, I am thankful for the real autonomy she gave me so that I could explore the topic by myself and fulfil my own ideas.

I am very grateful to Dr. Anthony Coleman from Université Claude Bernard Lyon 1, especially for correcting the manuscript, and his students for their collaboration to the work on amphiphilic calixarene compounds.

I would like to thank all my former and current colleagues from Department II for help, friendliness and constructive scientific discussions, especially Dr. Oksana Danylyuk, Dr. Edyta Kołodziejczyk, Ms Barbara Leśniewska, Dr. Kuba Luboradzki and Dr. Dariusz Świerczyński.

I would like to thank my wife, Agnieszka, and son, Aleksander, for their understanding, patience and emotional support during all the long stressful years of my PhD studies.

I would like to give special thanks to my parents, Aleksander and Anna, for teaching me to think independently.

CONTENTS

1   INTRODUCTION

Crystal engineering efficiently use intermolecular interactions which can vary from weak, such as van der Waals interactions or induced dipoles, through medium like aromatic stacking or hydrogen bonds to strong such as metal coordination bonds or electrostatic interactions. However, spatial unpredictability of the hydrophobic effect is still a great problem. It is even more confusing, if one takes into account the importance of hydrophobic effect in liquid phase; it plays a key role in micelle and membrane formation, chromatographic retention, protein folding, ligand-protein and protein-protein binding, and partitioning of drugs, metabolites and toxins throughout the environment and living systems *etc*.[1]

Calix[n]arenes are flexible phenol oligomers, which are cheaply and easy to prepare and modify in high yields.[2] Calix[n]arene-based surfactants were firstly obtained by Shinkai *et al*.[3] in 1986 but recently they have attracted more attention[4–11] due to much lower critical micelle concentration, higher kinetic stability, stronger viscosifying effect and stronger foaming power then classic 'monomeric' surfactants.

Better understanding of amphiphilic calix[n]arene self-assembly can be used in engineering and design of different kinds of sensors[12], for construction of nanoparticle shells, vesicles and solid lipid nanoparticles *etc*.

Obviously it might be expected that the stronger interactions should dominate and control the solid state assembly. But if an approximate balance between different types of intermolecular forces exist in solid, non-predictable packing might occur, multiple types of crystal may be present or the system simply becomes reluctant to crystallise. O-Alkylated calix[n]arenes are good example of such a situation. The goal of my thesis is to try to answer questions: Could O-alkylated calixarenes be treated as amphiphiles? In which cases this approach might be used? And what about the influence of the nature, size and number of substituents? As good model compounds three classes of O-alkylated calix[n]arenes were chosen: non-substituted at the upper rim (possible C–H···π and π-π stacking interactions), substituted at *para*-positions with *tert*-butyl groups (possibility for π-π stacking interactions is blocked), and substituted at *para*-positions with nitro groups calix[n]arenes (more polar molecules with additional possibility for C–H···O hydrogen binding).

2 LITERATURE REVIEW

2.1 Amphiphiles: nature and self-assembly in liquid phase

The pioneer researcher in the area of studying amphiphilic molecules was Hartley,[13] who investigated properties of aqueous solutions of paraffin chain salts nearly 80 years ago and introduced the term *'amphipathy'* (from Greek αμφις – both and πάθος – feeling) which indicates the possession of affinity to both water and oil. Later it was replaced by the term *'amphiphile'* (φιλία – love) which relates to molecules or ions having both hydrophilic (water-loving) and lipophilic (fat-loving) regions. The dual nature of amphiphilic compounds results in different kinds of interactions between molecule and environment, therefore the situation when each part of the molecule is located in the environment of the same nature is preferable.[14] This occurs, for instance, at the air/water interfaces.[15] When the interface is saturated, the individual amphiphilic molecules (monomers) penetrate into the bulk solution. The interaction between the hydrophobic surface and, *e.g.* water, is attractive due to the dispersion forces but the interaction between water molecules is much more attractive. This is why hydrophobic surfaces are not 'wetted' by water. For example, if we put *n*-propylamine into water, the water molecules reorganise themselves *around* the alkyl moiety in such a way, that the solvent molecules take part in hydrogen bond formation like in bulk water (hydrophobic solvation). The amino group, as a hydrophilic part of the molecule, is involved in the hydrogen bond framework. Energetically, the O–H⋯O and N–H⋯O hydrogen interactions are of the same order of magnitude. *n*-Propylamine clathrate hydrate formation at -35 °C is a solid-state example of such hydration[16] (Fig. 1). While the amphiphilic compound concentration is rising, more and more solvent molecules are

a   **b**   **c**
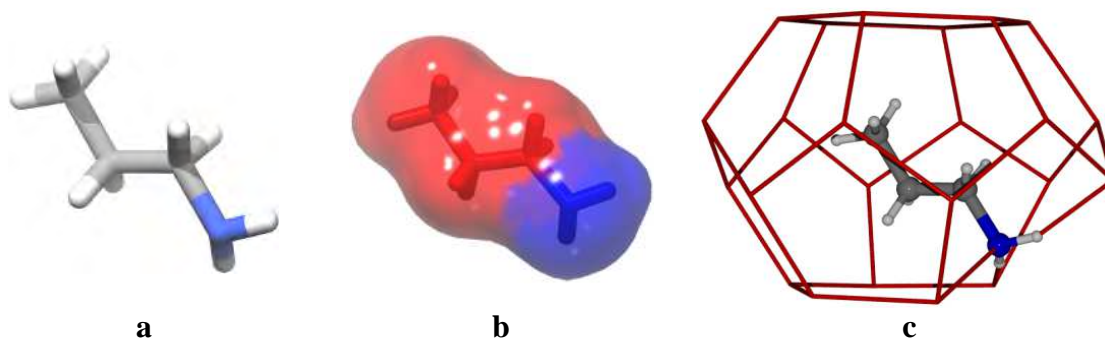
Fig. 1. *n*-Propylamine hydrate clathrate: (a) *n*-propylamine stick model; (b) surface, hydrophobic region coloured in red and hydrophilic in blue; (c) *n*-propylamine in the clathrate 'cage' (red line).

imposed to be arranged in the framework around the non-polar surfaces. Such re-arrangement is entropically very unfavourable, so at certain concentration (*critical micelle concentration*, CMC) amphiphilic molecules dispersed in the solution combine into micelles of different sizes and shapes, while the solvent molecules are released into the bulk phase (Fig. 2).
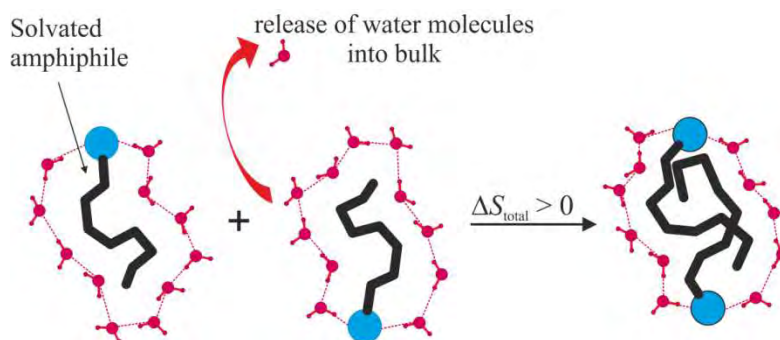
Fig. 2. Schematic representation of hydrophobic effect.

Further increase of the *n*-propylamine concentration results in precipitation of the *n*-propylamine semihydrate, where lamellar structure is formed[17] (Fig. 3). The model described was proposed by Frank and Evans[18] in 1945 and it was improved further in details, *e.g.* hydrophobic solvation proposed by Yamaguchi *et al.*[19] or thermodynamic aspects of the micelle formation process of Rusanov *et al.*[20,21]
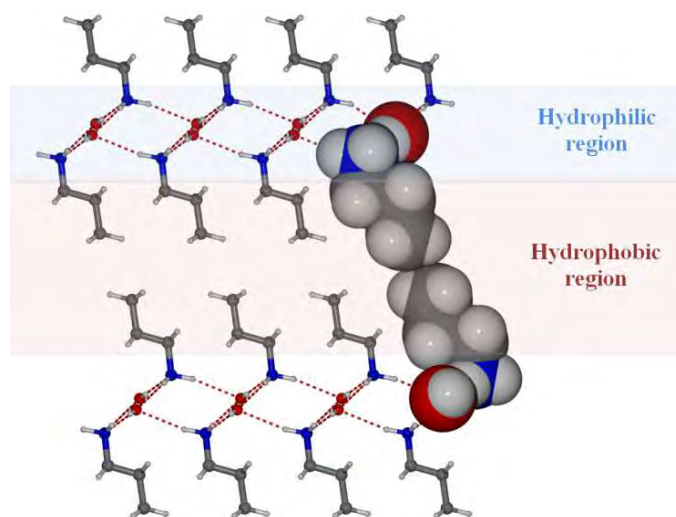
Fig. 3. *n*-Propylamine self-aggregation into lamellar structure. The solvent H$_2$O molecule is disordered over two positions and, like in water, each of them participates in four hydrogen bonds (two O–H···N and two N–H···O).

Thermochemical measurements reveal,[22] that the enthalpy of self-aggregation into micelles in aqueous solutions is usually endothermic (ΔH_{mic} is about 2–4 kJ per one mole of an amphiphile). This means that ΔS_{mic} should be positive (because $\Delta G < 0$) and

12

usually is between 80–140 $JK^{-1}mol^{-1}$ at room temperature. The total energetic effect is called *hydrophobic* and then *hydrophobic interactions* means stronger attraction between hydrophobic molecules (or parts of molecules) in water compared with their attraction in vacuum (usually by 2–4 times).

Hydrophobic interactions play the main role not only in micelle formation but also in molecular self-assembly,[23] in determining the conformation and aggregation of proteins,[24] in biological membrane structures,[25] and in many other surface phenomena.[26] This is why the role of hydrophobic interactions in self-assembly processes is one of the most widely studied.

There are two main aspects of the thermodynamics of micelle formation: kinetic and phase equilibria,[27,28] which are described in the *Mass Action Model* and *Pseudo-Phase Separation Model* approaches, respectively. Both models have their advantages and limitations, and they are complementary to each other.

Any experimental technique sensitive to the solution property modified by micellisation or sensitive to a probe (molecular or ion) property modified by micellisation is generally adequate to quantitatively estimate the onset of micellisation.[29] Determination of CMC is usually done by finding the singularity on the plot of the experimentally measured property or response as a function of the logarithm of the amphiphile concentration. A listing of the most popular experimental techniques used to determine CMC is given in Table 1.

It is necessary to stress the important role of temperature in the micellisation process. Both too high and too low temperatures cause phase separation processes and destroy micelles (see diagram in Fig. 4a). The Krafft point is the temperature (more

Table 1. List of techniques and observables for determination of CMC[29]

1. Conductance	12. MNR	23. Surface tensions
2. Density	13. Neutron scattering	24. Taylor diffusion
3. Diffusion coefficient	14. Optical probe	25. Turbidometry
4. Dye decomposition kinetics	15. Partial volume	26. Ultracentrifugation
5. Electromotive force	16. Polarographic maximum	27. Ultrafiltration
6. ESR probe	17. Potentiometry	28. Vapour pressure lowering
7. Flocculation rate	18. Refractive index	29. Velocity of sound
8. Foaming power	19. Solubilisation	30. Viscosity
9. Freezing point	20. Solubilisation rate	31. Voltammetry of electroactive probe
10. Heat of dilution	21. Specific heat	32. Wein effect
11. Light scattering	22. Streaming current	33. X-ray scattering

precisely, narrow temperature range) above which the solubility of an amphiphile rises sharply. At this temperature the solubility of the amphiphile becomes equal to CMC.[30] Consequently, it looks impossible to obtain single crystals of micelles by cooling. The other way to obtain crystals is to increase the amphiphile concentration. For instance, for an amphiphile which forms a lyotropic liquid crystal phases, the solid phase S is kindred with the liquid crystal phase (the similarity degree remains a question). An example of such a diagram is shown in the Fig. 4b. A comprehensive review of phase transitions in the liquid crystal states was published by Singh.[31]

a

b
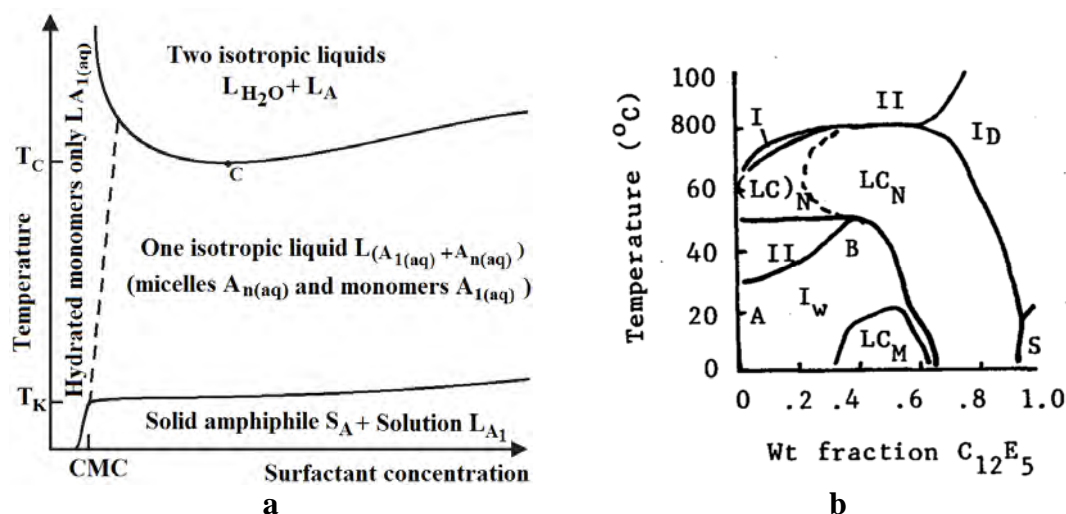
Fig. 4. (a) Schematic phase diagram of a binary non-ionic surfactant-water system. The dashed line indicates CMC; TK is the Krafft point and TC is the cloud point at the CMC = C (lower consolute temperature). (b) Phase diagram for the system water-$C_{12}H_{25}O(CH_2CH_2O)_5H$. I and II denote one- and two-phase regions, respectively. LC is a liquid crystal; S is a solid amphiphile phase.[32]

The term 'micelle' in the consideration above means all possible forms shown in Fig. 5. The form of the micelle depends not only on the total amphiphile concentration in the solution, but also on *averaged molecular shape* of the amphiphile molecules,
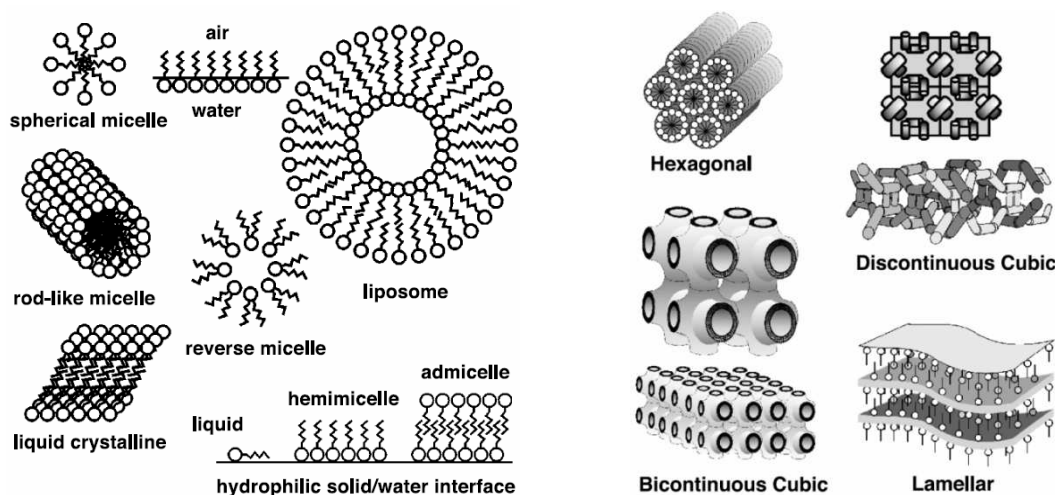
Fig. 5. Examples of amphiphile aggregates.[33]

14
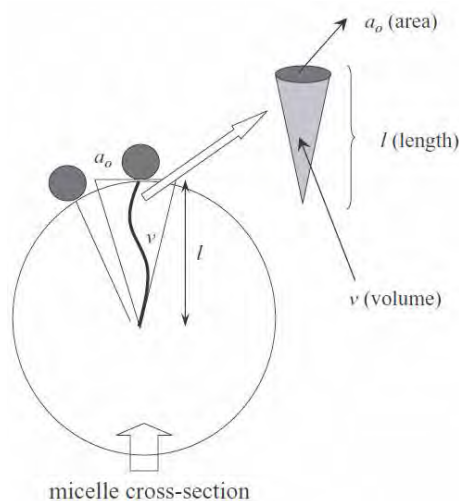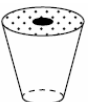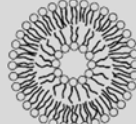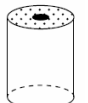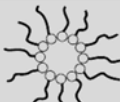
Fig. 6. Amphiphile (or micelle) packing parameter v/a_0l.

described by the ratio of *optimal headgroup area* a_0, *critical chain length* l ($l \leq l_{max}$) and *volume* of the hydrocarbon chain v (Fig. 6).[22] The optimal headgroup area a_0 is proportional to the headgroup repulsion and increase when polarity (for non-ionic amphiphiles), charge (for ionic surfactants) or the number of hydrophilic groups increases. The ratio of chain volume v to its linearity l gives the hydrophobic surface area and is proportional to the hydrophobic attraction between chains. Therefore, hydrophobic interactions are stronger between hydrophobic parts of molecules which are more tangled or have more chains. The dependence between *averaged molecular shape* and aggregate form is illustrated in Table 2. Each of these structures corresponds

Table 2. Packing parameter and geometries of amphiphilic structures.[22]

Effective shape of the amphiphile molecule	Packing parameter, v / a_0l	Aggregate morphology
cone	< 1/3	spherical micelles
truncated cone	1/2–1/3	tubular micelles
truncated cone	1/2–1	vesicles
cylinder	~ 1	bilayers,
inverted (truncated) cone	> 1	inverted micelles

15

to the minimum-sized aggregate in which all the amphiphiles are at the minimum free energy. Larger structures will be entropically unfavoured, while smaller structures, where packing constraints forces increase the surface area above a_0, will be enthalpy unfavoured.

For charged surfactants the *optimal headgroup area* a_0 depends on the ionic strength of the solution. In presence of an electrolyte, hexagonal or lamellar phases are formed. In absence of electrolytes, self-aggregation into spherical micelles is preferred.

It should be noted, that amphiphiles with longer chains prefer to form lamellar structures in which chains are in hexagonal close packing. Different chain lengths, the presence of unsaturated bonds or partial fluorination result in disruption of regular packing of long alkyl chains and decrease the hydrophobic attraction.

In conclusion, despite the long history of amphiphile investigations, there is a lot to do both in theory and application. Unfortunately, the images obtained from physicochemical methods are extremely complex and additional quantum chemistry modelling can help a deeper understanding of amphiphilic self-assembly processes. The synthesis of new class of amphiphiles and their self-assembly investigation is another hot topic in chemistry. X-ray crystallography could give important information about amphiphilic self-aggregation in the solid-state, which could be a useful starting point for molecular modelling of the aggregation processes for new classes of amphiphiles.

2.2 Amphiphiles: self-assembly in the solid-state

In spite of all the achievements in crystal chemistry, crystal structure prediction remains an unpleasant sticking point in the field of crystal engineering.[34,35] The main difficulty is in taking into account all the large number of intermolecular interactions (often with similar magnitude of energy), while even tiny changes in molecular structure can cause global changes in the overall crystal packing.

Contrary to solid crystals, in liquid ones, block copolymers or lyotropic amphiphilic systems just a few topologies are the norm because thermal motions cause a dynamical character of micelles and liquid crystal phases and the vagaries of individual energetic terms are averaged. The polymer science approach to the self-assembly of blocks in bulk polymers is to use the volume ratio between copolymer components of different nature (Fig. 7). If one of the components is a minor component, then minimisation of the surface area between the components will lead to a spherical impurity inside the major component. If the two components are equal in amount,

16
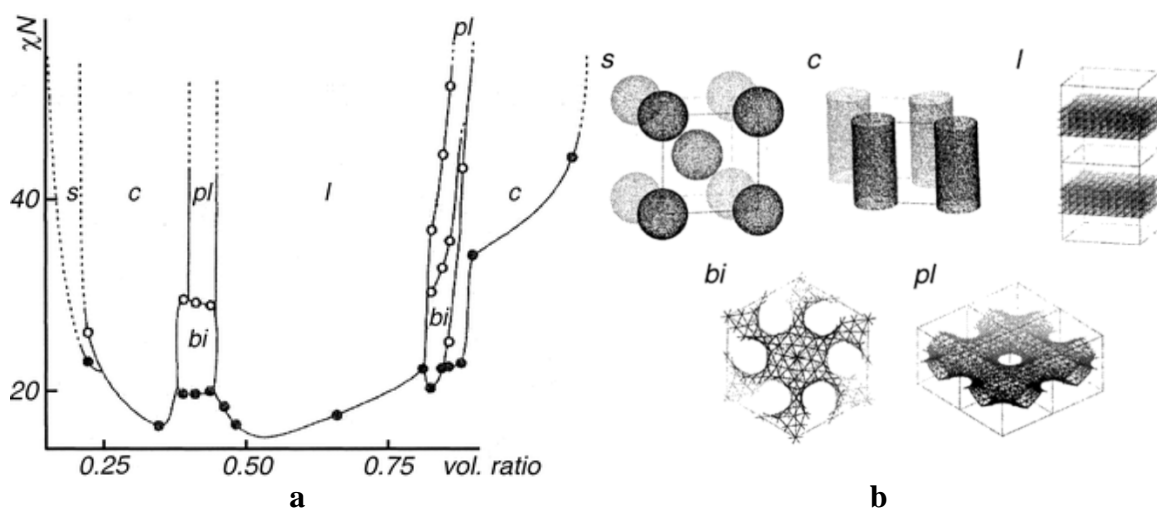
Fig. 7. (a) Experimentally determined phase diagram for polystyrene-polyisoprene diblock copolymers. (b) *s*: spheres, *c*: columns, *l*: layers, *bi*: bicontinuous, *pl*: perforated layers.

a lamellar structure with alternating layers will form. Because the two components have often different hydrophobicity, the volume ratio between components can be expressed as the *hydrophobic-to-total volume ratio,* which is an analogue of the *packing parameter* v/a_0l in the previous chapter. This approach concerning self-assembly of molecular crystals was developed by Lee and co-workers, and was tested on more than 150 structures.[36–40]

According to Lee *et al.*, topology prediction is based on tabulated data of distances and angles, not on crystal data (it implies ideal tetrahedral angles for sp^3-carbon atoms, C_{sp3}–C_{sp3} distances are equal to 1.53 Å, van der Waals radii for C, H and O are equal to 1.70, 1.20 and 1.52 Å, respectively, *etc.*). Examples of such structure type to hydrophobic-to-total volume ratio correlation for 120 systems of small organic molecules (aromatic polyethers and polyalcohols, aromatic ammonium carboxylates *etc.*) are presented in Table 3. It should be noted that structural classification was based on closest contacts defined as less than 1.30 times the sum of the van der Waals radii. It is easy to notice that generally at ratios 20-30%, the *s* and *c* topology is the most common, while the *l* and *bi* phases predominate for volume ratios of 40-50%, and at 70-80%, the *ic* and *is* topologies are prevalent. Finally, the *pl* and *ipl* phases are found at volume ratios intermediate between the *s* or *c* and *bi* or *l*, and *bi* or *l* and *is* or *ic*, respectively.

In conclusion, it is clear that the force of *hydrophobic-to-total volume ratio* approach is both simple to calculate and general. Unfortunately, the weakness of the approach is the same. Weak intermolecular interactions, however, play important role in

Table 3. Correlation between structure types and hydrophobic-to-total volume ratios.[40]

Vol. ratio, %	*s* or *c*	*pl*	*bi* or *l*	*ipl*[*]	*ic* or *is*[*]
0-10	1				
10-20	2				
20-30	14		3		
30-40	10	3	10		
40-50	1	6	35		1
50-60			12	5	1
60-70			1	2	0
70-80					6
80-90					2
90-100					1

[*] '*i*' before *s*, *c* and *pl* means 'inverted' to distinguish these phases from those with lower vol. ratio.

molecular self-assembly and result in deviation from the main tendency. For example, as Table 3 shows, there is one structure where the volume ratio is less than 10%. We might suppose that only spherical assemblies would have been found at such low ratios, but this particular one is columnar. The columns in question are formed by π-π stacking of parallel aromatic rings. Thus, the energetic stability of such stacking overbalances the minimisation of hydrophobic-to-hydrophilic contacts.

Nevertheless, the volume ratio approach can be used for these compounds where both surface effects and local geometry predispose the molecules to pack in one unique and obvious way.

2.3 Intermolecular interactions

Intermolecular interactions are based on forces that are exerted by molecules on each other. An application of intermolecular interactions to rational design of supramolecular systems is a holy grail of supramolecular chemistry.

Intermolecular interactions include:

1) ion-dipole interactions. There are no such interactions in the thesis;

2) dipole-dipole interactions usually are divided in interaction between permanent dipoles (orientation interaction) and permanent dipole-induced dipole interaction (polarisation interaction);

3) atom-atom interaction (dispersion interaction);

4) complex interactions, such as hydrogen bonding, $O_{NO_2} \cdots \pi(N)_{NO_2}$ interaction *etc*.

For historical reasons interactions other than ion-dipole interaction are also often called van der Waals interactions in honour of the famous pioneer of intermolecular interaction studies.

Dispersion interactions always occur between adjacent molecules. It is responsible *e.g.* for the noble gas condensation. Dipole-dipole interactions additionally arise when functional groups composed of atoms with different electronegativity present in the molecule. Dispersion interaction contribution can be insignificant (*e.g.* in strong hydrogen bonding) but it always presents in general energy of intermolecular interaction.

Contrary to dispersion and polarisation interactions (which are orientationally independent) orientation interaction strength depends on the dipoles mutual orientation. Because of diversity of chemical compounds, complex interactions consisting of electrostatic, covalent, orientation, induction, dispersion and repulsive interactions are possible. To distinguish complex directional interactions, such as hydrogen bonding, π-interactions, halogen-halogen interactions *etc.*, some authors[41] restricted van der Waals forces to directionally independent dispersion and repulsion interactions only. Below, only complex directional interactions occurring in analysed crystal structures are discussed.

2.3.1 Hydrogen bonding

According to IUPAC the hydrogen bond is "an attractive interaction between a hydrogen atom from a molecule or a molecular fragment X–H in which X is more electronegative than H, and an atom or a group of atoms in the same or a different molecule, in which there is evidence of bond formation".[30] During the twentieth century usually only strong hydrogen bonds were discussed. A hydrogen bond was treated as a special 'stronger' type of intermolecular interactions, highly electrostatic and partly covalent. Since about 1990 new types of interactions have been identified as weak hydrogen bonding and discussed, *e.g.* C–H⋯O,[42] C–H⋯π, O–H⋯π, N–H⋯π, S–H⋯π,[43] C–H⋯F,[44] C–H⋯Cl,[45] , N–H⋯S,[46] agostic[47] etc. Some examples of strong and weak hydrogen bonding are shown in Fig. 8.

The distance profile of potential energy of a typical hydrogen bond is shown in Fig. 8b. It was found for hydrogen bonds in crystals,[48] that the H⋯A distances cluster in a narrow range around the energy minimum at d_e and only a few hydrogen bonds have energies differing by more than 4.1 kJ·mol^{-1} from optimum. For weaker hydrogen bonds

19
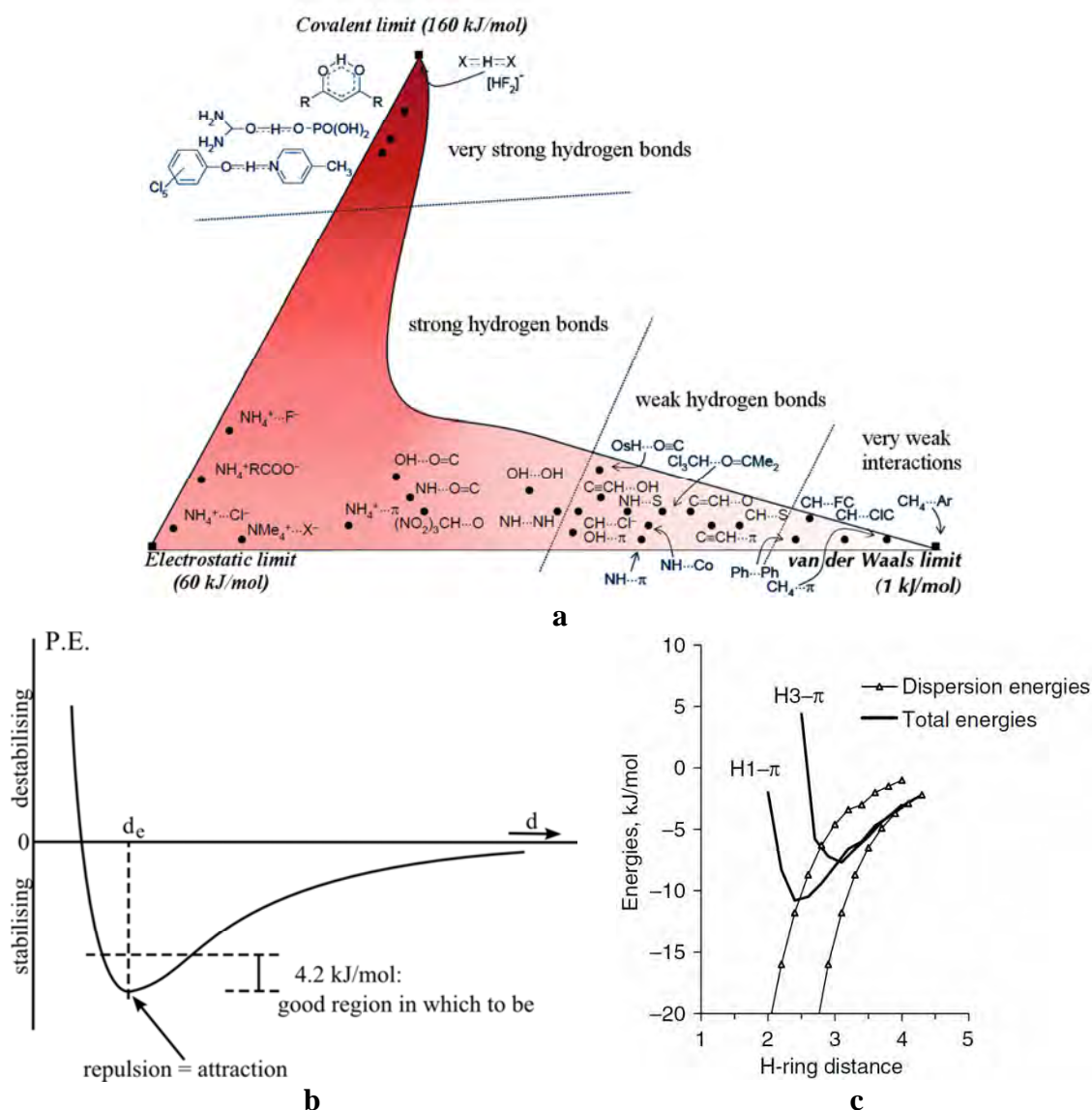
Fig. 8. (a) Hydrogen bonding diversity and energy scales.[49] (b) Schematic representation of a hydrogen bond potential as a function of H···A distance;[41] (c) Total energy and dispersion contribution for acetylene-benzene (H1) and butane-benzene (H3) C–H···π interactions.[50]

the minimum is shallow and shifted to longer distances (Fig. 8c). The weak hydrogen bonds have substantial dispersive contribution comparable with the coulombic term which results in well width 0.5–1.0 Å,[50] where they can be easily distorted without a significant energy penalty and with small electron density changes only. It should be noted, that for weak hydrogen bonds sum of van der Waals radii of both hydrogen and the acceptor roughly bisects a *d*-distance distribution. Therefore, van der Waals cut-off criterion in the H···A distance for the assignment of hydrogen bond character is inappropriate for weak hydrogen bonds.

The main driving force for self-assembly of calixarene molecules discussed in this thesis are isotropic van der Waals forces. Directionally dependent specific

interactions, such as C–H···O hydrogen bonding, C–H···π and π-π stacking interactions *etc.*, play only an additional stabilizing role. The threshold question is important in this case. For C–H···O hydrogen bonding, H···O distances lower than 3.0 Å (4.0 Å for C···O distances) and C–H···O angles up to 90° have been suggested as recommended thresholds.[41]

2.3.2 π-interactions

In the case of phenyl···phenyl interactions, there are two main cases, perpendicular phenyl rings (C–H···π or face-to-edge interactions) and parallel phenyl rings (π-π stacking or face-to-face interactions), and continuum of intermediate states (Fig. 9a).

The border line in the case of C–H···π interaction is a more complex problem. The donor ability decreases in the order acetylenic > phenyl > aliphatic hydrogen. The C–H···π interaction energy-distance profile with highly acidic donors looks almost like for C–H···O interaction. For less activated C–H bonds, the interaction is so close to van der Waals type that it can be called the weakest type of hydrogen bond.[51] Nevertheless, substantial attraction still exists in alkane-phenyl systems even when molecules are well separated (Fig. 9b) due to electrostatic and dispersion interactions.[52] Reported equilibrium distances and well widths for the same C–H···π cluster strongly depends on quantum chemistry method used. For instance, the PIXEL method[50] gives the distances equal to 2.9 and 3.2 Å for benzene-benzene and *n*-butane-benzene complexes, respectively, and the well widths ca. 0.8 Å, while *ab initio* calculations[53] suggest H···π
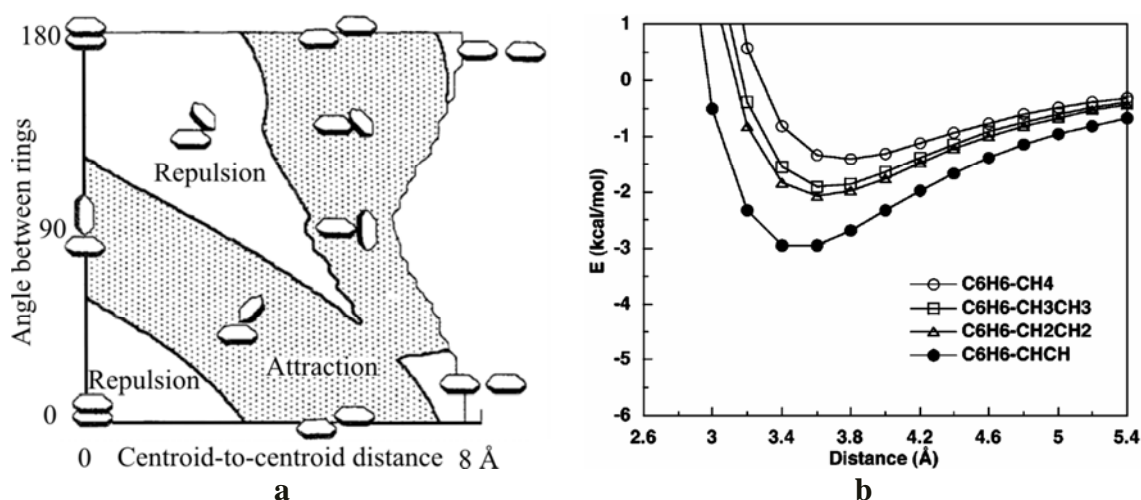
Fig. 9. (a) Schematic representation of π-interactions between two phenyl rings;[54] (b) calculated interaction energies of model C–H···π complexes at the MP2/cc-pVTZ level.[52]

distances of 2.7±0.3 Å for both the clusters. Moreover, it was also shown that for almost apolar C–H donors both the orientation[52] and lateral displacement of the donor group does not greatly affect the interaction.[55] All this makes the thresholds of C–H···π interaction very subjective. The only distances between hydrogen atoms of the donors and benzene rings closer than 3.2 Å (C···π distances closer than 4.3 Å) were taken into account in this thesis.

In the case of π-interaction between two benzene rings, dihedral angle between planes of rings is a threshold to distinguish face-to-edge (> 45°) and face-to-face (< 45°) interactions. Maximum distance between planes of two interacting rings of 3.8 Å was assumed.

2.3.3 O···π interactions between nitro groups

The last intermolecular interaction which I would like to mention here is O···π interaction between two perpendicular nitro groups, which occurs in crystal structures of the nitro calix[4]arenes being one of the calixarenes studied within this work. It was found in 104 structural fragments deposited in the Cambridge Structural Database,[56] that in the most cases, distance between oxygen atom of one nitro group and the plane of the other nitro group O_{NO_2}···$\pi(N)_{NO_2}$ is shorter than 3.0 Å and the angle between the planes of two interacting nitro groups (Fig. 10) is approximately 90°. *Ab initio* calculations of the interaction energy indicates the attractive nature of this interaction in the range of 13–29 kJ·mol^{-1}.
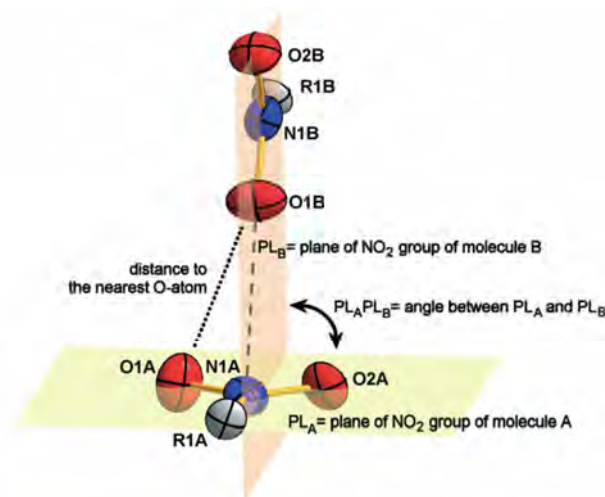
Fig. 10. Geometry parameters used for description of O_{NO_2}···$\pi(N)_{NO_2}$ interaction.[56]

At the end of this present survey of intermolecular interactions, I would like to emphasise that choice of limit distance values is still under investigation, especially in

the case of very weak interactions. The question where the specific interactions end and van der Waals interactions start is the subject of discussion between the scientists dealing with this issue.

2.4 Calixarenes: introduction

The calix[n]arenes are cyclic oligomers synthesised from phenol and formaldehyde. The term 'calix' was introduced by Gutsche since the shape of the molecule resembled the calyx krater vases of ancient Greece (Fig. 11). Calix[n]arenes can adopt various conformations and form cavities. They are also easy to prepare in high yields from inexpensive starting compounds and easy to modify with a wide variety of functional groups at the aromatic rings and/or the O-centres of the phenolic groups.

a   **b**

Fig. 11. (a) Molecular model of calix[4]arene; (b) a calyx krater at the Metropolitan Museum of Art (Euphronios and Euxitheos, Attic, *ca.* 515 B.C.).

It was first recognised by Cornforth[2] that the calix[4]arene can exist in four main conformations, with various numbers of aryl groups oriented upward (*u*) or downward (*d*) relative to an average plane defined by the bridge methylene groups (Fig. 12). Non-substituted calix[4]arene (Fig. 11a) is a flexible molecule but at room temperature it exists mainly in the cone conformation, which is stabilised by four O–H···O hydrogen bonds at the lower rim. *para-tert*-Butyl-tetramethoxycalix[4]arene is also flexible (conformational isomers can interconvert at room temperature with a rate of *ca.* 100 s^{-1})[57] but the partial cone conformation is the most stable one, while the tetraethyl

Cone   Partial cone   1,3-Alternate   1,2-Alternate
u,u,u,u   u,u,u,d   u,d,u,d   u,u,d,d
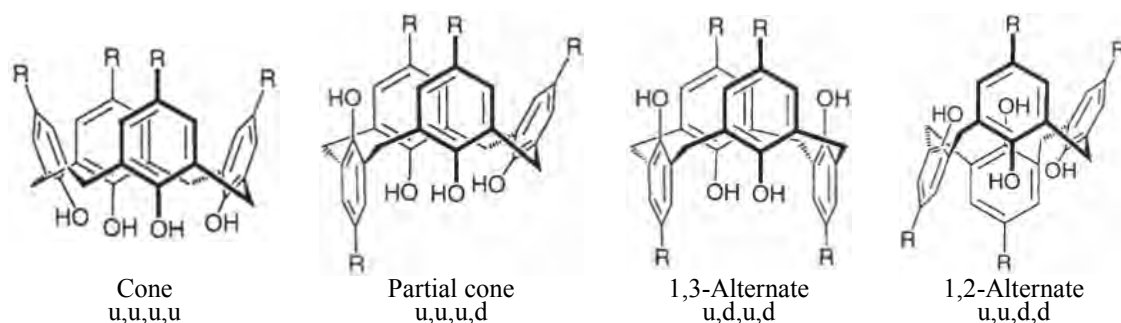
Fig. 12. Four possible conformations of calix[4]arenes.

23

ether is flexible only at temperatures above 100 °C and then it exists as an equal mixture of partial cone and 1,2-alternate cone conformers[58] (in 1,1,2,2-tetrachloroethane).

As the number of aryl groups in the macrocyclic ring rises, the number of conformers increases rapidly. Thus calix[5]arenes have only four pure '*up-down*' conformers (like calix[4]arenes), calix[6]arenes have eight, calix[8]arenes have sixteen, *etc*. Moreover, for all of them deviations from the true up/down orientations are possible. For example, a phenyl ring projecting down and outward is denoted as a 'do' orientation and that projecting down and inward ring is a 'di' orientation[59] (Fig. 13).

| (u,u,u,u,u,u) | (u,d,d,u,d,d) | (uo,u,d,do,d,u) | (ui,d,u,di,u,d) |
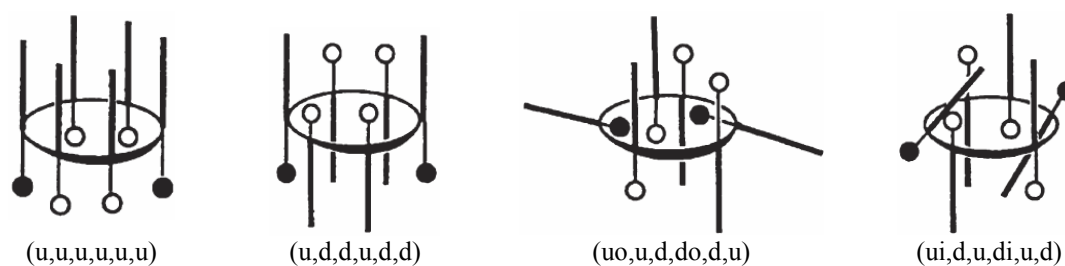
Fig. 13. Some possible conformations of calix[6]arenes.

The conformations of the calix[6]arenes are variously described as distorted cone, compressed cone, pinched cone, double partial cone, winged, 1,2,3-alternate, 1,3,5-alternate and distorted 1,2,3-alternate. In the case of the calix[8]arenes such term as 'pleated loop', 'pinched cone', 'inverted double cone' or '1,2,3,4-alternate structure' are in use.[2] As the number of phenyl rings in the macrocyclic ring increases, the conformational specification becomes increasingly difficult and less precise. Some suggestions for solving this problem have been published.[59,60]

a   **b**

Fig. 14. Two double partial cone conformations of calix[6]arenes: (a) 'up-up'; (b) 'up-down'.

In the solid-state, the cone conformation is dominant for calix[4]arenes, while for calix[6]arene their conformation depends on the solvent used for crystallisation. When the solvent cannot participate in hydrogen bonding with the hydroxyl groups of the calixarene, the 'up-up' double partial cone conformation is observed (Fig. 14a) in which all six OH groups are involved in cyclic intramolecular hydrogen bonding.

However, when the solvent participates in hydrogen bonding, the molecule assumes 'up-down' double partial cone (or inverted double partial cone) conformation (1,2,3-alternate)[61] (Fig. 14b).

The much larger macrocyclic rings of the calix[8]arenes can adopt 16 'up-down' conformations and numerous others in which one or more aryl rings project 'outward'.[2] Nevertheless, the pleated loop conformation (Fig. 15) is dominant for calix[8]arenes in both solution and solid state but the situation is much more complicated if the H-atoms of the hydroxyl groups are substituted.
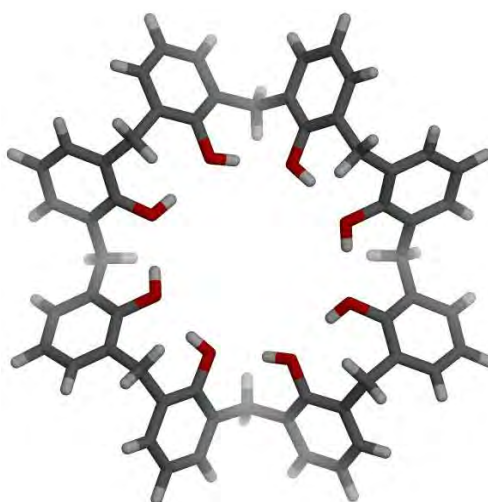
Fig. 15. Pleated loop conformation of calix[8]arene.

It should be noted, that calix[n]arenes with n = 4, 8, 12, 16 and 20 are all conformationally less mobile than their immediate neighbours[62] as a consequence of favourable shapes that maximize intramolecular hydrogen bond interactions.

2.5 Calix[4]arenes as amphiphiles: self-assembly in the solid-state

Non-substituted calix[4]arene has a hydrophilic lower rim, formed by four hydroxyl groups, while the four phenyl rings make up both a hydrophobic upper rim and cavity. Such an amphiphilic nature of the calixarene projects onto its self-organisation in the solid-state. There are 19 crystal structures of non-substituted calix[4]arene in the Cambridge Structural Database (CSD).[63] In the majority of cases, calix[4]arenes self-assembled in cyclic trimers, stabilised by C–H···π interactions between the mutually partially included calixarene rings (Fig. 16a). The trimers are combined into the crystal structure by van der Waals interactions. Between columns of trimers channels are formed, where small molecules of guest can be incorporated. In the case of guest molecules capable to form strong C–H···π interactions (acetone,[64]

25

$(CH_3)_4N^{+}$ [65] and DMF[66]) the guest is included into hosts' macrocyclic cavities and then inclusion complexes rather than clathrates are formed (Fig. 16b).
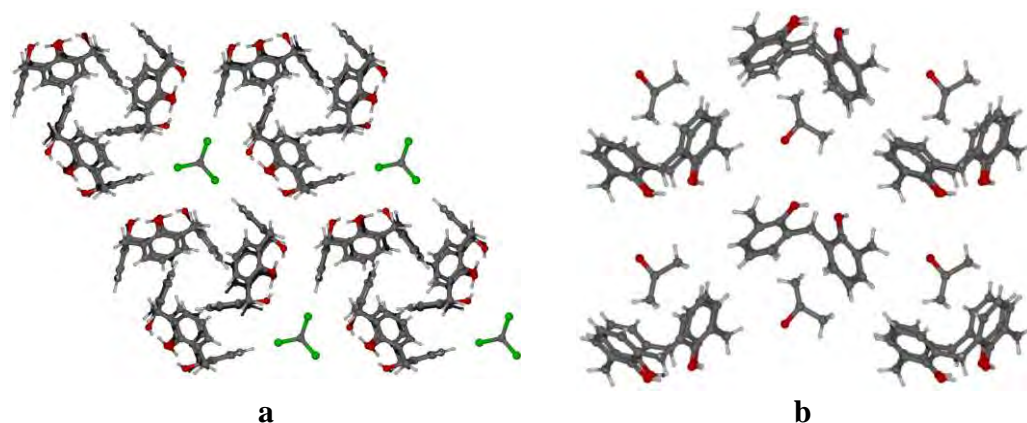
Fig. 16. Self-organisation of calix[4]arene in the solid-state: (a) trimers formation (clathrate with CCl₄ [67]); (b) inclusion complex formation (with acetone).

Calix[4]arene, as already mentioned, can be easily modified at both upper and lower rims. If the substituents are nonpolar and are located at the upper rim, the calixarene remains amphiphilic. The most examined groups, which count 77 and 34 structures, are solvates of tetra-*para-tert*-butylcalix[4]arene and tetra-*para*-acylcalix[4]arene, respectively. For tetra-*para-tert*-butylcalix[4]arene the driving force of calix[4]arene self-assembly is π-π-interaction, which results in double-layer formation. Small guest molecules can be included into calixarene cavities present on both sides of each double-layer (Fig. 17a). If the guest molecule is longer than 8.5 Å, then the adjacent double layers are adjusted to form larger cavities (Fig. 17b).
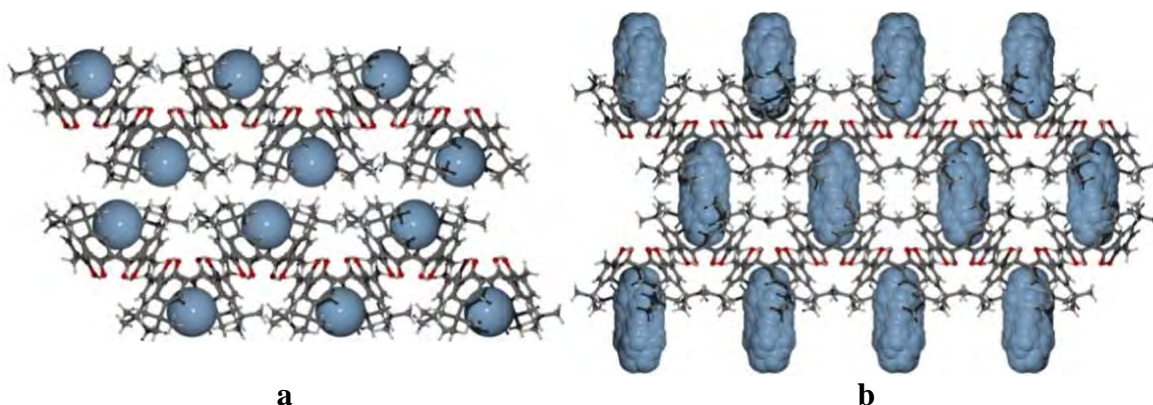
Fig. 17. Crystal structures of tetra-*para-tert*-butylcalix[4]arene inclusion compounds: (a) with xenon;[68] (b) with *n*-butylamine.[69] Guest molecules are in pale blue.

There are other self-assembling patterns. Thus, for tetra-*para*-acylcalix[4]arenes without guest molecules or with guests such as ethanol[70] or *tert*-butylamine,[71] calixarene self-inclusion is observed: the cavity of the macrocyclic host is occupied by

the alkyl substituent of the neighbouring acylcalixarene while guest molecules are located in the voids between the alkyl substituents (Fig. 18a). However, the preferable location for the guest molecule in the *para*-acylcalix[4]arene structures is the hydrophobic calixarene cavity. The *para*-acylcalix[4]arene·THF solvates are interesting examples of the shape/size relationship between host cavity on the one hand and guest molecule(s) on the other hand. In the crystal structure of the 1:1 (host:guest ratio) butanoylcalix[4]arene·THF inclusion complex[72] (Fig. 18b), calixarene molecules self-assemble in columns in head-to-tail mode and THF the molecules are located in the calixarene cavities. In the case of the hexanoylcalix[4]arene, in both known stoichiometries 1:1[73] and 1:1.5,[72] the calixarenes form van der Waals nanocapsules (Fig. 18c). The self-assembly pattern in the case of octanoyl-calix[4]arene·THF[74] complex is the same as for butanoylcalix[4]arene one. The only difference is that, due to longer alkyl chains, the cavity formed is much larger and accommodates both guest molecules and alkyl substituents of the neighbouring calixarene.

a

b   **c**
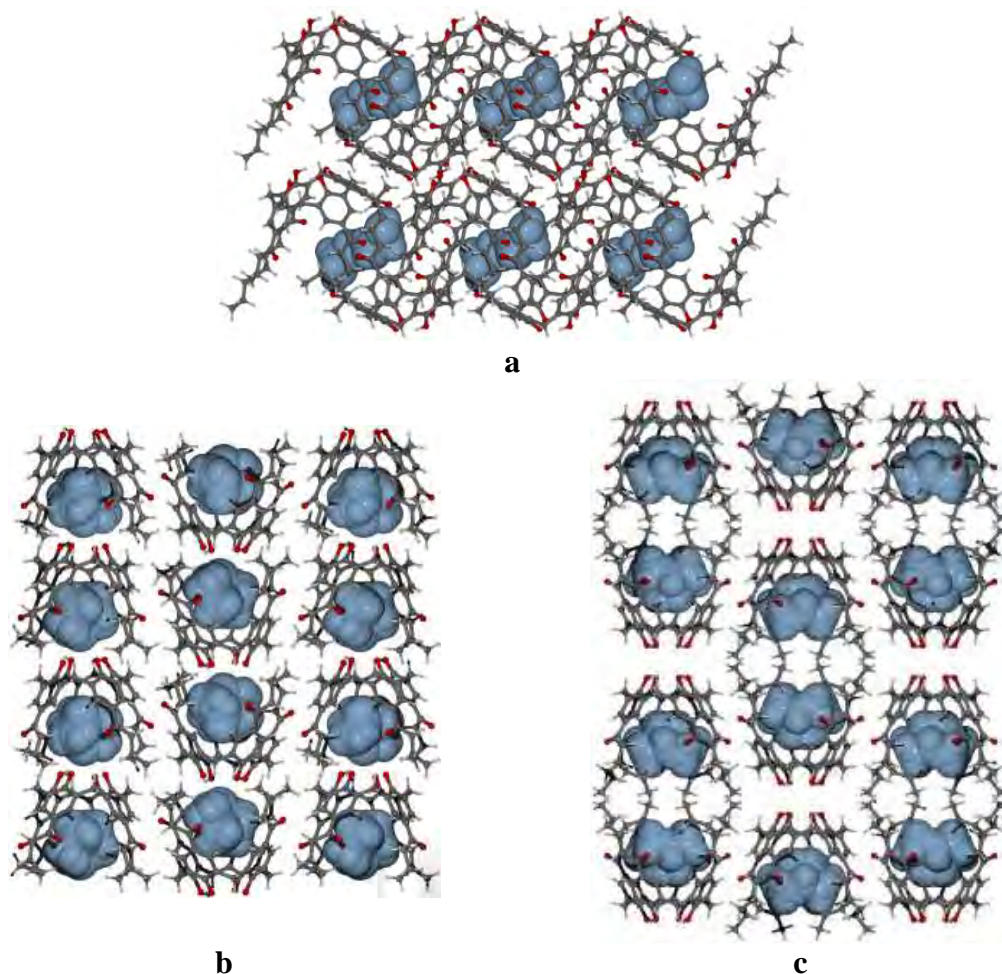
Fig. 18. Crystal structures of *para*-acylcalix[4]arene solvates: (a) hexanoylcalix[4]arene·ethanol clathrate;[70] (b) butanoylcalix[4]arene·THF and (c) hexanoylcalix[4]arene·THF inclusion complexes[72] (guest molecules are in pale blue).

27

As it was noticed by Pojarova *et al.*,[70] that the presence of carbonyl group at α-position makes the cavity in acyl calix[4]arenes accessible for guest molecules. It was also found that the position of carbonyl group is important for the type of self-assembly.[75] Tetra-*para*-2-oxooctanoylcalix[4]arene molecules self-assembly to give cuboctahedral inverted micelle-like self-assembly (Fig. 19). The location of the carbonyl group at β-position provides the micelle stabilisation due to C–H···O hydrogen bond formation.

a

c   **b**
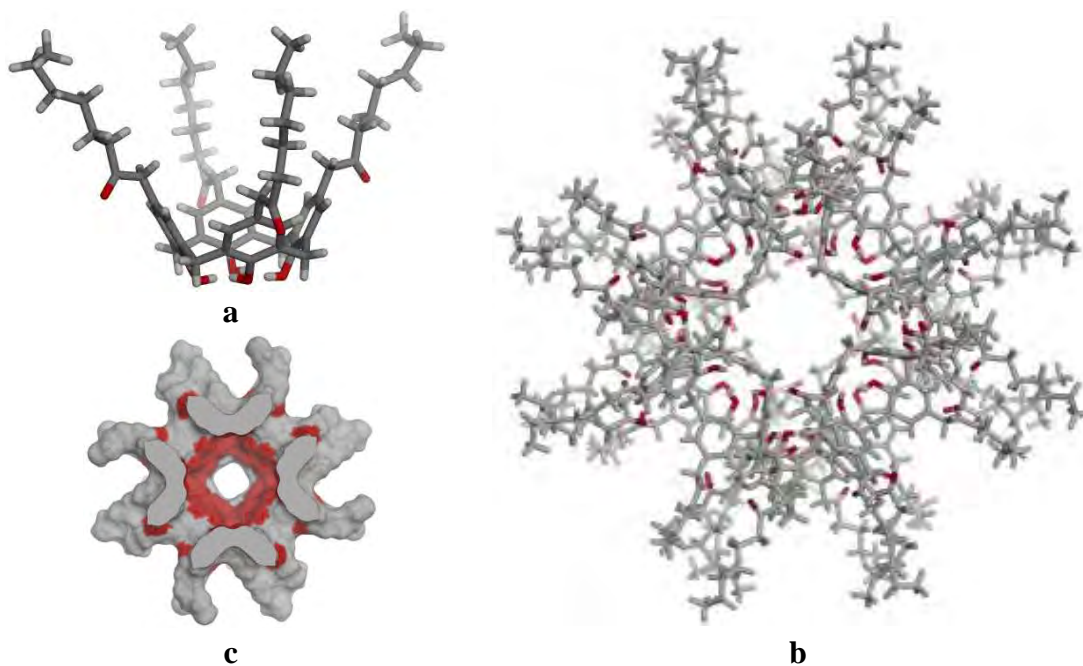
Fig. 19. Tetra-*para*-2-oxooctanoylcalix[4]arene: (a) molecular structure; (b) inverted micelle self-assembly; (c) internal hydrophilic cavity of about 1200 Å³.

It should be mentioned here, that bilayer[76] and spherical[77] self-assembly was also observed for other calixarenes but they are not of amphiphilic character and are not discussed in this thesis.

2.5.1 Crystal structures of the non-substituted at the upper rim alkoxycalix[4]arenes

As already mentioned, calixarenes can be easily modified at both upper and lower rims. It is obvious that if the substituent at the upper rim is non-polar, the calixarene remains amphiphilic as described above. If calixarene is alkylated at the lower rim, the situation becomes more complicated and then several questions arise. Could such calixarenes be treated as amphiphiles? For which cases this approach might be used? And what about the influence of the nature, size and number of substituents? I will try to answer some of these questions below.

Initially one non-substituted at the upper rim monomethoxycalix[4]arene ($HC[4]mOC_1$) was reported, by Hanna *et al.*[78] as a chloroform monosolvate, but no description or illustration of the structure was given. Then Maharaj *et al.*[79] showed that in solid state, as well as in solution, individual calixarene molecules exist in cone conformation, which is stabilised by O–H⋯O hydrogen bonding (Fig. 20a). The methoxy group of one calixarene molecule is located within another calixarene bowl and weak C–H⋯π interactions are present between the two molecules (H⋯π distance equals to 2.63 Å). Repetition of this construction mode creates head-to-tail zigzag chains (Fig. 20b), which are assembled in 3D structure *via* van Waals interactions. Chloroform molecules are disordered and located in cavities between chains, and participate in C–H⋯π interactions with the nearest calixarene phenyl ring ($d(H⋯π) = 2.41–2.60$ Å).

a   **b**   **c**
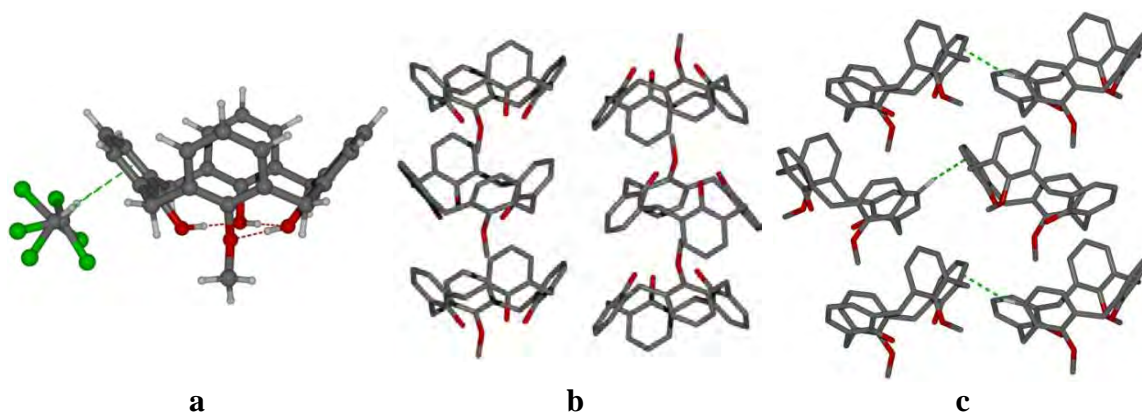
Fig. 20. (a) Crystallographically independent unit of $HC[4]mOC_1·CHCl_3$ structure. Two neighbouring chains of: (b) the monomethyl ether $HC[4]mOC_1$ and (c) the dimethyl ether $HC[4]diOC_1$ (hydrogen atoms are omitted for clarity).

Crystal structure of 1,3-dimethyl ether of calix[4]arene ($HC[4]diOC_1$) is also reported in the literature.[80] There are two calix[4]arene molecules in the asymmetric unit. Each of them forms 1D head-to-tail zigzag chain by inclusion of one methyl group into bowl of the neighbouring symmetric equivalent. The difference between monoether and diether (Fig. 20c) is, firstly, in the symmetry of calixarene chains: mirror plane *m* in the monoether *vs.* screw axis 2_1 in the diether. Secondly, contrary to the monoether, crystal structure of diether is stabilised by C–H⋯π interactions between adjacent chains.

The crystal structure of 1,3-diethoxycalix[4]arene ($HC[4]diOC_2$) chloroform clathrate[81] reveals a dramatic change in the self-assembly: elongation of the alkyl substituent by one carbon atom results in head-to-head dimers formation due to π-π interactions (Fig. 21). The distance between parallel phenyl rings is 3.35 Å and the

centroid-centroid distance equals to 3.88 Å. The chloroform molecule position was not reported by the authors.

a   **b**
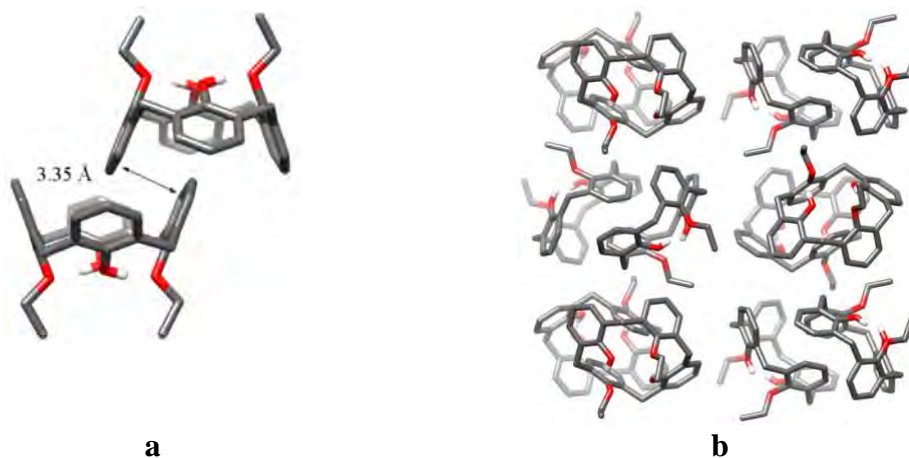
Fig. 21. 1,3-Diethoxycalix[4]arene: (a) head-to-head dimers; (b) packing diagram. Hydrogen atoms are omitted for clarity.

1,3-Dipropoxycalix[4]arene molecules (HC[4]diOC$_3$) also organise in head-to-head dimers.[82,83] The distance between two parallel phenyl rings of the neighbouring calixarenes equals to 3.46 Å, the displacement angle is 30.44 ° (angles between the centroid-centroid vector and normal to one of the phenyl ring) and the centroid-centroid distance is 4.00 Å. According to Janiak,[84] these parameters correspond to weak π-π interaction. This kind of dimerisation was observed in some other disubstituted calix[4]arene derivatives.[85] Hydrogen atoms of a first methylene group of a propyl substituent participate in C–H···π interactions with the phenyl rings of the adjacent calix[4]arenes, thereby the dimers are assembled in hexameric tubes (Fig. 22a). The same tubular self-assembly is observed in crystal structures of 1,3-bis(carboxy

a   **b**
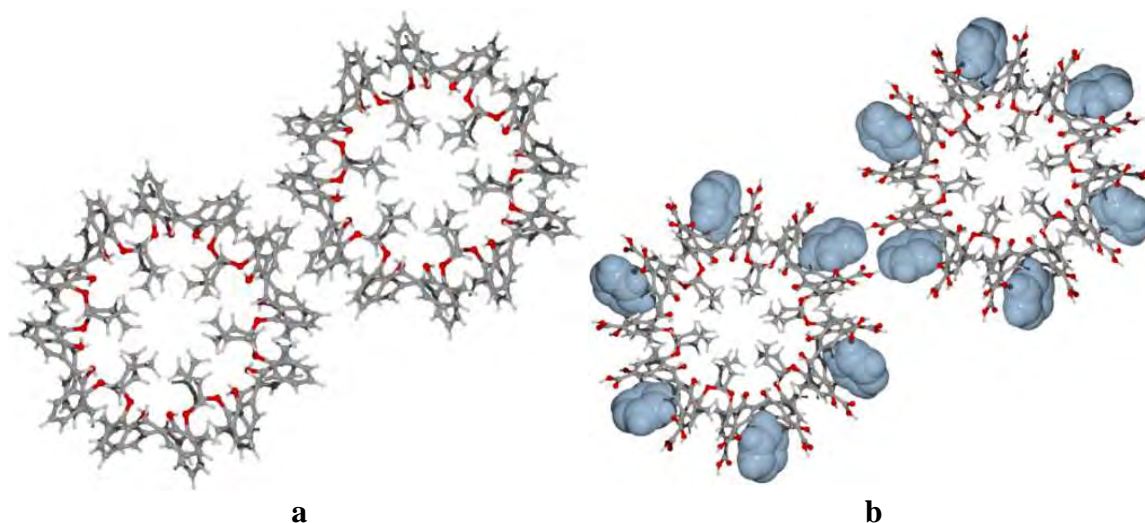
Fig. 22. Tubular intermeshing gear type self-assembly of: (a) 1,3-dipropoxycalix[4]arene; (b) tetra-*para*-carboxylato-25,27-dipropoxycalix[4]arene.[81]

30

methoxy)calix[4]arene·3.3H$_2$O,[86] 1,3-bis(methoxycarbonylmethoxy) calix[4]arene,[85,87] 5,17-diphenyl-25,27-di-propoxycalix[4]arene·3.5H$_2$O,[88] tetra-*para*-   *tert*-butyl-1,3-allyloxycalix[4]arene·CH$_3$OH[89] and tetra-*para*-carboxylato-25,27-dipropoxycalix[4]-arene·pyridine·0.5H$_2$O[81] (Fig. 22b).

Likewise the di-O-alkylated calix[4]arenes with shorter alkyl substituents, 1,3-dioctyloxycalix[4]arene (HC[4]diOC$_8$)[90] also organises in head-to-head dimers (Fig. 23a). The distance between two interacting phenyl rings of the neighbouring calixarenes equals to 3.46 Å and it is the same as in the case of HC[4]diOC$_3$, while the centroid-centroid distance is elongated to 4.26 Å. Weak C–H···π contacts of 2.78 Å combine the HC[4]diOC$_8$ molecules in infinite chains in 'up-down' mode (Fig. 23b). As a result of both π-π and C–H···π interactions the calix[4]arene molecules are assembled in corrugated sheets (Fig. 23c).
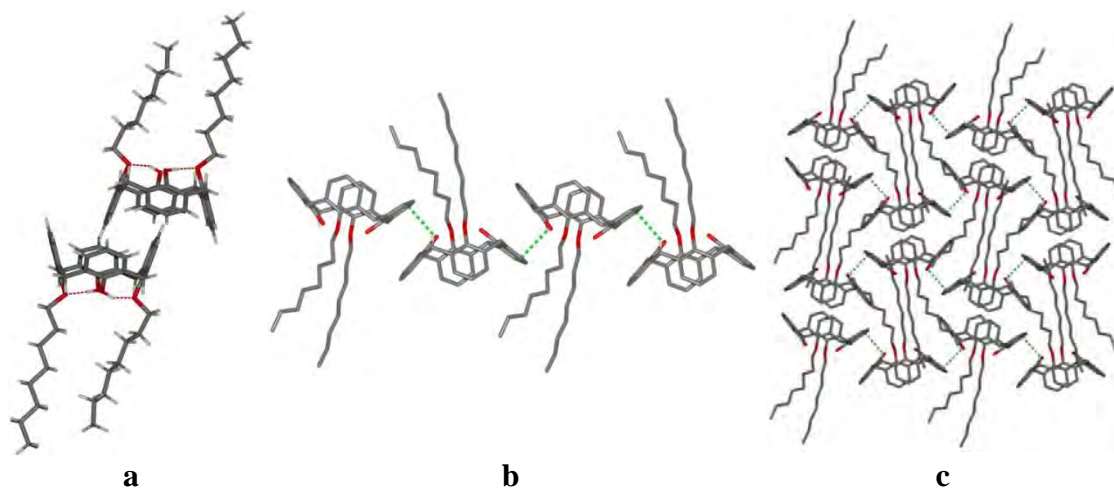
Fig. 23. Structure of 1,3-dioctyloxycalix[4]arene: (a) head-to-head dimer; (b) infinite chains; (c) packing diagram the *a* crystallographic axis.

Only one crystal structure of a non-substituted at the upper rim trialkoxycalix[4]arene has been reported.[91] Tripropoxycalix[4]arene (HC[4]triOC$_3$·CH$_3$CN) forms neither head-to-head dimer nor head-to-tail chain because the hydrophobic calix[4]arene cavity is occupied by an acetonitrile guest molecule (Fig. 24). The guest molecule is bound to two distal phenyl rings *via* C–H···π interactions. Authors noted, that the stabilisation of the complex in the crystal lattice can be mainly attributed to intramolecular O–H···O hydrogen bonds and C–H···π interactions, and intermolecular phenyl offset π-π stacking interactions.

Sykora *et al.*[92] analysed seven crystal structures of tetrapropoxycalix[4]arene (HC[4]OC$_3$) in 1,3-alternate conformation (non-substituted at the upper rim and *para*-

31

a   **b**
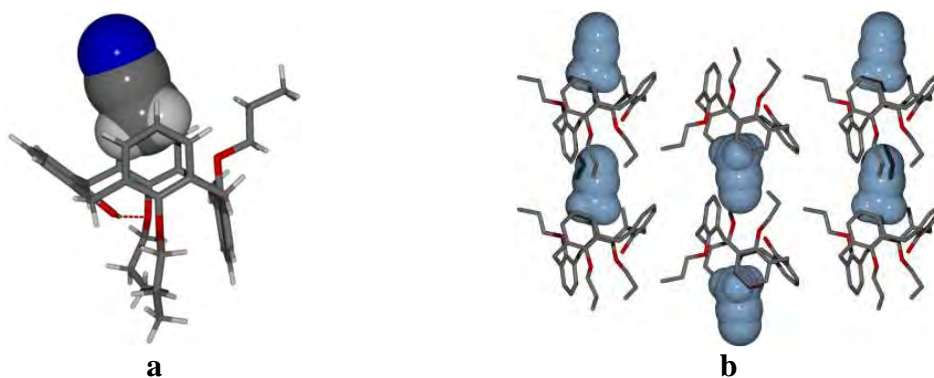
Fig. 24. Structure of HC[4]triOC$_3$· CH$_3$CN: (a) inclusion complex, acetonitrile molecule is shown in spacefill mode; (b) selected layer along diagonal between a and *c* crystallographic axes.

substituted by *tert*-butyl groups or bromine atoms, Fig. 25a). The authors showed that both conformation and crystal packing are independent of the number and nature of the substituents. The calixarene molecules in the solid state simply interlock like a box of bricks (Fig. 25b). All the molecules are combined together *via* van der Waals interactions only.

a   **b**
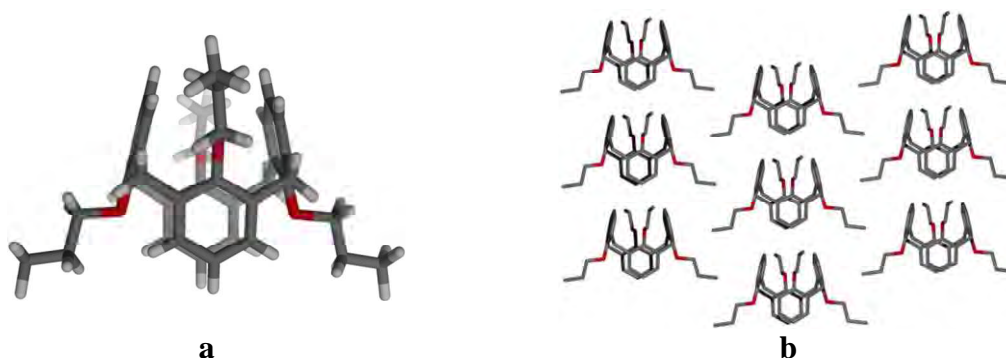
Fig. 25. Structure of HC[4]OC$_3$ in the 1,3-alternate conformation: (a) molecule; (b) columnar arrangement of the molecules.

The crystal structure of tetrapropoxycalix[4]arene (HC[4]OC$_3$) in partial cone conformation (Fig. 26a) was deposited in CSD by Tabatabai *et al.* as private

a   **b**   **c**
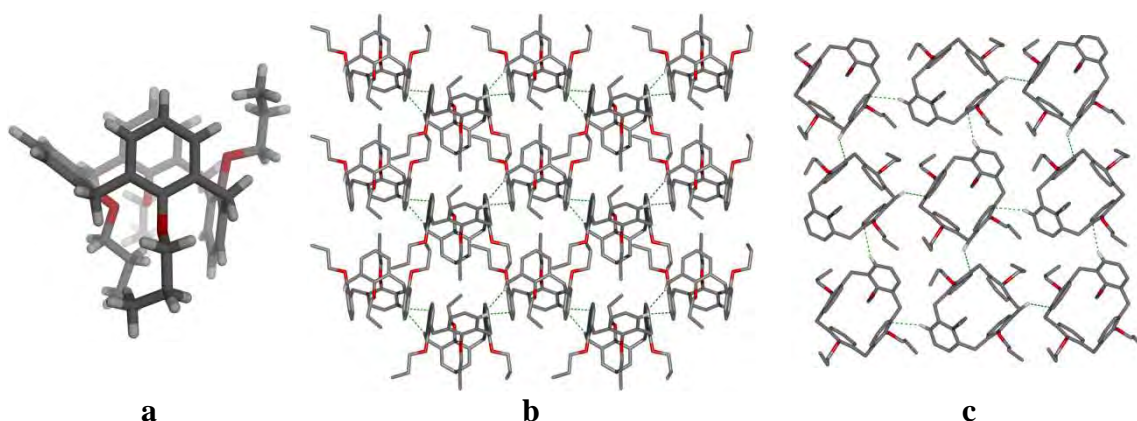
Fig. 26. Crystal structure of HC[4]OC$_3$ (partial cone): (a) molecule; (b) packing along the *c* crystallographic axis; (b) packing along the *a* crystallographic axis.

32

communication.[93] Calix[4]arene molecules are self-assembled, by C–H⋯π interactions between *meta*-H-atoms of the ring distal to the alternated one and H-atoms of methylene bridge bound to alternated ring and benzene ring of neighbouring calix[4]arene molecules, in corrugated layers shown in Fig. 26b.

The crystal structure of tetrapropoxycalix[4]arene (HC[4]OC$_3$) in the pinched cone conformation was deposited in CSD by M. Bolte and P. Sakhaii as a private communication.[94] There are two HC[4]OC$_3$ molecules in the asymmetric unit, which differ from each other by spatial orientation of the alkyl chains and form van der Waals capsules (Fig. 27a). The capsules are arranged in columns (Fig. 27b) and van der Waals interactions between columns are additionally stabilised by C–H⋯π contacts of 2.76 Å length between one type of symmetrically equivalent HC[4]OC$_3$ molecules.

| a | b | c |
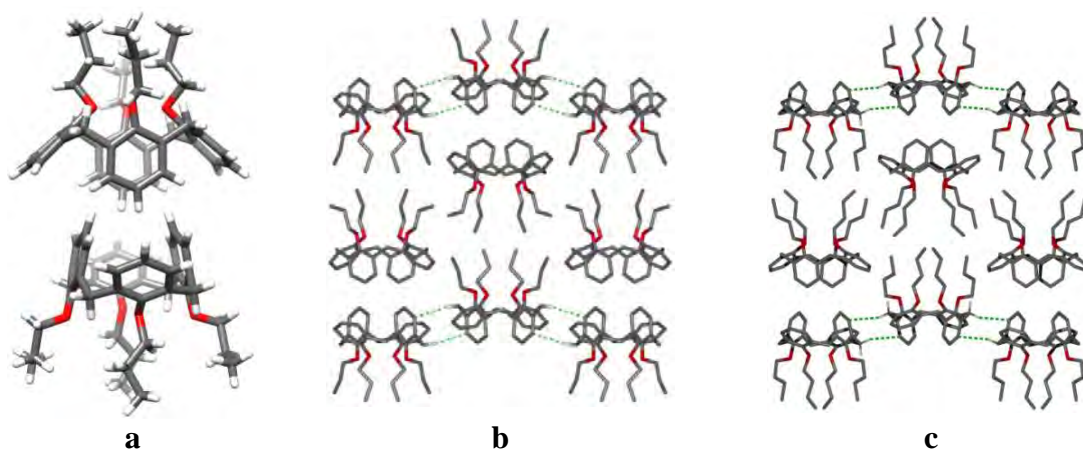
Fig. 27. Crystal structure of HC[4]OC$_3$ in a pinched cone conformation: (a) the asymmetric unit; (b) columnar arrangement of the molecules; (c) self-organisation of HC[4]OC$_4$ molecules.

Surprisingly, in the case of tetrabutoxycalix[4]arene (HC[4]OC$_4$)[95] in the pinched cone conformation, elongation of the alkyl substituents by one carbon atom results in the same self-assembling pattern (Fig. 27c) as for HC[4]OC$_3$ in the pinched cone conformation described above. The difference is in higher order of the crystal structure and only one molecule in the asymmetric unit. Each HC[4]OC$_4$ molecule participates in four C–H⋯π interactions (2.79 Å) to two neighbouring molecules of the calix[4]arene.

According to Shahgaldian *et al.*[96] tetradodecoxycalix[4]arene (HC[4]OC$_{12}$) (Fig. 28a) reveals amphiphilic behaviour: it forms ordered Langmuir monolayers at the air/water inter-phase. In the crystal structure, molecules with the same orientation are arranged in chains (all are oriented up or all down in the same chain) down the *y*-axis *via* C–H⋯π interactions between *meta*-H-atoms of calix-phenyl ring of adjacent

33

calixarenes. Such chains are bound in corrugated layers by C–H···π interactions (Fig. 28b, green dotted lines), where H-atoms belong to the methylene bridges of the calixarene macrocyclic rings. The corrugated layers are combined together by van der Waals interactions between alkyl chains.

a   **b**
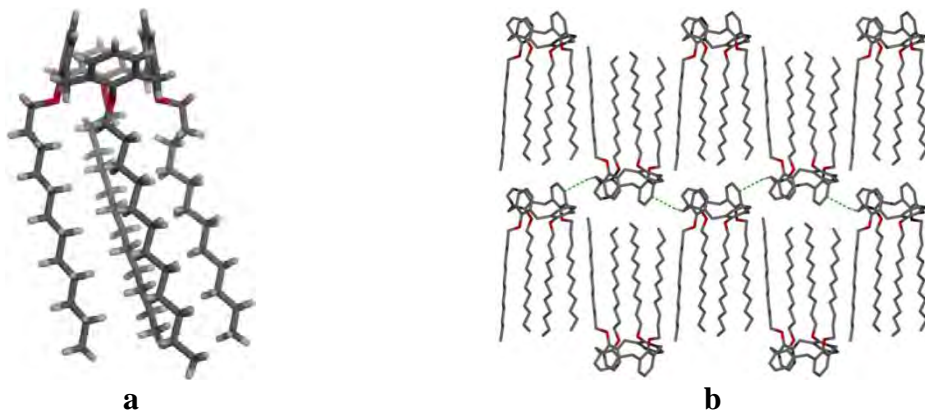
Fig. 28. Crystal structure of HC[4]OC$_{12}$: (a) molecule; (b) antiparallel arrangement of the calixarenes.

It was shown by Raston group[97] that another polymorph of HC[4]OC$_{12}$, and also HC[4]OC$_{14}$ and HC[4]OC$_{16}$ behave like amphiphiles forming bilayers (Fig. 29).

a   **b**   **c**
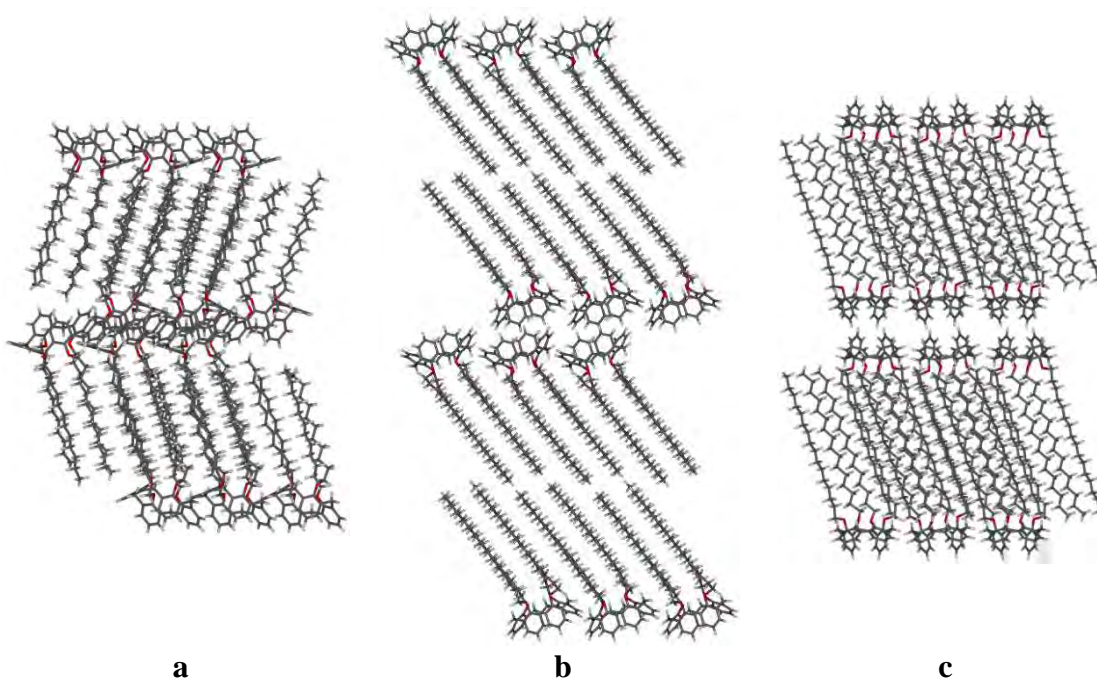
Fig. 29. The bilayers formation in crystal structures: (a) HC[4]OC$_{12}$; (b) HC[4]OC$_{14}$; (c) HC[4]OC$_{16}$·5H$_2$O.

The calix[4]arene macrocyclic rings are bound together by a net of C–H···π interactions between phenyl ring of adjacent calixarenes and, in case of HC[4]OC$_{12}$, H-atoms of methylene bridges and first methylene group of the alkyl substituents, and, in the case

of HC[4]OC$_{14}$ and HC[4]OC$_{16}$, the H-atoms of the first methylene group and *meta*-H of phenyl rings. Surprisingly, the tetratetrdecoxycalix[4]arene (HC[4]OC$_{14}$) spatial arrangement distinctly differs from its homologues with twelve and sixteen carbon atoms: the molecules pack without the alkyl chains being interdigitated (Fig. 29b).

In the case of HC[4]OC$_{18}$,[98] the bilayer arrangement of the calix[4]arene molecules was found in crystal structures of clathrates with both toluene and benzene (Fig. 30). Solvent molecules occupy sites between head-to-tail arrangement of calixarenes and between the layers of calixarenes. For the benzene clathrate there are several C–H⋯π interactions between the guest molecule and the neighbouring host molecules: with the terminal methyl group of alkyl substituent (2.67 Å); with the *O*-methylene group (the first CH$_2$-group of the alkyl substituent) (2.60 Å); with the calixarene methylene bridge hydrogens (2.60 Å).

a　　　　　　　　　　　　　　**b**
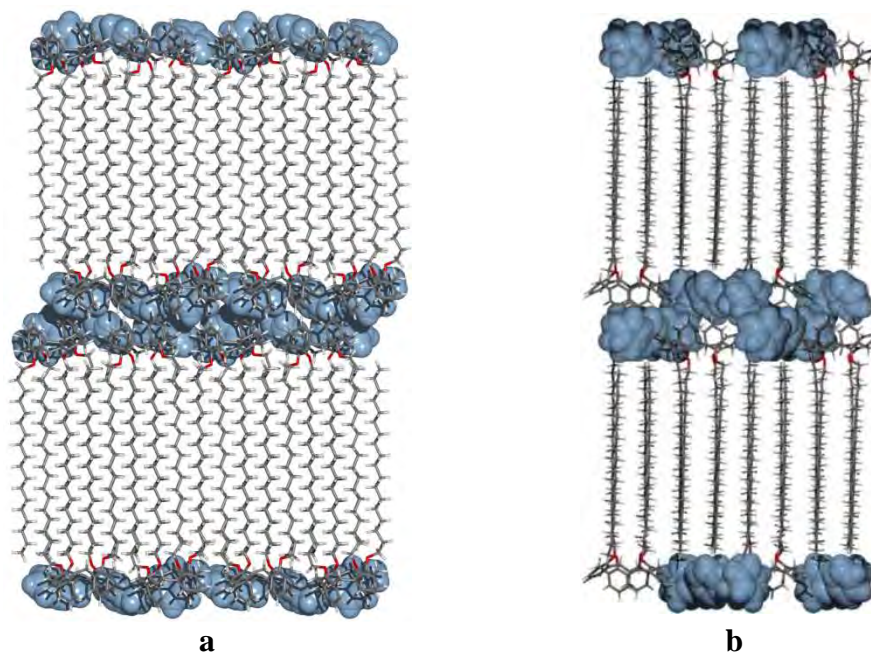
Fig. 30. The bilayer arrangement of HC[4]OC$_{18}$: (a) the toluene clathrate, projection along the *a* crystallographic axis; (b) benzene clathrate, projection along the *c* crystallographic axis.

For the toluene clathrate similar contacts were found, namely two C–H⋯π interactions of 2.72 and 2.87 Å from H-atoms of *meta*-H of calix-phenyl ring to toluene.

2.5.2 Crystal structures of O-alkylated *para-tert*-butylcalix[4]arenes

Preparative syntheses of *para-tert*-butylcalix[4]arene monoalkylethers tBuC[4]mOC$_n$H$_{2n-1}$ with n = 3, 4, 8 and 10 were developed in the Kalchenko group.[99] For these compounds ^{1}H and ^{13}C NMR spectroscopic but no crystal structure analyses were performed.

In the case of the above described dialkoxycalix[4]arenes HC[4]diOalkyl, the head-to-head dimer formation was typical, whereas substituted by *tert*-butyl group at *para*-position tBuC[4]diOalkyl are deprived of such possibility.

Grootenhuis and co-workers[79] published a crystal structure of tBuC[4]diOC$_1$ (Fig. 31a). The main goal of the article was calixarene conformational analysis, so unfortunately crystal packing was not described. There is a developed net of C–H⋯π contacts between *para-tert*-butyl groups and the phenyl rings of the neighbouring calix[4]arenes. The shortest one is 2.81 Å and self-assemble the dimethoxy ether molecules in zigzag chains, then longer one equals to 2.84 Å combine chains in layers (Fig. 31b) and finally the weakest contacts of 2.88 Å construct the 3D-structure. In the toluene solvate, tBuC[4]diOC$_1$·3toluene,[100] one molecule of the guest is included into the calix[4]arene bowl and such complexes are arranged in 'up-down' mode (Fig. 31c). Additional toluene molecules are located in cavities, which are formed in the crystal lattice.

| a | b | c |
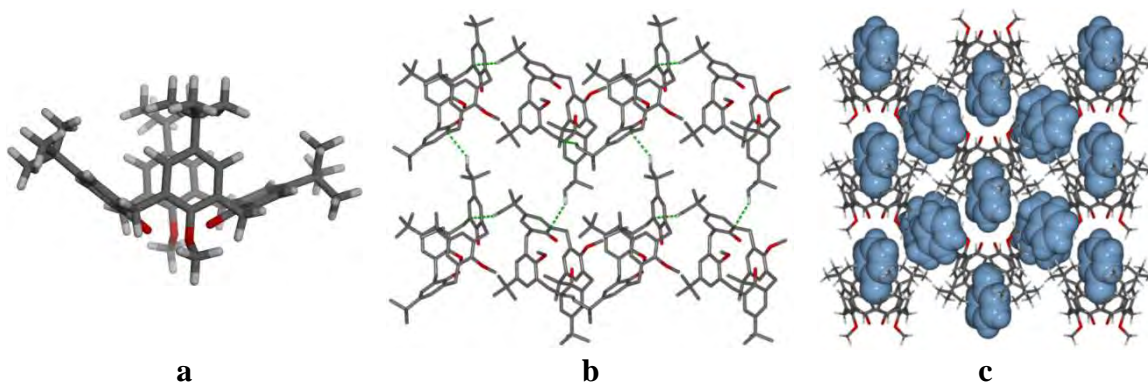
Fig. 31. (a) Molecule of tBuC[4]diOC$_1$; (b) self-assembling of tBuC[4]diOC$_1$ in layers; (c) packing diagram for tBuC[4]diOC$_1$·3toluene solvate.

In the inclusion complex of tBuC[4]diOC$_2$·ethanol,[101] two types of van der Waals pseudo-capsules are present: the calix[4]arene-ethanol complexes are oriented head-to-head (Fig. 32a). The pseudo-capsules of the same type are arranged in the plane of (110) family. Room temperature (298 K) modification of acetone inclusion complex, tBuC[4]diOC$_2$·acetone[102] reveals to be isostructural with the ethanol one, where ethanol molecules are isomorphically substituted by acetone. In the low temperature modification (153 K), only one type of the pseudo-capsules is present (Fig. 32b). Ethyl substituents of each complex participate in C–H⋯π interactions with phenyl rings of the neighbouring calix[4]arenes. In this way the complexes are joined in parallel

ribbons, which are perpendicular to the plane of the Fig. 32b. The spatial coherence between the ribbons is responsible for pseudo-capsule formation.

a   **b**
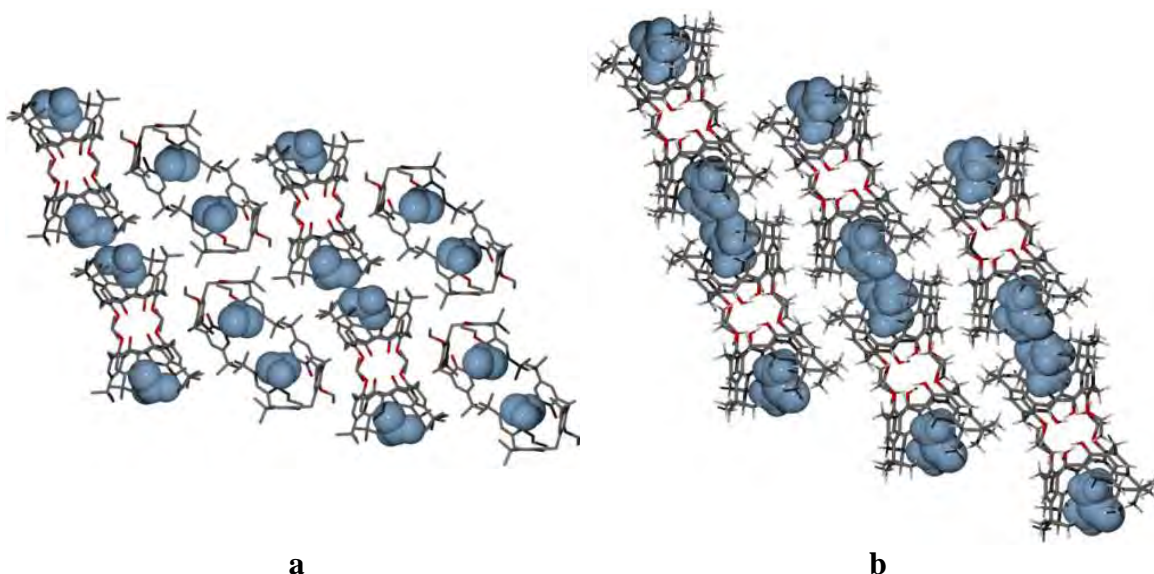
Fig. 32. Inclusion complexes of tBuC[4]diOC$_2$ with: (a) ethanol; (b) acetone.

Similarly to tBuC[4]diOC$_2$ with distal location of the ethyl groups, in the tBuC[4]diOC$_3$·CH$_3$CN[103] inclusion complex the calix[4]arene molecules are bound in ribbons *via* C–H···π interactions between terminal H atoms of the alkyl substituents and π-electrons of neighbouring calix[4]arene molecules (Fig. 33a). The difference is in the ribbon packing: the adjacent ribbons are rotated by the angle of 90° (Fig. 33b), therefore the van der Waals pseudo-capsules do not form.

a   **b**
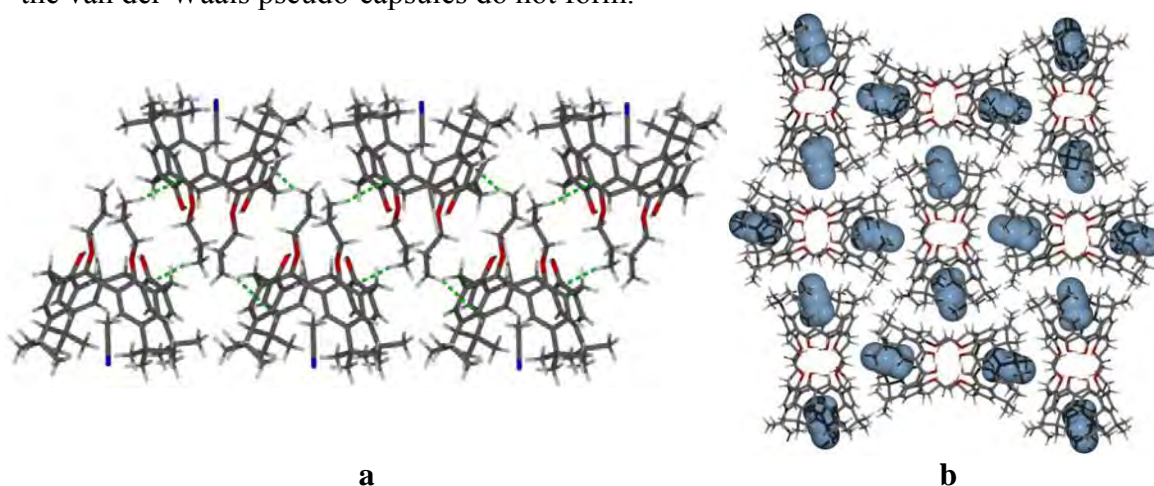
Fig. 33. Self-assembly of tBuC[4]diOC$_3$·CH$_3$CN complexes: (a) ribbon along the *c* crystallographic axis; (b) the ribbons arrangement in the crystal.

In the inclusion complex of tBuC[4]diOC$_3$ with chloroacetonitrile,[104] a hydrogen atom of the second carbon of only one propyl chain takes part in C–H···π interaction, which results in self-assembly in dimers, not ribbons (Fig. 34a). The spatial coherence

in the dimer arrangements causes formation of capsules oriented along diagonal between a and *b* crystallographic axes (Fig. 34b).

a   **b**
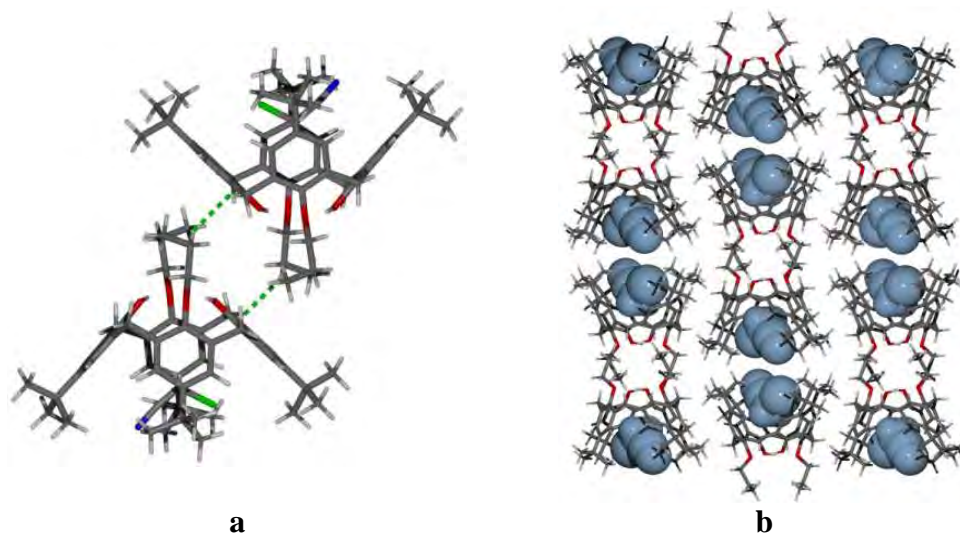
Fig. 34. tBuC[4]diOC$_3$·ClCH$_2$CN complex: (a) dimer; (b) the packing diagram along the *c* crystallographic axis.

Exchange chloroacetonitrile with a maleonitrile-dioxane mixture[104] induces substantial changes in the calix[4]arene self-assembly. The calix[4]arene·maleonitrile inclusion complexes are combined in chains along the *a* crystallographic axis *via* C–H···π interactions between H-atom of a *tert*-butyl group and phenyl ring of an adjacent calix[4]arene (Fig. 35a). Molecules of dioxane play the role of the binding component. Unlike the described above tBuC[4]diOC$_3$ solvate structures, in this crystal structure no capsule formation is observed: the calix[4]arene molecules are arranged in a head-to-tail mode (Fig. 35b).

a   **b**
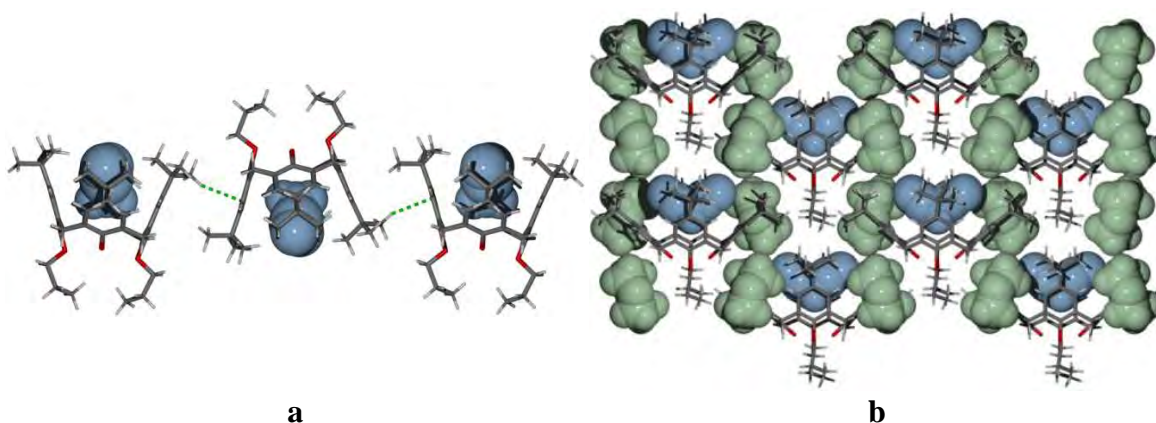
Fig. 35. Crystal structure of tBuC[4]diOC$_3$·maleonitrile·2dioxane solvate: (a) self-assembly of tBuC[4]diOC$_3$·maleonitrile inclusion complexes in chain; (b) packing diagram along the *a* crystallographic axis. Molecules of maleonitrile are in pale blue, the dioxane ones are in pale green.

Gruber *et al.* reported two[105] isostructural solvates of tBuC[4]diOC$_3$ with DMF and DMF-methanol guests. The crystal packing diagrams, which are displayed in Fig. 36, show molecular layers extending parallel to the crystallographic *ab* plane. Inclusion complexes are arranged in herringbone motifs. Methanol molecules present in the second structure come from the crystallisation mixture and are located in the cavities present in the crystal lattice (Fig. 36b). Both crystal structures are additionally stabilised by C–H⋯O bonds between inclusion complexes and DMF molecules.

a   b
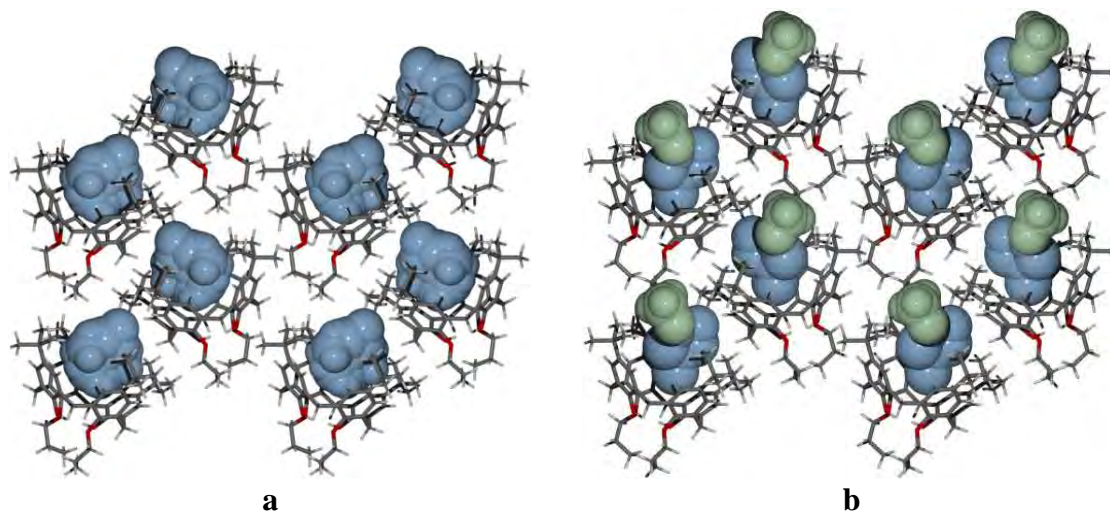
Fig. 36. View along the *c* crystallographic axis on the herringbone motifs: (a) tBuC[4]diOC$_3$·DMF; (b) tBuC[4]diOC$_3$·DMF·0.5CH$_3$OH.

Only one crystal structure of tri-O-alkylated at the lower rim *para-tert-*butylcalix[4]arene (tBuC[4]triOC$_1$) was reported so far by Grootenhuis *et al.*[80] (Fig. 37). Due to the non-polar nature of the calixarene, the crystal structure is dominated by weak intermolecular interactions. The cone conformation of the calix[4]arene is stabilised by
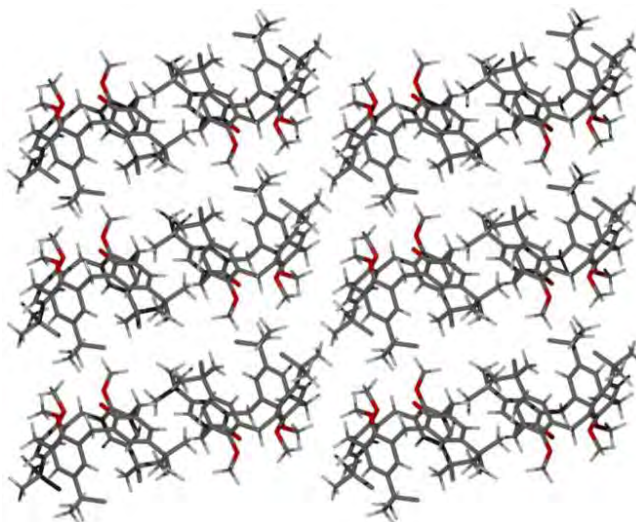
Fig. 37. tBuC[4]triOC$_1$: packing diagram along the *a* crystallographic axis.

39

intramolecular O–H···O hydrogen bond at the lower rim. The crystal packing is a rather complicated interplay of the calix[4]arene conformation (shape) and weak intermolecular van der Waals type arene-alkyl and alkyl-alkyl contacts.

As already mentioned above (page 23), the tetramethyl ether tBuC[4]OC$_1$ conformation undergoes interconvertion at room temperature. Quantum chemistry calculations[80] predict the 1,3-alternate conformation to be the most stable one. Nevertheless, in solution and the solid-state the partial cone conformation, in which all the methoxy groups point outwards, is preferred. Firstly, Grootenhuis *et al.*[80] reported the solvent-free tBuC[4]OC$_1$ crystal structure. Later the isostructural clathrates with THF[106] and CH$_2$Cl$_2$[107] were published by Fischer *et al*. In all three crystal structures, there are two independent molecules in the asymmetric unit and therefore two types of molecular layers, parallel to the *bc* crystallographic planes at a = 0 and a = 0.5, are present (Fig. 38). Each of them consists of only one type of molecules and additionally can contain solvent molecules in cavities between the calix[4]arene molecules. In the case of tBuC[4]OC$_1$·0.5CH$_2$Cl$_2$, the solvent molecules are present only in planes at a = 0.5.

a   **b**
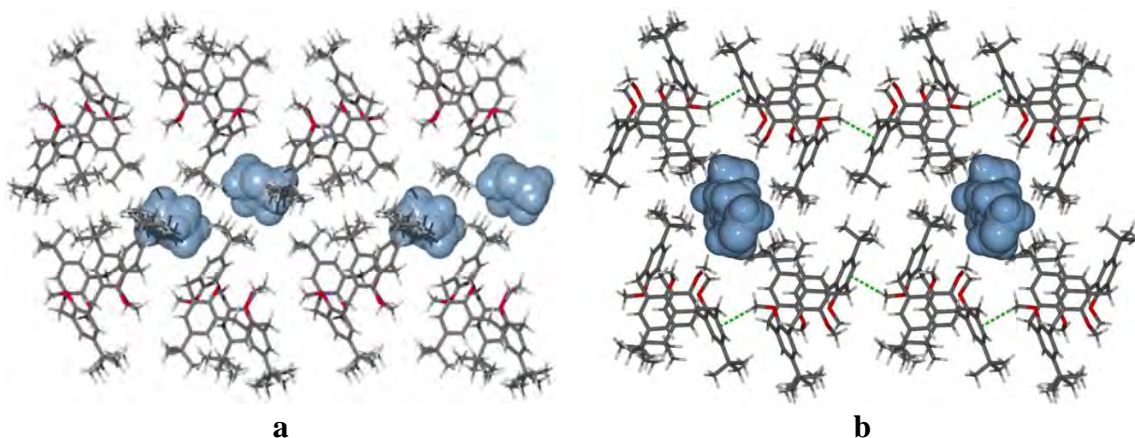
Fig. 38. Selected layers in tBuC[4]OC$_1$·THF clathrate parallel to *bc* crystallographic planes: (a) at a = 0; (b) at a = 0.5.

Both liquid and solid-state investigation of tBuC[4]OC$_2$ in the 1,2-alternate conformation were reported by Groenen *et al.*[58] The host calix[4]arene molecules are assembled by the guest CH$_2$Cl$_2$ molecules *via* C–H···π and Cl···π interactions in ribbons (Fig. 39a). The ribbons are packed in the 'up-down'-mode along the *c* crystallographic axis (Fig. 39b).

In the inclusion complex of the tetrapropyl ether tBuC[4]OC$_3$ with acetonitrile,[108] the calix[4]arene molecule adopts the cone conformation. Calix[4]arenes with the same spatial orientation, 'up' or 'down', are bound by C–H···π interaction

a

b
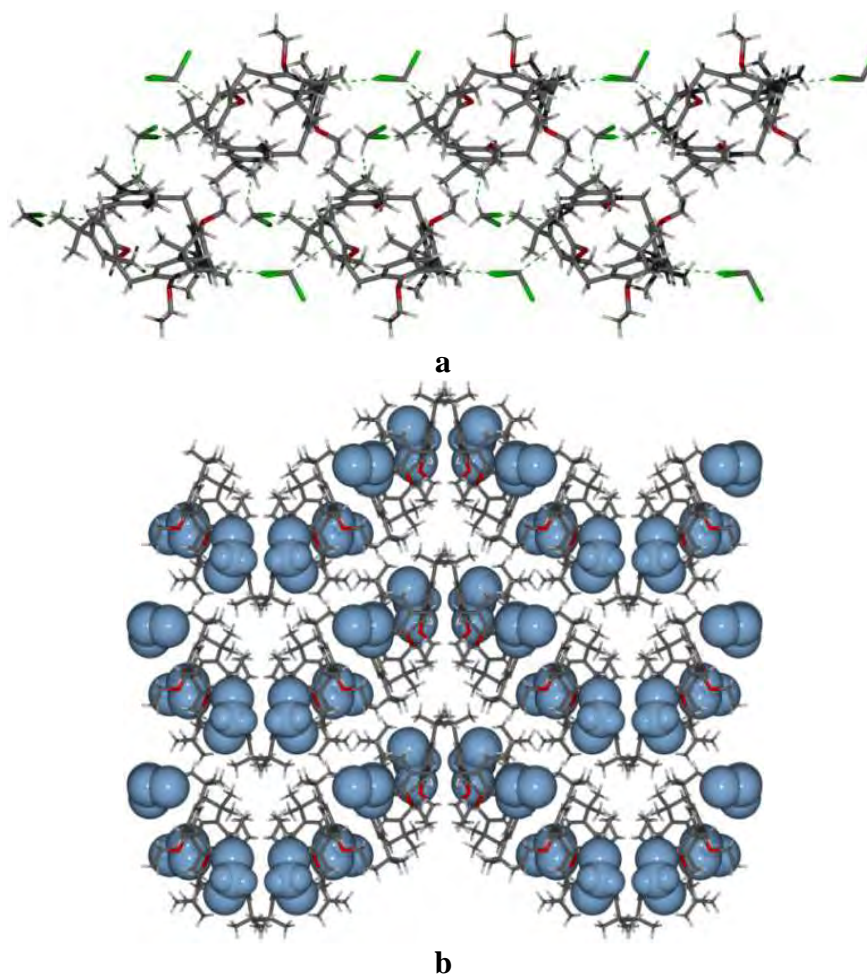
Fig. 39. Crystal structure of tBuC[4]OC$_2$·CH$_2$Cl$_2$ clathrate: (a) ribbon; (b) the packing diagram along the *c* crystallographic axis.

between H atoms of *tert*-butyl groups and calix[4]arene phenyl rings in chains along the *a* crystallographic axis. By the same type of bonds, the individual chains with 'antiparallel' calix[4]arene orientation are combined in ribbons (Fig. 40a). This structural motif is repeated in the crystal structure due to translational symmetry (Fig. 40b).

a

b
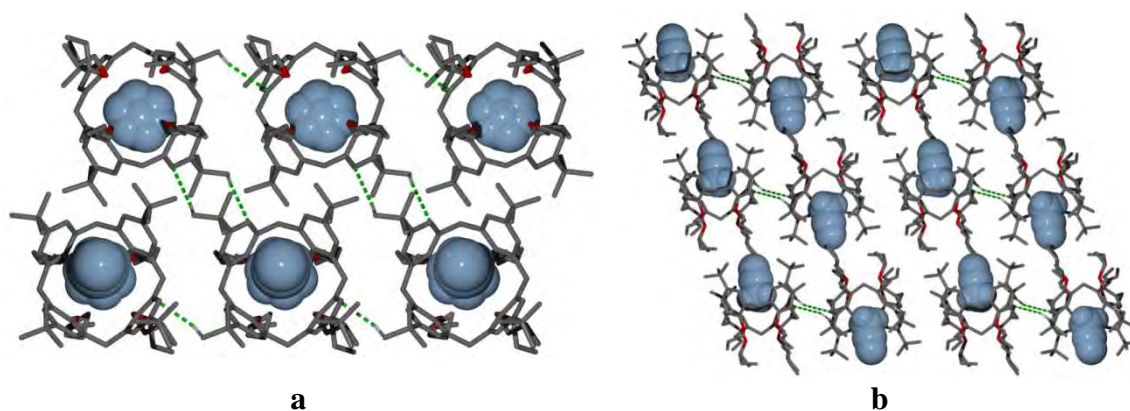
Fig. 40. Crystal structure of tBuC[4]OC$_3$·CH$_3$CN inclusion complex: (a) self-aggregation in ribbon along the *a* crystallographic axis; (b) packing diagram, view along the ribbons.

41

In the tBuC[4]OC$_3$·0.5THF clathrate, the calix[4]arene molecule assumes the partial cone conformation.[105] Orientation of the aromatic rings is such that the terminal carbon atom of the propoxy substituent, being attached to the alternate aromatic ring, is in close contact to the *tert*-butyl groups. Such a conformation of the calixarene causes closing of the cavity, which obviously prevents encapsulation of a guest molecule such as THF. As illustrated in Fig. 41a, the calixarene adopts a bilayer type of arrangement with solvent molecules located in the lattice cavities between double layers.

a   **b**   **c**
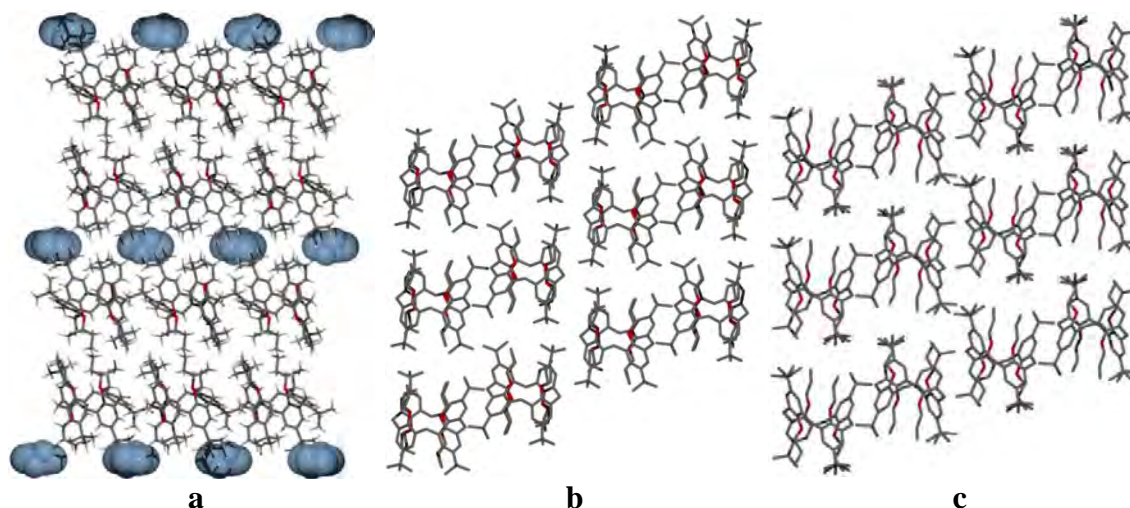
Fig. 41. Packing diagrams of tBuC[4]OC$_3$ crystal structures: (a) tBuC[4]OC$_3$·0.5THF clathrate viewed along the *b* crystallographic axis; (b) 1,2-alternate conformation along the *a* crystallographic axis; (c) 1,3-alternate conformation along the *a* crystallographic axis.

In the crystal structure of tBuC[4]OC$_3$ in the 1,2-alternate conformation,[109] calix[4]arene molecules are self-assembled, by C–H⋯π interactions of *tert*-butyl groups and calix[4]arene phenyl rings, in molecular layers parallel to (011) planes (Fig. 41b). All of the propyl chains are disordered over two or even three positions.

The crystal structure of tBuC[4]OC$_3$ in the 1,3-alternate conformation[92] is composed of molecular zigzag chains lying in the *ac* crystallographic plane: H-atoms of ordered *tert*-butyl groups take part in C–H⋯π interactions between adjacent calix[4]arene molecules. Apart from the mentioned C–H⋯π interactions, the crystal structure is stabilised by intermolecular arene-alkyl and alkyl-alkyl contacts. The packing diagram is shown in Fig. 41c.

Li *et al.*[110] reported structural study of tBuC[4]OC$_4$·4CHCl$_3$·2H$_2$O. Such high solvent content is quite unusual for alkoxycalix[4]arene crystal chemistry. Calix[4]arene molecules are arranged in columns along the *b* crystallographic axis in the head-to-tail mode. The role of the guest molecules is to bind the neighbouring calix[4]arene

molecules *via* C–H⋯Cl and C–H⋯O hydrogen bonds (Fig. 42a). All guest molecules are located between the adjacent calix[4]arene columns, the calix[4]arene internal cavity remains unoccupied.

a　　　　　　　　**b**
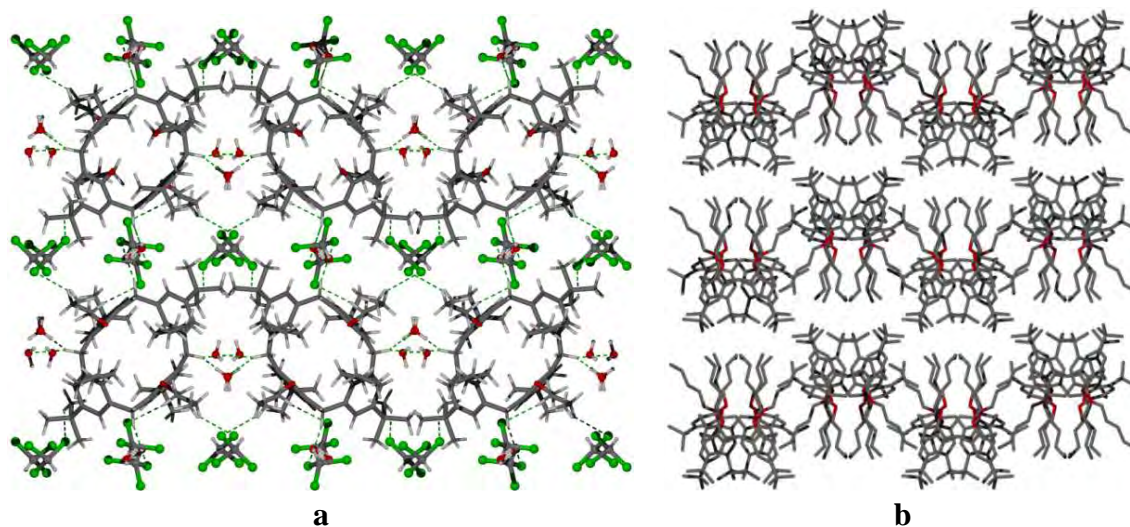
Fig. 42. Packing diagram: (a) tBuC[4]OC$_4$·4CHCl$_3$·2H$_2$O clathrate, view along the *b* crystallographic axis; (b) tBuC[4]OC$_5$, view along the diagonal between *a* and *c* crystallographic axes.

The tetrapentoxy ether tBuC[4]OC$_5$ molecules in the solid state[111] combine in centrosymmetrical dimers due to two C–H⋯π interactions between *tert*-butyl groups and phenyl rings of two adjacent calix[4]arene macrocyclic rings. Dimers are packed in the crystal in such a way, that the calix[4]arene molecules are arranged in parallel mode along the diagonal between a and *c* crystallographic axes (Fig. 42b) and in anti-parallel mode in perpendicular direction. The crystal structure is dominated by intermolecular van der Waals interactions.

2.5.3   Crystal structures of O-alkylated *para*-nitrocalix[4]arenes

The *para*-nitro-alkoxycalix[4]arenes NO$_2$C[4]Oalkyl are expected to be more polar than *para-tert*-butyl tBuC[4]Oalkyl or non-substituted HC[4]Oalkyl because of negative both inductive and mesomeric effects of the nitro group in the *para*-position. In addition, if a solvent molecule is present in the *para*-nitro-alkoxycalix[4]arene crystal structure, it would be expected to interact *via* its H-atom(s) with the negatively charged oxygen atoms of the nitro group rather than with the π-electrons of the calix[4]arene macrocyclic ring.

Nevertheless, in the crystal structure of NO$_2$C[4]OC$_1$·DMF inclusion complex, reported by Kumar *et al.*,[96] guest molecule is included into electron-deficient

43

calix[4]arene cavity (Fig. 43a). Hydrogen atoms in *meta*-position of the phenyl rings other than alternated one, H-atoms of methylene bridges and one methoxy group participate in C–H⋯O hydrogen bonds of length 2.53–2.84 Å, which combine inclusion complex molecules in three-dimensional framework. A selected layer with the calix[4]arene molecules with the same orientation is shown in Fig. 43b.
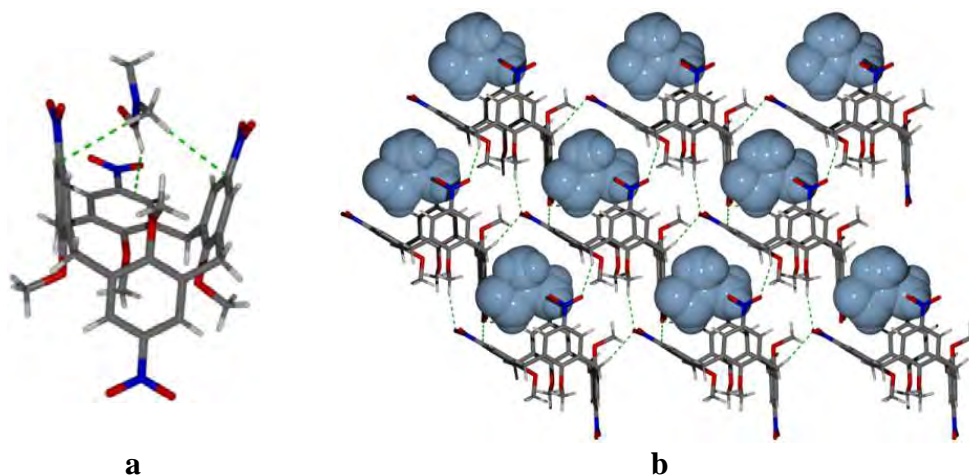
Fig. 43. Crystal structure of NO$_2$C[4]OC$_1$·DMF inclusion complex: (a) inclusion of DMF molecule; (b) a half of the layer with the calix[4]arene molecules with the same spatial orientation.

Two crystal structures of the tetraethoxycalix[4]arene NO$_2$C[4]OC$_2$·chloroform clathrates were published by Kunsági-Máté *et al.*[112] In the first structure, NO$_2$C[4]OC$_2$·2CHCl$_3$, the calix[4]arene adopts the partial cone conformation. Similarly to the crystal structure of the tetramethoxycalix[4]arene·DMF inclusion complex described above, calix[4]arene molecules with the same spatial orientation are arranged in the head-to-tail mode and form layers (Fig. 44a). The layers above and below are shifted due to the presence of a *c*-plane normal to the *b* crystallographic axis. The main difference between the two crystal structures is in the solvent location: chloroform
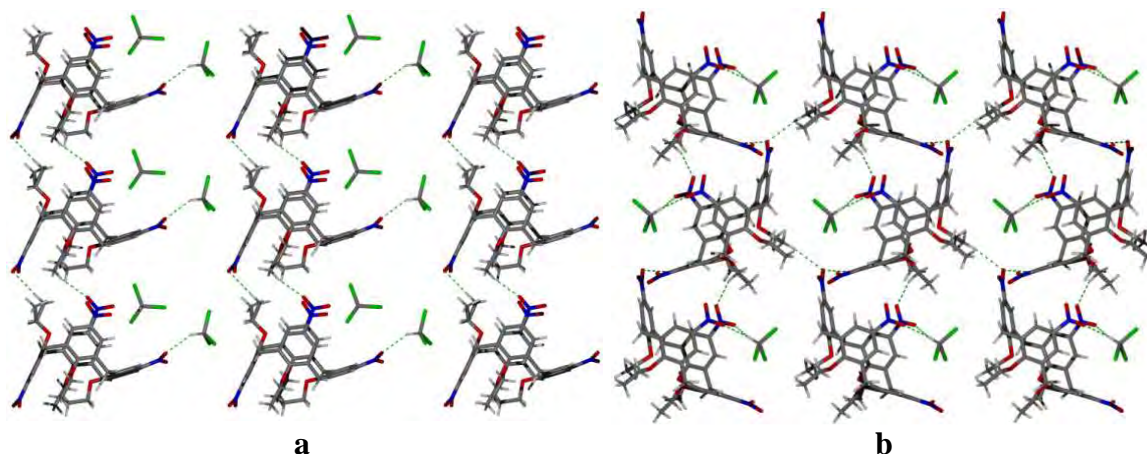
Fig. 44. Calixarene arrangements in NO$_2$C[4]OC$_2$·chloroform clathrates: (a) parallel for NO$_2$C[4]OC$_2$·2CHCl$_3$ (partial cone); (b) the herringbone-type for NO$_2$C[4]OC$_2$·CHCl$_3$ (cone).

molecules prefer to participate in C–H⋯O or C–H⋯Cl hydrogen bonds rather than in C–H⋯π interactions and, as a consequence, the *exo* complexation is realised. In Fig. 44a, location of the chloroform molecules between chains of the calix[4]arenes is shown. Chloroform molecules combine the calix[4]arene chains in layers and the layers in 3D structure.

In the second crystal structure, $NO_2C[4]OC_2 \cdot CHCl_3$, the calix[4]arene molecule assumes the cone conformation and a clathrate with stoichiometry 1:1 is formed. The calix[4]arene molecules are arranged in herringbone-type motif in the layers parallel to the *bc* crystallographic plane at a = 0.25 (Fig. 44b). The layers are self-assembled in 3D structure due to the presence of C–H⋯O hydrogen bonds between calixarene molecules from the adjacent layers. The guest molecules are included in cavities formed within the layers and, unlike the structure described above, do not participate in binding the layers by specific interactions other than van der Waals.

Tetra-O-propylated *para*-nitrocalix[4]arenes $NO_2C[4]OC_3$ have been more widely investigated than other *para*-nitroalkoxycalix[4]arenes. Kenis *et al.*[113] published four crystal structures: one structure of each main calix[4]arene conformers. The calix[4]arene in the cone conformation is a clathrate with unknown solvent, in 1,3-alternate conformation crystallises with methanol and the remaining two conformers form solvent-free crystals. The solid-state structure of the dichloromethane clathrate of the *para*-nitropropoxycalix[4]arene in the cone conformation was reported by Kelderman *et al.*[114] Klimentova *et al.*[115] report the crystal structures of $NO_2C[4]OC_3$ as tetrahydrofuran clathrate and solvent-free one where the calix[4]arene also adopts the cone conformation. Surprisingly, there is a self-assembling pattern which is common for all four crystal structures of the tetrapropoxycalix[4]arenes $NO_2C[4]OC_3$ in the cone conformation. The calix[4]arene molecules are self-assembled in infinite chains in 'up-down' mode *via* C–H⋯O hydrogen bonds between adjacent calixarenes (Fig. 45). There is a strong possibility that the nature of solvent plays an important role in the spatial orientation of the chains. When the solvent molecules are hydrogen donors in C–H⋯O hydrogen bonds with nitro groups of only one *para*-nitrocalix[4]arene, then the neighbouring chains are identical (Fig. 45a). When the solvent molecule is able to play a bridging role between chains, then calix[4]arene molecules in the neighbouring chains are oriented 'head-to-head' and 'tail-to-tail' Fig. 45b. In the absence of the solvent in the crystal, the chains become zigzag chains and the distances between them are shorter
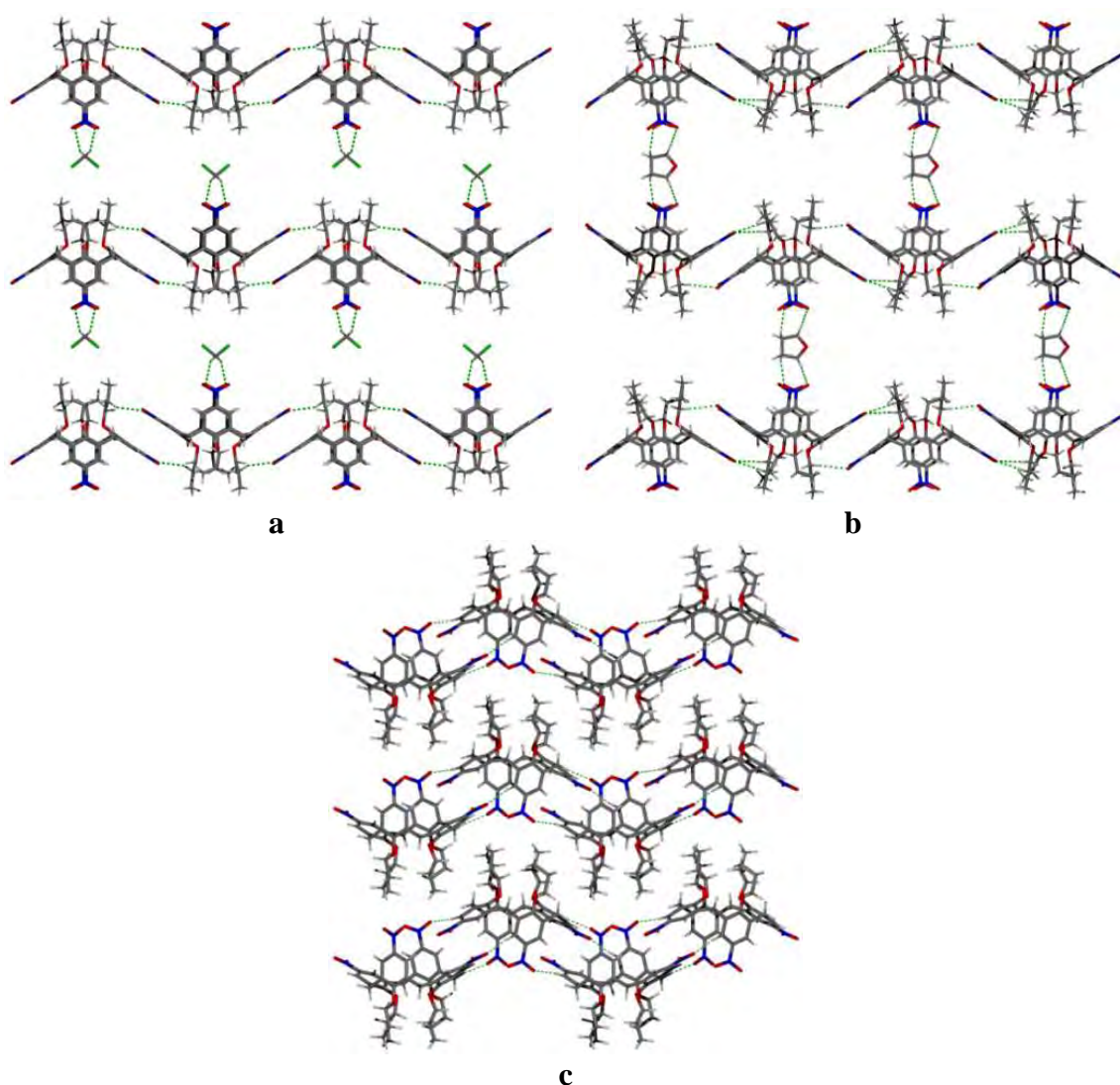
Fig. 45. Selected layers in NO₂C[4]OC₃ crystals: (a) (002) plane in CH₂Cl₂ clathrate[114]; (b) (404) plane in THF clathrate; (c) (004) plane in solvent-free NO₂C[4]OC₃.[115]

in order to minimize interactions between the hydrophobic propyl substituents and the calix[4]arene macrocyclic rings (Fig. 45c).

The crystal structures of NO₂C[4]OC₃ clathrates have similar fragments (Fig. 45a and b), their spatial arrangement depends on the space group of the each structure. H-atoms of propyl substituents and calixarene macrocyclic rings take part in C–H⋯O hydrogen bonds and bind flat fragments in three-dimensional structure.

In the case of the tetrabutoxycalix[4]arene NO₂C[4]OC₄·2acetone clathrate,[116] the strongest intermolecular interactions are C–H⋯O bonds between *meta*-H-atoms of the calix[4]arene phenyl rings and nitro groups and equals to 2.59 Å which bound the calix[4]arene molecules with the same spatial orientation in chains along the *a* crystallographic axis (Fig. 46a). Each acetone molecule forms two C–H⋯O bonds of the length 2.64 and 2.66 Å, and plays a bridging role between the calix[4]arene chains

combining them in corrugated layers (Fig. 46b). The last methylene group of the disordered butyl substituent forms in one of the positions C–H···O contact equal to 2.69 Å to the nitro group of the adjacent calix[4]arene but the angle value (132°) suggests a low contribution of this interaction in the whole crystal structure stabilisation.

| a | b |
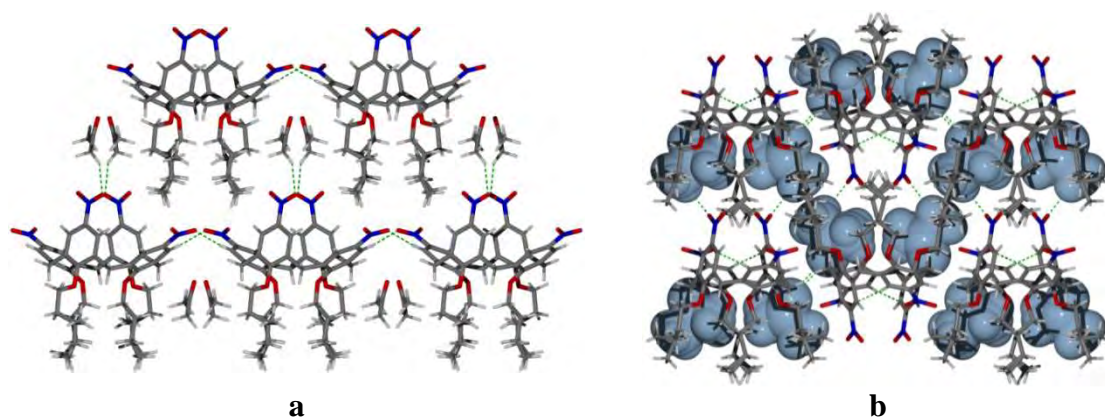
Fig. 46. NO$_2$C[4]OC$_4$·2acetone clathrate crystal structure: (a) chains formation along the *a* crystallographic axis; (b) packing diagram, view along the chains.

In the crystal structure of tetrapentoxycalix[4]arene NO$_2$C[4]OC$_5$, reported by Vysotsky *et al.*,[117] the calix[4]arene molecules with the same spatial orientation are connected by C–H···O hydrogen bonds but in different way than in the tetrapropoxy derivative (Fig. 47a). Nitro groups of two distal phenyl rings of each calix[4]arene molecule are hydrogen acceptors in one strong hydrogen bond of 2.55 Å (H-atom of the first methylene group of pentyl substituent), and one weak contact of 2.70 Å (with H-atom of the calixarene bridging methylene group). As a result of such interactions, the calix[4]arene molecules with the same spatial orientation are assembled in layers, which are parallel to the *ab* crystallographic plane. The layers with the opposite spatial

| a | b |
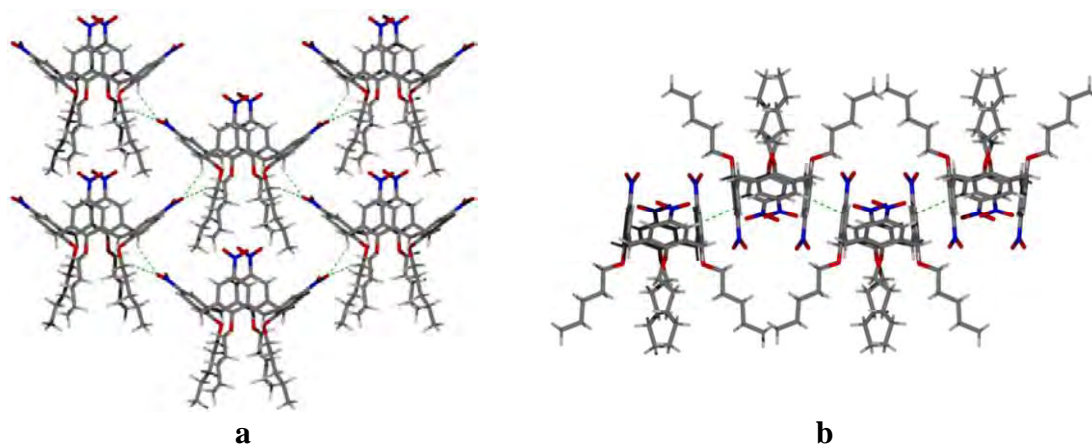
Fig. 47. Intermolecular interactions in NO$_2$C[4]OC$_5$ crystal structure: (a) layers formed by C–H···O interactions; (b) C–H···π interactions between layers.

orientation are joined by weak C–H···π contacts of length 2.79 Å between *meta*-H-atoms of the calix[4]arene and π-electrons of the phenyl ring of the adjacent one (Fig. 47b).

2.5.4   Calix[6]arenes as amphiphiles

Calix[6]arenes, as already mentioned in chapter 2.4, are much more conformationally flexible, than calix[4]arenes. Additionally, in both dominant conformations, 'up-down' double partial cone and 'up-up' double partial cone (Fig. 14), the macrocyclic cavity is more accessible for guest molecules than in the case of calix[4]arenes. These factors result in much more complicated crystal chemistry: the CSD contains 301 structures of calix[6]arenes, which belong to different classes of compounds, but only 4 are hexa-O-alkylated calix[6]arenes and *para-tert*-butylcalix[6]arenes.

Only one non-substituted in *para*-positions hexa-O-alkylated calix[6]arene was reported so far by Clark *et al.*:[118] it is hexakis(octadecyloxy)calix[6]arene HC[4]OC$_{18}$. Calix[6]arene bearing linear C$_{18}$ alkyl chains crystallises in 'up-down' double partial cone conformation with three alkyl chains on each side of the macrocyclic ring (Fig. 48a). The conformation is stabilised by intramolecular C–H···O hydrogen contacts between *meta*-H-atoms of phenyl moieties, H-atoms of second methylene groups of two distal alkyl substituents, which close the calix[6]arene cavity from the oxygens'

a   b
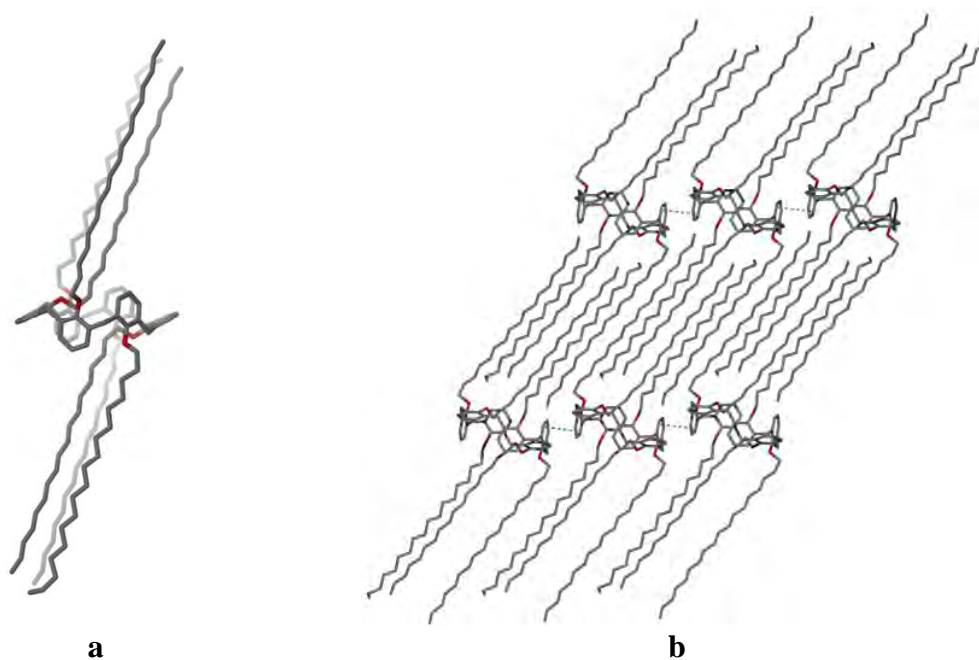
Fig. 48. Crystal structure of HC[6]OC$_{18}$:[118] (a) molecule in inverted partial cone conformation; (b) packing diagram along the *a* crystallographic axis. Hydrogen atoms are omitted for clarity.

side, and O-atoms of adjacent phenoxy moieties. Additionally, intramolecular C–H⋯π interactions between H-atoms of first methylene groups of two alkyl substituents closing the cavities and π-electrons of proximal benzene rings occur.

Each calix[6]arene macrocyclic ring connects through C–H⋯π and offset π-π interactions to other calix[6]arene macrocyclic rings, forming layers with the alkyl chains being almost parallel and protruding either side. The interdigitation of the alkyl chains from the neighbouring layers and gives a pseudo bilayer arrangement (Fig. 48b) similar to these observed in the crystal structures of HC[4]OC$_{18}$ clathrates with benzene and toluene (chapter 2.5.1). The Hirshfeld surface analyses at different temperatures (100, 200 and 300 K) clearly show that the thermal expansion of the structure particularly correlates with elongation of C–H⋯π contacts between the calix[6]arene macrocyclic rings: d(*meta*-H⋯π) equal to 3.14, 3.17 and 3.20 Å at 100, 200 and 300 K, respectively.

The crystal structure of hexamethoxy *para-tert*-butylcalix[6]arene tBuC[6]OC$_1$ was published by Tsue *et al.*[119] The calix[6]arene molecule assumes the 'up-down' double partial cone conformation (Fig. 49a) stabilised by intramolecular C–H⋯O hydrogen contacts between *meta*-H and O-atoms of adjacent alternated phenoxy moieties similarly to HC[6]OC$_{18}$.[118] Methyl groups of two distal phenyl rings with disordered *tert*-butyl groups close the calix[6]arene cavity from the oxygens' side and stabilise the calix[6]arene conformation by C–H⋯O hydrogen contacts and C–H⋯π interactions to proximal phenoxy moieties. Surprisingly, there are no intermolecular C–H⋯π or π–π-interactions present in the crystal structure. The C–H⋯O hydrogen

| a | b |
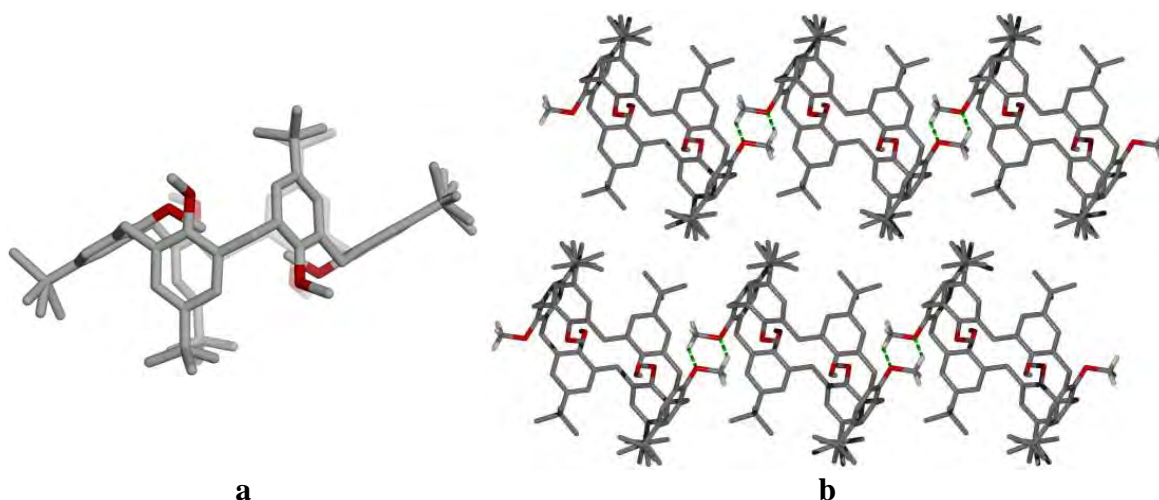
Fig. 49. Structure of tBuC[6]OC$_1$: (a) molecule in inverted double partial cone conformation; (b) chains formation *via* C–H⋯O hydrogen bonds. Hydrogen atoms are omitted for clarity.

bonds between H-atom of a methoxy groups and O-atom of the adjacent calix[6]arene methoxy groups (Fig. 49b) combine the calix[6]arene molecules in infinite chains along the *b* crystallographic axis. Between the chains only van der Waals interactions occur.

Two crystal structures of the hexaethoxy *para-tert*-butylcalix[6]arene tBuC[6]OC$_2$, solvent-free[120] (Fig. 50) and benzophenone clathrate[121] (Fig. 51), are deposited in the CSD as private communication by Zhang and Coppens. In both structures the calix[6]arene conformations are the same (inverted double partial cone) and are stabilised by C–H⋯O hydrogen contacts between the alternated phenoxy moieties and C–H⋯O hydrogen contacts and C–H⋯π interactions between H-atoms of alkyl substituents closing the cavities and proximal phenoxy moieties (Fig. 50a and Fig. 51a). The difference occurs in the calix[6]arene self-assembly. Solvent free calix[6]arene forms C–H⋯O hydrogen bonds between terminal H-atoms of the ethyl substituents and oxygen atoms of the ethoxy groups, which are directed towards the macrocyclic cavities (Fig. 50b). As a result, the calix[6]arene molecules are stacked along the *c* crystallographic axis (Fig. 50c).
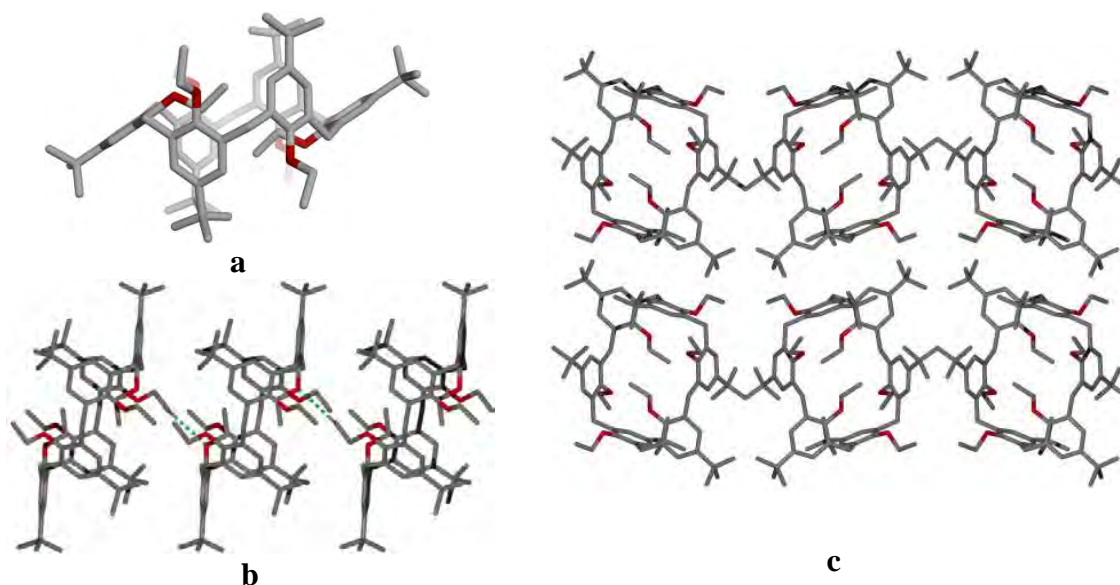
Fig. 50. Crystal structure of tBuC[6]OC$_2$: (a) molecule in inverted double partial cone conformation; (b) chain formation; (c) packing diagram, view along the *c* crystallographic axis. Hydrogen atoms are omitted for clarity.

In the crystal structure of benzophenone clathrate two tBuC[6]OC$_2$ molecules in the asymmetric unit exist. Terminal H-atom of the ethyl chain of one calixarene host molecule forms C–H⋯O hydrogen bond with oxygen atom of the guest molecule. Each symmetrically independent molecule of the calix[6]arene participates in a wide net of

C–H⋯π interactions with another symmetrically independent one and with benzophenone molecule located in the cavity existing in the crystal lattice (Fig. 51b).
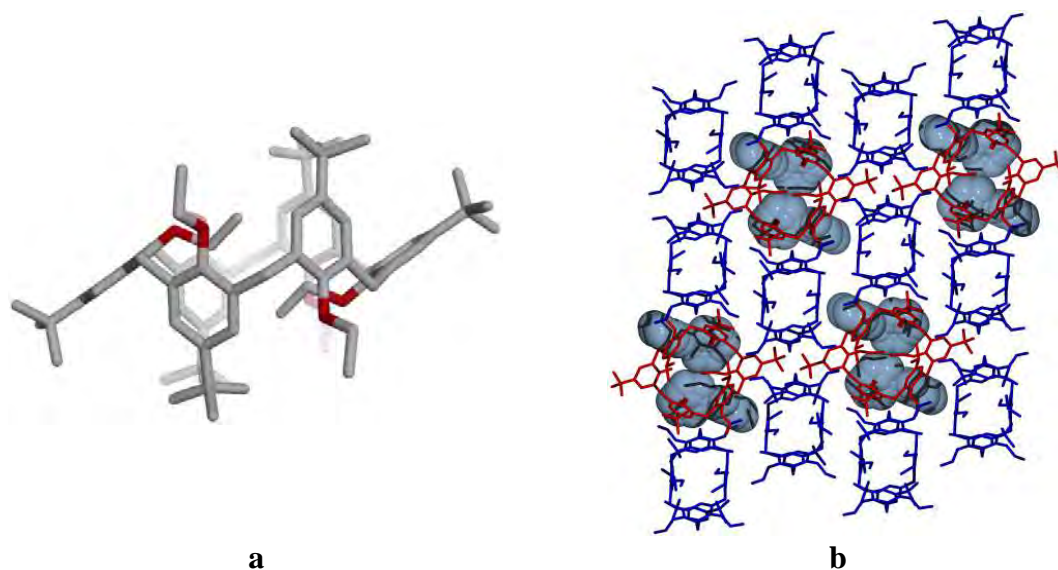
Fig. 51. Crystal structure of tBuC[6]OC$_2$·benzophenone clathrate: (a) molecule in inverted double partial cone conformation; (b) packing diagram, view along the *a* crystallographic axis; two symmetrically independent calix[6]arene molecules are in red and blue. Hydrogen atoms are omitted for clarity.

The discussed above O-alkylated *para-tert*-butylcalix[6]arenes, contrary to HC[6]OC$_{18}$, do not reveal amphiphilic behaviour probably simply due to a small difference in hydrophobicity between different parts of the molecule.

2.6 Application of amphiphilic calixarenes

The amphiphilic materials based on calix[n]arene moieties have attracted much attention due mainly to two reasons. Firstly, the alkoxycalix[n]arenes belong to the class of oligomeric surfactants, which, contrary to classic 'monomeric' surfactants, are characterized by much lower critical micelle concentration (*ca.* 1-2 orders of magnitude), higher kinetic stability, stronger viscosifying effect and stronger foaming power.[5,15] Secondly, both synthesis and selective functionalization of calix[n]arenes are well developed. Thus, the development of chemistry of amphiphilic calixarenes with focus on synthesis and self-assembly in water have recently been summarised in short review by Helttunen and Shahgaldian.[4] The ability of amphiphilic calixarenes to self-assemble at interfaces and proper functionalization allows their application in, e.g. different kinds of sensors:[12] chromogenic,[122] fluorescent,[123] ion- and molecule-selective electrodes[124] *etc.* Calixarenes are also useful materials for construction of nanoparticle shells: they provide the nanoparticle stability, the desired surface functionality and

51

spatial arrangement.[125] Vesicles and solid lipid nanoparticles based on amphiphilic calixarenes can be used as carriers for active pharmaceutical ingredients.[126–128] Thin films of amphiphilic calixarenes can reveal nonlinear optical properties[113] or pyroelectric effect.[129] O-Alkylated calixarenes are also known of their complexation ability to proteins[130,131] and DNA.[132,133]

The field of amphiphilic calixarene usage is mainly covered with amphiphilic compounds in general, and it is too wide to be present in full in this thesis.

2.7 Summary

All O-alkylated calixarenes which are presented in the literature review are compiled in Table 4 according to the alkyl chain(s) length. The table demonstrates that mostly crystal structures of calix[4]arenes with short alkyl substituents (≥ 5) are known. The long alkyl substituent O-alkylated calix[4]arenes are: $HC[4]diOC_8$,[90] two polymorphs of $HC[4]OC_{12}$,[96,97] $HC[4]OC_{14}$,[97] $HC[4]OC_{16}$[97] and two solvated of $HC[4]OC_{18}$.[98] Only one crystal structure of calix[6]arene with long alkyl substituents is known ($HC[6]OC_{18}$).[118]

It seems to be extremely difficult or even impossible to obtain crystals of amphiphilic compound by slow cooling of the solution. More elaborated techniques, like solvent evaporation, solvent/non-solvent diffusion, vapour diffusion and variations of these methods must be used.

Mono- and di-O-methylated calix[4]arenes $HC[4]mOC_1$ and $HC[4]diOC_1$[80] self-assembly in infinite chains based on the inclusion of methoxy group of one molecule into the cavity of the neighbouring calixarene molecule. Dialkoxycalix[4]arenes with longer alkyl substituents ($HC[4]diOC_2$, $HC[4]diOC_3$, $HC[4]diOC_8$) form head-to-head dimers due to weak π-π-stacking interaction, which can be assumed as weak appearance of amphiphilicity. Nevertheless, neither $HC[4]mOC_1$ and $HC[4]diOC_1$ nor $HC[4]diOC_2$, $HC[4]diOC_3$ and even $HC[4]diOC_8$ form classical amphiphilic arrangements. Probably, one or two alkyl substituents are not hydrophobic enough for this purpose.

Tetra-O-alkylated calix[4]arenes look to be more amphiphilic: $HC[4]OC_3$ and $HC[4]OC_4$ form van der Waals head-to-head dimers, while $HC[4]OC_n$, with n = 12, 14, 16 and 18, self-assemble in classical bilayers. It remains unknown where the border between the two types of self-assembling should be located.

In the case of $tBuC[4]OC_n$ (n = 1–5) there is no calix[4]arene amphiphilic behaviour.

Table 4. Crystal structures of non-substituted at *para*-positions, *para-tert*-butyl and *para*-nitro O-alkylated calix[4]arenes and calix[6]arenes.

n	HC[4]OCn				tBuC[4]OCn				NO$_2$C[4]OCn	XC[6]OCn
	mono	di	tri	tetra	mono	di	tri	tetra		
1	HC[4]mOC$_1$ cone ·CHCl$_3$[78,79]	HC[4]diOC$_1$ cone[80]				tBuC[4]diOC$_1$ cone[80] ·3toluene[100]	tBuC[4]triOC$_1$ cone[80]	tBuC[4]OC$_1$ paco[80] ·0.5CH$_2$Cl$_2$[107] ·THF[106]	NO$_2$C[4]OC$_1$ paco ·DMF[134]	tBuC[6]OC$_1$[119]
2		HC[4]diOC$_2$ cone ·CHCl$_3$[81]				tBuC[4]diOC$_2$ cone ·ethanol[101] ·acetone – 2 polym.[102]		tBuC[4]OC$_2$ 1,2-alt ·CH$_2$Cl$_2$[58]	NO$_2$C[4]OC$_2$ paco ·2CHCl$_3$[112] NO$_2$C[4]OC$_2$ cone ·CHCl$_3$[112]	tBuC[6]OC$_2$[120] ·Ph$_2$CO[121]
3		HC[4]diOC$_3$ cone[82,83]	HC[4]triOC$_3$ paco ·CH$_3$CN[91]	HC[4]OC$_3$ 1,3-alt[92] HC[4]OC$_3$ paco[93] HC[4]OC$_3$ cone[94]		tBuC[4]diOC$_2$ cone ·CH$_3$CN[103] ·ClCH$_2$CN[104] ·maleonitrile·2dioxan[104] ·DMF[106] ·DMF·0.5CH$_3$OH[106]	tBuC[4]OC$_3$ cone ·CH$_3$CN[108] tBuC[4]OC$_3$ paco ·0.5THF[105] tBuC[4]OC$_3$ 1,2-alt[109] tBuC[4]OC$_3$ 1,3-alt[92]		NO$_2$C[4]OC$_3$ cone[115] ·unknown solv.[113] ·0.5CH$_2$Cl$_2$[114] ·0.5THF[115] NO$_2$C[4]OC$_3$ paco[113] NO$_2$C[4]OC$_3$ 1,3-alt ·CH$_3$OH[113] NO$_2$C[4]OC$_3$ 1,2-alt[113]	
4				HC[4]OC$_4$ cone[95]				tBuC[4]OC$_4$ cone ·4CHCl$_3$·2H$_2$O[110]	NO$_2$C[4]OC$_4$ cone ·2acetone[116]	
5								tBuC[4]OC$_5$ cone[111]	NO$_2$C[4]OC$_5$ cone[117]	
6										
7										
8		HC[4]diOC$_8$ cone[90]								
9										
10										
11										
12				HC[4]OC$_{12}$ cone 2 polymorphs[96,97]						
13										
14				HC[4]OC$_{14}$ cone[97]						
15										
16				HC[4]OC$_{16}$ cone[97]						
17										
18				HC[4]OC$_{18}$ cone ·toluene[98] ·2benzene[98]						HC[6]OC$_{18}$[118]

* Conformation abbreviation: PACO – partial cone, 1,2-ALT – 1,2-alternate, 1,3-ALT – 1,3-alternate

Tetra-O-propylated *para*-nitrocalix[4]arenes $NO_2C[4]OC_n$ ($n = 1$–5) also reveal no amphiphilic behaviour.

Only one O-alkylated non-substituted at *para*-positions calix[6]arene, $HC[6]OC_{18}$, was reported in the literature. $HC[6]OC_{18}$ molecules, like their calix[4]arene analogues, self-assemble in layered structure due to presence of long alkyl substituents. Alkyl chains of known *para-tert*-butyl O-alkylated calix[6]arene are too short to cause amphiphilicity of the molecules.

Conformations of all known so far calixarenes are stabilised by intramolecular O–H⋯O bonding (partially O-alkylated calix[4]arenes), C–H⋯O contacts (fully O-alkylated calix[4]arenes), and C–H⋯π interactions (calix[6]arenes). Crystal structures of O-alkylated calixarenes are dominated by van der Waals interactions and additionally stabilised by intermolecular C–H⋯O, C–H⋯π and π-π interactions.

The self-assembly of alkoxycalix[*n*]arenes, especially these with $n > 4$, in the solid-state is rather unexplored. On the other hand, it is expected to play important role in rational design of novel surfactants, therefore undertaking studies in this area is very important for understanding the self-assembly process and further application of amphiphilic calixarenes.

3 EXPERIMENTAL

In this chapter the procedures for data collecting and processing, structure solution and refinement, and crystal structure analyses are described.

All compounds described in this thesis were synthesised in the group of Dr. Anthony W. Coleman from the Institute of Biology and Chemistry of Proteins in Lyon. Single crystals suitable for X-ray diffraction studies were obtained by slow diffusion of solvents or slow evaporation from mixed chloroform-methanol systems.

There are several stages in which one may influence the final quality of structural model. One of them is selecting a good quality crystal of pure composition of appropriate size and regular shape, and with no large internal imperfections, such as cracks or twinning. The ideal size of the crystal should be approx. 0.2–0.3 mm for organic compounds. Unfortunately, the calixarenes with long alkyl substituents usually form crystals of thin plate or needle habits and such crystals have to be cut to achieve appropriate size and as regular shape, as possible.

Single crystals suitable for X-ray crystallographic analysis were selected after examination under an optical microscope. Crystals were scooped up in a tiny loop with a small quantity of oil, because the amount of the oil in the X-ray beam influences background considerably. The loop was made of nylon and attached to a solid bronze rod. Crystals of $NO_2C[4]OC_8$ were sealed with a drop of mother liquor in thin-walled Lindemann glass capillary.

The last stage in the selection was crystal prescanning on the diffractometer, *i.e.* collecting a few quick exposure times and checking the images visually on spot size, shape and distribution. Almost all measurements were performed at low temperature (100 K) in order to prevent crystal decomposition, reduce thermal vibrations, enhance signal-to-noise ratio and reduce dynamic disorder. Crystals of the calixarenes with long alkyl chains should be frozen slowly, because flash freezing, in most cases, was strongly increasing the mosaicity or even caused cracking of the crystal into small pieces. For crystals of such compounds as $HC[4]OC_{11}$ (220 K), $tBuC[4]OC_{12} \cdot CHCl_3$ (200 K), $tBuC[4]OC_{14} \cdot CHCl_3$ (250 K) and $NO_2C[4]OC_{14} \cdot 2CHCl_3$ (140 K), even slow freezing (0.5 K·min^{-1}) to temperature 10K lower than the temperature of measurement (shown in brackets) resulted in increasing of mosaicity by 7–9 times.

When a crystal is mounted and exposed to an intense beam of X-rays, it scatters the X-rays into a pattern of reflections. The relative intensities and distribution of reflections provide the information about the electron density distribution in the unit cell, the basic building block of the crystal. It is further possible to determine type and spatial distribution of atoms in the unit cell (chemical composition), as well as absolute configuration and symmetry of both molecule and crystal. Crystal structure analysis can be complicated when substantial, positional, static and dynamic disorders, pseudosymmetry, twinning and superstructures occurs.

Single-crystal X-ray diffraction data for all compounds described along this thesis (except tBuC[4]OC$_9$), were collected on a Nonius KappaCCD diffractometer (Fig. 52), which was later upgraded to an KappaAPEXII, using Mo$K\alpha$ radiation (λ = 0.71073 Å). The first stage of the measurement was determination of the unit cell on the basis of ten frames collected during rotation by ten degrees (scan angle 1° per frame). Having the unit cell parameters and point group symmetry the strategy for data collection was calculated, *i.e.* the number of frames grouped in sets together with the time needed per degree of rotation to get a dataset with reflections up to a specific
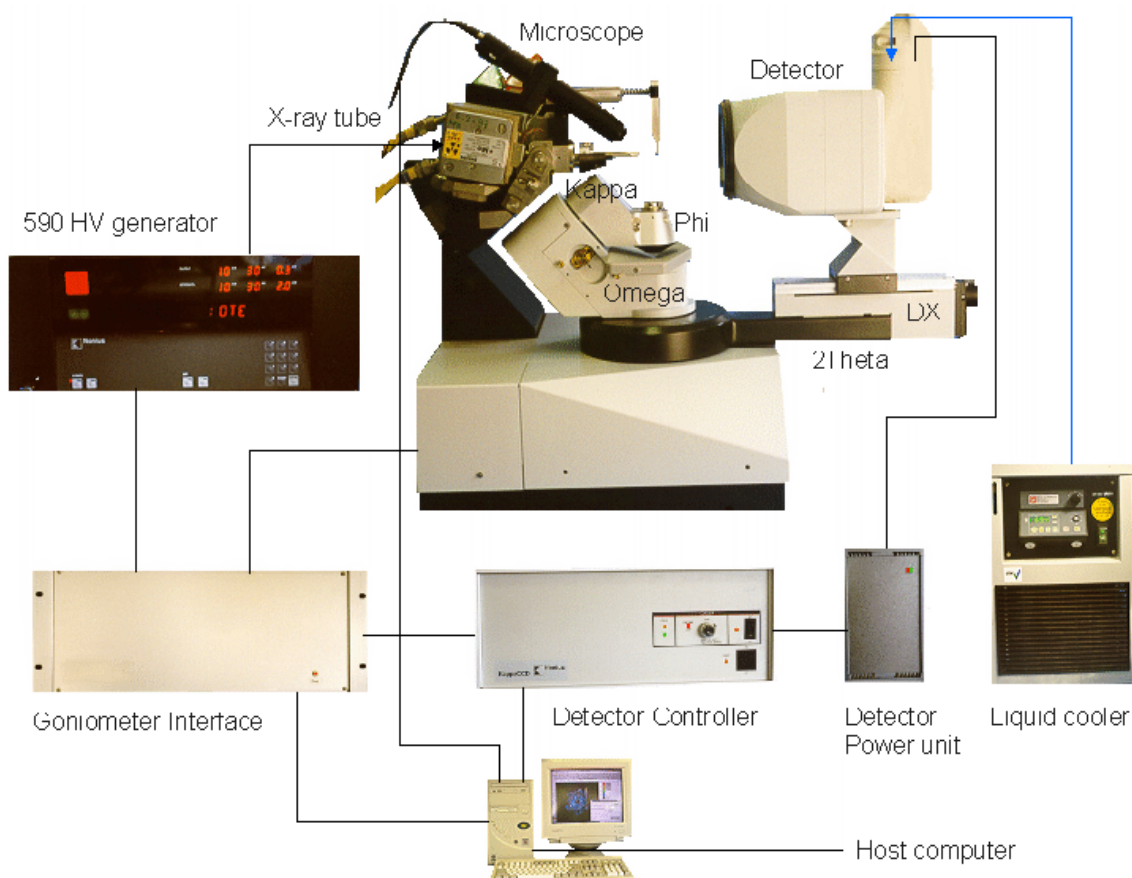
Fig. 52. Functional scheme of Nonius Kappa diffractometer.

diffraction angle. The raw data collected during the diffraction experiment were integrated and scaled in order to obtain the indexed reflections with a consistent intensity scale.

Data collection and data processing were carried out using programs COLLECT,[135] HKL2000[136] and program package maXus.[137]

Data for crystal structure of tBuC[4]OC$_9$ were collected on an Agilent SuperNova Dual Source diffractometer equipped with an Atlas detector using Cu$K\alpha$ radiation (λ = 1.54184 Å). Data collection and data processing were carried out using program CrysAlisPro.[138] Procedures of crystal quality checking, unit cell finding, data collection and processing are, in general, the same as in the case of the Nonius diffractometer.

Structures were solved by direct methods using the program SHELXS-97[139] and refined by full matrix least squares using the program SHELXL-97.[139] Unless specified, all non-hydrogen atoms were refined anisotropically. Hydrogen atoms were placed in geometrically calculated positions and refined as riding atoms. Hydrogen atoms of methyl and hydroxyl groups were refined in geometric positions for which the calculated sum of the electron density is the highest (rotating group refinement). Torsion angles were then refined during the least-squares refinement. All hydrogen atoms were refined isotropically with temperature factors 1.2 times of U_{eq} of their parent atoms (1.5 times for methyl and hydroxyl groups).

In the case of low quality diffraction data and disorder, DFIX and DANG geometrical restraints were applied in order to retain the reasonable molecular geometry. Distortion in molecular geometry can be an effect of atomic motion or/and static disorder but usual diffraction experiment performed in one temperature does not distinguish between the two of them. Only considerable changes of populations of disordered sites and apparent atomic positions with temperature can suggest dynamic disorder. If both, temperature-independent disorder and vibrations are observed, it is also possible to separate their contribution to atomic distortion parameters,[140] except the case when atomic sites are related by symmetry and close to each other.

In most of the considered structures the alkyl substituents and the solvent molecules are disordered even at the temperature of 100K. Because of the lack of strong interactions, the disorder is probably caused by thermal motions of groups or molecules in larger available space for occupation (dynamic disorder) or the possibility to occupy the available space in more than one manner (static disorder).

The most often observed is the disorder of *n*-alkyl substituents. The methyl and ethyl groups are always ordered in considered O-alkylated calixarenes. In the case of the medium length of *n*-alkyl substituents (3–7 carbon atoms), at least one of the chains is disordered and in tBuC[4]OC$_7$ (partial cone) crystal structure all four heptyl chains are strongly disordered. Whereas the whole arsenal of restraints was applied in crystal structure of NO$_2$C[4]OC$_8$·CHCl$_3$ (AFIX 66 command to idealize geometry of benzene rings; DFIX and DANG commands to restrain geometry of alkyl chains; SIMU and DELU commands to restrain thermal parameters of atoms of alkyl chains), the octyl substituents in crystal structures of tBuC[4]OC$_8$ (partial cone) and tBuC[4]OC$_8$ (1,3-alternate) are ordered. Pseudo-hexagonal close packing of long alkyl substituents (9 and more carbon atoms) does not protect them against the disorder: at least one chain is disordered even at 100K (except perfectly ordered structures of NO$_2$C[4]OC$_{14}$·CHCl$_3$ and NO$_2$C[4]OC$_{14}$·CHCl$_3$). In one case it was decided not to divide the undecyl substituent at the phenoxy moiety C in crystal structure of HC[4]OC$_{11}$ because of medium libration of carbon atoms.

Disorder of *para-tert*-butyl groups is observed in half of the structures. It is usually treated as rotation around C$_{benz}$–C$_{tBu}$ bond, except of the two structures, tBuC[4]OC$_1$·0.125CHCl$_3$ (partial cone) and tBuC[4]OC$_4$ (partial cone), where out-of-plane vibrations were additionally modelled. For extremely distorted *tert*-butyl groups C–C bond lengths and thermal parameters were restrained using DFIX, DANG and DELU commands in SHELXL-97 program.

In discussed crystal structures three types of disorder of chloroform molecules are observed. The first is positional disorder of loosely bound guest molecule, which occupies two or more positions in void between the host molecules (crystal structures of tBuC[4]OC$_1$·0.125CHCl$_3$ (partial cone), tBuC[4]OC$_4$·0.5CHCl$_3$ (partial cone), tBuC[6]OC$_4$·CHCl$_3$ and tBuC[6]OC$_6$·2CHCl$_3$). The second is positional disorder of strongly bound guest molecule, when CHCl$_3$ molecule forms strong C–H···O hydrogen bond in each of the two positions (crystal structure of NO$_2$C[4]OC$_8$·CHCl$_3$). The third is rotational disorder, when the guest molecule participates in strong C–H···O hydrogen bond (crystal structure of NO$_2$C[4]OC$_1$·CHCl$_3$) or C–H···π interactions (crystal structures of tBuC[4]OC$_{10}$·CHCl$_3$, tBuC[4]OC$_{12}$·CHCl$_3$ and tBuC[4]OC$_{14}$·CHCl$_3$) with the host molecule and rotate around the C···O or C···Cg(π) line.

In the case of chiral crystal structures of tBuC[4]OC$_3$ (cone) and tBuC[4]OC$_4$ (space group $P3_12$) absolute structures were not defined due to senseless Flack parameters (weak anomalous dispersion of Mo$K\alpha$ radiation on the C, H, and O atoms).

Sometimes to distinguish between centrosymmetric and non-centrosymmetric space group was not a straightforward task, like for tBuC[4]OC$_8$ (1,3-alternate) crystal structure. <E^2-1> criterion[141] of 0.909 suggested the structure to be centrosymmetric (0.968 for centrosymmetric, 0.736 for non-centrosymmetric). Taking into account systematic absences of reflections with even l in groups $h0l$ and $00l$ (which suggest symmetry operation c and 2_1) the structure was firstly solved in centrosymmetric space group $P2/c$ (No.13). The n-alkyl chains were disordered and the residual factor for significantly intense reflections (R for $F_o > 4\sigma(F_o)$) was 0.194. The solution in non-centrosymmetric Pc space group (No.7) resulted with two ordered molecules in the asymmetric unit and the R-factor decreased to 0.073.

All the above mentioned problems faced during structure solution were carefully checked and examined. It has to be mentioned here that in all these cases the structure solution was time-consuming and needed a lot of efforts on the way to obtain the final structural model. For some structures the time needed for refinement was counted in weeks and even months.

All crystallographic calculations were carried out with the WINGX[142] program package. All the figures were prepared using the DIAMOND[143] and USCF Chimera.[144] Hydrogen atoms, not taking part in hydrogen bonding or C–H⋯π interactions and disordered atoms with lower occupancy, usually were omitted from the drawings for clarity. A consistent numbering scheme was used for the calixarene molecules for all structures (Fig. 53). Numbering of alkyl substituent at phenyl oxygen atom starts from C8. If more than one calixarene molecule is present in the asymmetric part of the unit cell, subsequent letters (E,F,G...) are used to label the rings in the next molecules.
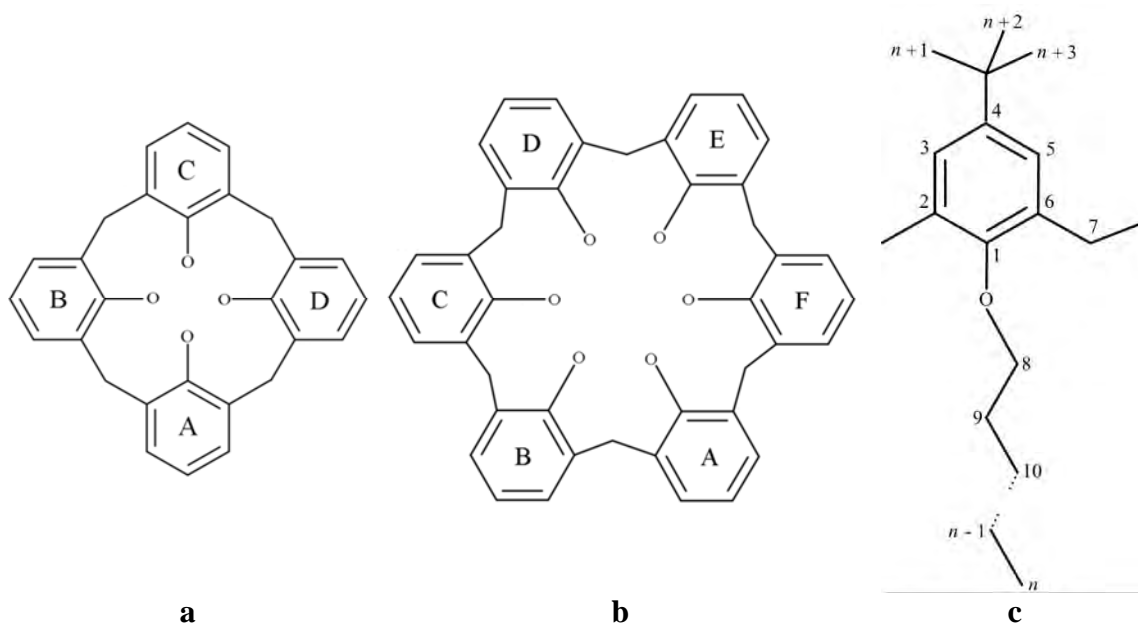
Fig. 53. Ring labelling scheme: (a) calix[4]arene; (b) calix[6]arene; (c) general atom numbering scheme for C atoms.

The two parameters used to describe calix[4]arene macrocyclic ring conformation: dihedral angle between plane of benzene ring and the mean plane of the four methylene groups and distance between distal C4 atoms are shown in Fig. 54.

MOLINSPIRATION INTERACTIVE PROPERTY CALCULATOR[145] was used for volume calculations of the calixarene molecules and their parts. Volume calculations were based on functional group contributions into the volume of a whole molecule and in this way do not depend on calixarene and alkyl chain conformations (*i.e.* calix[4]arene in the cone conformation and straight *n*-alkyl chains).
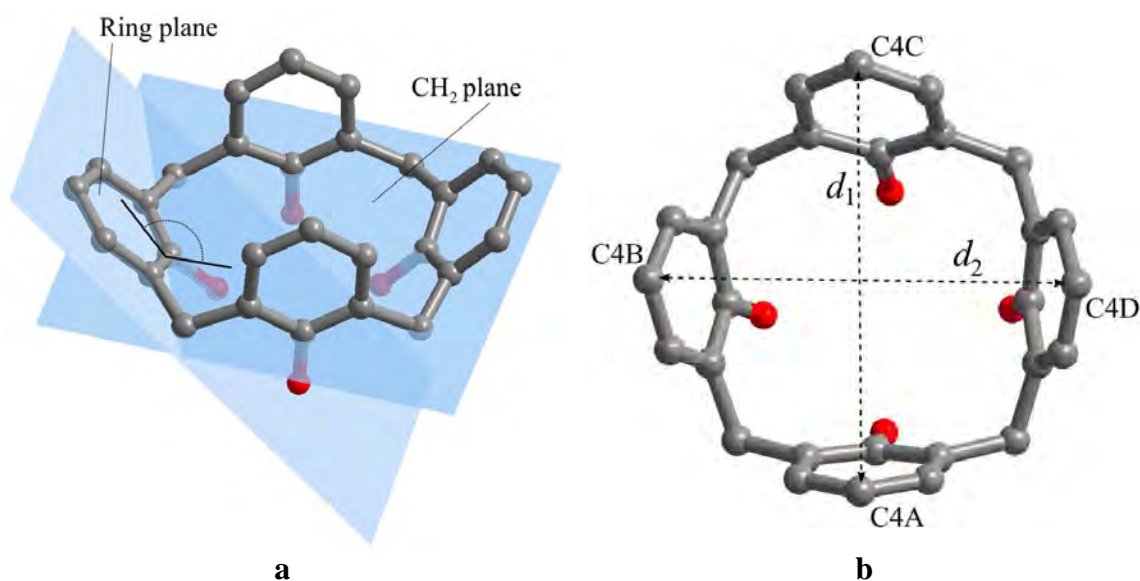
Fig. 54. (a) Dihedral angle between plane of benzene ring and the mean plane of the four methylene groups; (b) distances between distal C4 atoms, $d_1 < d_2$.

4 RESULTS

4.1 Crystal structures of non-substituted at the upper rim O-alkylated calix[4]arene

4.1.1 Crystal structure of O-heptylated calix[4]arene (cone)

Crystals of the non-substituted at the upper rim O-heptylated calix[4]arene (HC[4]OC$_7$) crystallise from a methanol/chloroform mixture in the monoclinic crystallographic system (Table 5). They display extremely poor diffraction, which

Table 5. Crystal data and structure refinement for HC[4]OC$_7$ (cone)

Molecular formula	C$_{56}$H$_{80}$O$_4$
Formula weight	817.20
Crystal system	Orthorhombic
Space group	*Pbca*
Unit cell dimensions	a = 19.2160(9) Å
	b = 19.076(1) Å
	c = 55.167(3) Å
Volume	20222(2) Å^3
Z	16
Temperature	100.0(5) K
Radiation and wavelength	Mo $K\alpha$ radiation, λ = 0.71073 Å
Monochromator	graphite
Density (calculated)	1.074 Mg·m^{-3}
Absorption coefficient	0.07 mm^{-1}
F(000)	7168
Crystal size	0.05 × 0.08 × 0.11 mm
θ range for data collection	2.6–18.9°
Index ranges	-16 ≤ h ≤ 17, -17 ≤ k ≤ 17, -50 ≤ l ≤ 50
Reflections collected	103307
Independent reflections	7945 [R_{int} = 0.382]
Completeness	93.3 %
Absorption correction	None
Refinement method	Full-matrix least-squares on F^2
Weighting scheme	$[\sigma^2(F_o^2) + 147.4872P]^{-1}$ *
Data / restraints / parameters	7945 / 426 / 1019
Goodness-of-fit on F^2	1.16
Final R indices [$I > 2\sigma(I)$]	R = 0.142, wR = 0.201
R indices (all data)	R = 0.243, wR = 0.229
Extinction coefficient	Not refined
Largest diff. peak and hole	0.32 and -0.34 e·Å^{-3}

* $P = (F_o^2 + 2F_c^2)/3$

reflects in high *R* parameters. The asymmetric unit comprises two independent molecules of calixarenes that differ from one another by spatial orientation of the alkyl chains (Fig. 55a and b). Carbon atom numbering scheme is shown in Fig. 55c. Two last atoms of heptyl substituent at the ring G are disordered over three positions with occupancy factors of 0.70, 0.15 and 0.15.
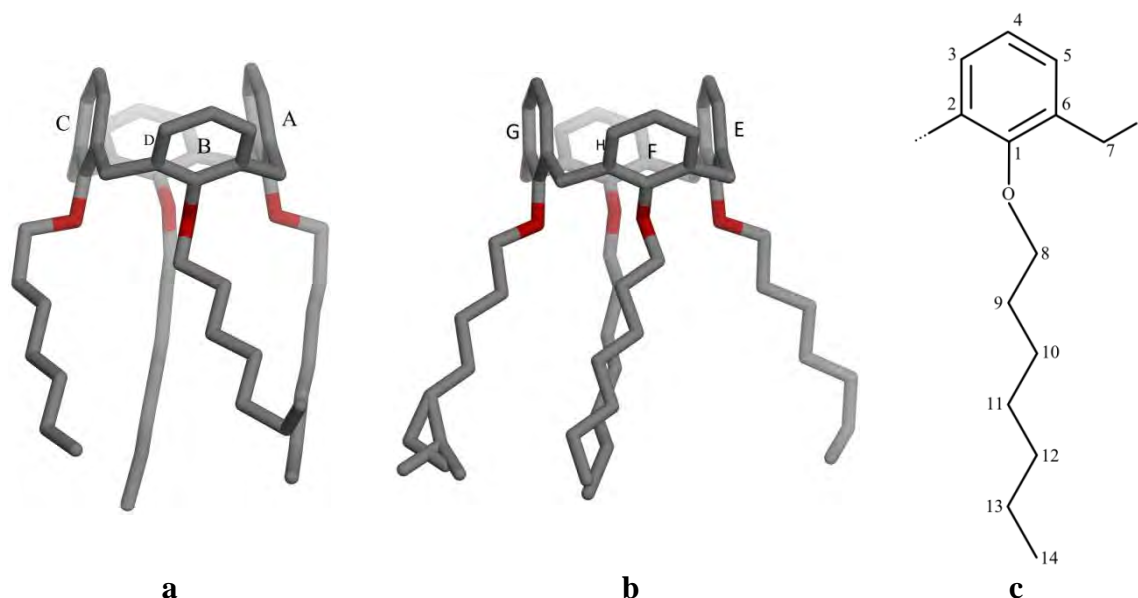
Fig. 55. HC[4]OC$_7$: (a) molecule 1; (b) molecule 2; (c) numbering scheme.

Analysis of dihedral angles between planes of each benzene ring and the mean plane of the four methylene groups and distances between distal C4 atoms (Table 6) reveals that molecule 1 is flattened slightly more than molecule 2.

Table 6. Calix[4]arene macrocyclic ring geometry for HC[4]OC$_7$

	∠(ring-to-CH$_2$-plane),°			Distal C4···C4 distances, Å	
A	81.4(3)	E	86.3(3)	C4A···C4C	4.33(1)
B	137.0(2)	F	133.2(3)	C4B···C4D	9.78(1)
C	80.3(3)	G	88.9(3)	C4E···C4G	5.17(1)
D	140.2(3)	H	136.7(3)	C4F···C4H	9.46(1)

The pinched cone conformation of each calix[4]arene macrocyclic rings is stabilised by one normal and one bifurcated intramolecular C–H···O contacts (Table 7) of H-atoms the second methylene groups of chain D and oxygen atoms of phenoxy moieties A, B and C (molecule 1), and the second methylene group of chain H with oxygen atoms of phenoxy moieties E, F and G (molecule 2) (Fig. 56).

In the case of molecule 2, there is one additional intramolecular C–H···O interaction between phenolic O1E oxygen atom and H-atom of the first methylene group of the alkyl chain C8F···O1E 3.48(1) Å.

62

Table 7. Weak interactions in HC[4]OC$_7$ (cone)

Hydrogen bonds

D–H$\cdots$A	d(D–H), Å	d(H$\cdots$A), Å	d(D$\cdots$A), Å	∠D–H$\cdots$A
C8F–H8F2$\cdots$O1E	0.99	2.98	3.48(1)	112
C9D–H9D2$\cdots$O1A	0.99	2.89	3.61(2)	120
C9D–H9D2$\cdots$O1B	0.99	2.88	3.45(1)	131
C9D–H9D1$\cdots$O1C	0.99	2.55	3.49(1)	160
C9H–H9H2$\cdots$O1E	0.99	2.77	3.59(1)	140
C9H–H9H1$\cdots$O1F	0.99	2.98	3.62(1)	123
C9H–H9H1$\cdots$O1G	0.99	2.56	3.38(1)	140

C–H$\cdots\pi$ interactions

C–H$\cdots$Cg	d(H$\cdots$Cg)	⊥d(H$\cdots\pi$)	d(C$\cdots$Cg)	∠C–H$\cdots$Cg	∠C–H$\cdots\pi$
C3D–H3D$\cdots$CgA[1]	3.27	2.82	4.18(1)	160	156
C5H–H5H$\cdots$CgB	3.59	2.30	4.32(1)	136	141
C7B–H7B2$\cdots$CgD[2]	2.90	2.69	3.83(1)	158	142
C7E–H7E2$\cdots$CgH[3]	3.05	2.75	3.92(1)	147	137

Symmetry codes: (1) 0.5 + x, y, 0.5 – z; (2) 2.5 – x, 0.5 + y, z; (3) 1.5 – x, –0.5 + y, z.

a　　　　　　　　　　**b**
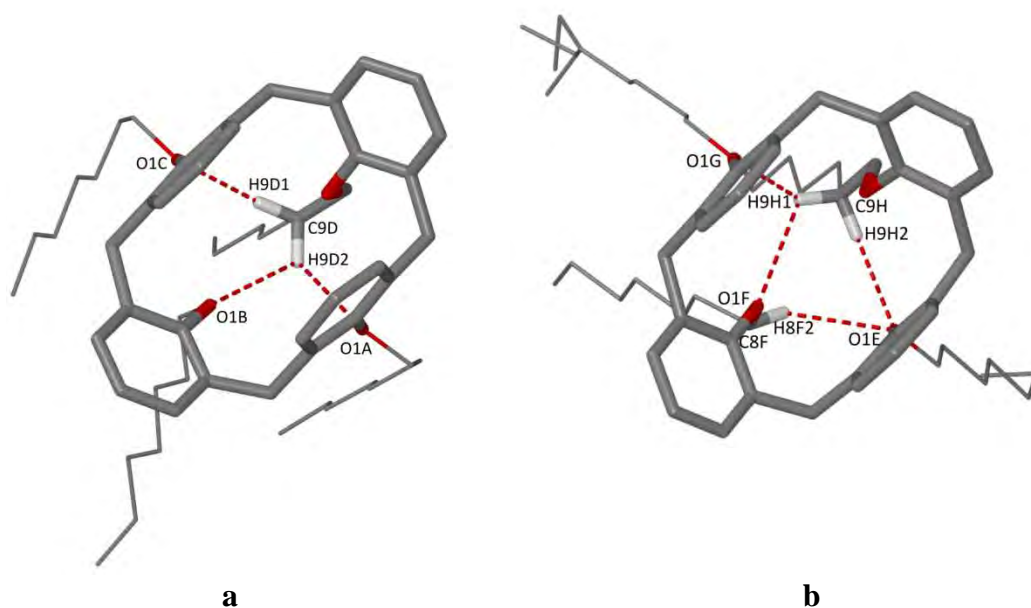
Fig. 56. Conformation stabilised by C–H$\cdots$O intramolecular contacts: (a) molecule 1; (b) molecule 2.

In crystal structure of HC[4]OC$_7$, similarly to tetraalkoxycalix[4]arenes with shorter alkyl substituents, HC[4]OC$_3$ and HC[4]OC$_4$,[94,95] head-to-head dimer formation due to van der Waals interaction between the upper rims of two opposite calixarene cones which are twisted ~90° one to another is observed (Fig. 57a).

The dimers (and the calix[4]arene molecules) of the same spatial orientation form chains down the *b* crystallographic axis *via* C–H$\cdots\pi$ interactions of methylene bridges of calix[4]arene macrocyclic rings and aromatic rings of adjacent calixarenes [C7B$\cdots$ring D and C7E$\cdots$ring H, Table 7] (Fig. 57b).

63
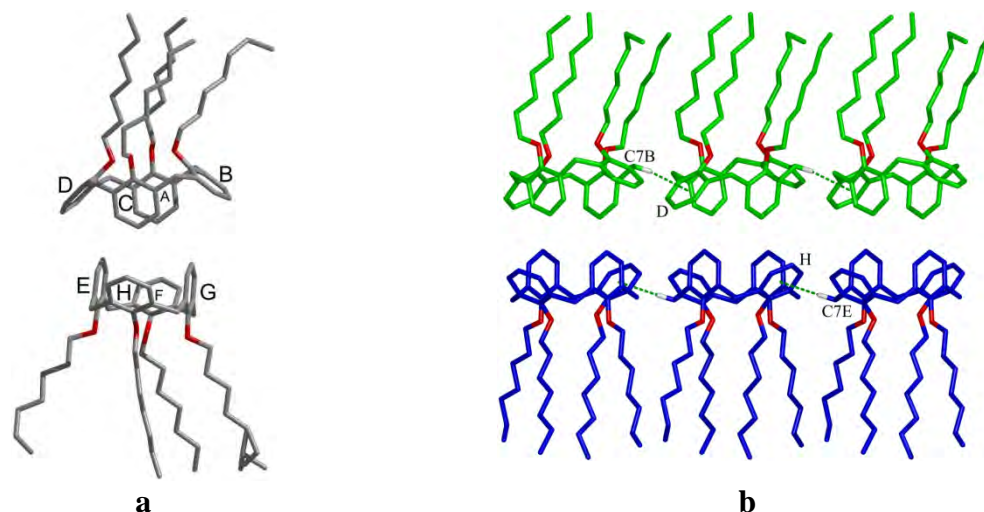
Fig. 57. (a) Van der Waals dimer of HC[4]OC$_7$; (b) intermolecular C–H⋯π interactions between the dimers of the same spatial orientation.

The self-organisation of the dimers in the opposite spatial orientation is additionally stabilised by C–H⋯π contacts of aromatic rings of adjacent calixarenes of molecules of the same and the opposite orientation [C3D⋯ring A, C5H⋯ring B, Table 7] (Fig. 58a).
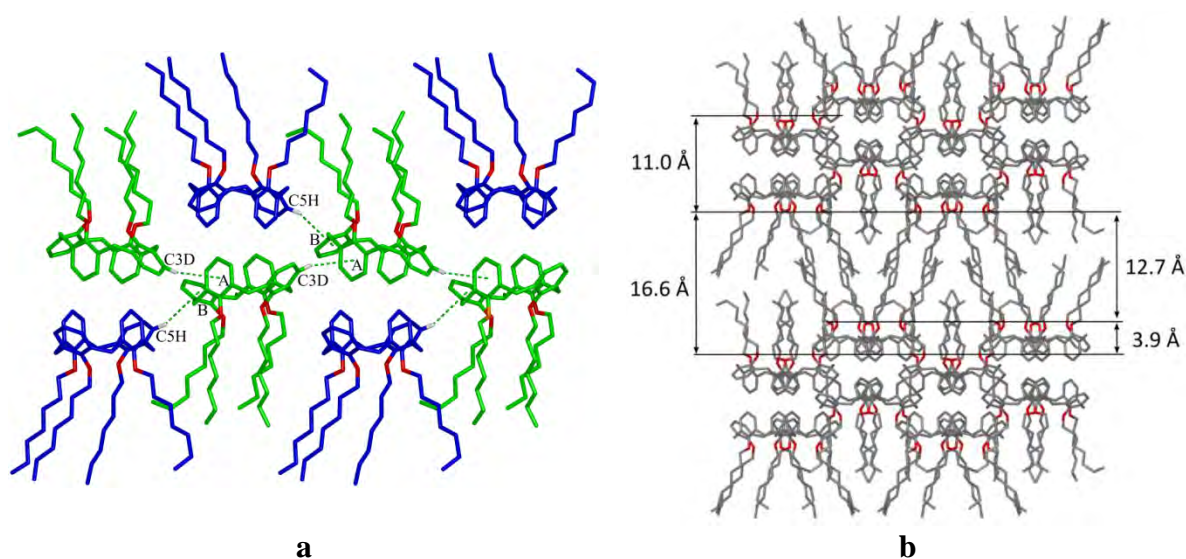
Fig. 58. HC[4]OC$_7$: (a) intermolecular C–H⋯π interactions between dimers in opposite spatial orientation; (b) packing diagram, view along the *b* crystallographic axis.

Thus, the net of C–H⋯π contacts joins the dimers in corrugated bilayers (Fig. 58b). The thickness of aromatic regions is *ca.* 11.0 Å while the thickness of aliphatic layers changes from 12.7 to 16.6 Å. Due to a small interdigitation of the relatively long alkyl substituents of the neighbouring layers, the HC[4]OC$_7$ self-assembling motif is an intermediate link between crystal packing of HC[4]Oalkyl molecules with shorter (3, or 4 carbon atoms)[94,95] and longer (12, 12, 14, 16, and 18 carbon atoms in chain)[96–98] alkyl chains.

4.1.2 Crystal structure of O-undecylated calix[4]arene (cone)

Non-substituted at the upper rim O-undecylated calix[4]arene (HC[4]OC$_{11}$) crystallises from a methanol/chloroform mixture in the triclinic crystallographic system and presents no disorder. Crystal data are presented in Table 8. Data collection was performed at 220 K. Below this temperature a sharp rise in the mosaicity up to 3.7° was observed and below 200 K crystal cracking occurs.

The asymmetric unit comprises only one molecule of HC[4]OC$_{11}$. The calix[4]arene macrocyclic ring assumes the pinched cone conformation (Fig. 59a). Carbon atom numbering scheme is shown in Fig. 59b.

Table 8. Crystal data and structure refinement for HC[4]OC$_{11}$ (cone)

Molecular formula	C$_{72}$H$_{112}$O$_4$
Formula weight	1041.62
Crystal system	Triclinic
Space group	$P\bar{1}$
Unit cell dimensions	$a = 11.9204(2)$ Å $\qquad \alpha = 93.173(1)°$
	$b = 16.8983(3)$ Å $\qquad \beta = 95.871(1)°$
	$c = 17.1660(4)$ Å $\qquad \gamma = 104.488(2)°$
Volume	3318.5(1) Å^3
Z	2
Temperature	220.0(5) K
Radiation and wavelength	Mo $K\alpha$ radiation, $\lambda = 0.71073$ Å
Monochromator	graphite
Density (calculated)	1.042 Mg·m^{-3}
Absorption coefficient	0.06 mm^{-1}
$F(000)$	1152
Crystal size	0.15 × 0.15 × 0.45 mm
θ range for data collection	2.8–22.7°
Index ranges	-12 ≤ h ≤ 12, -18 ≤ k ≤ 18, -18 ≤ l ≤ 18
Reflections collected	35579
Independent reflections	8894 [$R_{int} = 0.046$]
Completeness	99.9 %
Absorption correction	None
Refinement method	Full-matrix least-squares on F^2
Weighting scheme	$[\sigma^2(F_o^2) + (0.0615P)^2 + 1.4101P]^{-1}$ *
Data / restraints / parameters	8894 / 0 / 689
Goodness-of-fit on F^2	1.05
Final R indices [$I > 2\sigma(I)$]	$R = 0.058$, $wR = 0.139$
R indices (all data)	$R = 0.082$, $wR = 0.149$
Extinction coefficient	Not refined
Largest diff. peak and hole	0.18 and -0.20 e·Å^{-3}

* $P = (F_o^2 + 2F_c^2)/3$
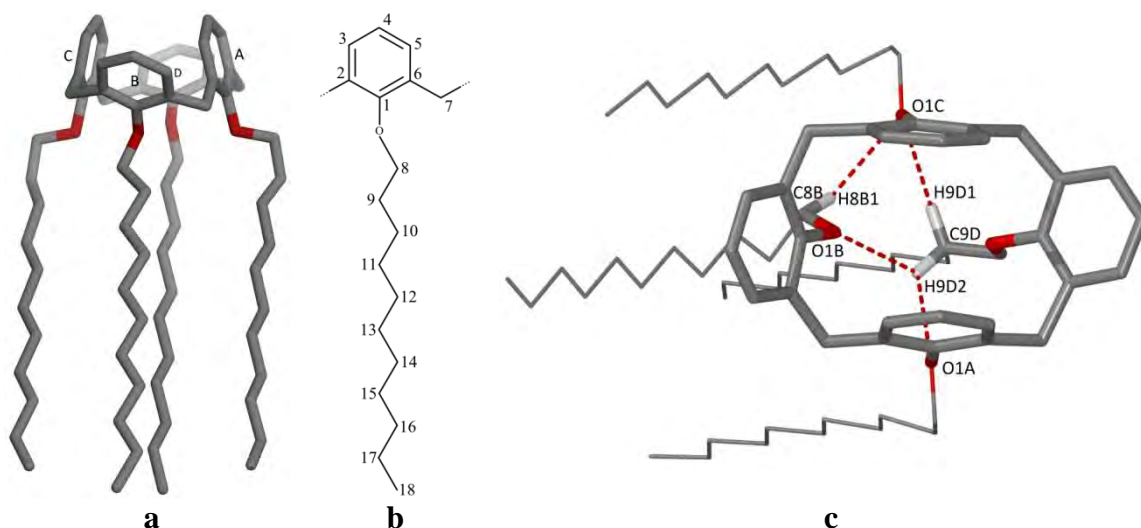
Fig. 59. HC[4]OC$_{11}$ (cone): (a) asymmetric unit; (b) numbering scheme; (c) conformation stabilised by C–H⋯O intramolecular contacts.

Values of dihedral angles between planes of each benzene ring and the mean plane of the four methylene groups and distances between distal C4 are presented in Table 9. Comparison with HC[4]OC$_7$ reveals that HC[4]OC$_{11}$ is more pinched.

Similarly to the molecule 2 of the HC[4]OC$_7$ structure, the conformation of HC[4]OC$_{11}$ is stabilised by two normal [C8B⋯O1C and C9D⋯O1C] and one bifurcated [C9D⋯O1A, C9D⋯O1B] C–H⋯O intramolecular contacts (Table 10) between H-atoms

Table 9. Calix[4]arene macrocyclic ring geometry for HC[4]OC$_{11}$

∠(ring-to-CH$_2$-plane), °		Distal C4⋯C4 distances, Å	
A	77.77(6)	C4A⋯C4C	4.114(4)
B	135.78(7)		
C	79.72(7)	C4B⋯C4D	9.865(4)
D	142.50(4)		

Table 10. Weak interactions in HC[4]OC$_{11}$ (cone)

Hydrogen bonds

D–H⋯A	d(D–H), Å	d(H⋯A), Å	d(D⋯A), Å	∠D–H⋯A
C8B–H8B1⋯O1C	0.98	2.93	3.360(3)	108
C9D–H9D1⋯O1C	0.98	2.97	3.821(3)	146
C9D–H9D2⋯O1A	0.98	2.75	3.471(3)	131
C9D–H9H2⋯O1B	0.98	2.93	3.561(3)	123

C–H⋯π interactions

C–H⋯Cg	d(H⋯Cg)	⊥d(H⋯π)	d(C⋯Cg)	∠C–H⋯Cg	∠C–H⋯π
C7A–H7A2⋯CgA[1]	3.09	2.79	4.022(3)	160	153
C7C–H7C2⋯CgC[2]	3.21	2.82	4.146(3)	160	153
C4D–H4D⋯CgB[3]	2.72	2.68	3.610(3)	159	166

Symmetry codes: (1) –x, –y, 1 – z; (2) 1 – x, 1 – y, 1 – z; (3) 1 + x, y, z.

of methylene groups of alkyl substituents and oxygen atom of phenoxy moieties A, B and C (Fig. 59c).

Two distal methylene bridges A and C participate in two C–H···π interactions with aromatic rings of the neighbouring calix[4]arene molecules at opposite orientation (Fig. 60a). C–H···π interactions of *para*-H-atoms of aromatic rings and phenyl groups of the adjacent calixarene macrocyclic rings in the same orientation (Fig. 60b) and van der Waals interactions between alkyl substituents result in the bilayer pattern of the calix[4]arene self-assembly with the thickness of the aromatic and aliphatic layers *ca.* 5.7 and 11.4 Å, respectively.

| a | b |
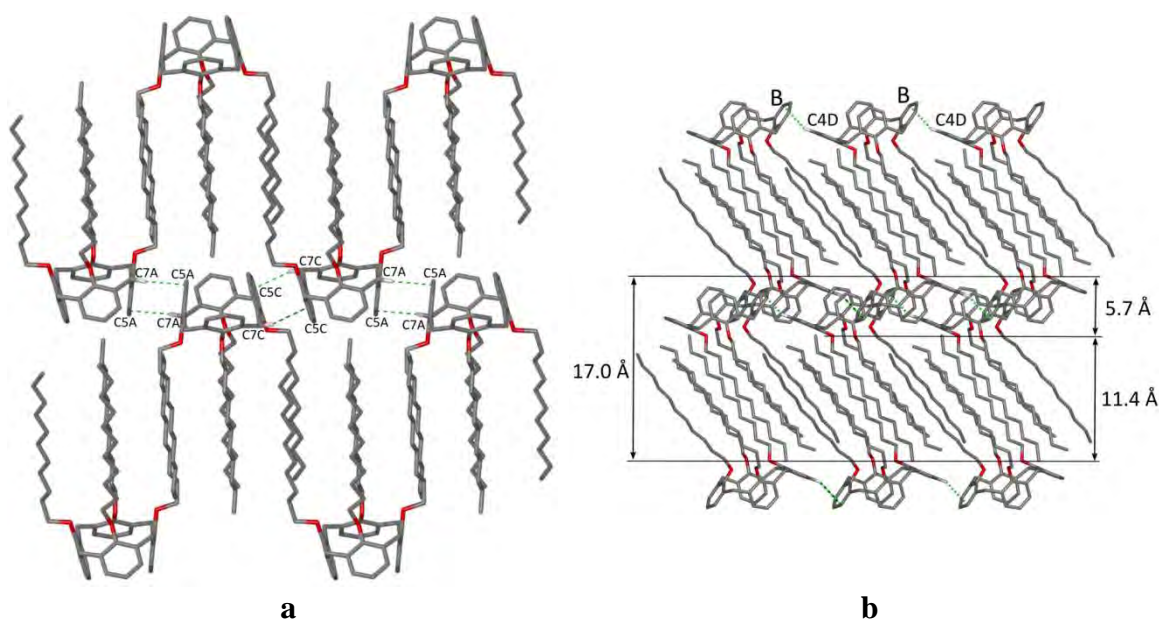
Fig. 60. HC[4]OC$_{11}$ (cone): (a) packing diagram, view along the *a* crystallographic axis; (b) packing diagram, view along the *b* crystallographic axis.

Therefore, the arrangement of HC[4]OC$_{11}$ molecules is similar to the 'real-amphiphiles' found in the crystal structures of HC[4]OC$_{12}$, HC[4]OC$_{16}$ and both HC[4]OC$_{18}$ systems.[96–98]

4.2 Crystal structures of *para-tert*-butyl-O-alkylated calix[4]arenes

4.2.1 Crystal structure of O-methylated *para-tert*-butylcalix[4]arene (partial cone) chloroform sescuncisolvate

O-Methylated *para-tert*-butylcalix[4]arene crystallises from methanol/ chloroform mixture in the monoclinic crystallographic system as a calix[4]arene-chloroform solvate with stoichiometry 8:1 (tBuC[4]OC$_1$·0.125CHCl$_3$). The crystal is isostructural (crystal data are presented in Table 11) with the solvent-free form and the

THF and CH_2Cl_2 solvates.[80,106,107] The asymmetric unit which comprises two molecules of the host and one-fourth of the guest molecule is shown in Fig. 61a. Carbon atom numbering scheme is shown in Fig. 61b.

Two *tert*-butyl groups of one host molecule are disordered each over two positions with occupancy factors of 0.51 and 0.49, and 0.64 and 0.36. In the case of the calixarene molecule **2**, there is only one disordered *tert*-butyl group with occupancy factors of 0.54 and 0.46. Both calix[4]arene molecules adopt a partial cone conformation (Fig. 62).

Table 11. Crystal data and structure refinement for tBuC[4]OC$_1$·0.125CHCl$_3$

Molecular formula	$C_{48}H_{64}O_4 \cdot 0.125CHCl_3$
Formula weight	719.91
Crystal system	Monoclinic
Space group	$P2_1/c$
Unit cell dimensions	$a = 16.7480(2)$ Å
	$b = 19.6593(2)$ Å $\quad \beta = 103.713(1)°$
	$c = 27.9952(4)$ Å
Volume	$8954.8(2)$ Å^3
Z	8
Temperature	$100.0(5)$ K
Radiation and wavelength	Mo $K\alpha$ radiation, $\lambda = 0.71073$ Å
Monochromator	graphite
Density (calculated)	1.068 Mg·m^{-3}
Absorption coefficient	0.09 mm^{-1}
$F(000)$	3130
Crystal size	$0.13 \times 0.25 \times 0.45$ mm
θ range for data collection	2.8–23.6°
Index ranges	$-18 \leq h \leq 18$, $-22 \leq k \leq 22$, $-31 \leq l \leq 31$
Reflections collected	97749
Independent reflections	13276 [$R_{int} = 0.093$]
Completeness	99.9 %
Absorption correction	None
Refinement method	Full-matrix least-squares on F^2
Weighting scheme	$[\sigma^2(F_o^2) + (0.0516P)^2 + 6.9594P]^{-1}$ *
Data / restraints / parameters	13276 / 52 / 1126
Goodness-of-fit on F^2	1.05
Final R indices [$I > 2\sigma(I)$]	$R = 0.057$, $wR = 0.127$
R indices (all data)	$R = 0.095$, $wR = 0.142$
Extinction coefficient	$0.0012(2)$
Largest diff. peak and hole	0.39 and -0.33 e·Å^{-3}

$* P = (F_o^2 + 2F_c^2)/3$
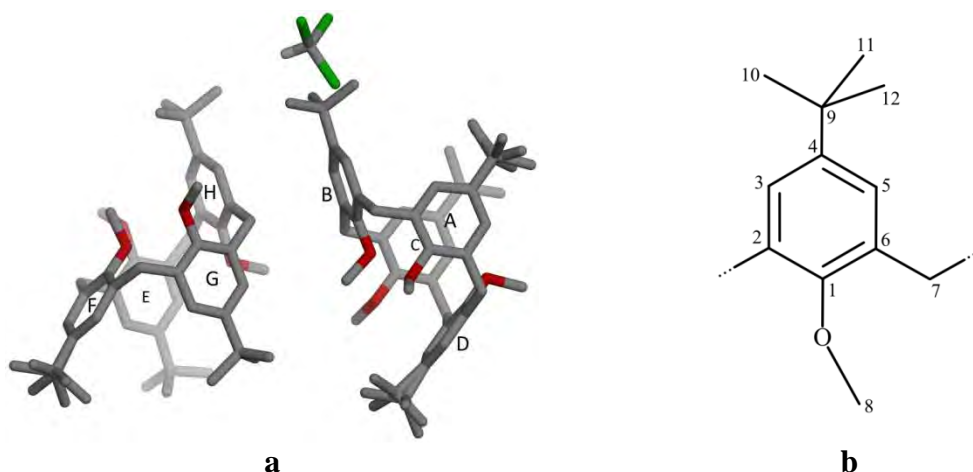
Fig. 61. tBuC[4]OC$_1$·0.125CHCl$_3$ (partial cone) solvate: (a) asymmetric unit; (b) numbering scheme.
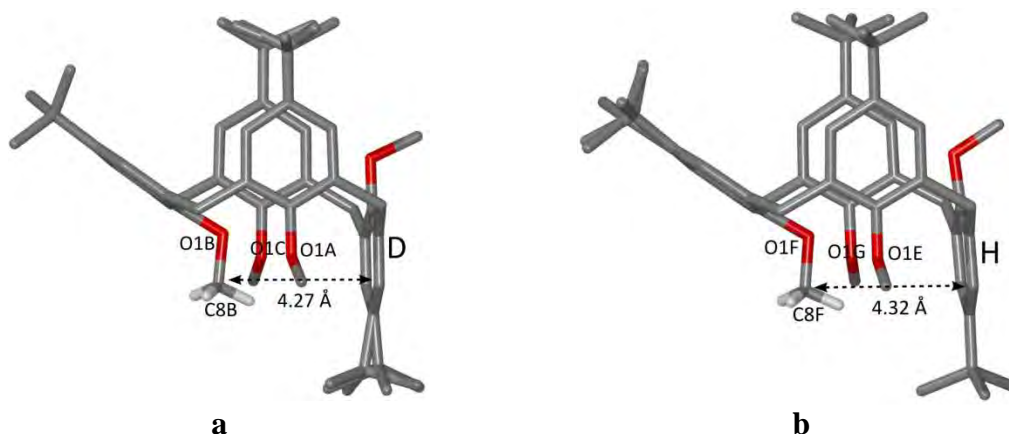
Fig. 62. tBuC[4]OC$_1$·0.125CHCl$_3$ in the partial cone conformation: (a) molecule 1 and (b) molecule 2.

Analysis of dihedral angles between planes of each benzene ring and the mean plane of the four methylene groups and distances between distal C4 atoms reveals that conformations of calix[4]arene macrocyclic ring of molecules **1** and **2** are almost identical (Table 12).

Since the downward pointing benzene rings are far from the distal methoxy groups [4.268(3) and 4.325(3) Å for atoms C8B and C8F and rings D and H, respectively (Fig. 62)], there is no evidence of intramolecular C–H⋯π interactions, except for an orientation of C–H bonds towards benzene ring (which were visible on difference Fourier synthesis maps). On the other hand, C⋯O distances for C8B and C8F proximal oxygen atoms are quite short [3.149(4), 3.113(4), 3.158(3) and 3.153(3) Å for atom pairs C8B⋯O1A, C8B⋯O1C, C8F⋯O1E and C8F⋯O1G, respectively], but the CHO angles are too small [90.1, 95.3, 92.2 and 93.3°] to provide evidence of C–H⋯O hydrogen binding.

8;

Table 12. Calix[4]arene macrocyclic ring geometry for tBuC[4]OC$_1$ (partial cone) ·0.125CHCl$_3$

∠(ring-to-CH$_2$-plane), °			
1		**2**	
A	92.82(7)	E	94.62(6)
B	144.69(9)	F	144.55(8)
C	94.33(6)	G	91.01(6)
D	-90.86(6)	H	-93.40(6)
Distal C4···C4 distances, Å			
1		**2**	
C4A···C4C	5.689(4)	C4E···C4G	5.633(3)
C4B···C4D	8.826(4)	C4F···C4H	8.905(4)

Two kinds of layers can be distinguished in crystal structure of tBuC[4]OC$_1$·0.125CHCl$_3$ (Fig. 63a and b) both extending parallel to the *bc* crystallographic plane: each of them comprises either molecules **1** and CHCl$_3$ or exclusively molecules **2**. Molecules **2** are self-assembled in infinite chains along the *b* crystallographic axis due to C–H···π interactions (Table 13) of methoxy group of the downward pointing benzene ring H and *tert*-butyl groups of the opposite benzene ring F (Fig. 64a). Infinite chains of molecules **2** are arranged parallel to the *bc* crystallographic plane. Molecules **1** are also involved in C–H···π interactions but with molecules **2** only (Fig. 64b). They are hydrogen donors in C–H···π interactions of methoxy groups A and D and hydrogen acceptors of H-atoms of methylene bridge E, methoxy group E and *meta*-H-atom of the ring F. Therefore, molecules **1** play a role of bridge between molecules **2**.

a	b
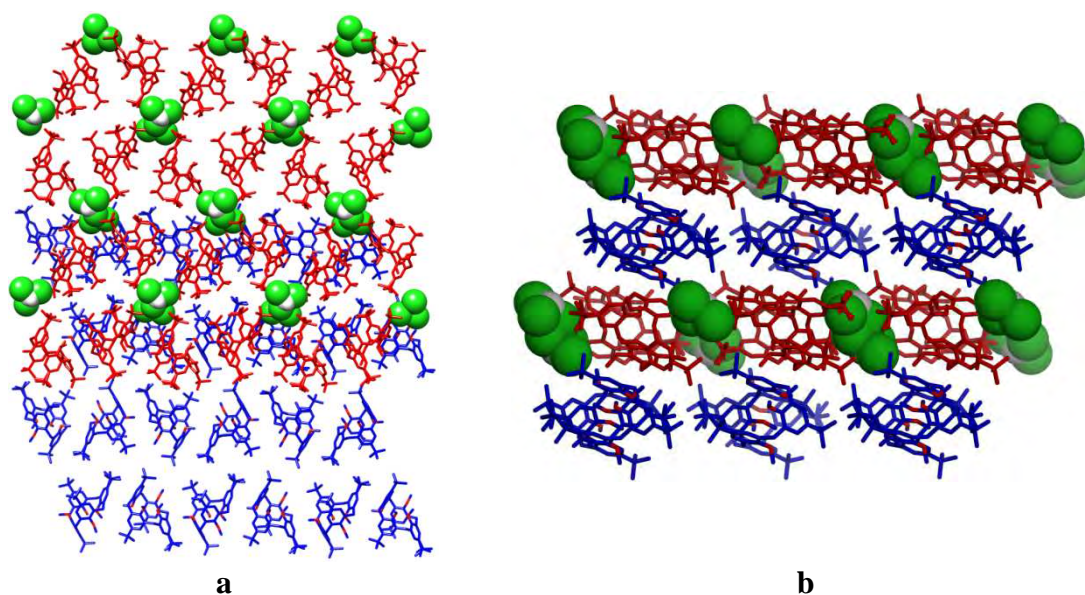
Fig. 63. Two kind of layers in crystal structure of tBuC[4]OC$_1$·0.125CHCl$_3$ (partial cone):
(a) partial superposition, view along the *a* crystallographic axis; (b) view along the *b* crystallographic axis. Molecules 1 in red, molecules 2 in blue.

Table 13. Weak interactions in tBuC[4]OC$_1$·0.125CHCl$_3$

Hydrogen bonds

D–H···A	d(D–H), Å	d(H···A), Å	d(D···A), Å	∠D–H···A
C7A–H7A2···Cl2	0.99	3.08	3.929(5)	145
C10B–H10F···Cl3[1]	0.98	2.96	3.776(6)	142
C12B–H12D···Cl3[1]	0.98	2.95	3.802(6)	146
C12B–H12E···Cl1[1]	0.98	2.86	3.469(6)	121
C12D–H12J···Cl3[2]	0.98	2.99	3.653(7)	126
C12J–H125···Cl1[2]	0.98	2.88	3.52(2)	126
C8E–H8E2···Cl1[3]	0.98	3.04	3.913(4)	149
C8E–H8E2···Cl2[3]	0.98	3.06	3.801(4)	134

Symmetry codes: (1) 1 − x, 1 − y, –z; (2) 1 − x, –0.5 + y, 0.5 − z; (3) –1 + x, y, z.

C–H···π interactions

C–H···Cg	d(H···Cg)	⊥d(H···π)	d(C···Cg)	∠C–H···Cg	∠C–H···π
C8A–H8A1···CgE[1]	2.670	2.67	3.464(3)	138	140
C8D–H8D1···CgG[2]	2.746	2.71	3.519(3)	136	144
C7E–H7E2···CgC[3]	2.839	2.84	3.710(3)	147	147
C8E–H8E1···CgA[4]	3.224	2.95	3.154(3)	159	135
C3F–H3F···CgC[5]	3.724	2.91	4.370(3)	128	141
C10F–H10P···CgH[5]	3.023	3.01	3.524(6)	113	117
C8H–H8H1···CgF[2]	2.877	2.68	3.592(4)	131	151

Symmetry codes: (1) 1 + x, y, z; (2) 1 − x, –0.5 + y, 0.5 − z; (3) − x, 0.5 + y, 0.5 − z;
(4) –1 + x, y, z; (5) –x, 0.5 + y, 0.5 − z.
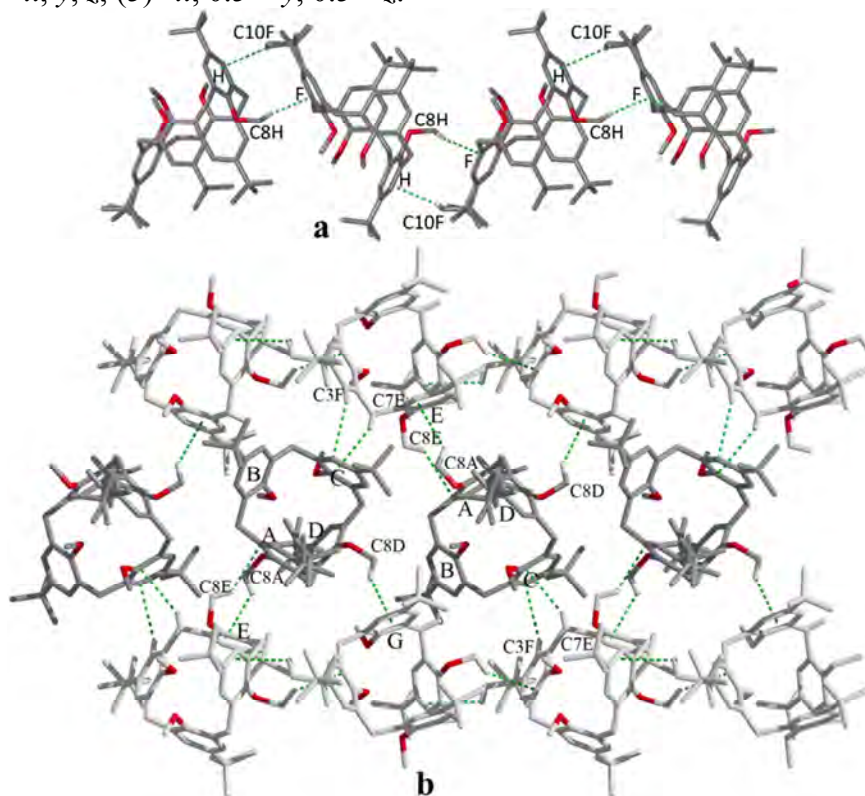
Fig. 64. tBuC[4]OC$_1$·0.125CHCl$_3$ (partial cone): (a) C–H···π interactions between molecules 2; (b) binding role of molecules 1.

Chloroform molecules are disordered in voids present within layers of molecules **1** and participate in C–H⋯Cl hydrogen bonds between H-atoms of methylene bridge C7A, methoxy group at the ring E and *tert*-butyl groups B and J and Cl atoms of chloroform (Table 13).

4.2.2 Crystal structure of O-ethylated *para-tert*-butylcalix[4]arene (partial cone)

O-Ethylated *para-tert*-butylcalix[4]arene (tBuC[4]OC$_2$ (partial cone)) crystallises from methanol/chloroform mixture in the monoclinic crystallographic system and does not contain any solvent. Crystal data are presented in Table 14.

Table 14. Crystal data and structure refinement for tBuC[4]OC$_2$ (partial cone)

Molecular formula	C$_{52}$H$_{72}$O$_4$
Formula weight	761.10
Crystal system	Monoclinic
Space group	$P2_1/c$
Unit cell dimensions	a = 14.1432(2) Å
	b = 17.1326(2) Å β =107.879(1)°
	c = 20.0987(2) Å
Volume	4634.9(1) Å^3
Z	4
Temperature	100.0(5) K
Radiation and wavelength	Mo $K\alpha$ radiation, λ = 0.71073 Å
Monochromator	graphite
Density (calculated)	1.091 Mg·m^{-3}
Absorption coefficient	0.07 mm^{-1}
F(000)	1664
Crystal size	0.20 × 0.22 × 0.25 mm
θ range for data collection	2.8–26.7°
Index ranges	-17 ≤ h ≤ 17, -17 ≤ k ≤ 21, -25 ≤ l ≤ 25
Reflections collected	45588
Independent reflections	9783 [R_{int} = 0.041]
Completeness	99.6 %
Absorption correction	None
Refinement method	Full-matrix least-squares on F^2
Weighting scheme	$[\sigma^2(F_o^2) + (0.0308P)^2 + 5.1616P]^{-1}$ *
Data / restraints / parameters	9783 / 0 / 522
Goodness-of-fit on F^2	1.03
Final R indices [$I > 2\sigma(I)$]	R = 0.062, wR = 0.123
R indices (all data)	R = 0.089, wR = 0.133
Extinction coefficient	0.0015(2)
Largest diff. peak and hole	0.30 and -0.25 e·Å^{-3}

* $P = (F_o^2 + 2F_c^2)/3$

74

The asymmetric unit comprises one molecule of the calix[4]arene which adopts a partial cone conformation (Fig. 65a) with pseudo-C_s symmetry. Carbon atom numbering scheme is shown in Fig. 65b.

a   **b**   **c**

Fig. 65. tBuC[4]OC$_2$ (partial cone): (a) asymmetric unit; (b) numbering scheme; (c) partial cone conformation stabilised by C–H···O intramolecular contacts, *tert*-butyl groups are omitted for clarity.

Dihedral angles between planes of each benzene ring and the mean plane of the four methylene groups and distances between distal C4 atoms are presented in Table 15. The partial cone conformation of calix[4]arene macrocyclic ring is stabilised by two C–H···O intramolecular contacts (Fig. 65c) between H-atoms of terminal carbon atom of the ethyl group and oxygen atoms of phenoxy moieties A and C (Table 16).

Table 15. Calix[4]arene macrocyclic ring geometry for tBuC[4]OC$_2$ (partial cone)

∠(ring-to-CH$_2$-plane), °		Distal C4···C4 distances, Å	
A	94.73(5)	C4A···C4C	5.645(3)
B	141.13(6)		
C	90.53(5)	C4B···C4D	8.996(3)
D	-94.92(4)		

Table 16. Weak interactions in tBuC[4]OC$_2$ (partial cone)

Hydrogen bonds

D–H···A	d(D–H), Å	d(H···A), Å	d(D···A), Å	∠D–H···A
C9B–H9B3···O1A	0.98	2.49	3.264(3)	136
C9B–H9B1···O1C	0.98	2.45	3.308(3)	146

C–H···π interactions

C–H···Cg	d(H···Cg)	⊥d(H···π)	d(C···Cg)	∠C–H···Cg	∠C–H···π
C8A–H8A2···CgC[1]	2.63	2.62	3.449(3)	141	145
C8D–H8D2···CgD[2]	3.55	2.99	4.315(3)	136	114
C11C–H11I···CgA[3]	3.12	3.03	4.094(3)	177	165

http://rcin.org.pl

Symmetry codes: (1) x, $1.5 - y$, $0.5 + z$; (2) $-x$, $1 - y$, $-z$; (3) x, $1.5 - y$, $-0.5 + z$.

Molecules of the calix[4]arene are self-assembled in infinite chains shown in Fig. 66a due to strong C–H···π interaction between an H-atom of the first methylene group of ethyl substituent A and the aromatic ring C of a neighbouring calix[4]arene. The chain formation is additionally enforced by weaker C–H···π interaction between an H-atom of the *tert*-butyl C and the aromatic ring A. C–H···π interactions (Fig. 66b) between H-atoms of the terminal carbon atom of the ethyl A to phenyl ring B (Table 16) combine the chains in corrugated layers parallel to the *bc* crystallographic plane (Fig. 66c).

a

b

c
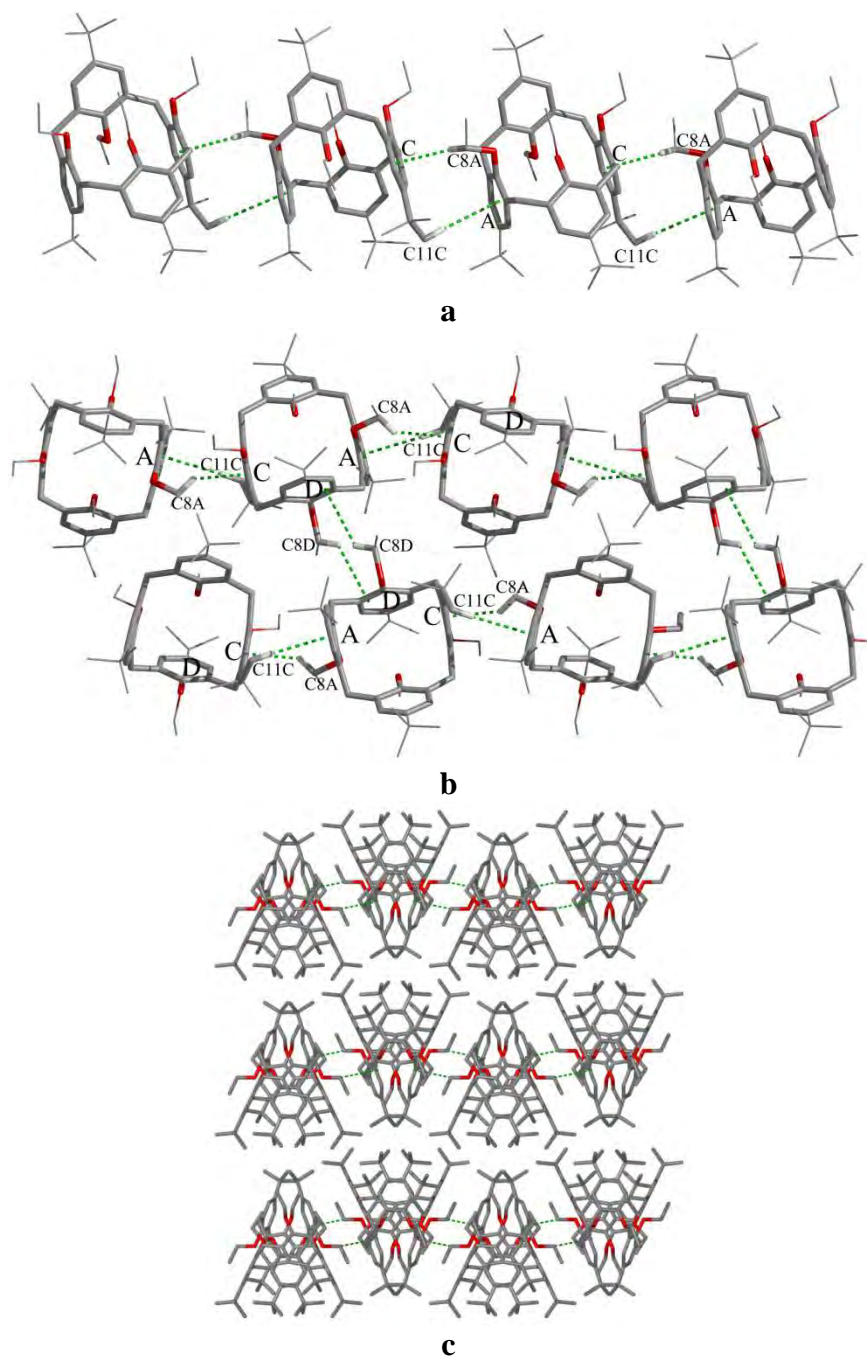
Fig. 66. tBuC[4]OC$_2$ (partial cone): (a) infinite chain self-assembly; (b) broad network of C–H···π interactions between the chains; (c) packing diagram, view along the *c* crystallographic axis, most of C–H···π interactions are omitted for clarity.

4.2.3 Crystal structure of O-propylated *para-tert*-butylcalix[4]arene (cone)

O-Propylated *para-tert*-butylcalix[4]arene (tBuC[4]OC$_3$ (cone)) crystallises from methanol/chloroform mixture in the trigonal crystallographic system. Crystal data are presented in Table 17. The asymmetric unit comprises half of the calix[4]arene molecule which adopts slightly flattened cone conformation with C_{2v}-symmetry (Fig. 67a). Carbon atom numbering scheme is shown in Fig. 67b. Two opposite propyl chains at rings B are disordered over three positions with occupancy factors of 0.50, 0.32 and 0.18. The cone conformation is stabilised by six C–H···O intramolecular contacts (Fig. 67c) between H-atoms of disordered propyl substituents and oxygen atoms O1A (Table 18).

Table 17. Crystal data and structure refinement for tBuC[4]OC$_3$ (cone)

Molecular formula	$C_{56}H_{80}O_4$
Formula weight	817.20
Crystal system	Trigonal
Space group	$P3_12$
Unit cell dimensions	a = 12.9405(2) Å
	c = 25.4723(5) Å
Volume	3694.0(1) Å^3
Z	3
Temperature	100.0(5) K
Radiation and wavelength	Mo $K\alpha$ radiation, λ = 0.71073 Å
Monochromator	graphite
Density (calculated)	1.102 Mg·m^{-3}
Absorption coefficient	0.07 mm^{-1}
$F(000)$	1344
Crystal size	0.13 × 0.50 × 0.74 mm
θ range for data collection	2.4–27.5°
Index ranges	$0 \leq h \leq 16$, $-8 \leq k \leq 0$, $-32 \leq l \leq 33$
Reflections collected	15898
Independent reflections	3169 [R_{int} = 0.051]
Completeness	99.9 %
Absorption correction	None
Refinement method	Full-matrix least-squares on F^2
Weighting scheme	$[\sigma^2(F_o^2) + (0.0566P)^2 + 2.2672P]^{-1}$ *
Data / restraints / parameters	3169 / 4 / 318
Goodness-of-fit on F^2	1.03
Final R indices [$I > 2\sigma(I)$]	R = 0.052, wR = 0.124
R indices (all data)	R = 0.060, wR = 0.130

Extinction coefficient	Not refined
Largest diff. peak and hole	0.26 and -0.23 e·Å^{-3}

$$* P = (F_o^2 + 2F_c^2)/3$$

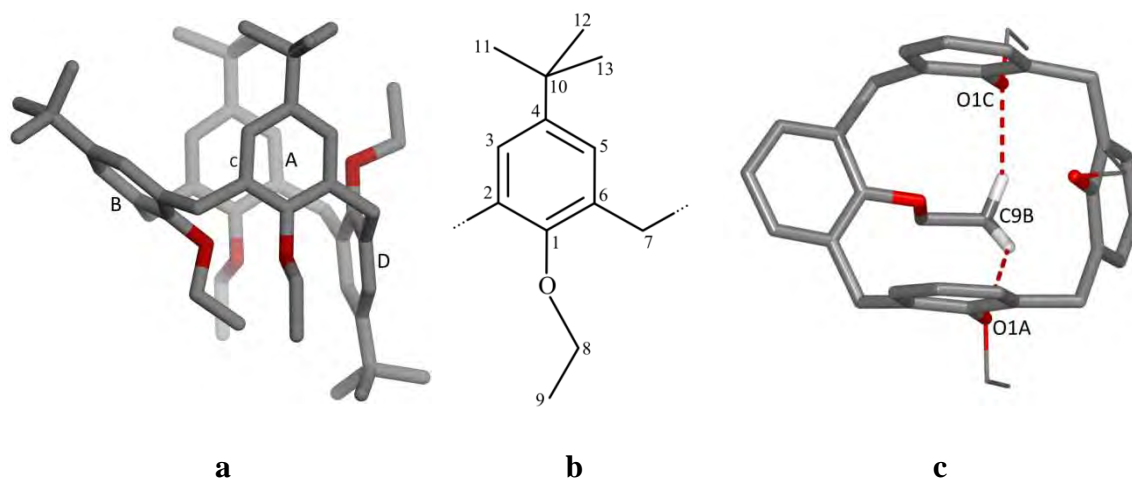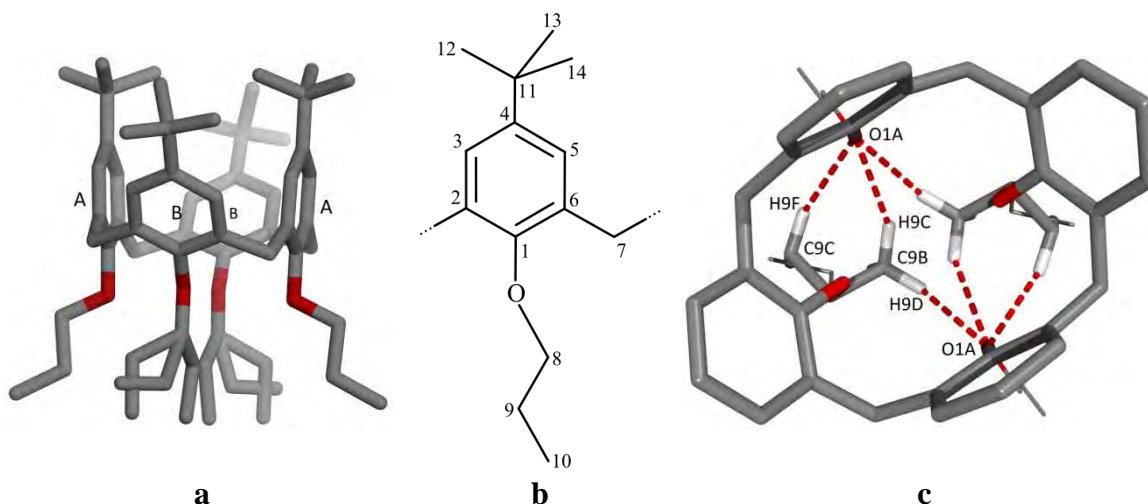**Fig. 67. tBuC[4]OC$_3$ (cone): (a) single molecule; (b) numbering scheme; (c) cone conformation stabilised by C–H···O intramolecular contacts, *tert*-butyl groups at the upper rim are omitted for clarity.**

Table 18. Weak interactions in tBuC[4]OC$_3$ (cone)

Hydrogen bonds

D–H···A	d(D–H), Å	d(H···A), Å	d(D···A), Å	∠D–H···A
C9B–H9C···O1A	0.99	2.50	3.372(8)	147
C9B–H9D···O1A[1]	0.99	2.56	3.426(7)	146
C9C–H9F···O1A[1]	0.99	2.62	3.46(1)	143

Symmetry codes: (1) $1 + x - y$, $2 - y$, $1.67 - z$.

C–H···π interactions

C–H···Cg	d(H···Cg)	⊥d(H···π)	d(C···Cg)	∠C–H···Cg	∠C–H···π
C12B–H3D···CgA[1]	3.12	2.97	4.061(4)	161	178
C13B–H3D···CgA[1]	3.42	3.04	4.310(7)	152	172

Symmetry codes: (1) $-x + y$, $2 - x$, $-0.33 + z$.

Dihedral angles between planes of each benzene ring and the mean plane of the four methylene groups are 92.85(6) and 129.90(5)°, and distances between distal C4 atoms are 5.640(5) and 9.144(5) Å for pairs of rings A and B, respectively.

At a first glance, the crystal packing of tBuC[4]OC$_3$ (cone) is composed of molecular layers parallel to the *ab* crystallographic plane (Fig. 68a). The subsequent layers are related by trigonal 3$_1$ screw symmetry (Fig. 68b and c).

Further analysis reveals that each calix[4]arene molecule participates in very weak intermolecular C–H···π interactions of 4.061(4) and 4.310(7) Å (Table 18) with four neighbouring ones (Fig. 69a): two from the layer above and two from the layer

78

below. *tert*-butyl groups of rings B interact with π-electrons of rings A of adjacent calix[4]arene.
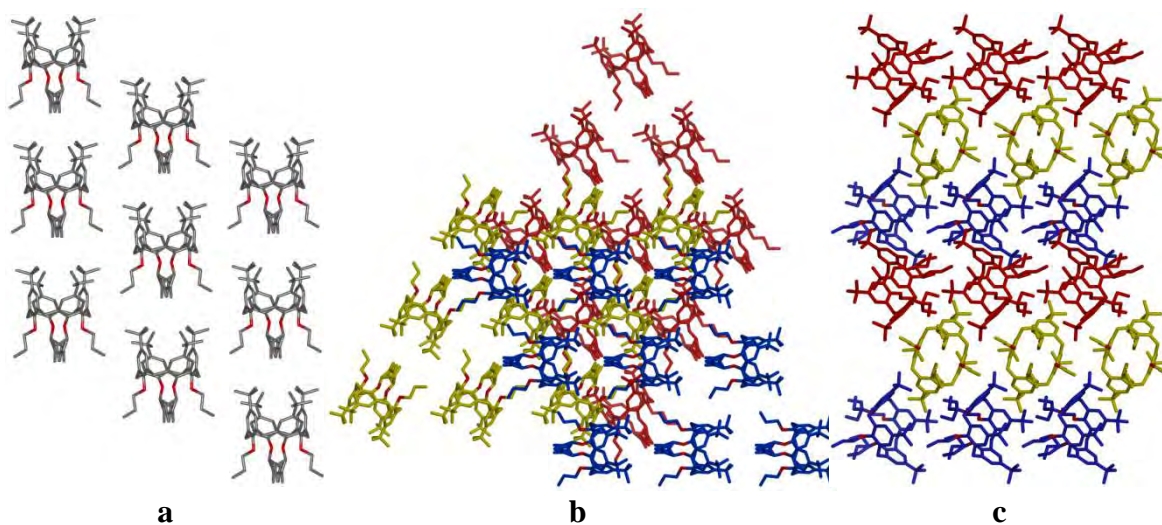
Fig. 68. tBuC[4]OC$_3$ (cone): (a) head-to-tail arrangement of the calix[4]arene molecules in the layer parallel to the *ab* crystallographic plane; (b) trigonal 3$_1$ screw symmetry relation between layers; (c) packing diagram, view along the *a* crystallographic axis.

Consequently, the calix[4]arene cores and *tert*-butyl groups form a relatively rigid channel type aromatic matrix with hexagonal distribution of channels formed by disordered flexible alkyl chains (Fig. 69b). The distance between centres of channels (12.9405(2) Å) defines the unit cell parameter *a*. The diameter of channels is *ca.* 8.1 Å while the thickness of aromatic 'walls' is *ca.* 4.8 Å.
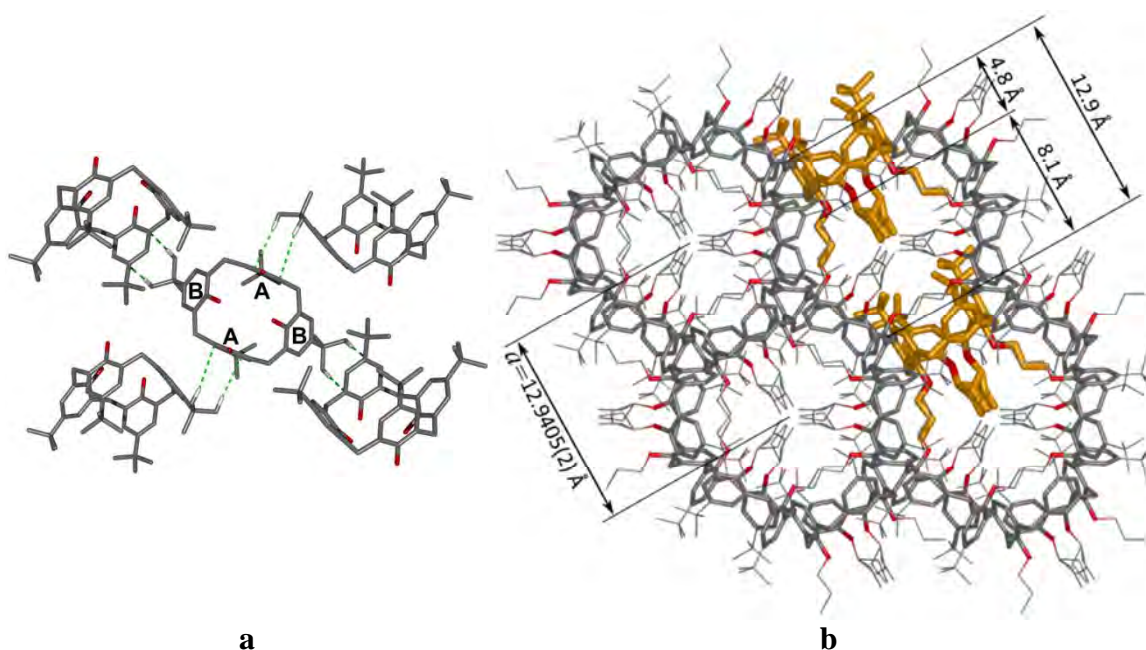
Fig. 69. tBuC[4]OC$_3$ (cone): (a) C–H···π interactions, propyl substituents are omitted for clarity; (b) packing diagram, view along the *c* crystallographic axis.

4.2.4 Crystal structure of O-propylated *para-tert*-butylcalix[4]arene (partial cone) chloroform semisolvate

O-Propylated *para-tert*-butylcalix[4]arene-chloroform semisolvate (tBuC[4]OC$_3$ (partial cone)·0.5CHCl$_3$) crystallises from methanol/chloroform mixture in the monoclinic crystallographic system and is isostructural with tBuC[4]OC$_3$ (partial cone)·0.5THF.[105] Crystal data for the solvate are presented in Table 19. The asymmetric unit comprises one molecule of the host and half molecule of the guest (Fig. 70a)

Table 19. Crystal data and structure refinement for tBuC[4]OC$_3$ (partial cone)·0.5CHCl$_3$

Molecular formula	C$_{56}$H$_{80}$O$_4$·0.5CHCl$_3$
Formula weight	876.88
Crystal system	Monoclinic
Space group	*C*2/*c*
Unit cell dimensions	*a* = 50.797(3) Å
	b = 10.6646(7) Å β = 110.337(4)°
	c = 20.528(1) Å
Volume	10428(1) Å^3
Z	8
Temperature	100.0(5) K
Radiation and wavelength	Mo *Kα* radiation, λ = 0.71073 Å
Monochromator	graphite
Density (calculated)	1.117 Mg·m^{-3}
Absorption coefficient	0.14 mm^{-1}
F(000)	3816
Crystal size	0.15 × 0.20 × 0.25 mm
θ range for data collection	3.0–25.0°
Index ranges	-42 ≤ *h* ≤ 60, -8 ≤ *k* ≤ 12, -24 ≤ *l* ≤ 24
Reflections collected	19768
Independent reflections	8594 [*R*$_{int}$ = 0.058]
Completeness	92.9 %
Absorption correction	None
Refinement method	Full-matrix least-squares on *F*^{2}
Weighting scheme	[$\sigma^2(F_o^2)$ + (0.0553*P*)^2 + 65.6737*P*]$^{-1}$ *
Data / restraints / parameters	8594 / 30 / 625
Goodness-of-fit on *F*^{2}	1.15
Final *R* indices [*I* > 2σ(*I*)]	*R* = 0.104, *wR* = 0.216
R indices (all data)	*R* = 0.134, *wR* = 0.231
Extinction coefficient	Not refined
Largest diff. peak and hole	0.47 and -0.79 e·Å^{-3}

* $P = (F_o^2 + 2F_c^2)/3$
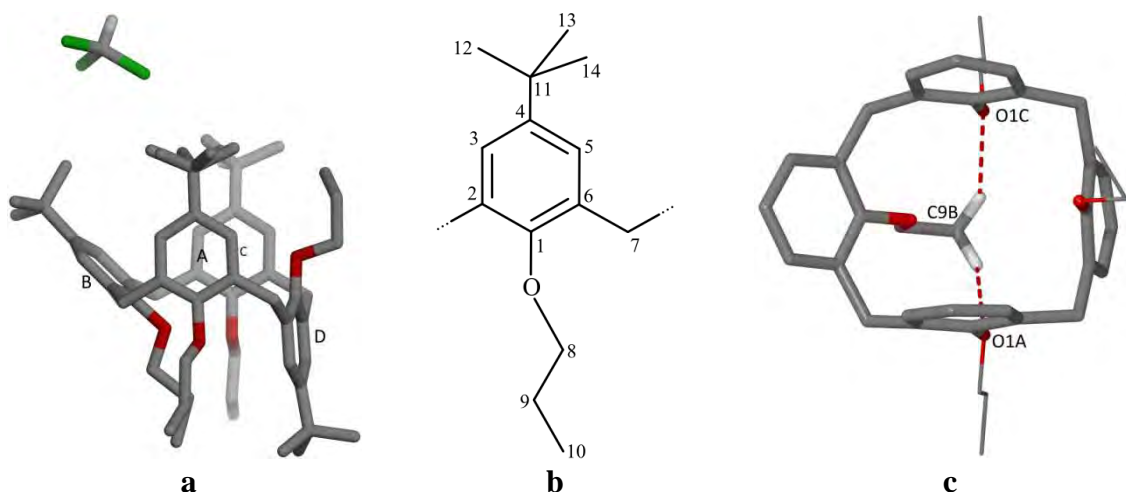
Fig. 70. tBuC[4]OC$_3$ (partial cone)·0.5CHCl$_3$ solvate: (a) asymmetric unit; (b) numbering scheme; (c) conformation stabilised by C–H···O intramolecular contacts, *tert*-butyl groups are omitted for clarity.

resulting in host:guest stoichiometry 2:1. Carbon atom numbering scheme is shown in Fig. 70b. *Tert*-butyl group of the ring A is disordered over two positions with occupancy factors of 0.52 and 0.48. The chloroform molecule lies on 2-fold crystallographic axis.

The calix[4]arene assumes a partial core conformation. Dihedral angles between planes of each benzene ring and the mean plane of the four methylene groups and distances between distal C4 atoms are presented in Table 20. Similarly to the tBuC[4]OC$_2$ (partial cone), the partial cone conformation of tBuC[4]OC$_3$ is stabilised by two C–H···O intramolecular contacts between H-atoms of the second methylene group of the chain B and oxygen atoms of phenoxy moieties A and C (Fig. 70c, Table 21).

Table 20. Calix[4]arene macrocyclic ring geometry for tBuC[4]OC$_3$ (partial cone)·0.5CHCl$_3$

∠(ring-to-CH$_2$-plane), °		Distal C4···C4 distances, Å	
A	90.1(1)	C4A···C4C	5.976(6)
B	135.2(1)		
C	101.4(1)	C4B···C4D	8.923(6)
D	-93.2(1)		

Contrary to tBuC[4]OC$_2$ (partial cone), self-assembly of tBuC[4]OC$_3$ (partial cone) molecules is realised through C–H···π interactions between *tert*-butyl groups and aromatic rings only [C14B···ring A, C14B···ring D and C13D···ring B, Table 21]. Each calix[4]arene participates in six C–H···π interactions with four neighbouring molecules (Fig. 71a).

As a result of C–H···π interactions between tBuC[4]OC$_3$ (partial cone) molecules the layered-type structure shown in Fig. 71b is formed. Layers are parallel to

9;

Table 21. Weak interactions in tBuC[4]OC$_3$ (partial cone)·0.5CHCl$_3$

Hydrogen bonds

D–H···A	d(D–H), Å	d(H···A), Å	d(D···A), Å	∠D–H···A
C9B–H9B1···O1A	0.99	2.67	3.504(5)	142
C9B–H9B2···O1C	0.99	2.51	3.357(5)	143
C13A–H13C···Cl3[1]	0.98	2.91	3.30(2)	105
C9D–H9D2···Cl3[2]	0.99	2.93	3.65(1)	131
C12E–H12O···Cl3[3]	0.98	2.74	3.54(2)	139

Symmetry codes: (1) x, $3 - y$, $-0.5 + z$; (2) x, $2 - y$, $-0.5 + z$; (3) $-x$, y, $0.5 - z$.

C–H···π interactions

C–H···Cg	d(H···Cg)	⊥d(H···π)	d(C···Cg)	∠C–H···Cg	∠C–H···π
C14B–H14E···CgA[1]	2.88	2.85	3.736(6)	147	153
C14B–H14D···CgD[2]	3.27	2.92	4.100(6)	144	133
C13D–H13L···CgB[3]	3.37	2.93	4.122(6)	136	152

Symmetry codes: (1) x, $3 - y$, $0.5 + z$; (2) x, $2 - y$, $0.5 + z$; (3) x, $2 - y$, $-0.5 + z$.

the *bc* crystallographic plane and only van der Waals interactions occur between layers of calixarenes. Molecules in the layer are symmetry related by *c*-glide planes and therefore all molecules in the plane are in the same spatial orientation: three *n*-propyl and one *tert*-butyl substituents are located above and one *n*-propyl and three *tert*-butyl substituents are located below the plane. Adjacent planes are symmetry related by 2$_1$-axis and centre of symmetry. Both sides of a layer are different. In crystal the layers are arranged in 'head-to-head' mode, *i.e.* the faces with the same structure of surface are in contact. Space between layers which is rich with *tert*-butyl groups accommodates

a   **b**
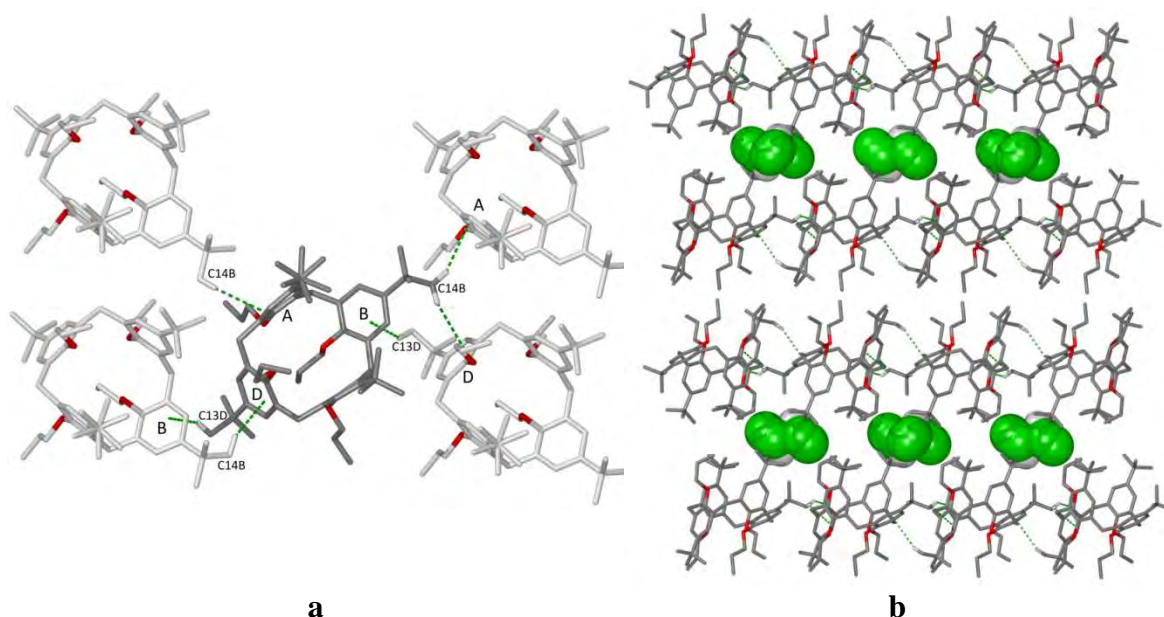
Fig. 71. tBuC[4]OC$_3$ (partial cone)·0.5CHCl$_3$: (a) intermolecular interactions; (b) packing diagram, view along the *b* crystallographic axis.

solvent molecules, while space between layers rich with *n*-propyl groups solvent is not present. Atom Cl3 participates in three C–H···Cl contacts (Table 21). Nevertheless, these interactions are not strong enough to avoid disorder of chloroform molecule.

4.2.5 Crystal structure of O-butylated *para-tert*-butylcalix[4]arene (cone)

O-Butylated *para-tert*-butylcalix[4]arene (tBuC[4]OC$_4$ (cone)) crystallises from a methanol/chloroform mixture in the trigonal crystallographic system and is isostructural with tBuC[4]OC$_3$ (cone). Crystal data are presented in Table 22. The asymmetric unit comprises half of the calix[4]arene molecule. Similarly to tBuC[4]OC$_3$ (cone), the calix[4]arene assumes the slightly flattened cone conformation with

Table 22. Crystal data and structure refinement for tBuC[4]OC$_4$ (cone)

Molecular formula	C$_{60}$H$_{88}$O$_4$
Formula weight	873.30
Crystal system	Trigonal
Space group	$P3_12$
Unit cell dimensions	a = 13.8697(7) Å
	c = 24.674(1) Å
Volume	4110.6(4) Å^3
Z	3
Temperature	100.0(5) K
Radiation and wavelength	Mo $K\alpha$ radiation, λ = 0.71073 Å
Monochromator	graphite
Density (calculated)	1.058 Mg·m^{-3}
Absorption coefficient	0.06 mm^{-1}
$F(000)$	1440
Crystal size	0.25 × 0.15 × 0.05 mm
θ range for data collection	2.5–26.4°
Index ranges	-17 ≤ h ≤ 17, -14 ≤ k ≤ 14, -30 ≤ l ≤ 30
Reflections collected	22987
Independent reflections	3126 [R_{int} = 0.041]
Completeness	99.6 %
Absorption correction	None
Refinement method	Full-matrix least-squares on F^2
Weighting scheme	$[\sigma^2(F_o^2) + (0.0378P)^2 + 2.9451P]^{-1}$ *
Data / restraints / parameters	3126 / 15 / 346
Goodness-of-fit on F^2	1.15
Final R indices [$I > 2\sigma(I)$]	R = 0.065, wR = 0.140
R indices (all data)	R = 0.069, wR = 0.142
Extinction coefficient	Not refined
Largest diff. peak and hole	0.25 and -0.20 e·Å^{-3}

* $P = (F_o^2 + 2F_c^2)/3$

C_{2v}-symmetry (Fig. 72a). Carbon atom numbering scheme is shown in Fig. 72b. Terminal methyl groups of *n*-butoxy substituents of rings A are disordered over two positions with occupancy factors of 0.72 and 0.28. *n*-Butoxy substituents at the ring B are disordered along whole length also over two positions with almost equivalent occupancy factors of 0.52 and 0.48. The cone conformation of the calix[4]arene is stabilised by six C–H···O intramolecular contacts (Fig. 72c) between H-atoms of *n*-butyl chains at rings B and oxygen atoms O1A (Table 23).
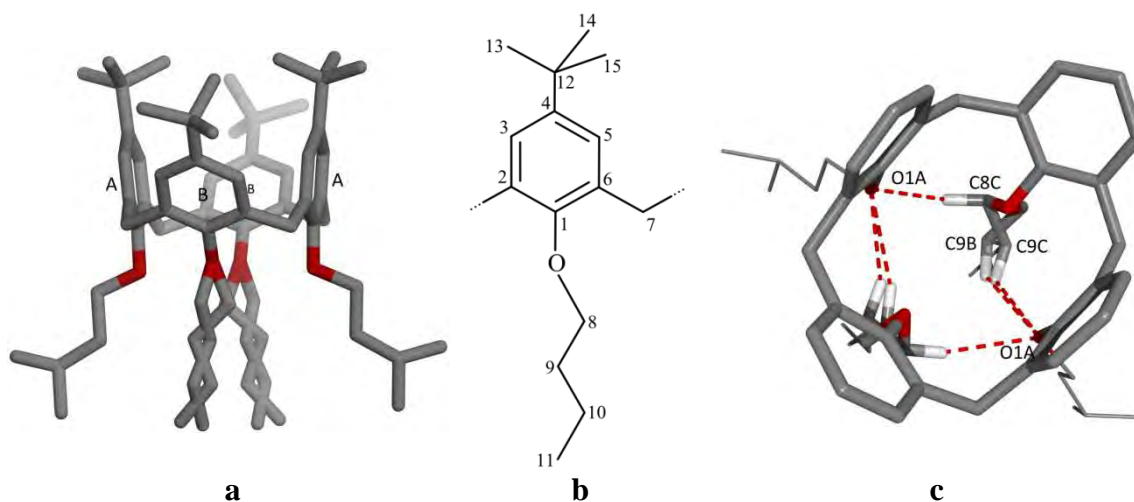
Fig. 72. tBuC[4]OC$_4$ (cone): (a) single molecule; (b) numbering scheme; (c) conformation stabilised by C–H···O intramolecular contacts, *tert*-butyl groups at the upper rim are omitted for clarity.

Contrary to tBuC[4]OC$_3$ in tBuC[4]OC$_4$, cone flattening is smaller: dihedral angles between planes of each benzene ring and the mean plane of the four methylene groups are equal to 95.10(8) and 131.67(7)°, and distances between distal C4 atoms are 5.903(7) and 9.224(6) Å for pairs of rings A and B, respectively. Similarly to tBuC[4]OC$_3$ (cone), in tBuC[4]OC$_4$ (cone) molecules with the same spatial orientation

Table 23. Weak interactions in tBuC[4]OC$_4$ (cone)

Hydrogen bonds

D–H···A	d(D–H), Å	d(H···A), Å	d(D···A), Å	∠D–H···A
C8C–H8F···O1A	0.99	2.47	3.258(9)	137
C9B–H9D···O1A[1]	0.99	2.90	3.69(1)	136
C9C–H9F···O1A[1]	0.99	2.77	3.45(2)	127

Symmetry codes: (1) $1 + x - y$, $2 - y$, $1.67 - z$.

C–H···π interactions

C–H···Cg	d(H···Cg)	⊥d(H···π)	d(C···Cg)	∠C–H···Cg	∠C–H···π
C14A–H12C···CgB[1]	3.67	2.94	4.514(5)	146	165
C14B–H14F···CgA[2]	2.91	2.88	3.624(5)	131	139
C15A–H15A···CgB[1]	3.08	3.00	4.059(6)	173	168

Symmetry codes: (1) $-x + y$, $2 - x$, $-0.33 + z$.

are parallel to the *ab* crystallographic plane. Each calix[4]arene molecule takes part in very weak intermolecular C–H⋯π interactions (Table 23) with two neighbouring molecules from the layer above and two other from the layer below: two H-atoms of *tert*-butyl group of ring A interact with π-electrons of ring B, and one H-atom of *tert*-butyl group of ring B interacts with π-electrons of ring A (Fig. 73a).

Comparison of the unit cell parameters of isostructural tBuC[4]OC$_4$ (cone) and tBuC[4]OC$_3$ (cone) reveals that a parameter for tBuC[4]OC$_4$ (cone) is almost 1 Å longer [13.8697(7) *versus* 12.9405(2) Å]. This corresponds to the longer alkyl chains in tBuC[4]OC$_4$ (cone). On the other hand, elongation of alkyl chains results in larger distances between calix[4]arene cores (Fig. 73b) and consequently, in more compact packing of calix[4]arene molecules and shortening of *c* parameter of the unit cell of tBuC[4]OC$_4$ (cone) [24.674(1) *versus* 25.4723(5) Å for tBuC[4]OC$_3$ (cone)]. Similarly to tBuC[4]OC$_3$ (cone) the calix[4]arene macrocyclic rings and *tert*-butyl groups form a relatively rigid channel type aromatic matrix with hexagonal distribution of channels formed by disordered flexible alkyl chains (Fig. 73c). The thickness of aromatic 'walls'
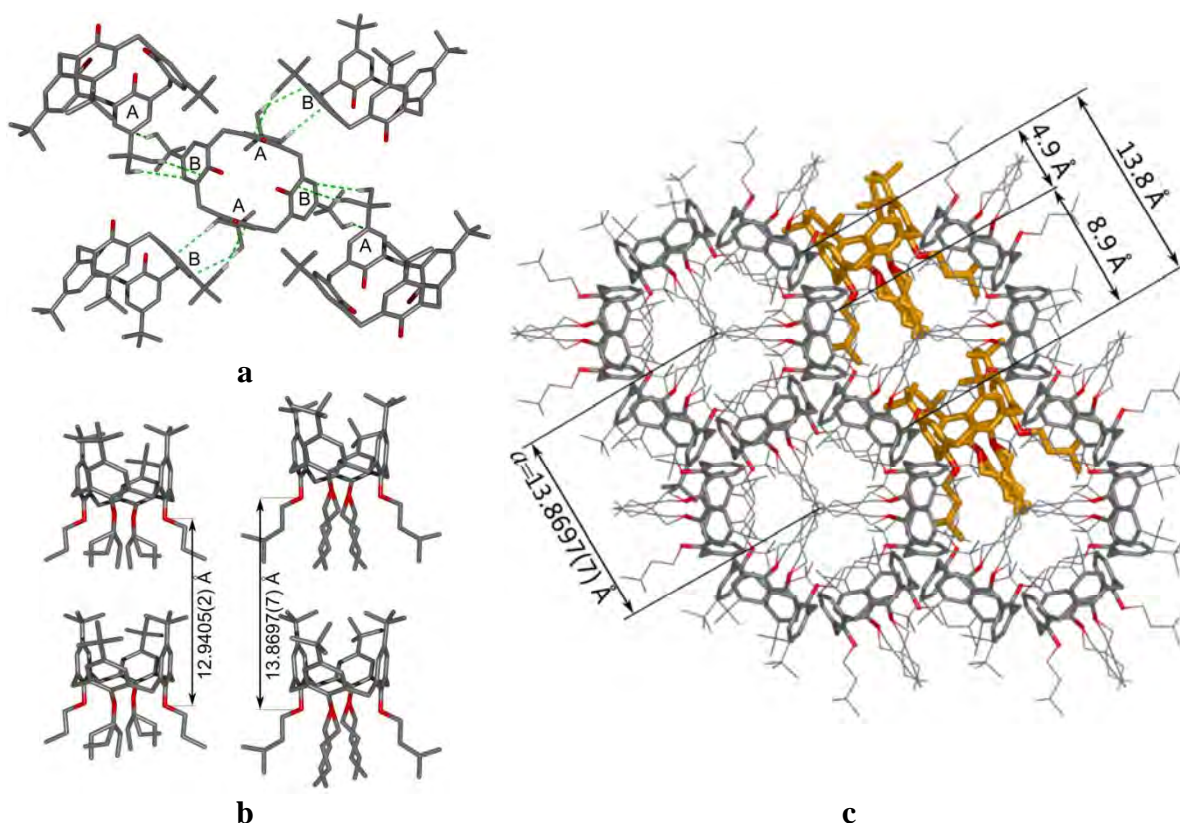
Fig. 73. tBuC[4]OC$_4$ (cone): (a) C–H⋯π interactions of the calix[4]arene molecule with adjacent molecules, *n*-butyl substituents are omitted for clarity; (b) distance between calix[4]arene cores in tBuC[4]OC$_3$ (cone) and tBuC[4]OC$_4$ (cone); (c) packing diagram, view along the *c* crystallographic axis.

85

is very similar (*ca.* 4.9 Å) while the diameter of channels is slightly larger [*ca.* 8.9 *versus* 8.1 Å for tBuC[4]OC$_3$ (cone)].

4.2.6   Crystal structure of O-butylated *para-tert*-butylcalix[4]arene (partial cone)

O-Butylated *para-tert*-butylcalix[4]arene (tBuC[4]OC$_4$ (partial cone)) crystallises from methanol/chloroform mixture in the triclinic crystallographic system. No solvent molecules exist in the crystal lattice. Crystal data are presented in Table 24. The asymmetric unit comprises two independent molecules of the calixarene which differs one from another in spatial orientation of the alkyl chains (Fig. 74a and b).

Table 24. Crystal data and structure refinement for tBuC[4]OC$_4$ (partial cone)

Molecular formula	C$_{60}$H$_{88}$O$_4$
Formula weight	873.30
Crystal system	Triclinic
Space group	$P\bar{1}$
Unit cell dimensions	a = 15.1575(3) Å α = 107.316(1)°
	b = 18.9060(3) Å β = 92.595(1)°
	c = 20.7254(5) Å γ = 104.599(1)°
Volume	5440.3(2) Å^3
Z	4
Temperature	100.0(5) K
Radiation and wavelength	Mo $K\alpha$ radiation, λ = 0.71073 Å
Monochromator	graphite
Density (calculated)	1.066 Mg·m^{-3}
Absorption coefficient	0.06 mm^{-1}
F(000)	1920
Crystal size	0.05 × 0.15 × 0.25 mm
θ range for data collection	2.8–23.3°
Index ranges	-16 ≤ h ≤ 16, -21 ≤ k ≤ 21, -23 ≤ l ≤ 22
Reflections collected	58711
Independent reflections	15558 [R_{int} = 0.066]
Completeness	99.9 %
Absorption correction	None
Refinement method	Full-matrix least-squares on F^2
Weighting scheme	$[\sigma^2(F_o^2) + (0.0897P)^2 + 6.8833P]^{-1}$ *
Data / restraints / parameters	15558 / 100 / 1452
Goodness-of-fit on F^2	1.05
Final R indices [$I > 2\sigma(I)$]	R = 0.083, wR = 0.200
R indices (all data)	R = 0.118, wR = 0.217
Extinction coefficient	Not refined
Largest diff. peak and hole	0.90 and -0.54 e·Å^{-3}

* $P = (F_o^2 + 2F_c^2)/3$

86
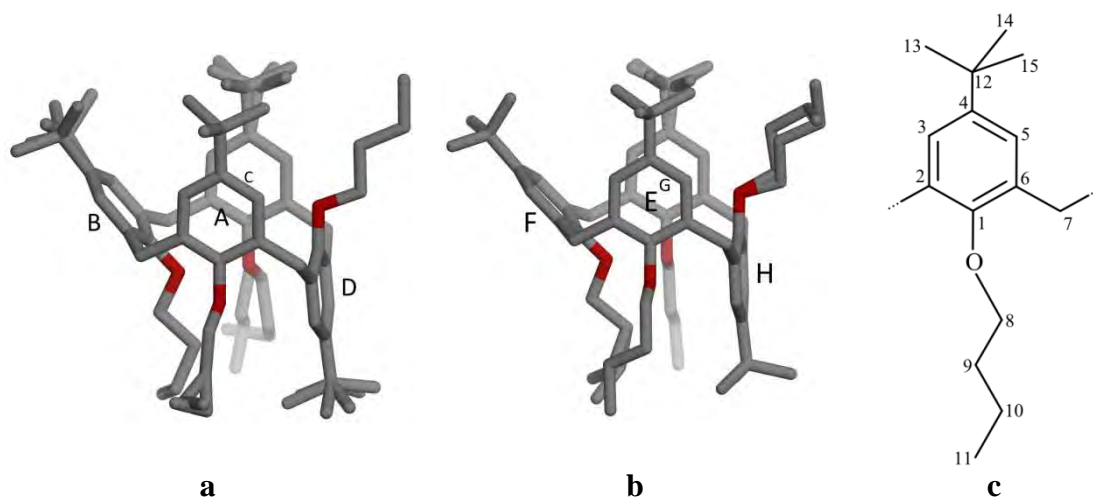
Fig. 74. tBuC[4]OC₄ (partial cone): (a) molecule 1 and (b) molecule 2; (c) numbering scheme.

Carbon atom numbering scheme is shown in Fig. 74c.*n*-Butyl chains at rings A and C of molecule **1** (proximal to turned ring D) are disordered over two positions (two end atoms of the chain at the ring A and the chain at the ring C along its whole length) with occupancy factors of 0.54 and 0.46, and 0.70 and 0.30 for ring A and C, respectively. Three of four *tert*-butyl groups (rings B, C and D) are also disordered [occupancy factors of 0.58 and 0.42, 0.65 and 0.35, and 0.60 and 0.40 for ring B, C and D, respectively]. In the case of the second calixarene molecule, there are also two disordered *n*-butyl chains. Two end atoms of the *n*-alkyl substituent at the ring F, distal to turned ring H, are disordered over two positions with occupancy factors of 0.61 and 0.39. The *n*-butyl chain on the downward pointing ring H is disordered along its whole length with similar occupancy factors of 0.60 and 0.40. Contrary to molecule **1**, there is only one disordered *tert*-butyl group (ring G) with equal occupancy factors of 0.5.

Both calix[4]arene molecules adopt a partial cone conformation. Analysis of dihedral angles between planes of each benzene ring and the mean plane of the four methylene groups and distances between distal C4 atoms reveals that conformation of

Table 25. Calix[4]arene macrocyclic ring geometry for tBuC[4]OC₄ (partial cone)

∠(ring-to-CH₂-plane), °			
1		**2**	
A	93.76(9)	E	92.60(7)
B	132.2(1)	F	134.92(9)
C	91.18(9)	G	91.85(7)
D	-95.90(9)	H	-93.01(8)
Distal C4···C4 distances, Å			
1		**2**	
C4A···C4C	5.609(5)	C4E···C4G	5.636(4)
C4B···C4D	9.015(5)	C4F···C4H	8.892(4)

the macrocyclic core for both molecules is almost identical (Table 25). The partial cone conformation of each calix[4]arene macrocyclic ring is stabilised by two C–H···O intramolecular contacts between H-atoms of the second methylene and oxygen atoms of phenol moieties (Fig. 75 and Table 26).
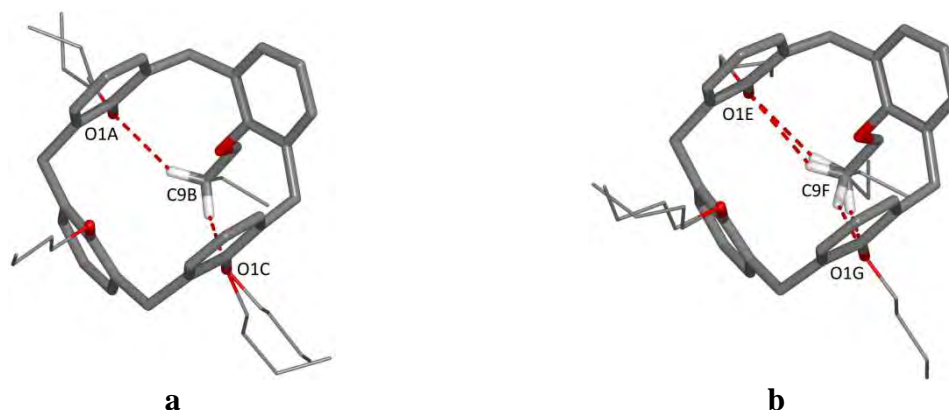
Fig. 75. tBuC[4]OC$_4$ (partial cone) conformation stabilised by C–H···O intramolecular contacts: (a) molecule 1; (b) molecule 2. *Tert*-butyl groups are omitted for clarity.

Table 26. Weak interactions in tBuC[4]OC$_4$ (partial cone)

Hydrogen bonds

D–H···A	$d(D$–H), Å	d(H···A), Å	$d(D$···A), Å	∠D–H···A
C9B–H9B1···O1A	0.99	2.73	3.617(6)	140
C9B–H9B2···O1C	0.99	2.78	3.617(6)	143
C9F–H9F1···O1E	0.99	2.84	3.673(4)	142
C9F–H9F2···O1G	0.99	2.61	3.421(4)	139
C9F–H9F3···O1E	0.99	2.92	3.673(4)	134
C9F–H9F4···O1G	0.99	2.55	3.421(4)	146

C–H···π interactions

C–H···Cg	d(H···Cg)	⊥d(H···π)	d(C···Cg)	∠C–H···Cg	∠C–H···π
C11A–H11A···CgF[1]	3.36	3.15	4.15(1)	140	140
C11A–H11C···CgB[2]	3.25	3.13	3.84(2)	121	135
C13F–H13P···CgA[1]	3.46	3.13	3.723(6)	102	118
C13F–H13R···CgE[3]	2.99	2.94	3.833(6)	145	155
C10G–H10M···CgC[4]	3.51	2.88	4.415(5)	154	146
C10H–H10O···CgC[5]	3.19	3.09	3.872(7)	127	115
C10I–H10R···CgB[2]	3.24	3.05	3.85(1)	122	137
C11I–H11···CgF[1]	3.00	2.91	3.82(1)	143	153
C11P–H210···CgD[6]	3.35	3.04	3.696(7)	103	128

Symmetry codes: (1) 2 –x,1 – y, 1 – z; (2) 1 – x, 1 – y, 1 – z; (3) 2 –x, –y, 1 – z; (4) 1 + x, y, z; (5) 1 – x,–y, –z; (6) x, –1 + y, z.

Each molecule **1** participates in C–H···π interactions with one related by centre of symmetry molecule **1** between H-atoms of two end carbon atoms of disordered

n-butyl chain at the ring A and phenyl moiety B (Fig. 76a). Molecule **1** also takes part in C–H···π interactions with four molecules 2 between H-atoms of terminal or second from the end carbon atoms of *n*-butyl chains and adjacent phenyl moieties (Table 26). There is also C–H···π interaction between H-atom of *tert*-butyl-group of the ring F and phenyl moiety A.
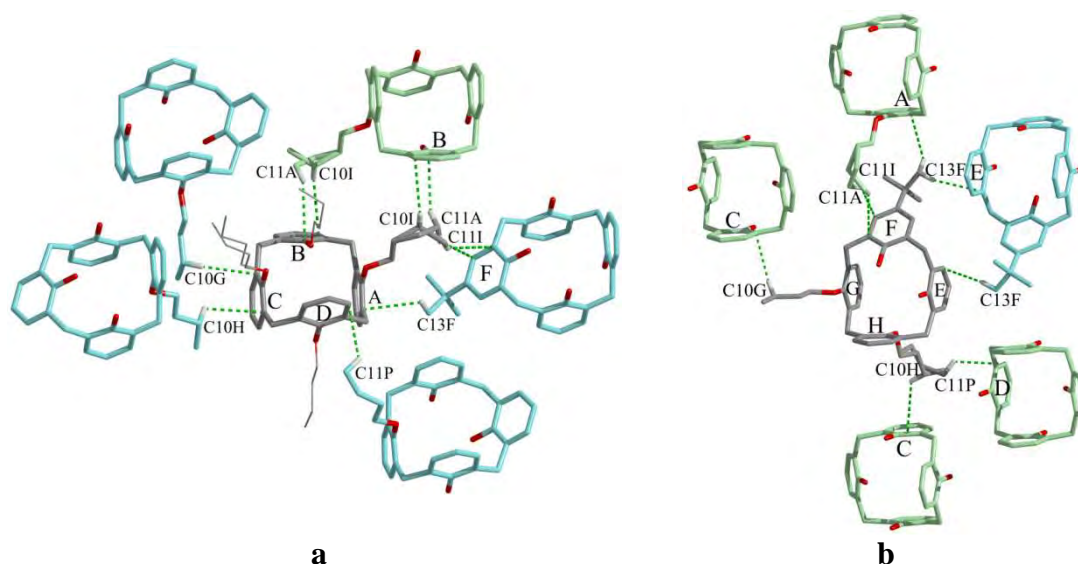
Fig. 76. tBuC[4]OC₄ (partial cone): C–H···π interactions with adjacent molecules (a) molecule 1 (greenish) and (b) molecule 2 (bluish). Only C–H···π interactions in which the central molecule takes part are shown.

The local environment of molecule **2** is similar to that found for molecule **1**. Each molecule **2** takes part in C–H···π interactions with one related by centre of symmetry molecule **2** and four molecules **1** (Fig. 76b). Two adjacent molecules **2** also form centrosymmetric dimer due to C–H···π interactions between H-atom of *tert*-butyl substituent at rings F and phenyl moieties E. Molecule **2** participates in C–H···π interactions with four molecules 1 between H-atoms of terminal or second from the end carbon atoms of *n*-butyl chains and adjacent phenyl moieties (Table 26). There is also C–H···π interaction between H-atom of *tert*-butyl-group of the ring F and phenyl moiety A.

It should be noted here, that C–H···π interactions in crystal structure of tBuC[4]OC₄ (partial cone) are not strong enough to avoid a disorder of *n*-butyl chains.

Due to widespread net of C–H···π interactions, calix[4]arene molecules are self-assembled in layers which are extending parallel to the *a*(*b*+*c*) crystallographic plane. Molecules **1** and molecules **2** in layers are arranged in rows along the *c* crystallographic axis (Fig. 77a) and rows are alternately arranged in layers. Molecules within rows and layers (shown in Fig. 77b) are related by centre of symmetry, so each layer consist of

molecules in both spatial orientations and both sides of the layer contain the same amount of *tert*-butyl and *n*-alkyl substituents. Only weak van der Waals interactions exist between layers.
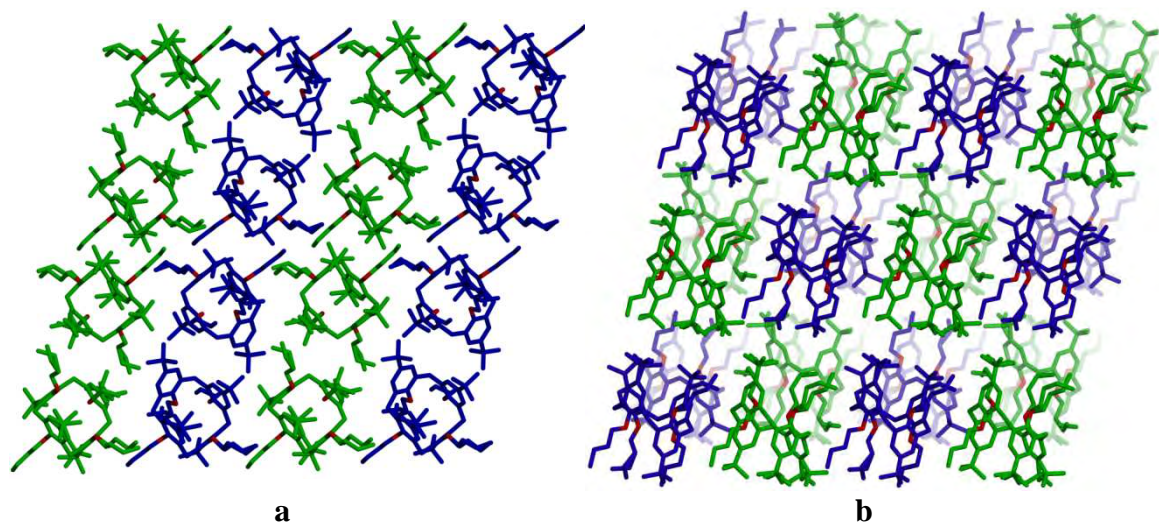
Fig. 77. tBuC[4]OC$_4$ (partial cone): (a) the top view on the layer; (b) packing diagram, view along the *c* crystallographic axis. Molecules 1 in green, molecules 2 in blue.

4.2.7   Crystal structure of O-pentylated *para-tert*-butylcalix[4]arene (partial cone)

O-Pentylated *para-tert*-butylcalix[4]arene (tBuC[4]OC$_5$ (partial cone)) crystallises from methanol/chloroform mixture in the triclinic crystallographic system. Crystal data are presented in Table 27. The asymmetric unit comprises two molecules of the calix[4]arene in a partial cone conformation (Fig. 78a and b) with different orientation of alkyl chains. Carbon atom numbering scheme is shown in Fig. 78c. *tert*-Butyl group at the ring C of molecule **1** is disordered over two positions with occupancy factors of 0.68 and 0.32. Terminal atom and two end atoms of pentyl substituents at
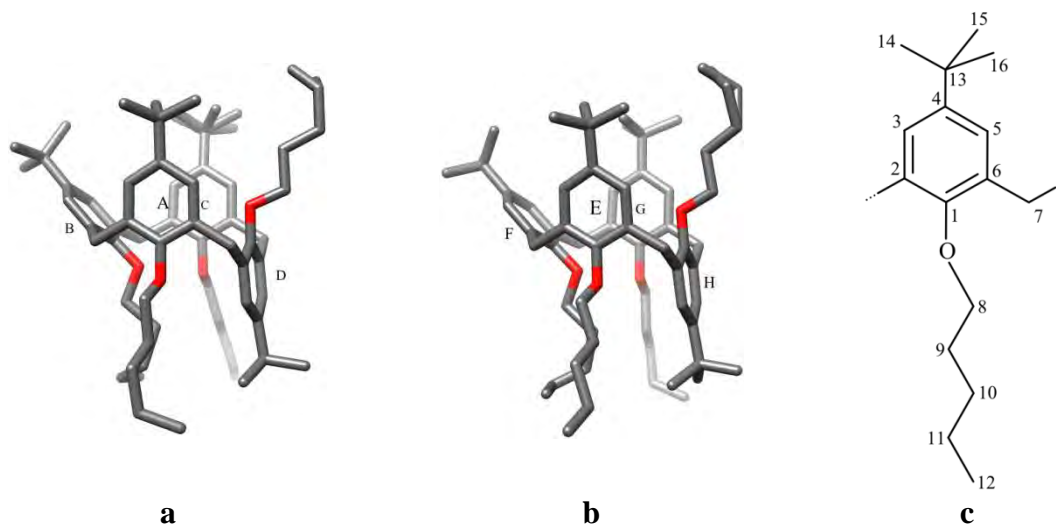
Fig. 78. tBuC[4]OC$_5$ (partial cone): (a) molecule 1; (b) molecule 2; (c) numbering scheme.

Table 27. Crystal data and structure refinement for tBuC[4]OC$_5$ (partial cone).

Molecular formula	C$_{64}$H$_{96}$O$_4$	
Formula weight	929.41	
Crystal system	Triclinic	
Space group	$P\,\overline{1}$	
Unit cell dimensions	a = 10.6235(3) Å	α = 107.251(1)°
	b = 20.3875(6) Å	β = 91.743(1)°
	c = 28.4196(1) Å	γ = 90.016(2)°
Volume	5875.4(3) Å^3	
Z	4	
Temperature	100.0(5) K	
Radiation and wavelength	Mo $K\alpha$ radiation, λ = 0.71073 Å	
Monochromator	graphite	
Density (calculated)	1.051 Mg·m^{-3}	
Absorption coefficient	0.06 mm^{-1}	
$F(000)$	2048	
Crystal size	0.20 × 0.15 × 0.08 mm	
θ range for data collection	2.9–20.8°	
Index ranges	-10 ≤ h ≤ 10, -20 ≤ k ≤ 20, -28 ≤ l ≤ 28	
Reflections collected	41084	
Independent reflections	11710 [R_{int} = 0.100]	
Completeness	94.4 %	
Absorption correction	None	
Refinement method	Full-matrix least-squares on F^2	
Weighting scheme	$[\sigma^2(F_o^2) + (0.0681P)^2 + 11.2286P]^{-1}$ *	
Data / restraints / parameters	11710 / 71 / 1320	
Goodness-of-fit on F^2	1.04	
Final R indices [$I > 2\sigma(I)$]	R = 0.080, wR = 0.171	
R indices (all data)	R = 0.135, wR = 0.192	
Extinction coefficient	Not refined	
Largest diff. peak and hole	0.62 and -0.30 e·Å^{-3}	

* $P = (F_o^2 + 2F_c^2)/3$

turned rings of both molecule **1** and molecule **2** are disordered over two positions with occupancy factors of 0.53 and 0.47 and 0.55 and 45 for rings D and H, respectively.

Analysis of dihedral angles between planes of each benzene ring and the mean plane of the four methylene groups and distances between distal C4 atoms (Table 28) reveals that calix[4]arene macrocyclic rings show a pseudo plane of symmetry running through the downward pointing ring and the one distal. This observation also correlates with the strength of C– H···O intramolecular contacts (Table 29). H-atoms of the second methylene group of the pentyl substituent at the ring distal to the downward pointing one interacts with oxygen atoms of two neighbouring phenyl rings in a slightly asymmetric way (Fig. 79).

: ;

Table 28. Calix[4]arene macrocyclic ring geometry for tBuC[4]OC$_5$ (partial cone)

	∠(ring-to-CH$_2$-plane),°			Distal C4⋯C4 distances, Å	
A	93.2(1)	E	99.0(1)	C4A⋯C4C	5.937(7)
B	133.80(8)	F	134.68(9)	C4B⋯C4D	8.953(7)
C	97.0(1)	G	93.7(1)	C4E⋯C4G	6.060(7)
D	-95.7(1)	H	-97.4(1)	C4F⋯C4H	9.000(7)

a　　　　　　　　　　　　**b**
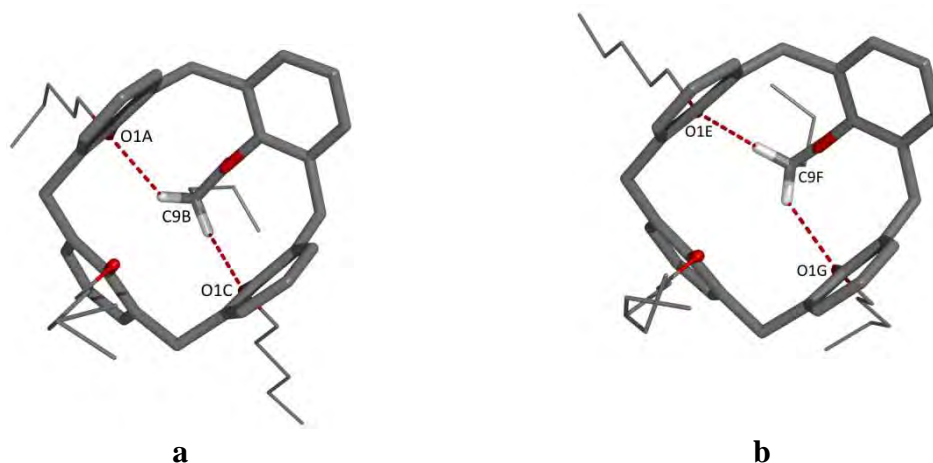
Fig. 79. tBuC[4]OC$_5$ (partial cone) conformation stabilised by C–H⋯O intramolecular contacts: (a) molecule 1; (b) molecule 2. *Tert*-butyl groups are omitted for clarity.

Table 29. Weak interactions in tBuC[4]OC$_5$ (partial cone)

Hydrogen bonds

D–H⋯A	d(D–H), Å	d(H⋯A), Å	d(D⋯A), Å	∠D–H⋯A
C9B–H9B1⋯O1A	0.99	2.71	3.517(7)	139
C9B–H9B2⋯O1C	0.99	2.71	3.502(7)	138
C9F–H9F1⋯O1E	0.99	2.67	3.461(7)	138
C9F–H9F2⋯O1G	0.99	2.70	3.507(7)	139

C–H⋯π interactions

C–H⋯Cg	d(H⋯Cg)	⊥d(H⋯π)	d(C⋯Cg)	∠C–H⋯Cg	∠C–H⋯π
C14B–H14E⋯CgG[1]	3.65	2.63	4.343(7)	130	151
C15B–H15E⋯CgG[1]	2.83	2.79	3.677(8)	145	155
C15B–H15D⋯CgH[2]	3.21	2.85	4.073(7)	148	136
C14F–H14Q⋯CgA[3]	2.88	2.84	3.707(7)	143	152
C14F–H14R⋯CgD	3.21	2.87	4.071(7)	147	135
C15F–H15R⋯CgA[3]	3.59	2.62	4.327(7)	134	153

Symmetry codes: (1) −1 + x, −1 + y, z; (2) x, −1 + y, z; (3) 1 + x, y, z.

C–H⋯π interactions are the driving force of self-assembly process of tBuC[4]OC$_5$ (partial cone) molecules in layers which are extending parallel to the *ab* crystallographic plane. Molecules **1** interact exclusively with molecules **2** and similarly, molecules **2** interact exclusively with molecules **1** (Fig. 80a).

92
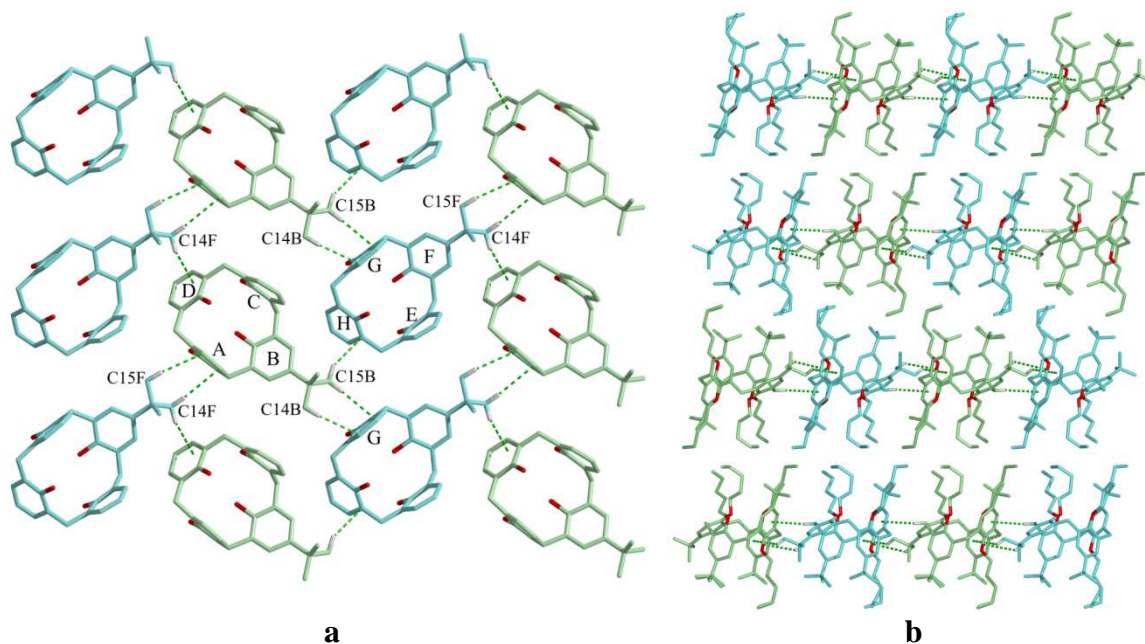
Fig. 80. tBuC[4]OC$_5$ (partial cone): (a) layer formation due to C–H···π interactions between molecules 1 (greenish) and molecules 2 (bluish), *n*-pentyl and *tert*-butyl substituents which do not participate in C–H···π interactions are omitted for clarity; (b) packing diagram, view along the *a* crystallographic axis.

There are six C–H···π interactions between molecules **1** and **2** (Table 29). Like the crystal structure of tBuC[4]OC$_3$ (partial cone)·0.5CHCl$_3$ and contrary to the crystal structures of tBuC[4]OC$_2$ (partial cone) and tBuC[4]OC$_4$ (partial cone), molecules of calix[4]arene in the layer are not related by centres of symmetry which results in difference between both sides of the layer. One side is richer in *tert*-butyl groups while the other one is richer in *n*-alkyl substituents. Layers are in contact by sides of the same nature. Additionally, two subsequent layers form bilayer with molecular arrangement:

···B···A···B···A···B···A···

···B···A···B···A···B···A···
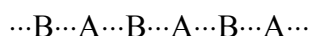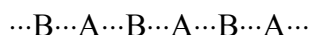
The next bilayers shifted to the adjacent ones by one calix[4]arene (Fig. 80b).

4.2.8 Crystal structure of O-hexylated *para-tert*-butylcalix[4]arene (cone)

O-Hexylated *para-tert*-butylcalix[4]arene (tBuC[4]OC$_6$ (cone)) crystallises from methanol/chloroform mixture in the monoclinic crystallographic system. Crystal data are presented in Table 30. The asymmetric unit comprises two independent molecules of calixarenes that differ one from another by spatial orientation of alkyl chains (Fig. 81a and b). Carbon atom numbering scheme is shown in Fig. 81c. Four end atoms of hexyl substituent at the ring C are disordered over two positions with occupancy factors of 0.78 and 0.22. Five atoms (except the first one) of hexyl substituent at the ring F are

Table 30. Crystal data and structure refinement for tBuC[4]OC$_6$ (cone)

Molecular formula	C$_{68}$H$_{104}$O$_4$
Formula weight	985.51
Crystal system	Monoclinic
Space group	$P2_1/c$
Unit cell dimensions	a = 19.3890(2) Å
	b = 16.8102(2) Å β = 115.215(1)°
	c = 41.9181(5) Å
Volume	12360.7(3) Å^3
Z	8
Temperature	100.0(5) K
Radiation and wavelength	Mo Kα radiation, λ = 0.71073 Å
Monochromator	graphite
Density (calculated)	1.059 Mg·m^{-3}
Absorption coefficient	0.06 mm^{-1}
F(000)	4352
Crystal size	0.37 × 0.45 × 0.50 mm
θ range for data collection	2.8–24.4°
Index ranges	-22 ≤ h ≤ 22, -19 ≤ k ≤ 19, -48 ≤ l ≤ 48
Reflections collected	118080
Independent reflections	20313 [R_{int} = 0.081]
Completeness	99.9 %
Absorption correction	None
Refinement method	Full-matrix least-squares on F^2
Weighting scheme	$[\sigma^2(F_o^2) + (0.0363P)^2 + 9.0257P]^{-1}$ *
Data / restraints / parameters	20313 / 77 / 1494
Goodness-of-fit on F^2	1.04
Final R indices [$I > 2\sigma(I)$]	R = 0.059, wR = 0.116
R indices (all data)	R = 0.091, wR = 0.126
Extinction coefficient	Not refined
Largest diff. peak and hole	0.63 and -0.32 e·Å^{-3}

* $P = (F_o^2 + 2F_c^2)/3$
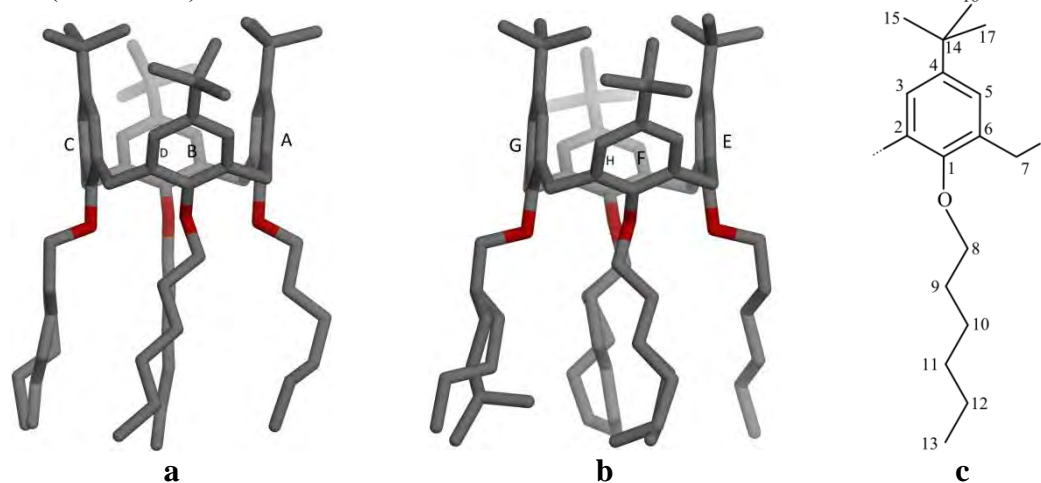
Fig. 81. tBuC[4]OC$_6$ (cone): (a) molecule 1; (b) molecule 2; (c) numbering scheme.

also disordered over two positions with occupancy factors of 0.54 and 0.46. Four last atoms of hexyl chain at the ring G are disordered over three positions with occupancy factors of 0.42, 0.36 and 0.22. Finally, four last atoms of hexyl chain at the ring H are disordered over two positions with occupancy factors of 0.68 and 0.32.

Analysis of dihedral angles between planes of each benzene ring and the mean plane of the four methylene groups and distances between distal C4 atoms (Table 31) reveals that the conformation of the molecule **1** can be described as flattened cone whereas the molecule **2** adopts the pinched cone conformation.

Table 31. Calix[4]arene macrocyclic ring geometry for tBuC[4]OC$_6$ (cone)

$\angle$(ring-to-CH$_2$-plane), °			
1		**2**	
A	95.08(6)	E	90.01(5)
B	131.76(6)	F	135.47(6)
C	92.32(6)	G	85.51(4)
D	132.50(5)	H	138.53(7)
Distal C4$\cdots$C4 distances, Å			
1		**2**	
C4A$\cdots$C4C	5.780(3)	C4E$\cdots$C4G	5.227(3)
C4B$\cdots$C4D	9.250(3)	C4F$\cdots$C4H	9.569(3)

The conformation of both molecules is stabilised by C–H$\cdots$O intramolecular contacts between H-atoms of the first and the second methylene groups of hexyl chains and oxygen atoms of phenoxy moieties (Table 32). In molecule **1** (Fig. 82a), the first and the second methylene group of chain B interact with oxygen atoms of two opposite rings A and C, and the second methylene group of the chain D interacts with oxygen atoms of rings A and C. In molecule **2** (Fig. 82b), the first and the second methylene groups of opposite chains interact with oxygen atoms of opposite phenyl rings E and G.

a	b
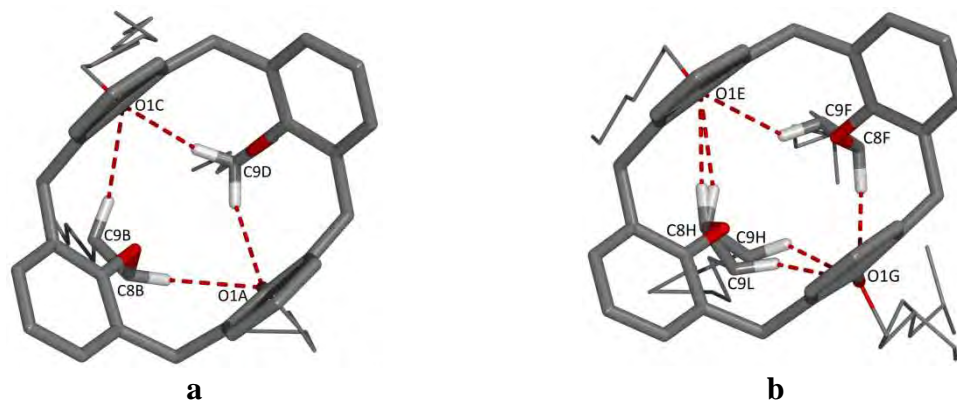
Fig. 82. tBuC[4]OC$_6$ (cone), conformation stabilised by C–H$\cdots$O intramolecular contacts: (a) molecule 1; (b) molecule 2. *Tert*-butyl groups at upper rims are omitted for clarity.

95

Table 32. Weak interactions in tBuC[4]OC$_6$ (cone)

Hydrogen bonds

D–H···A	d(D–H), Å	d(H···A), Å	d(D···A), Å	∠D–H···A
C8B–H8B2···O1A	0.99	2.76	3.374(3)	121
C9B–H9B1···O1C	0.99	3.00	3.780(3)	137
C9D–H9D1···O1C	0.99	2.73	3.574(3)	144
C9D–H9D2···O1A	0.99	2.88	3.682(3)	139
C8F–H8F1···O1G	0.99	2.64	3.417(3)	136
C9F–H9F2···O1E	0.99	2.92	3.588(3)	126
C8H–H8H1···O1E	0.99	2.52	3.298(3)	136
C8H–H8H3···O1E	0.99	2.60	3.298(3)	128
C9H–H9H2···O1G	0.99	2.57	3.324(7)	133
C9L–H9L2···O1G	0.99	2.85	3.572(9)	130

C–H···π interactions

C–H···Cg	d(H···Cg)	⊥d(H···π)	d(C···Cg)	∠C–H···Cg	∠C–H···π
C10A–H10B···CgF	3.09	2.97	3.910(3)	140	152
C12B–H12C···CgD[1]	3.37	3.09	3.917(3)	117	137
C13B–H13D···CgE[1]	3.27	2.83	4.248(3)	173	157
C8C–H8C1···CgG[2]	3.68	2.63	4.150(3)	112	153
C7G–H7G2···CgC[3]	2.70	2.70	3.637(3)	159	156
C15F–H15Q···CgB[4]	3.01	2.92	3.949(3)	162	158

Symmetry codes: (1) $-x$, $-0.5 + y$, $0.5 - z$; (2) $-1 + x$, y, z; (3) $1 + x$, y, z; (4) $-x$, $0.5 + y$, $0.5 - z$.

At the first glance, two types of layers parallel to the *bc* crystallographic plane may be distinguished in the crystal structure of tBuC[4]OC$_6$ (cone) each of them comprising exclusively molecules **1** or molecules **2** arranged in alternated 'up-down' or herringbone motif (Fig. 83a and Fig. 83b).

a **b**
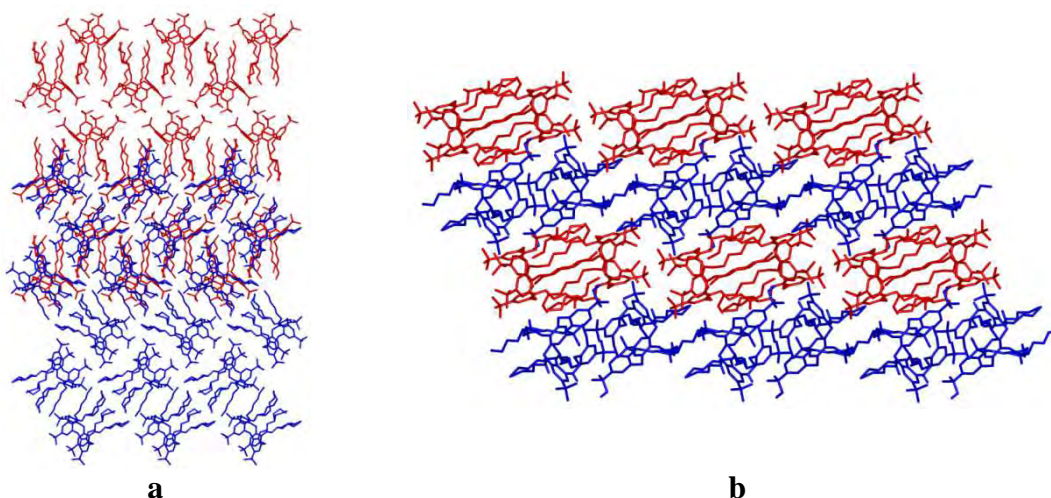
Fig. 83. tBuC[4]OC$_6$ (cone): (a) Layer arrangement, view along the *a* crystallographic axis; (b) Layer arrangement, view along the *b* crystallographic axis, molecules 1 in red, molecules 2 in blue.

Further analysis reveals that molecules **1** are self-assembled in infinite chains in an 'up-down' manner with alkyl chains interdigitated and the aggregation is enhanced by C–H···π interactions (Table 32) between H-atom of the last methylene group of the hexyl chain C13B and π electrons of the ring D (Fig. 84a Molecules **2** play a role of bridge between molecules **1** from adjacent chains (Fig. 84b) due to C–H···π interactions. The stronger C–H···π interactions occur between H-atoms of the first methylene group of the chain C8C and aromatic ring G and methylene bridge C7G and aromatic ring C. The weaker C–H···π interactions are between H-atoms of terminal atom C13B of the chain B and aromatic ring E and third methylene group of the chain C10A and aromatic ring F. The bridging role of molecules **2** results in the formation of a layer parallel to the *ab* crystallographic plane (Fig. 84c). Layers are combined in three-dimensional structure by weak van der Waals interactions only.
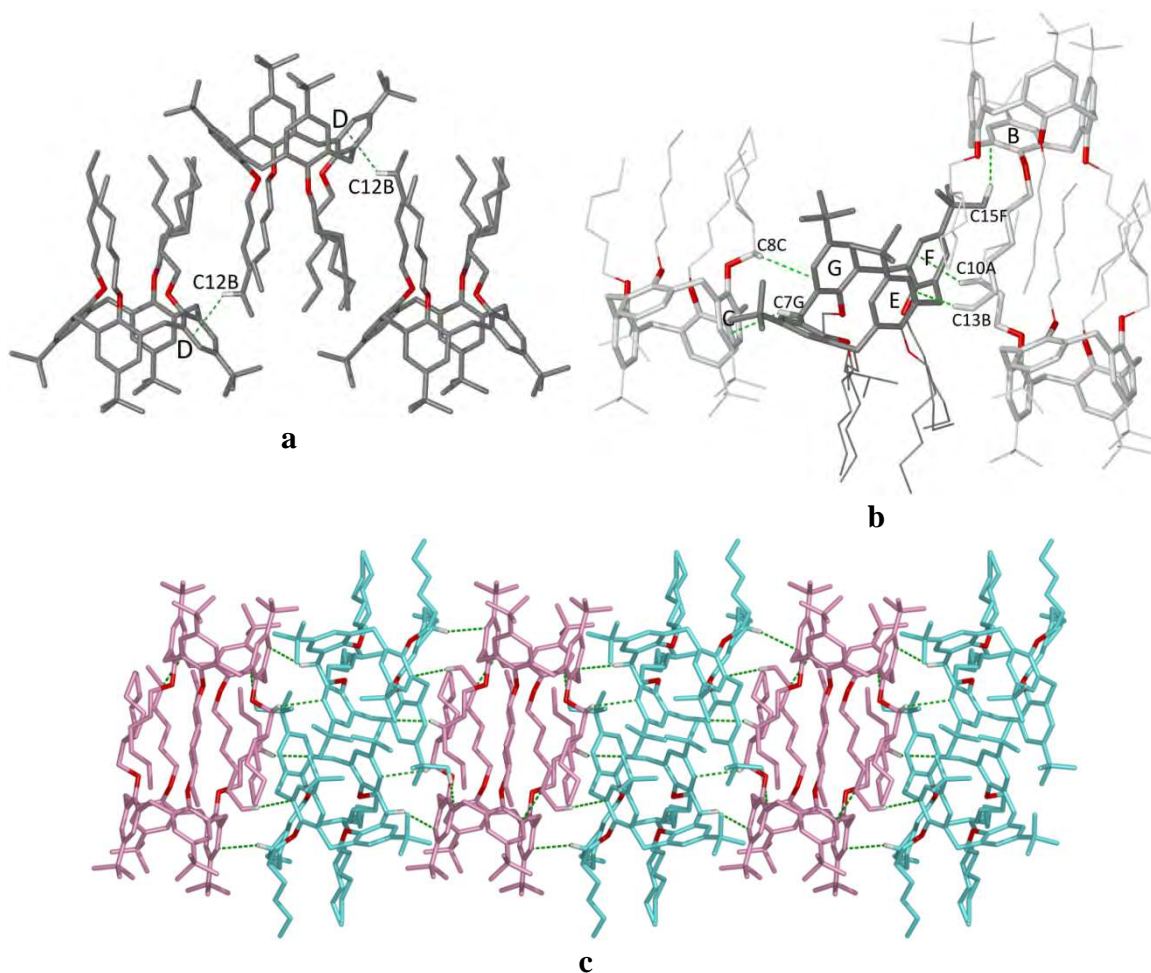
Fig. 84. tBuC[4]OC$_6$ (cone): (a) C–H···π interactions between molecules 1 itself; (b) C–H···π interactions between molecule 2 and adjacent molecules 1, (c) C–H···π interactions between molecules 1 (pink) and molecules 2 (bluish).

4.2.9 Crystal structure of O-hexylated *para-tert*-butylcalix[4]arene (partial cone)

O-Hexylated *para-tert*-butylcalix[4]arene in the partial cone conformation (tBuC[4]OC$_6$ (partial cone)) crystallises from methanol/chloroform mixture in the triclinic crystallographic system. Crystal data are presented in Table 33. Similarly to tBuC[4]OC$_5$ (partial cone), the asymmetric unit of tBuC[4]OC$_6$ (partial cone) comprises two independent molecules of calixarenes that differ by spatial orientation of alkyl chains (Fig. 85a and b). Carbon atom numbering scheme is shown in Fig. 85c. Hexyl chains at rings A, E and F on their whole lengths (except the first and the fourth atoms

Table 33. Crystal data and structure refinement for tBuC[4]OC$_6$ (partial cone)

Molecular formula	C$_{68}$H$_{104}$O$_4$
Formula weight	985.51
Crystal system	Triclinic
Space group	$P\bar{1}$
Unit cell dimensions	a = 10.6051(3) Å $\quad$ α = 90.399(4)°
	b = 20.272(1) Å $\quad$ β = 94.601(4)°
	c = 29.275(1) Å $\quad$ γ = 89.912(2)°
Volume	6273.3(5) Å^3
Z	4
Temperature	100.0(5) K
Radiation and wavelength	Mo $K\alpha$ radiation, λ = 0.71073 Å
Monochromator	graphite
Density (calculated)	1.043 Mg·m^{-3}
Absorption coefficient	0.06 mm^{-1}
$F(000)$	2176
Crystal size	0.07 × 0.10 × 0.25 mm
θ range for data collection	1.2–22.0°
Index ranges	-11 ≤ h ≤ 11, -21 ≤ k ≤ 21, -30 ≤ l ≤ 30
Reflections collected	206219
Independent reflections	15297 [R_{int} = 0.10]
Completeness	100 %
Absorption correction	None
Refinement method	Full-matrix least-squares on F^2
Weighting scheme	$[\sigma^2(F_o^2) + (0.0282P)^2 + 8.9018P]^{-1}$ *
Data / restraints / parameters	15297 / 91 / 1510
Goodness-of-fit on F^2	1.10
Final R indices [$I > 2\sigma(I)$]	R = 0.077, wR = 0.145
R indices (all data)	R = 0.118, wR = 0.157
Extinction coefficient	Not refined
Largest diff. peak and hole	0.31 and -0.23 e·Å^{-3}

* $P = (F_o^2 + 2F_c^2)/3$
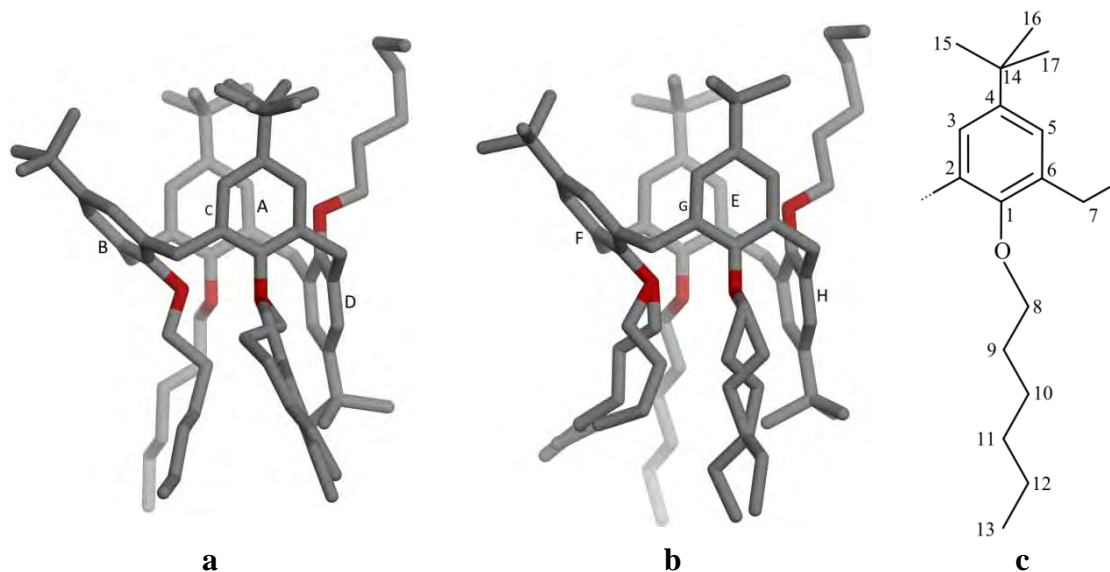
Fig. 85. tBuC[4]OC$_6$ (partial cone): (a) molecule 1; (b) molecule 2; (c) numbering scheme.

at the ring E) are disordered over two positions with occupancy factors of 0.62 and 0.38, 0.53and 0.47 and 0.65 and 0.35. Only one *tert*-butyl group (at the ring A) is disordered over two positions with occupancy factors of 0.82 and 0.18.

Dihedral angles between planes of each benzene ring and the mean plane of the four methylene and distances between distal C4 atoms are presented in Table 34.

Partial cone conformations of calix[4]arene macrocyclic rings are stabilised by two C–H···O intramolecular contacts (Fig. 86) between H-atoms of the second methylene group of hexyl substituents and oxygen atoms of two proximal phenoxy moieties A and C in the case of molecule **1**, and phenyl ring G in the case of molecule **2** (Table 35).
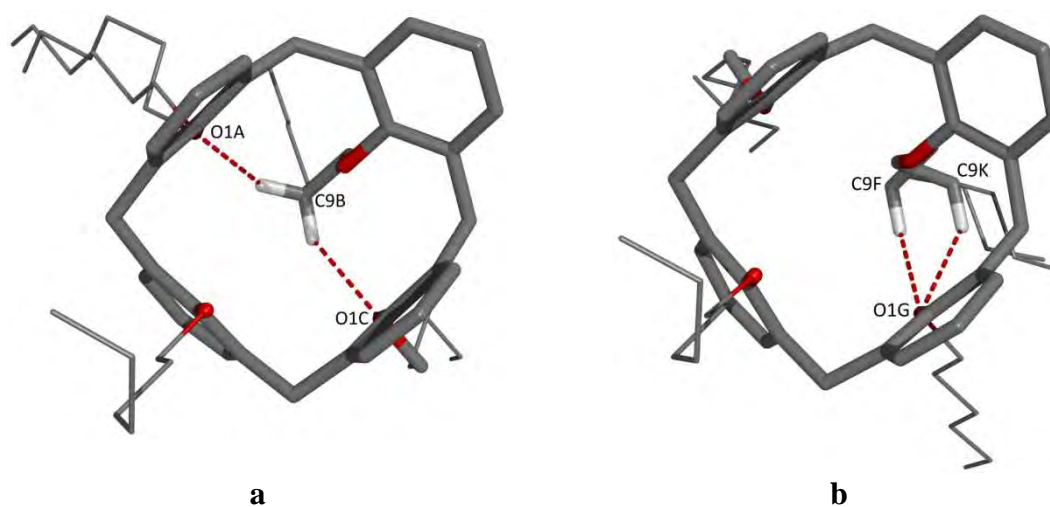
Fig. 86. tBuC[4]OC$_6$ (partial cone) conformation stabilised by C–H···O intramolecular contacts: (a) molecule 1; (b) molecule 2. *Tert*-butyl groups are omitted for clarity.

Table 34. Calix[4]arene macrocyclic ring geometry for tBuC[4]OC$_6$ (partial cone)

∠(ring-to-CH$_2$-plane), °			
1		**2**	
A	97.8(1)	E	92.46(9)
B	135.73(7)	F	133.47(7)
C	90.17(9)	G	99.2(1)
D	-94.24(9)	H	-98.65(9)
Distal C4···C4 distances, Å			
1		**2**	
C4A···C4C	5.834(5)	C4E···C4G	6.014(5)
C4B···C4D	8.932(5)	C4F···C4H	9.031(5)

Molecules **1** with the same spatial orientation (Fig. 87a) participate in C–H···π interactions between H-atoms of the third methylene group (C10A and C10I) of disordered hexyl chain at the ring A and aromatic ring B of adjacent calix[4]arene molecule. As previously observed in crystal structures of tBuC[4]OC$_5$ (partial cone) molecules **2** play a role of bridge between molecules **1** (Fig. 87b), which results in layered self-assembly (parallel to the *ab* crystallographic plane) shown in Fig. 87c. Molecule **2** is involved in five C–H···π interactions (Fig. 87b and Table 35).

Like the crystal structure of tBuC[4]OC$_3$ (partial cone)·0.5CHCl$_3$ and tBuC[4]OC$_5$ (partial cone) one side of the layer is richer in *tert*-butyl groups while the other one is richer in *n*-alkyl chains. Layers are joined by weak van der Waals

Table 35. Weak interactions in tBuC[4]OC$_6$ (partial cone)

Hydrogen bonds

D–H···*A*	*d*(*D*–H), Å	*d*(H···*A*), Å	*d*(*D*···*A*), Å	∠*D*–H···*A*
C9B–H9B1···O1A	0.99	2.57	3.412(5)	143
C9B–H9B2···O1C	0.99	2.73	3.566(5)	142
C9F–H9F1···O1G	0.99	2.77	3.589(7)	140
C9K–H9K1···O1G	0.99	2.69	3.48(1)	137

C–H···π interactions

C–H···Cg	*d*(H···Cg)	⊥*d*(H···π)	*d*(C···Cg)	∠C–H···Cg	∠C–H···π
C10A–H10B···CgB[1]	3.56	2.79	4.55(1)	175	137
C15B–H15E···CgE[2]	2.87	2.83	3.720(5)	145	154
C15B–H15F···CgH[3]	3.21	2.88	4.034(5)	143	133
C15F–H15Q···CgC[1]	3.63	2.70	4.348(6)	132	149
C16F–H16P···CgD	3.23	2.86	4.050(5)	142	133
C16F–H16Q···CgC[1]	2.91	2.89	3.743(5)	144	150
C10I–H10Q···CgB[1]	3.53	2.77	4.50(1)	167	144

Symmetry codes: (1) 1 + *x*, *y*, *z*; (2) −1 + *x*, −1 + *y*, *z*; (3) *x*, −1 + *y*, *z*.

; :
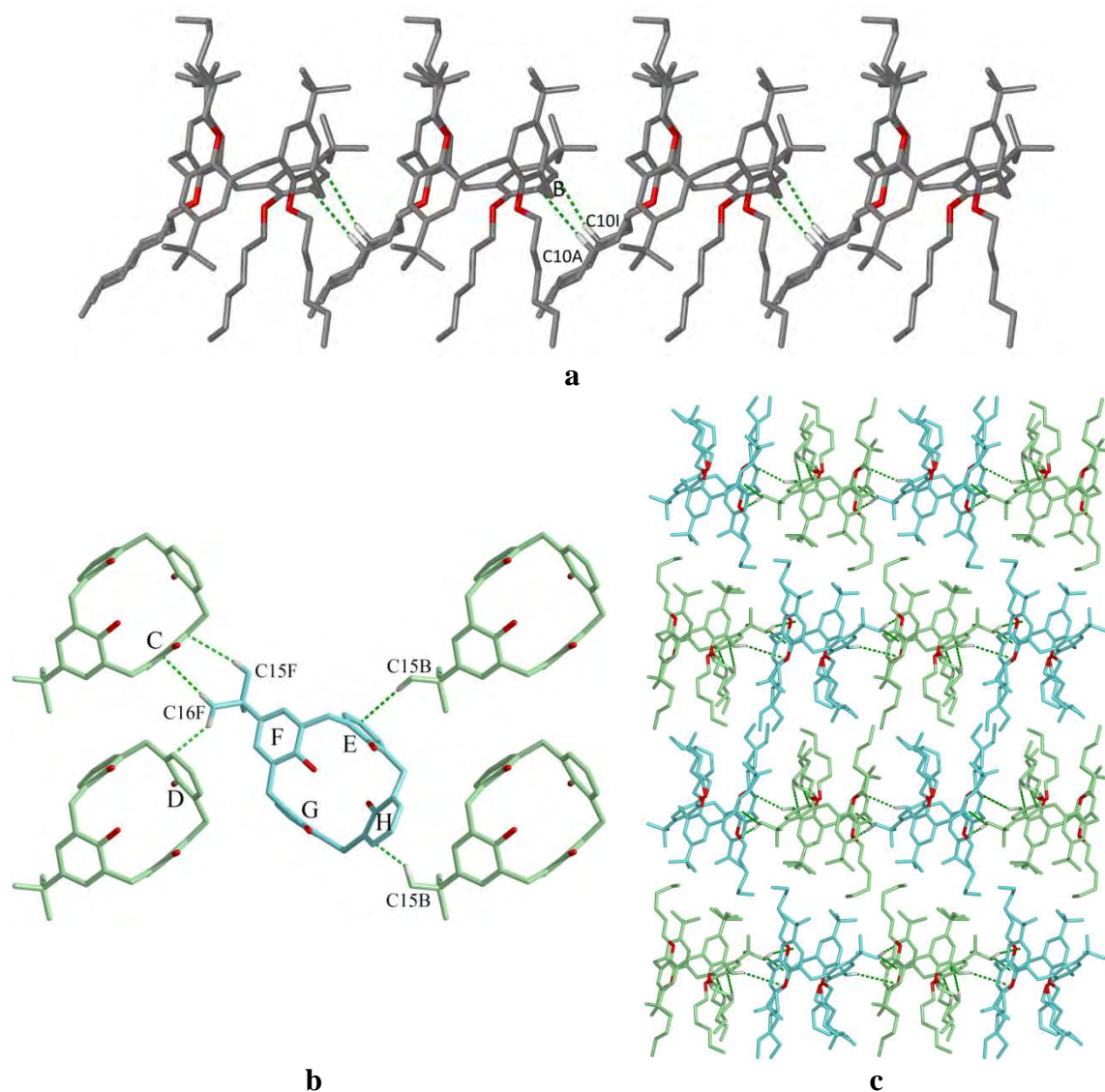
Fig. 87. tBuC[4]OC$_6$ (partial cone): (a) infinite chains of molecules 1 along the *a* crystallographic axis; (b) molecule 2 (bluish) plays a role of bridge between molecules 1 (greenish); (c) packing diagram, view along the *a* crystallographic axis.

interactions only and they are in contact by sides of the same nature forming bilayers with molecular arrangement:

$$\cdots B\cdots A\cdots B\cdots A\cdots B\cdots A\cdots$$

$$\cdots A\cdots B\cdots A\cdots B\cdots A\cdots B\cdots$$
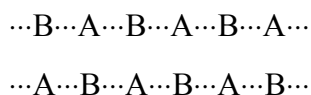
(the layers forming bilayer are shifted by one calixarene). Contrary to tBuC[4]OC$_5$ (partial cone), bilayers are not shifted.

4.2.10 Crystal structure of O-heptylated *para-tert*-butylcalix[4]arene (partial cone)

O-Heptylated *para-tert*-butylcalix[4]arene in the partial cone conformation (tBuC[4]OC$_7$ (partial cone)) crystallises from methanol/chloroform mixture in the

; ;

monoclinic crystallographic system. Crystal data are presented in Table 36. Contrary to tBuC[4]OC$_5$ (partial cone) and tBuC[4]OC$_6$ (partial cone), the asymmetric unit of tBuC[4]OC$_7$ (partial cone) comprises only one molecule of the calixarene (Fig. 88a). Carbon atom numbering scheme is shown in Fig. 88b. Alkyl substituents are highly disordered in this crystal structure. Three end atoms of heptyl chain at the ring A are disordered over two positions with occupancy factors of 0.71and 0.29. Heptyl chains at rings B, C and D on their whole length (except the first and last carbon atoms of the chain at the ring C) are also disordered over two positions. Occupancy factors are 0.67 and 0.33 [ring B], 0.73 and 0.27 [ring C] and 0.59 and 0.41 [ring D]. Terminal carbon

Table 36. Crystal data and structure refinement for tBuC[4]OC$_7$ (partial cone)

Molecular formula	C$_{72}$H$_{112}$O$_4$
Formula weight	1041.62
Crystal system	Monoclinic
Space group	*Cc*
Unit cell dimensions	*a* = 33.5463(6) Å
	b = 10.5294(3) Å β = 114.888(1)°
	c = 20.4909(5) Å
Volume	6565.7(3) Å^3
Z	4
Temperature	100.0(5) K
Radiation and wavelength	Mo *Kα* radiation, λ = 0.71073 Å
Monochromator	graphite
Density (calculated)	1.054 Mg·m^{-3}
Absorption coefficient	0.06 mm^{-1}
F(000)	2304
Crystal size	0.05 × 0.10 × 0.20 mm
θ range for data collection	2.8–21.2°
Index ranges	-34 ≤ *h* ≤ 34, -10 ≤ *k* ≤ 10, -20 ≤ *l* ≤ 20
Reflections collected	51632
Independent reflections	7257 [*R*$_{int}$ = 0.090]
Completeness	98.9 %
Absorption correction	None
Refinement method	Full-matrix least-squares on *F*^{2}
Weighting scheme	[$\sigma^2(F_o^2) + (0.0711P)^2 + 8.0872P$]$^{-1}$ *
Data / restraints / parameters	7257 / 331 / 1022
Goodness-of-fit on *F*^{2}	1.03
Final *R* indices [*I* > 2σ(*I*)]	*R* = 0.059, *wR* = 0.138
R indices (all data)	*R* = 0.073, *wR* = 0.148
Extinction coefficient	0.0017(2)
Largest diff. peak and hole	0.28 and -0.19 e·Å^{-3}

* $P = (F_o^2 + 2F_c^2)/3$
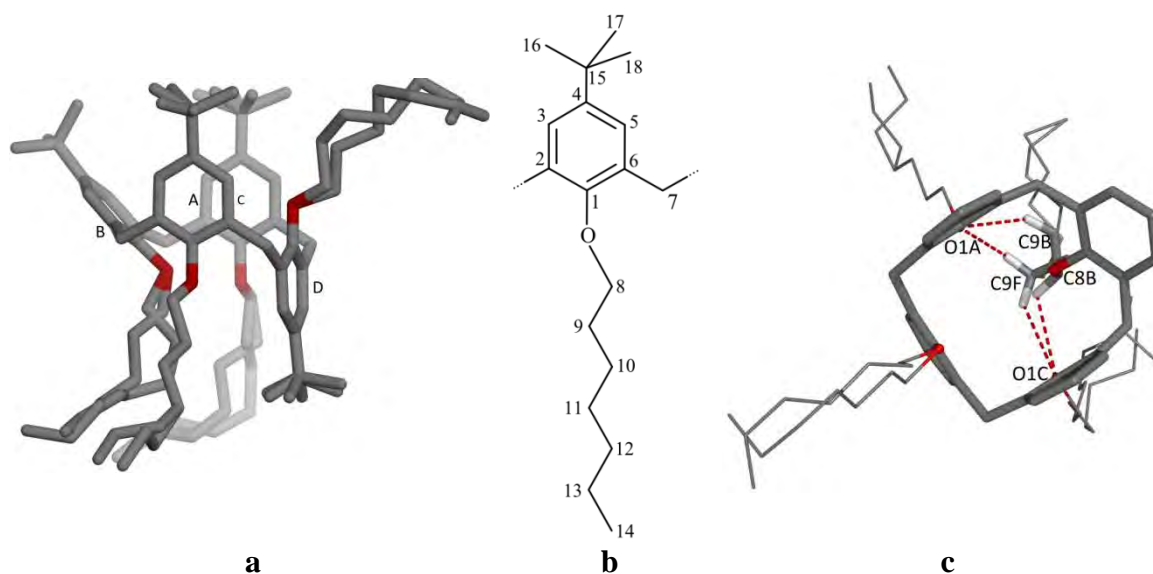
Fig. 88. tBuC[4]OC$_7$ (partial cone): (a) asymmetric unit; (b) numbering scheme; (c) conformation stabilised by C–H···O intramolecular contacts, *tert*-butyl groups are omitted for clarity.

atom of heptyl chain at the ring C is disordered over three positions with occupancy factors of 0.46, 0.27 and 0.27. Three of four *tert*-butyl groups are disordered over two positions with occupancy factors of 0.75 and 0.25, 0.51 and 0.49, and 0.54 and 0.46 for rings A, C and D, respectively.

Dihedral angles between planes of each benzene ring and the mean plane of the four methylene groups and distances between distal C4 atoms are presented in Table 37.

Table 37. Calix[4]arene macrocyclic ring geometry for tBuC[4]OC$_7$ (partial cone)

∠(ring-to-CH$_2$-plane), °		Distal C4···C4 distances, Å	
A	96.4(1)	C4A···C4C	5.788(6)
B	134.3(1)		
C	90.8(1)	C4B···C4D	8.880(6)
D	-93.2(1)		

A partial cone conformation of tBuC[4]OC$_7$ is stabilised by four C–H···O intramolecular contacts (Fig. 88c) between H-atoms of the first and the second methylene group of heptyl substituent at the ring B and oxygen atoms of phenoxy moieties A and C (Table 38).

As it was previously observed in tert-butyl C[4]OC$_5$ (partial cone) and tBuC[4]OC$_6$ (partial cone) structures, calix[4]arene molecule participates in C–H···π interactions with four adjacent calix[4]arene molecules and form layers parallel to the *bc* crystallographic plane (in tBuC[4]OC$_5$ (partial cone) and tBuC[4]OC$_6$ (partial cone) the layers were parallel to the *ab* crystallographic plane). C–H···π interactions occur between adjacent molecules (Fig. 89a, Table 38).

123

Table 38. Weak interactions in tBuC[4]OC$_7$ (partial cone)

Hydrogen bonds

D–H···A	d(D–H), Å	d(H···A), Å	d(D···A), Å	∠D–H···A
C8B–H8B1···O1C	0.99	2.97	3.36(1)	105
C9B–H9B2···O1A	0.99	2.77	3.563(8)	137
C9F–H9F1···O1C	0.99	2.95	3.41(1)	140
C9F–H9F2···O1A	0.99	2.64	3.76(1)	135

C–H···π interactions

C–H···Cg	d(H···Cg)	⊥d(H···π)	d(C···Cg)	∠C–H···Cg	∠C–H···π
C16B–H16D···CgD[1]	3.27	2.96	4.006(7)	134	131
C17B–H17D···CgC[2]	3.68	2.72	4.418(7)	134	149
C17H–H17X···CgB[3]	3.32	2.89	4.216(8)	154	159

Symmetry codes: (1) $x, -y, 0.5 + z$; (2) $x, -1 - y, 0.5 + z$; (3) $x, -y, -0.5 + z$.

Van der Waals interaction between layers are probably weaker than in the case of similar crystal structures of tBuC[4]OC$_5$ (partial cone) and tBuC[4]OC$_6$ (partial cone) because of significant disorder of *tert*-butyl and *n*-heptyl substituents located on the surface of each layer (Fig. 89b).

Fig. 89. tBuC[4]OC$_7$ (partial cone): (a) C–H···π interactions with neighbouring molecules, *n*-heptyl and *tert*-butyl substituents which do not take part in C–H···π interactions are omitted for clarity; (b) packing diagram, view along the *b* crystallographic axis.

4.2.11 Crystal structure of O-octylated *para-tert*-butylcalix[4]arene (partial cone)

O-Octylated *para-tert*-butylcalix[4]arene in a partial cone conformation (tBuC[4]OC$_8$ (partial cone)) crystallises from methanol/chloroform mixture in the monoclinic crystallographic system. Crystal data are presented in Table 39. The asymmetric unit comprises one molecule of the calix[4]arene which adopts a partial

Table 39. Crystal data and structure refinement for tBuC[4]OC$_8$ (partial cone)

Molecular formula	C$_{76}$H$_{120}$O$_4$
Formula weight	1097.72
Crystal system	Monoclinic
Space group	*Cc*
Unit cell dimensions	*a* = 36.544(2) Å
	b = 10.5863(7) Å *β* = 113.648(3)°
	c = 20.199(1) Å
Volume	7158.1(8) Å^3
Z	4
Temperature	100.0(5) K
Radiation and wavelength	Mo *Kα* radiation, *λ* = 0.71073 Å
Monochromator	graphite
Density (calculated)	1.019 Mg·m^{-3}
Absorption coefficient	0.06 mm^{-1}
F(000)	2432
Crystal size	0.10 × 0.12 × 0.24 mm
θ range for data collection	2.9–24.1°
Index ranges	-41 ≤ *h* ≤ 42, -12 ≤ *k* ≤ 12, -23 ≤ *l* ≤ 23
Reflections collected	13933
Independent reflections	9062 [*R*$_{int}$ = 0.015]
Completeness	99.5 %
Absorption correction	None
Refinement method	Full-matrix least-squares on *F*^{2}
Weighting scheme	[$\sigma^2(F_o^2) + (0.0871P)^2 + 37.494P$]$^{-1}$ *
Data / restraints / parameters	9062 / 2 / 738
Goodness-of-fit on *F*^{2}	1.11
Final *R* indices [*I* > 2σ(*I*)]	*R* = 0.092, *wR* = 0.225
R indices (all data)	*R* = 0.104, *wR* = 0.233
Extinction coefficient	0.0130(8)
Largest diff. peak and hole	0.35 and -0.35 e·Å^{-3}

* $P = (F_o^2 + 2F_c^2)/3$

cone conformation and is shown in Fig. 90a. Carbon atom numbering scheme is shown in Fig. 90b. Surprisingly, there is no disorder of alkyl chains.

Dihedral angles between planes of each benzene ring and the mean plane of the four methylene and distances between distal C4 are presented in Table 40.

Table 40. Calix[4]arene macrocyclic ring geometry for tBuC[4]OC$_8$ (partial cone)

| ∠(ring-to-CH$_2$-plane), °		Distal C4···C4 distances, Å	
A	99.8(2)	C4A···C4C	5.909(8)
B	133.2(2)		
C	90.5(1)	C4B···C4D	9.124(8)
D	-100.1(2)		
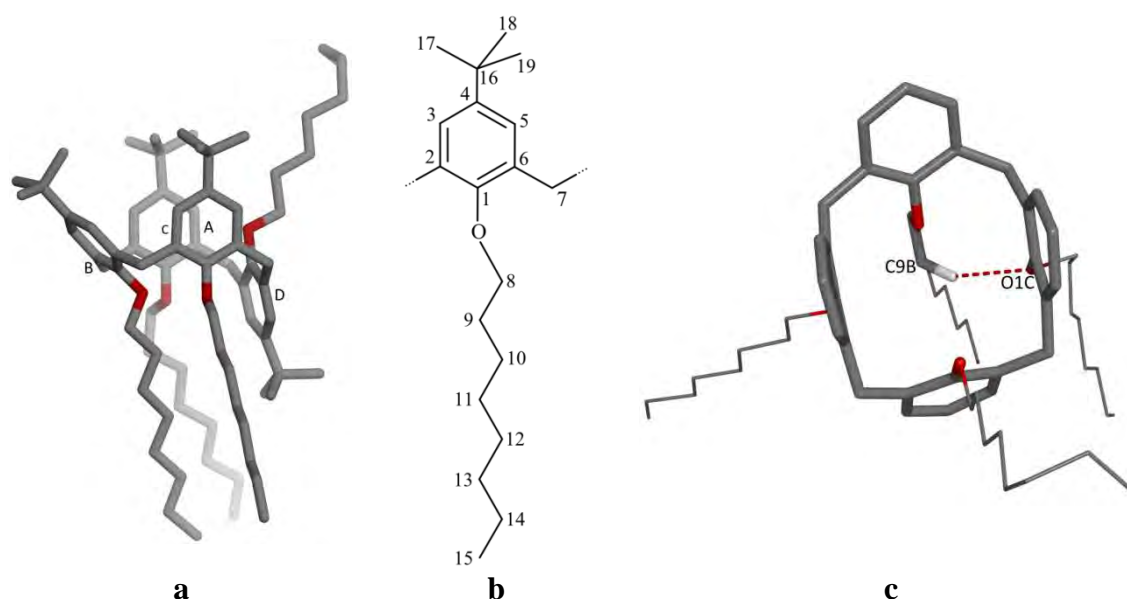
Fig. 90. tBuC[4]OC$_8$ (partial cone): (a) asymmetric unit; (b) numbering scheme; (c) conformation stabilised by C–H···O intramolecular contacts, *tert*-butyl groups are omitted for clarity.

Contrary to tBuC[4]OC$_7$ (partial cone), a partial cone conformation of tBuC[4]OC$_8$ (partial cone) is stabilised by only one C–H···O intramolecular contact between H-atoms of the second methylene group of octyl chain at the ring B and phenoxy moiety C (Fig. 90c) with C9B···O1C distance equals to 3.499(8) Å.

Table 41. Weak interactions in tBuC[4]OC$_8$ (partial cone)

Hydrogen bond				
D–H···A	$d(D$–H), Å	d(H···A), Å	$d(D$···A), Å	$\angle D$–H···A
C9B–H9B2···O1C	0.99	2.63	3.499(8)	147

C–H···π interactions					
C–H···Cg	d(H···Cg)	$\perp d$(H···π)	d(C···Cg)	$\angle$C–H···Cg	$\angle$C–H···π
C17B–H17E···CgC[1]	2.86	2.78	3.661(8)	139	153
C17B–H17F···CgD[2]	3.32	2.94	4.099(8)	138	130
C17D–H17L···CgB[3]	3.06	2.88	3.96(1)	154	155

Symmetry codes: (1) x, $-y$, $-0.5 + z$; (2) x, $1 - y$, $-0.5 + z$; (3) x, $1 - y$, $0.5 + z$.

Similarly to the three previously discussed structures, molecule of tBuC[4]OC$_8$ participates in C–H···π interactions to four adjacent calix[4]arene molecules but only H-atoms of *tert*-butyl substituents participate in these interactions (Fig. 91a and Table 41). C–H···π interactions result in self-assembly of tBuC[4]OC$_8$ molecules in corrugated layers, parallel to the *bc* crystallographic plane (Fig. 91b). Only van der Waals interactions between *tert*-butyl and *n*-octyl substituents from adjacent layers are observed.
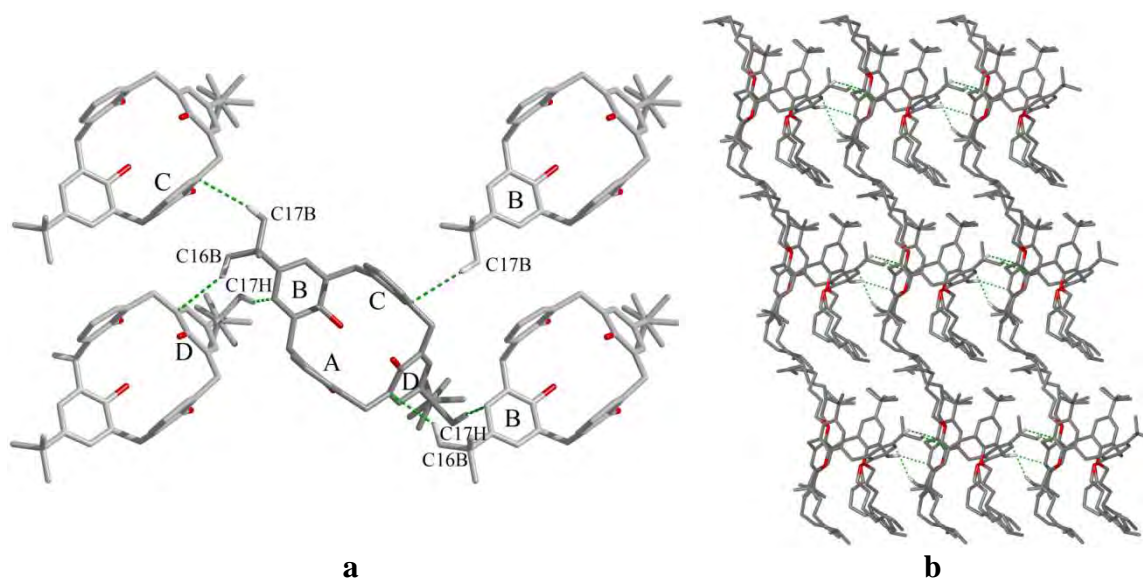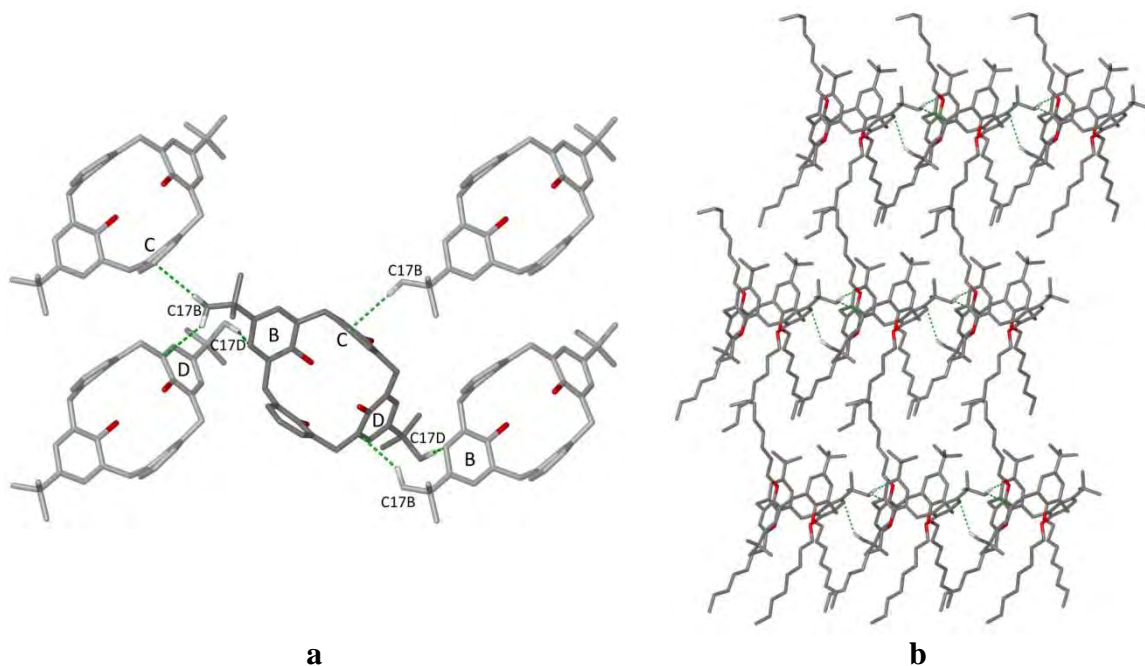
Fig. 91. tBuC[4]OC$_8$ (partial cone): (a) C–H···π interactions with neighbouring molecules, *n*-octyl and *tert*-butyl substituents which do not participate in C–H···π interactions are omitted for clarity; (b) packing diagram, view along the *b* crystallographic axis.

4.2.12 Crystal structure of O-octylated *para-tert*-butylcalix[4]arene (1,3-alternate)

O-Octylated *para-tert*-butylcalix[4]arene in 1,3-alternate conformation (tBuC[4]OC$_8$ (1,3-alternate)) crystallises from methanol/chloroform mixture in the monoclinic crystallographic system. Crystal data are presented in Table 42. The asymmetric unit comprises two molecules of the calix[4]arene which adopt the 1,3-alternate conformation (Fig. 92a and b). Carbon atom numbering scheme is shown in
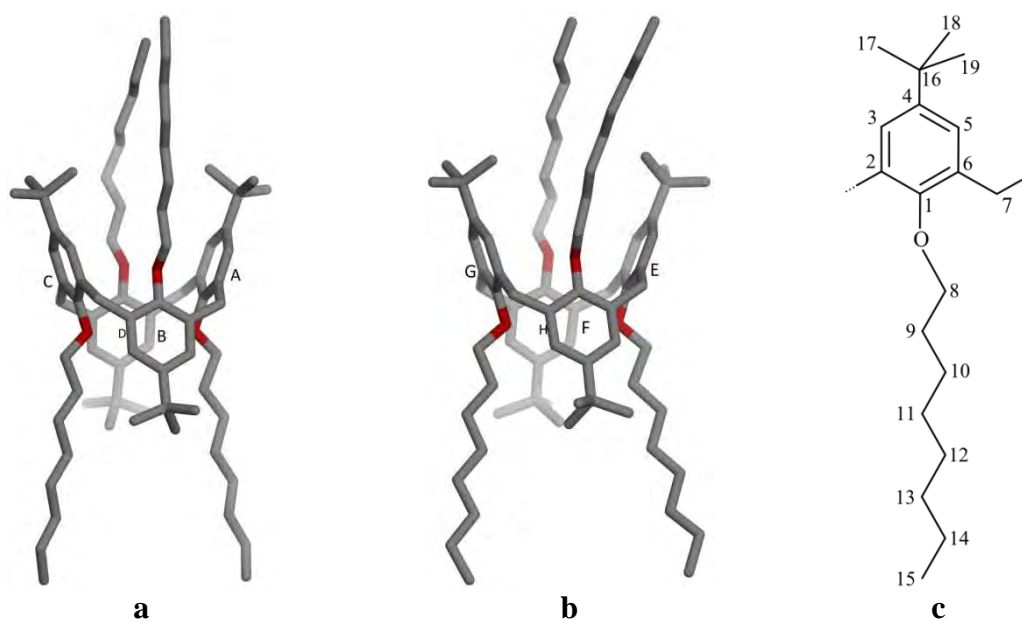
Fig. 92. tBuC[4]OC$_8$ (1,3-alternate): (a) molecule 1; (b) molecule 2; (c) numbering scheme.

107

Table 42. Crystal data and structure refinement for tBuC[4]OC$_8$ (1,3-alternate)

Molecular formula	C$_{76}$H$_{120}$O$_4$
Formula weight	1097.72
Crystal system	Monoclinic
Space group	Pc
Unit cell dimensions	a = 10.4600(4) Å
	b = 38.3011(8) Å $\quad$ β =109.653(1)°
	c = 18.6303(5) Å
Volume	7029.1(4)Å^3
Z	4
Temperature	100.0(5) K
Radiation and wavelength	Mo $K\alpha$ radiation, λ = 0.71073 Å
Monochromator	graphite
Density (calculated)	1.037 Mg·m^{-3}
Absorption coefficient	0.06 mm^{-1}
F(000)	2432
Crystal size	0.10 × 0.12 × 0.15 mm
θ range for data collection	2.8–20.5°
Index ranges	-10 ≤ h ≤ 10, -37 ≤ k ≤ 37, -18 ≤ l ≤ 17
Reflections collected	27923
Independent reflections	11437 [R_{int} = 0.111]
Completeness	95.5 %
Absorption correction	None
Refinement method	Full-matrix least-squares on F^2
Weighting scheme	$[\sigma^2(F_o^2) + (0.0687P)^2 + 10.6008P]^{-1}$ *
Data / restraints / parameters	11437 / 0 / 1473
Goodness-of-fit on F^2	1.08
Final R indices [$I > 2\sigma(I)$]	R = 0.073, wR = 0.176
R indices (all data)	R = 0.087, wR = 0.185
Extinction coefficient	Not refined
Largest diff. peak and hole	0.31 and -0.22 e·Å^{-3}

$* \ P = (F_o^2 + 2F_c^2)/3$

Fig. 92c. No disorder of the alkyl chains was observed.

Dihedral angles between planes of each benzene ring and the mean plane of the four methylene groups and distances between distal C4 atoms are presented in Table 43.

Table 43. Calix[4]arene macrocyclic ring geometry for tBuC[4]OC$_8$ (1,3-alternate)

∠(ring-to-CH$_2$-plane), °			
1		**2**	
A	108.6(2)	E	111.9(2)
B	-108.6(2)	F	-107.6(2)
C	107.4(2)	G	107.9(2)
D	-107.6(2)	H	-103.5(2)

Table 43. Continuation.

Distal C4···C4 distances, Å			
1		**2**	
C4A···C4C	6.982(9)	C4E···C4G	7.11(1)
C4B···C4D	6.845(9)	C4F···C4H	6.675(9)

Similarly to the previously discussed tBuC[4]OC$_8$ (partial cone) structure, molecules of tBuC[4]OC$_8$ (1,3-alternate) participate in C–H···π interactions between H-atoms of *tert*-butyl substituents and aromatic rings of four adjacent molecules (Fig. 93a and b). Molecules **1** interact exclusively with molecules **1** and similarly, molecules **2** interact exclusively with molecules **2** (Table 44). Molecules **1** and molecules **2** are self-assembled in layers parallel to the *ac* crystallographic plane (Fig. 93c). Calix[4]arene molecules in the layers are arranged in 'up-down' mode and are related by a *c*-glide plane.

Alkyl chains are located on both sides of the layer and interdigitate with these belonging to the adjacent layers.
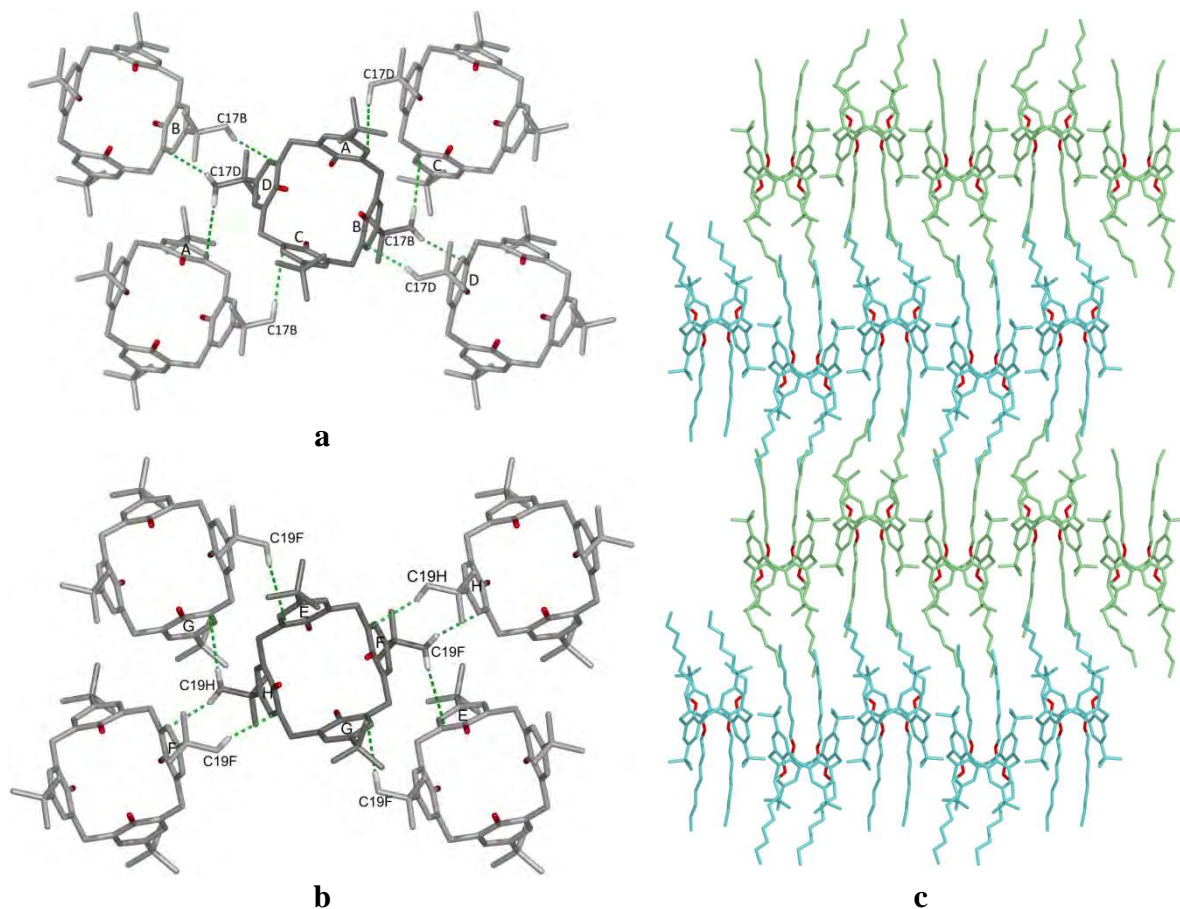
Fig. 93. tBuC[4]OC$_8$ (1,3-alternate): (a) C–H···π interactions between molecules 1; (b) C–H···π interactions between molecules 2, *n*-octyl substituents are omitted for clarity; (c) packing diagram, view along the *a* crystallographic axis.

Table 44. Weak interactions in tBuC[4]OC$_8$ (1,3-alternate)

C–H···π interactions

C–H···Cg	d(H···Cg)	⊥d(H···π)	d(C···Cg)	∠C–H···Cg	∠C–H···π
C17B–H17E···CgC[1]	3.09	3.01	3.828(1)	133	143
C17B–H17D···CgD[2]	3.18	2.67	4.137(1)	166	145
C17D–H17L···CgA[3]	3.07	2.98	3.822(1)	138	149
C17D–H17K···CgB[4]	3.20	2.66	4.127(1)	158	146
C19F–H19Q···CgE[5]	3.33	3.19	4.046(1)	131	145
C19F–H19R···CgH[6]	3.21	2.73	4.146(1)	160	148
C19H–H19W···CgF[7]	3.24	2.67	4.196(1)	164	145
C19H–H19V···CgG[8]	3.15	2.98	3.752(1)	122	138

Symmetry codes: (1) x, $1 − y$, $0.5 + z$; (2) $1 + x$, $1 − y$, $0.5 + z$; (3) x, $1 − y$, $−0.5 + z$; (4) $−1 + x$, $1 − y$, $−0.5 + z$; (5) x, $2 − y$, $−0.5 + z$; (6) $−1 + x$, $2 − y$, $−0.5 + z$; (7) $1 + x$, $2 − y$, $0.5 + z$.; (8) x, $2 − y$, $0.5 + z$.

4.2.13 Crystal structure of O-nonylated *para-tert*-butylcalix[4]arene (cone)

O-Nonylated *para-tert*-butylcalix[4]arene (tBuC[4]OC$_9$) crystallises from methanol/chloroform mixture in the monoclinic crystallographic system. Crystal data are presented in Table 45. The asymmetric unit comprises one molecule of the calix[4]arene which adopts a flattened cone conformation (Fig. 94a). Carbon atom numbering scheme is shown in Fig. 94b. The nonyl chain at the ring C is disordered over two positions on its whole length (except the first carbon atom) with equal occupancy factors of 0.5.

a   **b**   **c**
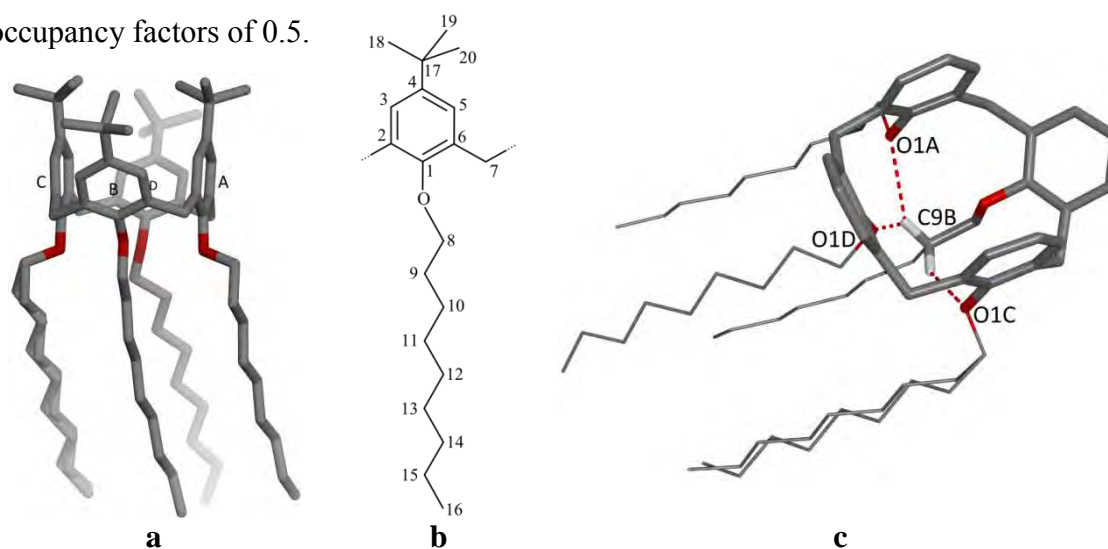
Fig. 94. tBuC[4]OC$_9$ (cone): (a) asymmetric unit; (b) numbering scheme; (c) conformation stabilised by C–H···O intramolecular contacts, *tert*-butyl groups at the upper rim are omitted for clarity.

Dihedral angles between planes of each benzene ring and the mean plane of the four methylene groups and distances between distal C4 atoms are presented in Table 46.

Table 45. Crystal data and structure refinement for tBuC[4]OC₉ (cone)

Molecular formula	$C_{80}H_{128}O_4$
Formula weight	1153.82
Crystal system	Monoclinic
Space group	$P2_1/c$
Unit cell dimensions	$a = 16.8347(7)$ Å
	$b = 32.617(1)$ Å $\beta = 100.109 (3)°$
	$c = 13.7053(4)$ Å
Volume	7408.6(5) Å^3
Z	4
Temperature	100.0(1) K
Radiation and wavelength	Cu $K\alpha$ radiation, $\lambda = 1.54184$ Å
Monochromator	Mirror
Density (calculated)	1.034 Mg·m^{-3}
Absorption coefficient	0.46 mm^{-1}
$F(000)$	2560
Crystal size	$0.05 \times 0.18 \times 0.23$ mm
θ range for data collection	3.0–72.1°
Index ranges	$-15 \leq h \leq 20, -37 \leq k \leq 39, -16 \leq l \leq 16$
Reflections collected	28405
Independent reflections	14289 [$R_{int} = 0.064$]
Completeness	100.0 %
Absorption correction	Multi-scan*
Refinement method	Full-matrix least-squares on F^2
Weighting scheme	$[\sigma^2(F_o^2) + (0.0349P)^2]^{-1}$ **
Data / restraints / parameters	14289 / 27 / 847
Goodness-of-fit on F^2	0.97
Final R indices [$I > 2\sigma(I)$]	$R = 0.073$, $wR = 0.142$
R indices (all data)	$R = 0.140$, $wR = 0.174$
Extinction coefficient	Not refined
Largest diff. peak and hole	0.26 and -0.23 e·Å^{-3}

> * Empirical absorption correction using spherical harmonics, implemented in SCALE3 ABSPACK scaling algorithm of *CrysAlis PRO* program package.[138]
> ** $P = (F_o^2 + 2F_c^2)/3$

Table 46. Calix[4]arene macrocyclic ring geometry for tBuC[4]OC₉ (cone)

	$\angle$(ring-to-CH₂-plane), °	Distal C4···C4 distances, Å	
A	92.16(7)	C4A···C4C	5.595(4)
B	131.13(5)		
C	90.79(7)	C4B···C4D	9.117(4)
D	128.12(7)		

The calix[4]arene conformation is stabilised by three C–H···O intramolecular contacts between H-atoms of the second methylene group of the alkyl chain B and oxygen atoms of phenoxy moieties A and C (Fig. 94c, Table 47).

Table 47. Weak interactions in tBuC[4]OC$_9$ (cone)

Hydrogen bonds

D–H⋯A	d(D–H), Å	d(H⋯A), Å	d(D⋯A), Å	∠D–H⋯A
C9B–H9B1⋯O1A	0.99	2.62	3.481(4)	145
C9B–H9B1⋯O1D	0.99	2.95	3.535(4)	119
C9B–H9B2⋯O1C	0.99	2.60	3.473(4)	147

C–H⋯π interactions

C–H⋯Cg	d(H⋯Cg)	⊥d(H⋯π)	d(C⋯Cg)	∠C–H⋯Cg	∠C–H⋯π
C18B–H18E⋯CgA[1]	2.82	2.81	3.631(4)	141	141
C19B–H19F⋯CgD[2]	2.75	2.70	3.673(4)	158	167
C3D–H3D⋯CgC[3]	3.75	2.89	4.652(4)	159	150

Symmetry codes: (1) x, $0.5 - y$, $0.5 + z$; (2) x, y, $1 + z$; (3) $2 - x$, $1 - y$, $2 - z$.

Molecules with the same spatial orientation related by c-glide plane are involved in C–H⋯π interactions between H-atoms of *tert*-butyl groups at rings B and π-electrons of rings A of adjacent calix[4]arene molecules (interaction C18B⋯ring A, Table 47) forming ribbons shown in Fig. 95a. Ribbons are additionally stabilised by C–H⋯π interactions between H-atom of C19B carbon atom of *tert*-butyl groups at the rings B and aromatic rings D of adjacent calix[4]arene molecules. Neighbouring ribbons with

a

b
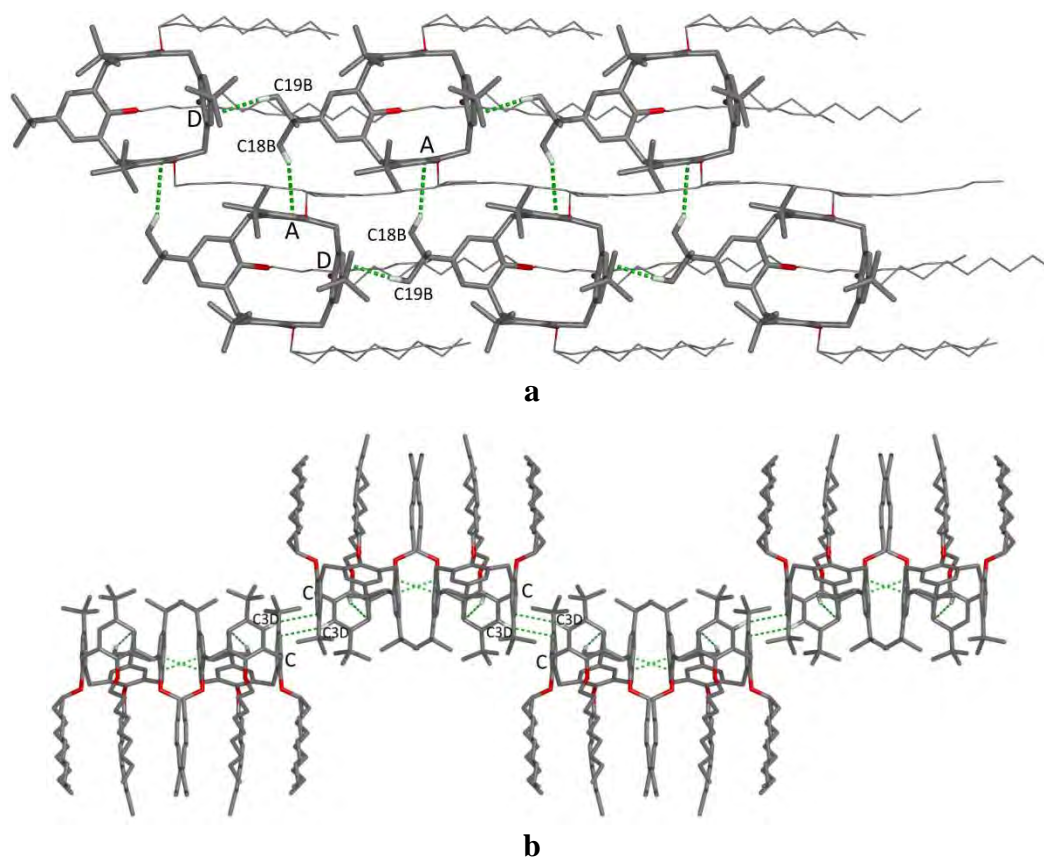
Fig. 95. tBuC[4]OC$_9$ (cone): (a) self-assembly of calix[4]arene molecules in ribbon along the c crystallographic axis; (b) corrugated layer.

112
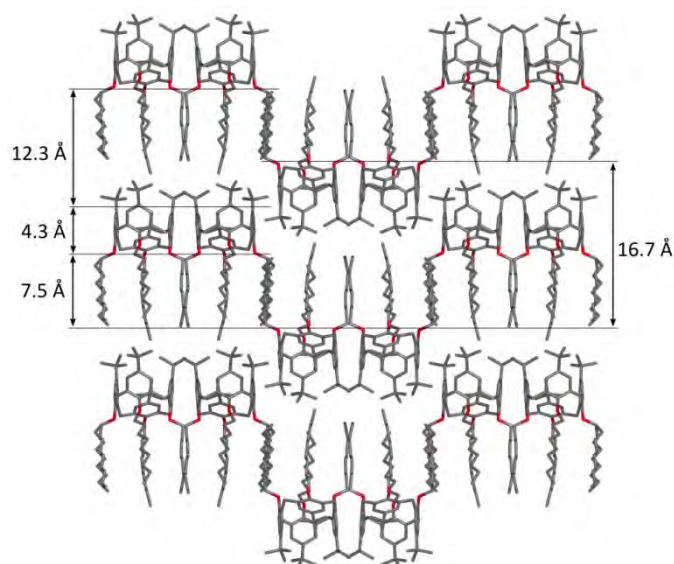
Fig. 96. tBuC[4]OC₉ (cone): packing diagram, view along the *c* crystallographic axis.

opposite spatial orientation of calix[4]arene molecules participate in weak C–H···π interactions [C3D···ring C] between centrosymmetrically related molecules forming corrugated layers parallel to the *bc* crystallographic plane (Fig. 95b). Layers are self-assembled by van der Waals interactions between long alkyl chains (Fig. 96). The thickness of aromatic layers is *ca.* 4.3 Å, whereas the thickness of aliphatic parts is *ca.* 12.3. Å.

4.2.14 Crystal structure of O-decylated *para-tert*-butylcalix[4]arene (cone) chloroform monosolvate

O-Decylated *para-tert*-butylcalix[4]arene crystallises from a methanol/chloroform mixture in the monoclinic crystallographic system as a calix[4]arene-chloroform solvate with stoichiometry 1:1 (tBuC[4]OC₁₀·CHCl₃). Crystal data are presented in Table 48.

Table 48. Crystal data and structure refinement for tBuC[4]OC₁₀ (cone)·CHCl₃

Molecular formula	$C_{84}H_{136}O_4 \cdot CHCl_3$
Formula weight	1329.30
Crystal system	Monoclinic
Space group	$P2_1/c$
Unit cell dimensions	$a = 26.9568(6)$ Å
	$b = 15.6435(4)$ Å $\beta = 105.384(1)°$
	$c = 20.3604(5)$ Å
Volume	$8278.3(3)$ Å^3
Z	4
Temperature	100.0(5) K
Radiation and wavelength	Mo Kα radiation, $\lambda = 0.71073$ Å
Monochromator	graphite

113

Table 48. Continuation.

Density (calculated)	1.067 Mg·m^{-3}
Absorption coefficient	0.16 mm^{-1}
F(000)	2920
Crystal size	0.03 × 0.04 × 0.37 mm
θ range for data collection	2.8–20.8°
Index ranges	-26 ≤ h ≤ 26, -15 ≤ k ≤ 15, -20 ≤ l ≤ 20
Reflections collected	51443
Independent reflections	8627 [R_{int} = 0.048]
Completeness	99.9 %
Absorption correction	None
Refinement method	Full-matrix least-squares on F^2
Weighting scheme	$[\sigma^2(F_o^2) + (0.092P)^2 + 22.8196P]^{-1}$ *
Data / restraints / parameters	8627 / 164 / 1057
Goodness-of-fit on F^2	1.06
Final R indices [$I > 2\sigma(I)$]	R = 0.094, wR = 0.225
R indices (all data)	R = 0.124, wR = 0.242
Extinction coefficient	Not refined
Largest diff. peak and hole	0.43 and -0.40 e·Å^{-3}

* $P = (F_o^2 + 2F_c^2)/3$

The asymmetric unit comprises one molecule of the host and one molecule of the guest (Fig. 97a). Carbon atom numbering scheme is shown in Fig. 97b. Decyl chain at the ring D is disordered over two positions with occupancy factors of 0.55 and 0.45 along its whole length. Two of four *tert*-butyl groups [rings B and C] are also disordered [occupancy factors of 0.56 and 0.44, and 0.77 and 0.23 for B and C, respectively]. Decyl
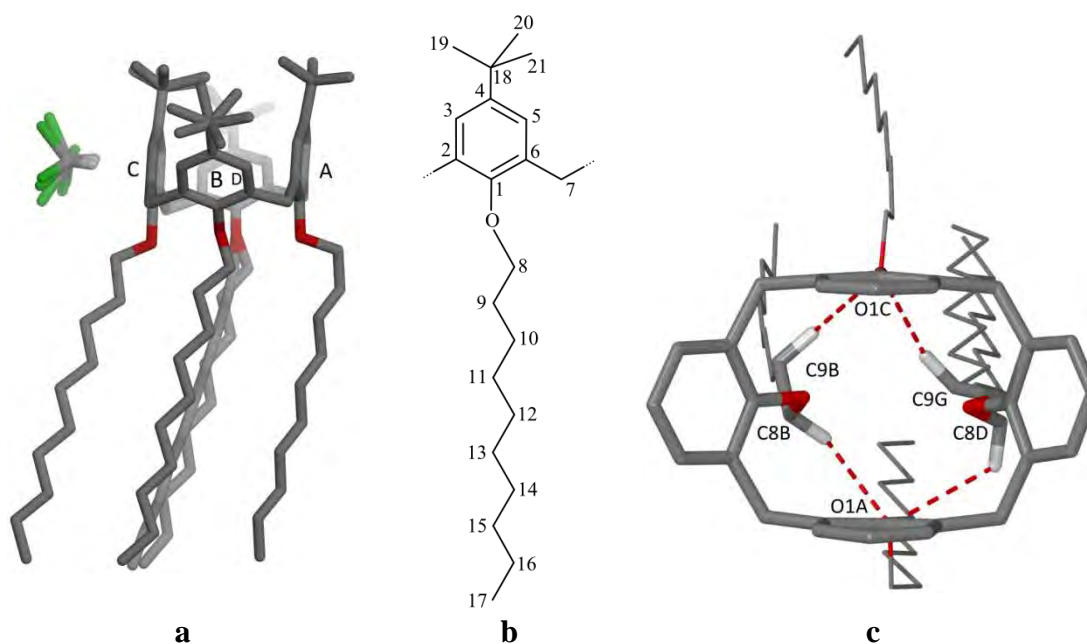

Fig. 97. tBuC[4]OC$_{10}$ (cone)·CHCl$_3$: (a) asymmetric unit; (b) numbering scheme; (c) C–H···O intramolecular contacts, *tert*-butyl groups at the upper rim are omitted for clarity.

substituents and *tert*-butyl groups, as well as the chloroform molecule, were modelled with restraints to retain the correct geometry and reasonable thermal parameters.

Dihedral angles between planes of each benzene ring and the mean plane of the four methylene groups and distances between distal C4 atoms are presented in Table 49.

Table 49. Calix[4]arene macrocyclic ring geometry for tBuC[4]OC$_{10}$ (cone)·CHCl$_3$

	∠(ring-to-CH$_2$-plane), °	Distal C4···C4 distances, Å	
A	97.0(1)	C4A···C4C	5.381(8)
B	137.4(1)		
C	83.8(1)	C4B···C4D	9.49(1)
D	133.5(1)		

Ring A is tilted slightly outwards the calix[4]arene cavity and ring C is tilted slightly inwards the cavity and this means that the calix[4]arene conformation is intermediate between the flattened cone and the pinched cone. The conformation is stabilised by four C–H···O contacts between first and second methylene groups of decyl chains and oxygen atoms of phenoxy moieties (Fig. 97c and Table 50).

Table 50. Weak interactions in tBuC[4]OC$_{10}$ (cone)·CHCl$_3$

Hydrogen bonds				
D–H···A	**d(D–H), Å**	**d(H···A), Å**	**d(D···A), Å**	**∠D–H···A**
C8B–H8B2···O1A	0.99	2.77	3.407(7)	122
C9B–H9B1···O1C	0.99	2.70	3.529(7)	141
C8D–H8D1···O1A	0.99	2.81	3.38(2)	117
C9G–H9G2···O1C	0.99	2.73	3.62(2)	150
C7A–H7A1···Cl1A[1]	0.99	2.80	3.617(8)	140
C7A–H7A1···Cl2B[1]	0.99	2.79	3.647(8)	146
C7C–H7C2···Cl3B	0.99	3.06	3.802(9)	133
C8C–H8C1···Cl2A	0.99	3.08	3.954(9)	148
C8C–H8C1···Cl2C	0.99	2.93	3.556(6)	122
C17C–H17H···Cl2C[2]	0.98	3.07	4.005(7)	160
C19D–H19P···Cl3A[3]	0.98	3.07	3.76(2)	129
C19D–H19R···Cl2C[3]	0.98	3.08	3.834(6)	135
C20A–H20B···Cl1C[1]	0.98	2.52	3.360(9)	143
C20A–H20B···Cl1A[1]	0.98	3.05	3.943(8)	152
C20C–H20K···Cl3A	0.98	2.99	3.61(2)	122
C20C–H20K···Cl1B	0.98	2.87	3.54(1)	127
C20C–H20J···Cl1C[4]	0.98	3.04	3.69(2)	125
C21F–H21O···Cl1B[4]	0.98	2.77	3.36(2)	119
C21F–H21O···Cl1C[4]	0.98	2.90	3.59(2)	128
C21F–H21O···Cl3A[4]	0.98	2.83	3.42(2)	119

Symmetry codes: (1) *x*, 0.5 − *y*, −0.5 + *z*; (2) 1 − *x*, 1 − *y*, 1 − *z*; (3) *x*, 1.5 − *y*, −0.5 + *z*; (4) 2 − *x*, 1 − *y*, 1 − *z*.

Table 43. Continuation.

C–H⋯π interactions

C–H⋯Cg	d(H⋯Cg)	⊥d(H⋯π)	d(C⋯Cg)	∠C–H⋯Cg	∠C–H⋯π
C17A–H17A⋯CgD[1]	3.10	3.01	3.654(7)	117	128
C17G–H17N⋯CgB[2]	2.77	2.73	3.71(5)	162	170
C22–H22A⋯CgC	2.42	2.32	3.379(6)	165	169
C22–H22B⋯CgC	2.41	2.33	3.379(6)	171	166
C22–H22C⋯CgC	2.42	2.39	3.379(6)	165	156

Symmetry codes: (1) $1 - x, 1 - y, -z$; (2) $1 - x, 0.5 + y, 0.5 - z$.

tBuC[4]OC$_{10}$ molecules are self-assembled in bilayers parallel to the *bc* crystallographic plane. The main attractive forces in the self-assembly of tBuC[4]OC$_{10}$ molecules are van der Waals interactions between H-atoms of long decyl chains. The bilayer motif (Fig. 98a) is additionally stabilised by C–H⋯π interactions between H-atoms of terminal carbons of decyl chains as shown in Fig. 98b and listed in Table 50.

The thickness of aromatic layer is *ca.* 4.8 Å, whereas thicknesses of each of aliphatic regions are 5.6 and 10.9 Å for the spaces formed by *tert*-butyl and *n*-decyl substituents, respectively.

The solvent molecule is disordered at least over three positions with occupancy factors equal to 0.43, 0.37 and 0.20 due to the rotation around C–H bond and participates in C–H⋯π interaction with benzene ring C [C22⋯ring C interaction, Table 50].
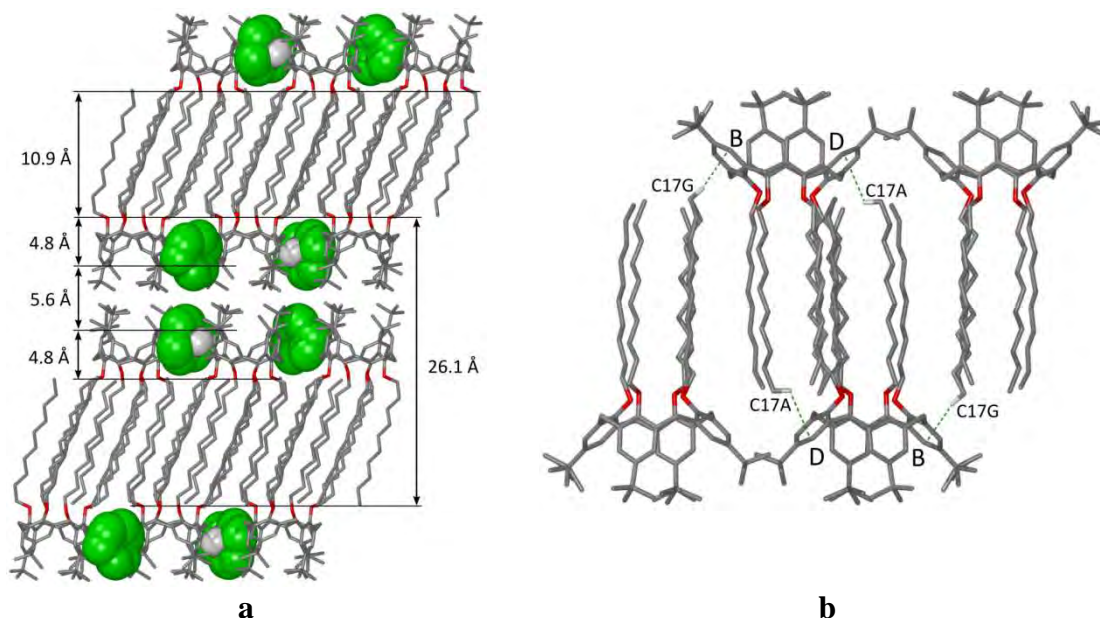

Fig. 98. tBuC[4]OC$_{10}$ (cone)·CHCl$_3$: (a) packing diagram, view along the *b* crystallographic axis; (b) the bilayer structure stabilised by C–H⋯π interactions.

4.2.15 Crystal structure of O-undecylated *para-tert*-butylcalix[4]arene (cone)

O-Undecylated *para-tert*-butylcalix[4]arene (tBuC[4]OC$_{11}$) crystallises from a methanol/chloroform mixture in the monoclinic crystallographic system. It is isostructural with tBuC[4]OC$_9$. Crystal data are presented in Table 51. The asymmetric unit comprises one calix[4]arene molecule which adopts a flattened cone conformation (Fig. 99a). Carbon atom numbering scheme is shown in Fig. 99b. Undecyl chain at the ring C is disordered over two positions with equal occupancy factors of 0.50. It was modelled with restraints to retain the correct geometry and reasonable thermal parameters.

Table 51. Crystal data and structure refinement for tBuC[4]OC$_{11}$ (cone)

Molecular formula	C$_{88}$H$_{144}$O$_4$
Formula weight	1266.03
Crystal system	Monoclinic
Space group	$P2_1/c$
Unit cell dimensions	a = 18.222(1) Å
	b = 32.651(2) Å β = 92.634(4)°
	c = 13.7086(6) Å
Volume	8147.3(8) Å^3
Z	4
Temperature	100.0(5) K
Radiation and wavelength	Mo Kα radiation, λ = 0.71073 Å
Monochromator	graphite
Density (calculated)	1.032 Mg·m^{-3}
Absorption coefficient	0.06 mm^{-1}
F(000)	2816
Crystal size	0.05 × 0.12 × 0.15 mm
θ range for data collection	2.9–18.2°
Index ranges	-15 ≤ h ≤ 15, -28 ≤ k ≤ 23, -12 ≤ l ≤ 12
Reflections collected	25308
Independent reflections	5621 [R_{int} = 0.128]
Completeness	98.0 %
Absorption correction	None
Refinement method	Full-matrix least-squares on F^2
Weighting scheme	$[\sigma^2(F_o^2) + (0.0212P)^2 + 22.7702P]^{-1}$ *
Data / restraints / parameters	5621 / 115 / 947
Goodness-of-fit on F^2	1.19
Final R indices [$I > 2\sigma(I)$]	R = 0.094, wR = 0.161
R indices (all data)	R = 0.142, wR = 0.174
Extinction coefficient	Not refined
Largest diff. peak and hole	0.20 and -0.21 e·Å^{-3}

* $P = (F_o^2 + 2F_c^2)/3$
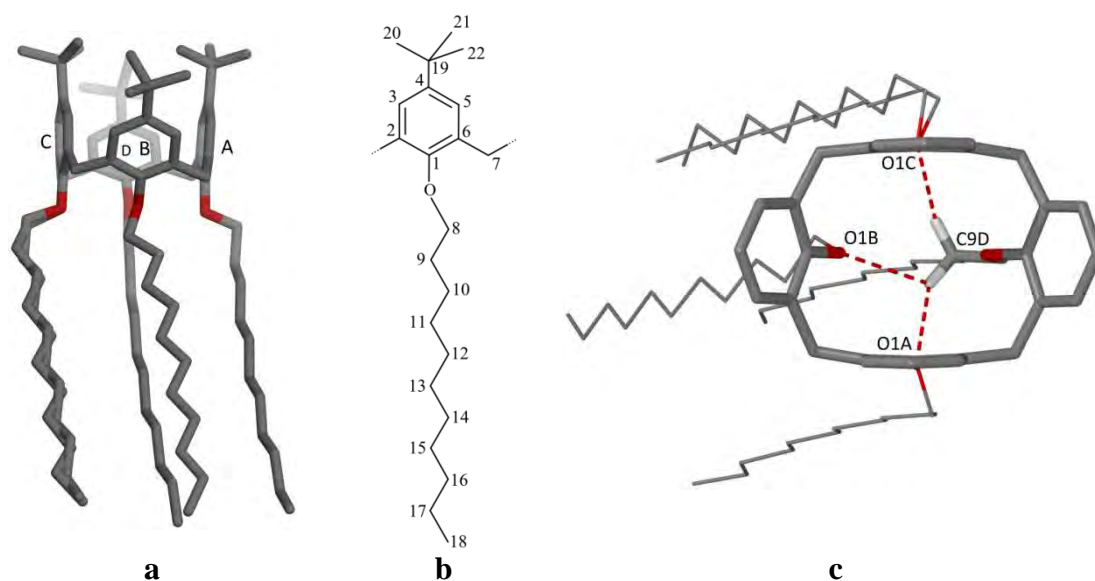
Fig. 99. tBuC[4]OC$_{11}$ (cone): (a) asymmetric unit; (b) numbering scheme; (c) C–H···O intramolecular contacts, *tert*-butyl groups at the upper rim are omitted for clarity.

Dihedral angles between planes of each benzene ring and the mean plane of the four methylene groups and distances between distal C4 atoms are presented in Table 52.

Table 52. Calix[4]arene macrocyclic ring geometry for tBuC[4]OC$_{11}$ (cone)

∠(ring-to-CH$_2$-plane), °		Distal C4···C4 distances, Å	
A	91.8(2)	C4A···C4C	5.59(1)
B	128.0(2)		
C	91.1(2)	C4B···C4D	9.10(1)
D	130.6(1)		

The calix[4]arene conformation is stabilised by one normal and one bifurcated C–H···O intramolecular contact (Fig. 99c) between H-atoms of the second methylene group of the alkyl chain D and oxygen atoms of phenoxy moieties A, B and C (Table 53).

Table 53. Weak interactions in tBuC[4]OC$_{11}$ (cone)

Hydrogen bonds

D–H···A	d(D–H), Å	d(H···A), Å	d(D···A), Å	∠D–H···A
C9D–H9D2···O1A	0.99	2.59	3.450(9)	146
C9D–H9D2···O1B	0.99	2.95	3.51(1)	117
C9D–H9D1···O1C	0.99	2.59	3.465(9)	148

C–H···π interactions

C–H···Cg	d(H···Cg)	⊥d(H···π)	d(C···Cg)	∠C–H···Cg	∠C–H···π
C5B–H5B···CgC[1]	3.78	2.88	4.673(9)	157	150
C20D–H20L···CgB[2]	2.76	2.72	3.699(7)	160	170
C22D–H22L···CgA[3]	2.80	2.79	3.607(7)	140	141

Symmetry codes: (1) $1 - x$, $-y$, $-z$; (2) x, y, $1 + z$; (3) x, $0.5 - y$, $0.5 + z$.

Similarly to tBuC[4]OC$_9$, molecules of tBuC[4]OC$_{11}$ in the same spatial orientation are self-assembled in infinite chains due to C–H⋯π interactions between H-atoms of *tert*-butyl group at the ring D and π electrons of adjacent aromatic ring B (Fig. 100a, Table 53). The chains, symmetry related by *c*-glide plane, are joined by C–H⋯π interactions between H-atom of the same *tert*-butyl group D and adjacent aromatic ring A in ribbons shown in Fig. 100b. Next, similarly to tBuC[4]OC$_9$, neighbouring ribbons with opposite spatial orientation of calix[4]arene molecules are organised in corrugated,

a

b

c
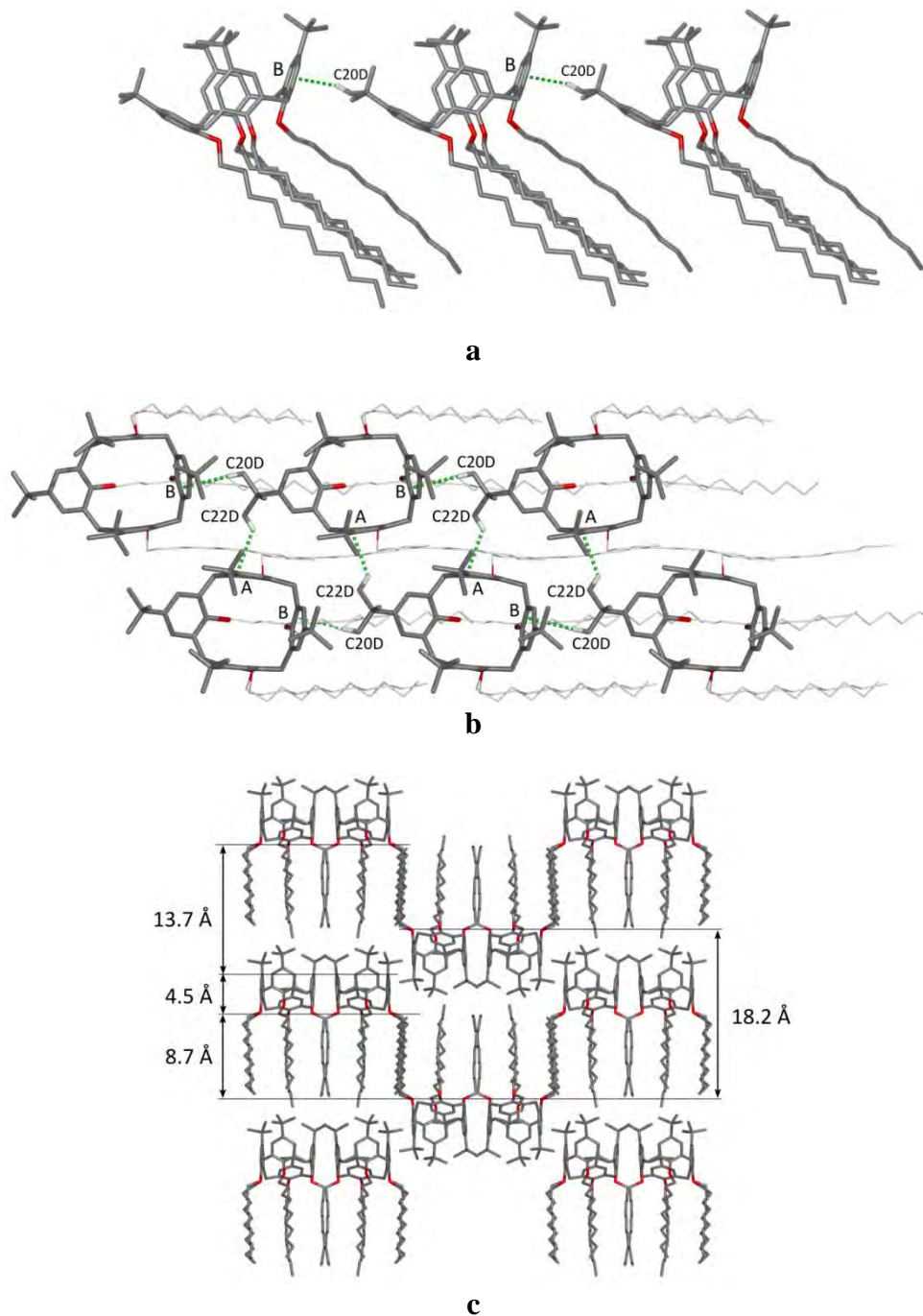
Fig. 100. tBuC[4]OC$_{11}$ (cone): (a) infinite chain along the *c* crystallographic axis; (b) self-assembly of two chains in ribbon; (c) packing diagram, view along the *c* crystallographic axis.

119

parallel to the *bc* crystallographic plane, layers by weak C–H⋯π interactions [C5B⋯ring C] between centrosymmetrically related molecules. Finally, intermolecular van der Waals interactions between *n*-undecyl substituents result in layered self-assemble (Fig. 100c) where *n*-undecyl and *tert*-butyl substituents form aliphatic regions (thickness varies in the range of *ca.* 8.7–13.7. Å), whereas aromatic calix[4]arene cores form aromatic regions with the thickness of *ca.* 4.5 Å.

4.2.16 Crystal structure of O-dodecylated *para-tert*-butylcalix[4]arene (cone) chloroform monosolvate

O-Dodecylated *para-tert*-butylcalix[4]arene crystallises from methanol/chloroform mixture in the monoclinic crystallographic system as calix[4]arene-chloroform solvate with stoichiometry 1:1 (tBuC[4]OC$_{12}$·CHCl$_3$). Data collection was performed at 200 K to avoid crystal cracking below 200 K. Crystal is isostructural (crystal data are presented in Table 54) with tBuC[4]OC$_{10}$·CHCl$_3$. The asymmetric unit comprises one molecule of the host and one molecule of the guest (Fig. 101a). Carbon atom numbering scheme is shown in Fig. 101b. Dodecyl chain at the ring B is disordered on its whole length over two positions with equal occupancy factors of 0.50. Three of four *tert*-butyl groups are also disordered [occupancy factors of 0.50 and 0.50, 0.72 and 0.28, 0.64 and 0.36 for groups A, C and D, respectively]. Dodecyl chains and *tert*-butyl groups, as well as chloroform molecule, were modelled with restraints to retain the correct geometry and reasonable thermal parameters.

a	b	c

Fig. 101. tBuC[4]OC$_{12}$ (cone)·CHCl$_3$: (a) asymmetric unit; (b) numbering scheme; (c) C–H⋯O intramolecular contacts, *tert*-butyl groups at the upper rim are omitted for clarity.

13:

Table 54. Crystal data and structure refinement for tBuC[4]OC$_{12}$ (cone)·CHCl$_3$

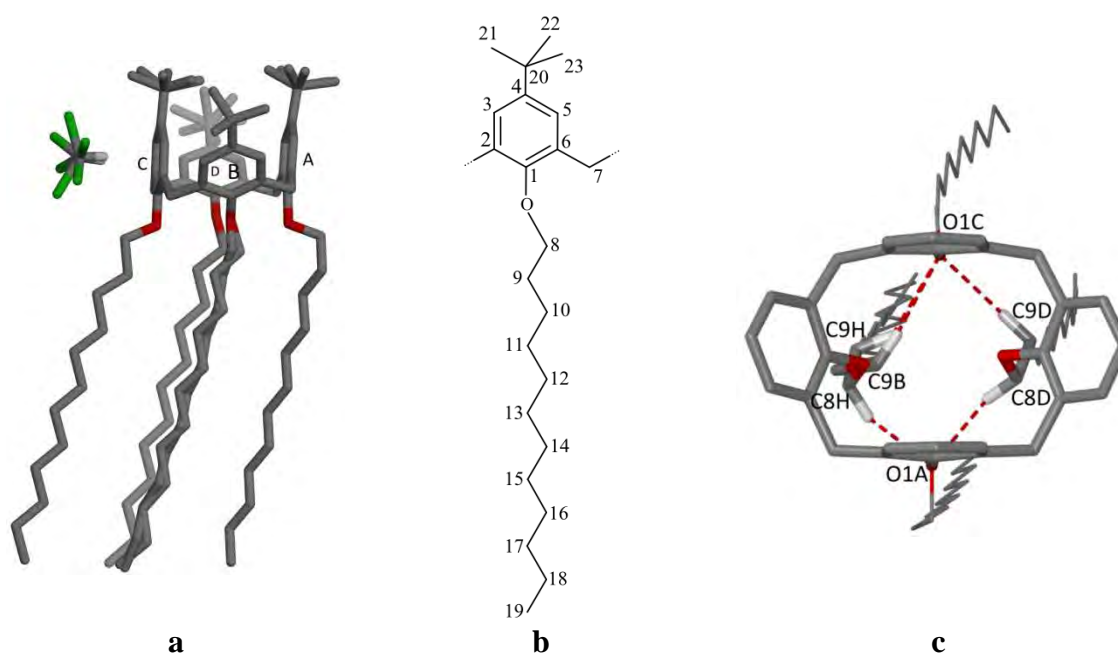|	
Molecular formula	C$_{92}$H$_{152}$O$_4$·CHCl$_3$
Formula weight	1441.50
Crystal system	Monoclinic
Space group	$P2_1/c$
Unit cell dimensions	a = 29.6303(5) Å
	b = 15.8179(2) Å β = 105.622(1)°
	c = 20.4554(2) Å
Volume	9233.1(2) Å^3
Z	4
Temperature	200.0(5) K
Radiation and wavelength	Mo Kα radiation, λ = 0.71073 Å
Monochromator	graphite
Density (calculated)	1.037 Mg·m^{-3}
Absorption coefficient	0.14 mm^{-1}
F(000)	3176
Crystal size	0.10 × 0.15 × 0.15 mm
θ range for data collection	2.9–20.8°
Index ranges	-29 ≤ h ≤ 29,-15 ≤ k ≤ 15, -20 ≤ l ≤ 20
Reflections collected	68417
Independent reflections	9582 [R_{int} = 0.073]
Completeness	99.9 %
Absorption correction	None
Refinement method	Full-matrix least-squares on F^2
Weighting scheme	$[\sigma^2(F_o^2) + (0.0953P)^2 + 5.5197P]^{-1}$ *
Data / restraints / parameters	9582 / 107 / 1149
Goodness-of-fit on F^2	1.03
Final R indices [$I > 2\sigma(I)$]	R = 0.066, wR = 0.170
R indices (all data)	R = 0.086, wR = 0.182
Extinction coefficient	0.0027(5)
Largest diff. peak and hole	0.37 and -0.27 e·Å^{-3}

* $P = (F_o^2 + 2F_c^2)/3$

Dihedral angles between planes of each benzene ring and the mean plane of the four methylene groups and distances between distal C4 atoms are presented in Table 55.

Table 55. Calix[4]arene macrocyclic ring geometry for tBuC[4]OC$_{12}$ (cone)·CHCl$_3$

	∠(ring-to-CH$_2$-plane), °	Distal C4···C4 distances, Å	
A	94.93(8)	C4A···C4C	5.436(4)
B	133.42(8)		
C	86.67(7)	C4B···C4D	9.512(5)
D	138.46(7)		

Similarly to tBuC[4]OC$_{10}$·CHCl$_3$, the calix[4]arene conformation is intermediate between the flattened cone and the pinched cone: ring A is tilted slightly outwards the

13;

calix[4]arene cavity and ring C is tilted slightly inwards the cavity. The conformation is stabilised by four C–H···O contacts (Fig. 101c and Table 56).

Table 56. Weak interactions in tBuC[4]OC$_{12}$ (cone)·CHCl$_3$

Hydrogen bonds

D–H···A	d(D–H), Å	d(H···A), Å	d(D···A), Å	∠D–H···A
C9B–H9B1···O1C	0.99	2.76	3.67(1)	153
C8D–H8D1···O1A	0.99	2.76	3.390(4)	122
C9D–H9D2···O1C	0.99	2.69	3.525(5)	142
C8H–H8H1···O1A	0.99	2.64	3.32(2)	127
C9H–H9H1···O1C	0.99	2.92	3.64(4)	130
C7D–H7D1···Cl3A[1]	0.99	2.77	3.608(5)	143
C21C–H21H···Cl1A	0.98	2.68	3.22(1)	115
C21E–H21M···Cl2B[1]	0.98	2.81	3.567(9)	134
C21F–H21P···Cl1A[2]	0.98	2.78	3.45(2)	126

Symmetry codes: (1) x, $1.5 - y$, $-0.5 + z$; (2) $1 - x$, $1 - y$, $1 - z$.

C–H···π interactions

C–H···Cg	d(H···Cg)	⊥d(H···π)	d(C···Cg)	∠C–H···Cg	∠C–H···π
C19A–H19C···CgB[1]	3.19	3.09	3.741(5)	117	129
C19D–H19E···CgD[2]	3.05	2.89	3.908(6)	148	165
C19H–H19N···CgD[2]	3.29	3.11	3.89(1)	122	140
C1S–H1SA···CgC	2.54	2.45	3.533(7)	171	172
C1S–H1SB···CgC	2.55	2.50	3.533(7)	167	159

Symmetry codes: (1) $- x$, $1 - y$, $-z$; (2) $- x$, $-0.5 + y$, $0.5 - z$.

Due to presence of dodecyl groups, similarly to the tBuC[4]OC$_{10}$, the main attractive force in self-assembly of tBuC[4]OC$_{12}$ are van der Waals interactions between H-atoms of long dodecyl chains. The resulting bilayer motif (Fig. 102a) is additionally
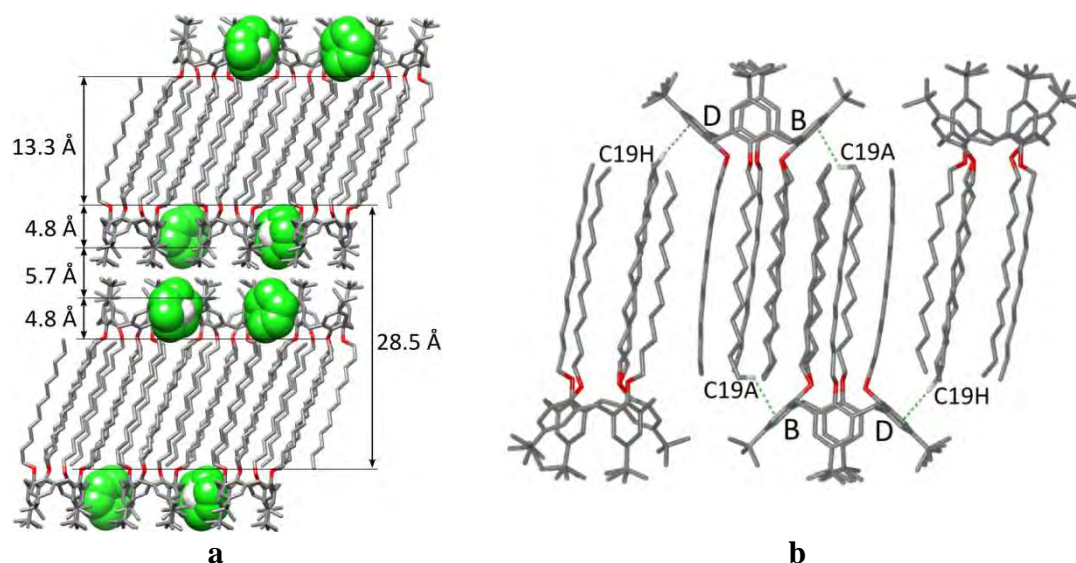

Fig. 102. tBuC[4]OC$_{12}$ (cone)·CHCl$_3$: (a) packing diagram, view along the *b* crystallographic axis; (b) stabilisation of the bilayer structure by C–H···π interactions.

stabilised by C–H⋯π interactions between H-atoms of terminal carbons of dodecyl chains shown in Fig. 102b and listed in Table 56.

The thickness of aromatic layers is *ca.* 4.8 Å, whereas thicknesses of aliphatic regions are 5.7 and 13.3 Å for these formed by *tert*-butyl and *n*-dodecyl substituents, respectively.

The solvent molecule present in the crystal structure is disordered over two positions with occupancy factors equal to 0.53 and 0.47 and takes part in C–H⋯π interaction with calix[4]arene benzene ring C.

4.2.17 Crystal structure of O-tetradecylated *para-tert*-butylcalix[4]arene (cone) chloroform monosolvate

O-Tetradecylated *para-tert*-butylcalix[4]arene crystallises from a methanol/chloroform mixture in the monoclinic crystallographic system as a calix[4]arene-chloroform solvate with stoichiometry 1:1 (tBuC[4]OC$_{14}$·CHCl$_3$). Crystal data are presented in Table 57. The crystal is isostructural with tBuC[4]OC$_{10}$·CHCl$_3$ and tBuC[4]OC$_{12}$·CHCl$_3$. Data collection was performed at 250 K to avoid crystal cracking which occurs below 240 K. The asymmetric unit comprises one molecule of the host and one molecule of the guest (Fig. 103a). Carbon atom numbering scheme is shown in Fig. 103b. Two dodecyl chains at distal rings B and D are disordered over two positions with occupancy factors of 0.56 and 0.44, and 0.63 and
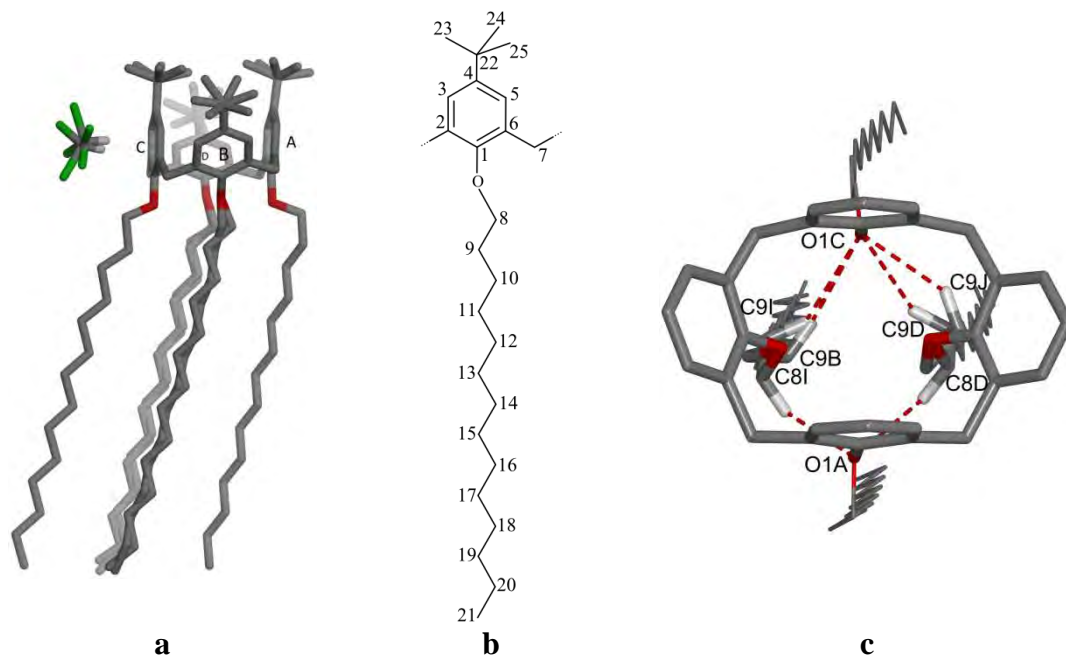

Fig. 103. tBuC[4]OC$_{14}$ (cone)·CHCl$_3$: (a) asymmetric unit; (b) numbering scheme; (c) conformation stabilised by C–H⋯O intramolecular contacts, *tert*-butyl groups at the upper rim are omitted for clarity.

Table 57. Crystal data and structure refinement for tBuC[4]OC$_{14}$ (cone)·CHCl$_3$

Molecular formula	C$_{100}$H$_{168}$O$_4$·CHCl$_3$
Formula weight	1553.71
Crystal system	Monoclinic
Space group	$P2_1/c$
Unit cell dimensions	a = 32.215(1) Å
	b = 15.9293(6)Å β = 105.890(2)°
	c = 20.5361(8)Å
Volume	10135.6(7) Å^3
Z	4
Temperature	250.0(5) K
Radiation and wavelength	Mo Kα radiation, λ = 0.71073 Å
Monochromator	graphite
Density (calculated)	1.018 Mg·m^{-3}
Absorption coefficient	0.14 mm^{-1}
$F(000)$	3432
Crystal size	0.07 × 0.27 × 0.50 mm
θ range for data collection	2.8–19.8°
Index ranges	-30 ≤ h ≤ 30, -15 ≤ k ≤ 14, -19 ≤ l ≤ 19
Reflections collected	32293
Independent reflections	9108 [R_{int} = 0.085]
Completeness	99.5 %
Absorption correction	None
Refinement method	Full-matrix least-squares on F^2
Weighting scheme	$[\sigma^2(F_o^2) + (0.0638P)^2 + 7.3452P]^{-1}$ *
Data / restraints / parameters	9108 / 503 / 1407
Goodness-of-fit on F^2	1.05
Final R indices [$I > 2\sigma(I)$]	R = 0.072, wR = 0.158
R indices (all data)	R = 0.112, wR = 0.177
Extinction coefficient	0.0013(3)
Largest diff. peak and hole	0.22 and -0.19 e·Å^{-3}

* $P = (F_o^2 + 2F_c^2)/3$

0.37 for chains at rings B and D, respectively. Also all four *tert*-butyl substituents are disordered with occupancy factors of 0.85 and 0.15, 0.83 and 0.17, 0.77 and 0.23(1), and 0.69 and 0.31 at rings A, B, C and D, respectively. Dodecyl chains and *tert*-butyl groups, as well as chloroform molecule, were modelled with restraints to retain the correct geometry and reasonable thermal parameters.

Dihedral angles between planes of each benzene ring and the mean plane of the four methylene groups and distances between distal C4 atoms are presented in Table 58. Ring A is tilted slightly outwards the calix[4]arene cavity and ring C is tilted slightly

inwards the cavity and this indicates that the calix[4]arene conformation. Similarly to tBuC[4]OC$_{10}$·CHCl$_3$ and tBuC[4]OC$_{12}$·CHCl$_3$ the calix[4]arene macrocycle adopts an intermediate conformation between the flattened cone and the pinched cone. The conformation is stabilised by C–H···O contacts (Fig. 103c and Table 59).

Table 58. Calix[4]arene macrocyclic ring geometry for tBuC[4]OC$_{14}$ (cone)·CHCl$_3$

	∠(ring-to-CH$_2$-plane), °	Distal C4···C4 distances, Å	
A	94.2(1)	C4A···C4C	5.453(6)
B	133.3(1)		
C	87.45(1)	C4B···C4D	9.530(7)
D	138.65(9)		

Similarly to the crystal structures of tBuC[4]OC$_{10}$·CHCl$_3$ and tBuC[4]OC$_{12}$·CHCl$_3$ the molecules self-assemble in bilayers (Fig. 104a). Self-assembly is stabilised by C–H···π interactions between H-atoms of terminal carbons of tetradecyl chains and adjacent aromatic rings of calix[4]arene macrocyclic rings. Thus C21A···ring B interactions (Table 59) join calix[4]arene molecules in centrosymmetric dimers shown in Fig. 104b, while C21B···ring D and C21I···ring D interactions enforce an infinite chain formation (Fig. 104c).

Table 59. Weak interactions in tBuC[4]OC$_{14}$ (cone)·CHCl$_3$

Hydrogen bonds

D–H···A	d(D–H), Å	d(H···A), Å	d(D···A), Å	∠D–H···A
C8D–H8D1···O1A	0.98	2.82	3.51(1)	128
C8I–H8I2···O1A	0.98	2.53	3.23(2)	129
C9B–H9B2···O1C	0.98	2.83	3.72(1)	151
C9D–H9D2···O1C	0.98	2.80	3.52(1)	131
C9I–H9I1···O1C	0.98	2.88	3.64(1)	135
C9J–H9J2···O1C	0.98	2.76	3.54(1)	137
C7D–H7D1···Cl3B[1]	0.98	2.79	3.607(7)	142
C25F–H25Q···Cl2B[2]	0.97	2.95	3.60(1)	125
C25F–H25R···Cl1B[2]	0.97	2.86	3.63(1)	137
C23G–H23S···Cl1B[3]	0.97	2.72	3.53(3)	142

Symmetry codes: (1) *x*, 1.5 − *y*, 0.5 − *z*; (2) *x*, 0.5 − *y*, 0.5 + *z*; (3) −*x*, 1 − *y*, − *z*.

C–H···π interactions

C–H···Cg	d(H···Cg)	⊥d(H···π)	d(C···Cg)	∠C–H···Cg	∠C–H···π
C21A–H21C···CgB[1]	3.26	3.15	3.793(6)	116	128
C21B–H21E···CgD[2]	3.14	2.97	3.99(1)	146	164
C21I–H21N···CgD[2]	3.36	3.16	3.90(1)	118	137
C1SA–H1SA···CgC	2.68	2.62	3.632(7)	161	157
C1SB–H1SB···CgC	2.55	2.44	3.516(7)	167	173

Symmetry codes: (1) 1 − *x*, 1 −*y*, 1 −*z*; (2) 1 − *x*, −0.5 + *y*, 0.5 − *z*.
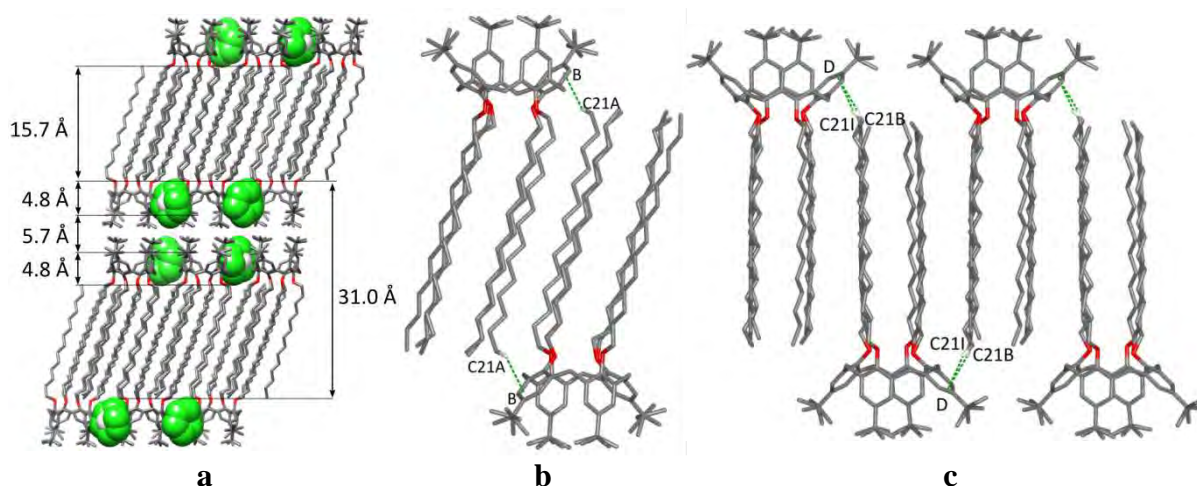
Fig. 104. tBuC[4]OC₁₄ (cone)·CHCl₃: (a) packing diagram, view along the *b* crystallographic axis; (b) self-assembly in dimers; (c) infinite chain formation.

The thickness of the aromatic layers is *ca.* 4.8 Å, whereas thicknesses of each of the aliphatic ones are 5.7 and 15.7 Å for regions formed by *tert*-butyl and *n*-tetradecyl substituents, respectively.

The chloroform molecule present in the crystal structure is disordered over two positions with occupancy factors equal 0.50 and participates in C–H···π interaction with benzene ring C of the calix[4]arene (Table 59).

4.3 Crystal structures of O-alkylated *para*-nitrocalix[4]arenes

4.3.1 Crystal structure of O-methylated *para*-nitrocalix[4]arene (partial cone) inclusion complex with chloroform

O-Methylated *para*-nitrocalix[4]arene crystallises from a methanol/chloroform mixture in the triclinic crystallographic system as the calix[4]arene-chloroform inclusion complex with stoichiometry 1:1 (NO₂C[4]OC₁·CHCl₃). The asymmetric unit comprises one molecule of the host and one molecule of the guest (Fig. 105a). Carbon atom numbering scheme is shown in Fig. 105b. Crystal data for the complex are presented in Table 60. The complex is isostructural with NO₂C[4]OC₁·DMF.[134] Unlike the DMF complex, the chloroform molecule, as was expected, takes part in C–H···O interaction with partially negatively charged oxygen atom of the nitro group, not with the π-electrons of the calix[4]arene macrocyclic ring (Fig. 105c). The chloroform molecule is disordered over two positions with equal occupancies of 0.5. In addition to C–H···O hydrogen bonds between chloroform hydrogen and oxygen atom O3A of nitro groups (Fig. 105c and Table 61), the solvate is stabilised by two Cl···π contacts between included Cl atoms of chloroform and calix[4]arene aromatic rings.

126

Table 60. Crystal data and structure refinement for NO$_2$C[4]OC$_1$ (partial cone)·CHCl$_3$

Molecular formula	C$_{32}$H$_{28}$N$_4$O$_{12}$·CHCl$_3$
Formula weight	779.95
Crystal system	Triclinic
Space group	$P\bar{1}$
Unit cell dimensions	a = 9.0081(2) Å α = 75.729(2)°
	b = 11.7486(3) Å β = 79.456(2)°
	c = 18.2748(5) Å γ = 71.649(2)°
Volume	1767.35(8) Å^3
Z	2
Temperature	100.0(5) K
Radiation and wavelength	Mo Kα radiation, λ = 0.71073 Å
Monochromator	graphite
Density (calculated)	1.466 Mg·m^{-3}
Absorption coefficient	0.33 mm^{-1}
F(000)	804
Crystal size	0.08 × 0.08 × 0.20 mm
θ range for data collection	3.4–26.0°
Index ranges	0 ≤ h ≤ 11, -13 ≤ k ≤ 14, -21 ≤ l ≤ 22
Reflections collected	46936
Independent reflections	6927 [R_{int} = 0.070]
Completeness	96.5 %
Absorption correction	None
Refinement method	Full-matrix least-squares on F^2
Weighting scheme	$[\sigma^2(F_o^2) + (0.0355P)^2 + 4.9519P]^{-1}$ *
Data / restraints / parameters	6927 / 0 / 499
Goodness-of-fit on F^2	1.06
Final R indices [$I > 2\sigma(I)$]	R = 0.076, wR = 0.151
R indices (all data)	R = 0.119, wR = 0.165
Extinction coefficient	Not refined
Largest diff. peak and hole	0.50 and -0.64 e·Å^{-3}

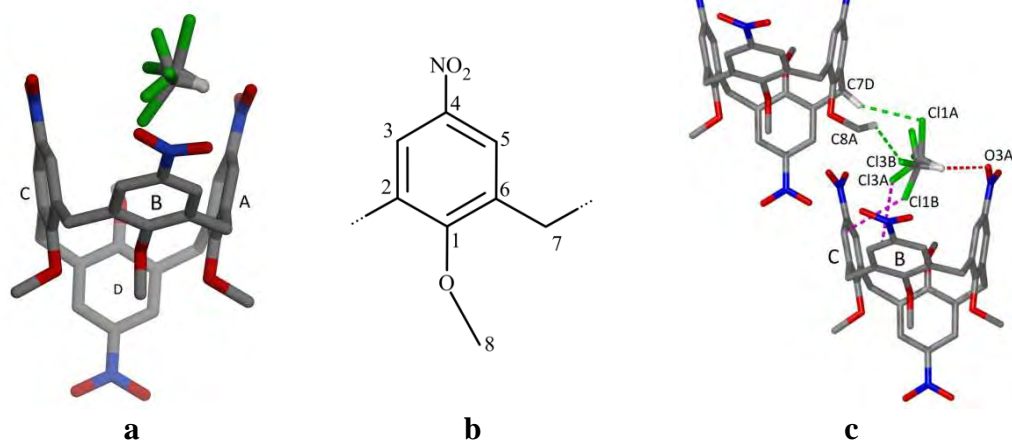* $P = (F_o^2 + 2F_c^2)/3$

a **b** **c**

Fig. 105. NO$_2$C[4]OC$_1$ (partial cone)·CHCl$_3$: (a) asymmetric unit; (b) numbering scheme; (c) interactions of CHCl$_3$ molecule with calixarenes.

Chloroform molecule also participates in C–H···Cl hydrogen bonds with H-atoms of the moiety D, methoxy group C8A and methylene bridge C7D of the adjacent calix[4]arene (Table 61).

Table 61. Weak interactions in NO$_2$C[4]OC$_1$ (partial cone)·CHCl$_3$

Hydrogen bonds

D–H···A	d(D–H), Å	d(H···A), Å	d(D···A), Å	∠D–H···A
C3A–H3A···O3B[1]	0.95	2.66	3.462(5)	142
C3B–H3B···O2B[2]	0.95	2.56	3.208(5)	125
C3C–H3C···O3D[3]	0.95	2.53	3.434(5)	159
C5A–H5A···O2B[2]	0.95	2.44	3.353(5)	162
C5B–H5B···O3D[3]	0.95	2.69	3.431(5)	135
C7A–H7A1···O2A[4]	0.99	2.48	3.383(5)	151
C7B–H7B2···O3C[4]	0.99	2.47	3.316(5)	144
C7C–H7C1···O2C[5]	0.99	2.83	3.360(4)	115
C7C–H7C2···O2D[6]	0.99	2.66	3.361(5)	162
C7D–H7D1···O3B[1]	0.99	2.57	3.456(5)	149
C8A–H8A1···O3A[7]	0.98	2.95	3.665(5)	131
C8A–H8A2···O3B[8]	0.98	2.62	3.573(5)	164
C8A–H8A3···O2A[7]	0.98	2.99	3.622(5)	123
C8B–H8B1···O2A[4]	0.98	2.84	3.811(4)	170
C8C–H8C1···O3C[4]	0.98	2.80	3.531(4)	132
C8C–H8C2···O2D[9]	0.98	2.90	3.860(4)	165
C8C–H8C3···O3C[5]	0.98	2.95	3.613(4)	126
C8D–H8D3···O2D[6]	0.98	2.90	3.806(5)	155
C1SA–H1SA···O3A	1.00	2.35	3.12(1)	133
C1SB–H1SB···O3A	1.00	2.36	3.22(2)	143
C5D–H5D···Cl3A[8]	0.95	2.99	3.907(4)	162
C7D–H7D2···Cl1A[8]	0.99	2.88	3.759(4)	148
C8A–H8A1···Cl3B[8]	0.98	2.65	3.369(5)	130

Symmetry codes: (1) $1 + x, -1 + y, z$; (2) $-x, 1 - y, 1 - z$; (3) $x, 1 + y, z$; (4) $-1 + x, y, z$; (5) $1 - x, 1 - y, -z$; (6) $1 - x, -y, -z$; (7) $1 - x, y, 1 - z$; (8) $x, -1 + y, z$; (9) $-x, -y, z$.

Cl···π interaction

C–Cl···Cg	d(Cl···Cg)	⊥(Cl···π)	∠C–Cl···Cg	∠C–Cl···π
C1SA–Cl3A···CgB	3.467(4)	3.170(4)	124.4(6)	138.5(6)
C1SB–Cl1B···CgC	3.827(4)	3.039(4)	160.4(8)	124.0(8)

π···π interactions

CgI···CgJ	d(CgI···CgJ)	α	β	γ	⊥(CgI···πJ)	⊥(CgJ···πI)
CgA···CgA[1]	4.665(5)	0	41	41	3.539(5)	3.539(5)
CgC···CgC[2]	4.785(6)	0	45	45	3.401(6)	3.401(6)

Symmetry codes: (1) $1 - x, -y, 1 - z$; (2) $1 - x, 1 - y, -z$.

d(CgI···CgJ) – distance between ring centroids I and J (Å), α – dihedral angle between planes I and J; β – angle between CgI···CgJ vector and normal to plane I; γ – angle between CgI···CgJ vector and normal to plane J (°), ⊥(CgI···πJ) – perpendicular distance of CgI on ring J; ⊥(CgJ···πI) – perpendicular distance of CgJ on ring I (Å).

The calix[4]arene adopts the partial core conformation: dihedral angles between planes of each benzene ring and the mean plane of the four methylene groups and distances between distal C4 atoms are presented in Table 62. The conformation is stabilised by interaction with included guest molecule and C–H···O contacts (Table 61) with adjacent calix[4]arene molecules.

Table 62. Calix[4]arene macrocyclic ring geometry for $NO_2C[4]OC_1$ (partial cone)·$CHCl_3$

	∠(ring-to-CH_2-plane), °	Distal C4···C4 distances, Å	
A	98.94(8)	C4A···C4C	6.118(5)
B	151.12(7)		
C	99.03(8)	C4B···C4D	8.806(5)
D	-92.16(8)		

Molecules of $NO_2C[4]OC_1$ show a similar to $NO_2C[4]OC_3$ solvates[113–115] mode of self-assembly: they are engaged in infinite chains (Fig. 106) along diagonal between $-b$ and c crystallographic axes in 'up-down' manner mainly due to π-π stacking interactions between the conjugated systems of the benzene rings and nitro groups of the neighbouring calixarenes. π-π Stacking interactions are additionally stabilised by C–H···O contacts between H-atoms of methoxy groups and nitro groups of adjacent calixarenes (Table 61).
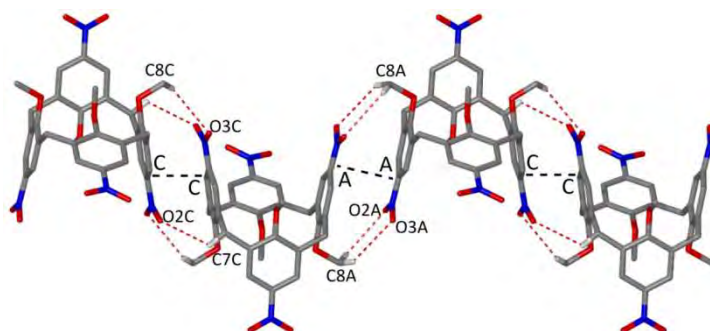
Fig. 106. Self-assembly of $NO_2C[4]OC_1$ in infinite chains due to both π-π stacking interactions and C–H···O contacts.

The crystal packing diagram shown in Fig. 107 reveals that solvent replacement does not change in self-assembly of the complexes compared to $NO_2C[4]OC_1$·DMF.[105] Hydrogen atoms in *meta*-position of the benzene rings, hydrogen atoms of methylene bridges and one methyl group participate in C–H···O contacts with oxygen atoms of nitro groups of neighbouring calix[4]arene molecules (Table 61). The network of C–H···O contacts combine in three dimensional structure, similarly to the complex with DMF.[134]
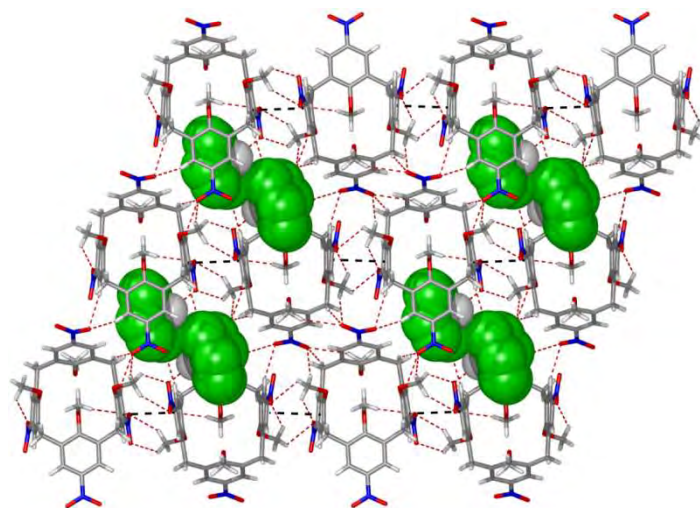
Fig. 107 NO$_2$C[4]OC$_1$ (partial cone)·CHCl$_3$. Packing diagram, view along the *a* crystallographic axis.

4.3.2 Crystal structure of O-octylated *para*-nitrocalix[4]arene (cone) chloroform monosolvate

O-Octylated *para*-nitrocalix[4]arene crystallises from methanol/chloroform mixture in the rhombohedral crystallographic system as a calix[4]arene-chloroform solvate with stoichiometry 1:1 (NO$_2$C[4]OC$_8$·CHCl$_3$). Crystal data are presented in Table 63. The asymmetric unit comprises half molecule of the host and half molecule of the guest. The calix[4]arene molecule assumes the pinched cone conformation with C_{2v}-symmetry (Fig. 108a). Carbon atom numbering scheme is shown in Fig. 108b. All alkyl substituents are strongly disordered. Each of them was localised in two positions with equal occupancy factors of 0.50 and was modelled using restraints to retain the correct geometry and reasonable thermal parameters.

| a | b | c |

Fig. 108. NO$_2$C[4]OC$_8$ (cone)·CHCl$_3$: (a) calix[4]arene molecule; (b) numbering scheme; (c) cone conformation stabilised by C–H···O intramolecular contacts.

14:

Table 63. Crystal data and structure refinement for NO$_2$C[4]OC$_8$ (cone)·CHCl$_3$

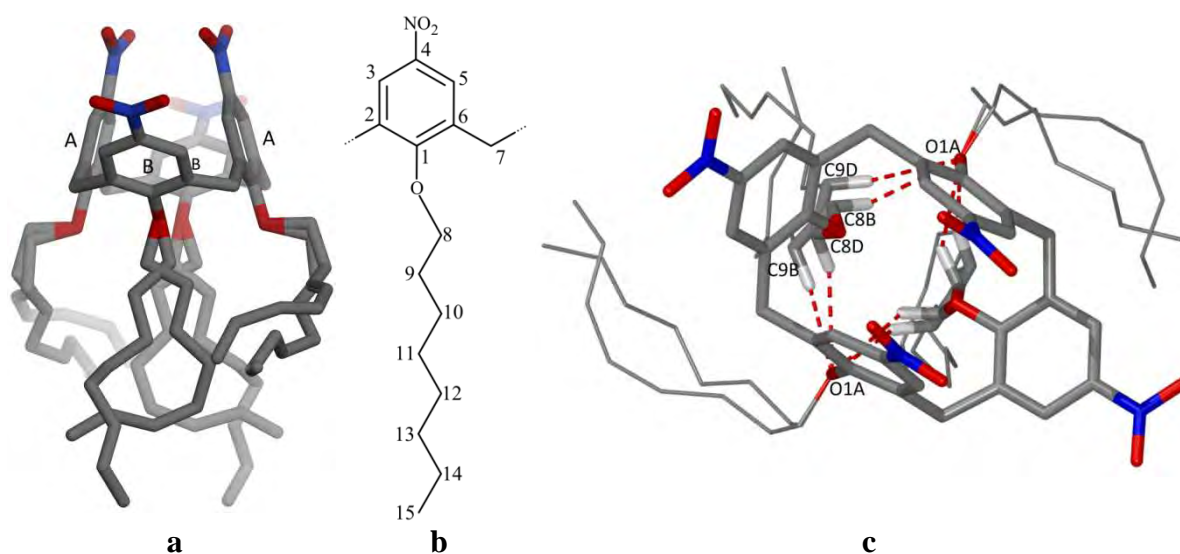|	
Molecular formula	C$_{60}$H$_{84}$N$_4$O$_{12}$·CHCl$_3$
Formula weight	1172.68
Crystal system	Rhombohedral
Space group	$R\bar{3}c$
Unit cell dimensions	a = 23.501(1) Å α = 111.206(4)°
Volume	9295(1) Å^3
Z	6
Temperature	100.0(5) K
Radiation and wavelength	Mo Kα radiation, λ = 0.71073 Å
Monochromator	graphite
Density (calculated)	1.257 Mg·m^{-3}
Absorption coefficient	0.21 mm^{-1}
F(000)	3756
Crystal size	0.13 × 0.15 × 0.30 mm
θ range for data collection	2.8–18.9°
Index ranges	-21 ≤ h ≤ 21, -21 ≤ k ≤ 21, -21 ≤ l ≤ 21
Reflections collected	49035
Independent reflections	2433 [R_{int} = 0.104]
Completeness	99.9 %
Absorption correction	None
Refinement method	Full-matrix least-squares on F^2
Weighting scheme	$[\sigma^2(F_o^2) + (0.2P)^2]^{-1}$ *
Data / restraints / parameters	2433 / 205 / 455
Goodness-of-fit on F^2	1.75
Final R indices [$I > 2\sigma(I)$]	R = 0.132, wR = 0.359
R indices (all data)	R = 0.158, wR = 0.387
Extinction coefficient	Not refined
Largest diff. peak and hole	0.64 and -0.46 e·Å^{-3}

* $P = (F_o^2 + 2F_c^2)/3$

Dihedral angles between planes of each benzene ring and the mean plane of the four methylene groups and distances between distal C4 are presented in Table 64.

Table 64. Calix[4]arene macrocyclic ring geometry for NO$_2$C[4]OC$_8$ (cone)·CHCl$_3$

	∠(ring-to-CH$_2$-plane), °	Distal C4···C4 distances, Å	
A	75.9(2)	C4A···C4A^1	3.88(1)
B	143.0(2)	C4B···C4B^1	9.96(1)

Symmetry codes: (1) 0.5 − x, 0.5 − y, 0.5 − z.

The calix[4]arene conformation is stabilised by intramolecular C–H···O bonds (Fig. 108c) between H-atoms of the first and the second methylene groups of disordered octyl chains and oxygen atoms of phenoxy moieties A (Table 65).

Surprisingly, self-assembly of $NO_2C[4]OC_8$ resembles the behaviour of $NO_2C[4]OC_1 \cdot CHCl_3$ and tetra-O-propylated *para*-nitrocalix[4]arenes[98–100] rather than the ones with longer alkyl chains: tetra-O-butylated[101] and tetra-O-pentylated.[102] Thus, the molecules of $NO_2C[4]OC_8$ self-assemble in infinite chains (Fig. 109) in 'up-down'

Table 65. Weak interactions in $NO_2C[4]OC_8$ (cone)·$CHCl_3$

Hydrogen bonds

D–H⋯A	d(D–H), Å	d(H⋯A), Å	d(D⋯A), Å	∠D–H⋯A
C8B–H8B1⋯O3B[1]	0.99	2.57	3.300(9)	130
C8B–H8B2⋯O1A	0.99	2.76	3.426(8)	125
C8D–H8D1⋯O1A[2]	0.99	2.74	3.351(9)	120
C8D–H8D2⋯O2B[1]	0.99	2.65	3.618(9)	165
C9B–H9B1⋯O1A[2]	0.99	2.85	3.626(9)	136
C9B–H9B2⋯O2B[1]	0.99	2.45	3.390(9)	158
C9D–H9D1⋯O3B[1]	0.99	2.57	3.247(9)	125
C9D–H9D2⋯O1A	0.99	2.52	3.404(8)	148
C1S–H1S⋯O3A	1.00	2.55	3.51(3)	161
C3B–H3B⋯Cl2[3]	0.95	3.00	3.86(3)	153
C5B–H5B⋯Cl1[4]	0.95	2.70	3.63(3)	168
C7B–H7B2⋯Cl2[5]	0.99	2.95	3.66(3)	129

Symmetry codes: (1) $-x, 1-y, -z$; (2) $0.5-x, 0.5-y, 0.5-z$; (3) $-z, 1-x, 1-y$; (4) $0.5-y, 0.5-x, -0.5-z$; (5) $z, x, -1+y$.

π⋯π interactions

CgI⋯CgJ	d(CgI⋯CgJ)	α	β	γ	⊥(CgI⋯πJ)	⊥(CgJ⋯πI)
CgA⋯CgA[1]	3.733(7)	9	24	24	3.401(8)	3.401(8)
CgB⋯CgB[2]	4.286(7)	0	36	36	3.481(8)	3.481(8)

Symmetry codes: (1) $0.5-z, 1.5-y, 0.5-x$; (2) $-x, 1-y, -z$.

d(CgI⋯CgJ) – distance between ring centroids I and J (Å), α – dihedral angle between planes I and J; β – angle between CgI⋯CgJ vector and normal to plane I; γ – angle between CgI⋯CgJ vector and normal to plane J (°), ⊥(CgI⋯πJ) – perpendicular distance of CgI on ring J; ⊥(CgJ⋯πI) – perpendicular distance of CgJ on ring I (Å).
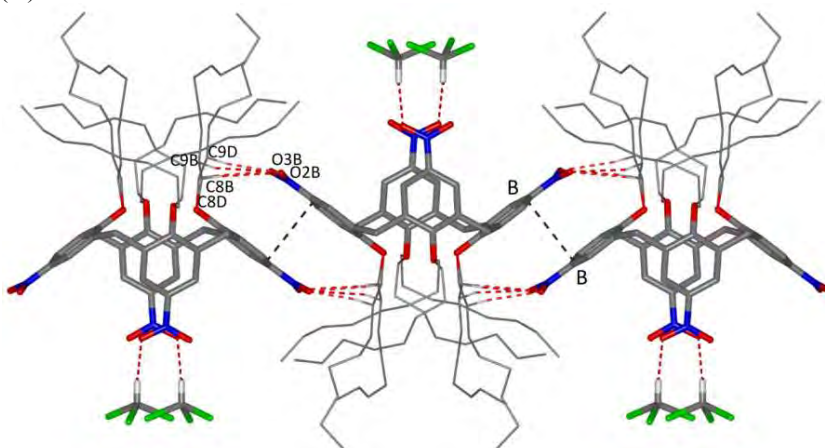
Fig. 109. Self-assembly of $NO_2C[4]OC_8$ (cone) in infinite chains due to both π-π stacking interactions and C–H⋯O contacts.

manner mainly due to π-π stacking interactions between the conjugated systems of the benzene rings and nitro groups of the neighbouring calixarenes. The distance between the planes of the interacting π-systems is equal to 3.439(9) Å and the interaction is additionally stabilised by C–H···O bonds (Table 65) between H-atoms of the first and the second methylene groups of the alkyl substituents and the nitro group of the adjacent calixarene.

Infinite chains of calix[4]arene molecules are oriented along each coordinate axis of the rhombohedral unit cell. π-π Interactions between adjacent calix[4]arenes of neighbouring chains are shown in Fig. 110a. The solvent molecule is disordered in two

a

b

c

Fig. 110. $NO_2C[4]OC_8$ (cone)·$CHCl_3$: (a) bridging role of chloroform molecule; (b) and (c) packing diagram down the $\bar{3}$ axis. Three infinite chains of π-π stacked molecules of $NO_2C[4]OC_8$ which run along each coordination axis are coloured in yellow, turquoise and pink.

133

symmetrically related by 2-fold axis positions located between the alkyl chains. In each position it acts as a hydrogen donor in C–H⋯O bond (Table 65) to nitro group of the same calix[4]arene and as a hydrogen acceptor in at least three C–H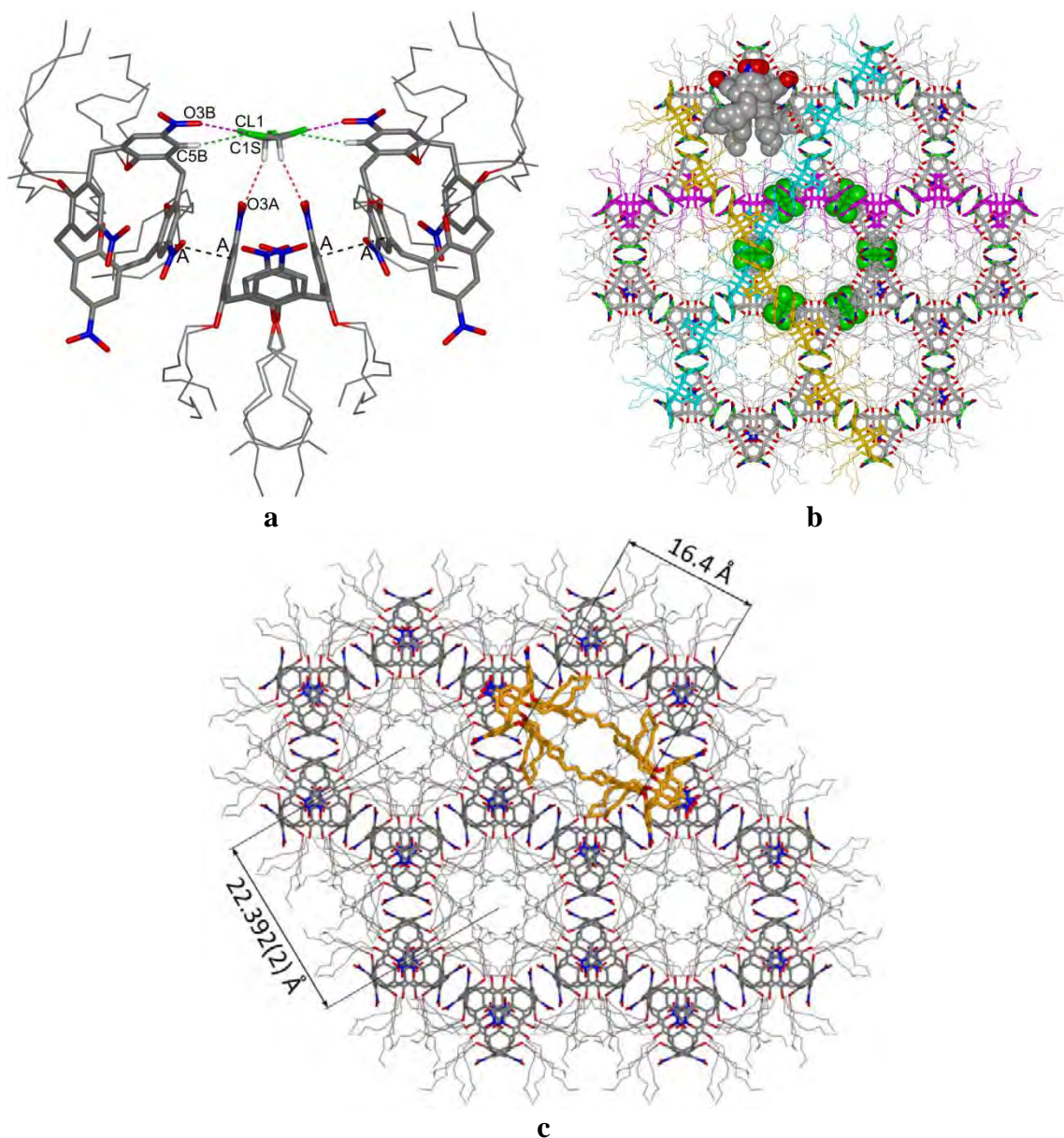⋯Cl hydrogen bonds, where H atoms are in meta-positions of benzene ring and methoxy bridge B (Table 65) of $NO_2C[4]OC_8$ molecule of the neighbouring infinite chain. Additionally, the chloroform molecule is in close O⋯Cl contact (3.08(2) Å) with the nitro groups of the same calix[4]arene molecule. In this way the calix[4]arene macrocyclic rings and solvent molecules form a relatively rigid framework with hexagonal distribution of 'channels' (diameter equal to 16.4 Å) formed by disordered flexible alkyl chains (Fig. 110b and c).

4.3.3 Crystal structure of O-dodecylated *para*-nitrocalix[4]arene (cone)

O-Dodecylated *para*-nitrocalix[4]arene ($NO_2C[4]OC_{12}$) crystallises from a methanol/chloroform mixture in the triclinic crystallographic system. Crystal data are presented in Table 66. The asymmetric unit comprises one calix[4]arene molecule which adopts the pinched cone conformation (Fig. 111a). Carbon atom numbering scheme is shown in Fig. 111b. The dodecyl chain at the ring D is disordered over two positions with equal occupancy factors of 0.5 and was modelled with restraints to retain the correct geometry and reasonable thermal parameters.
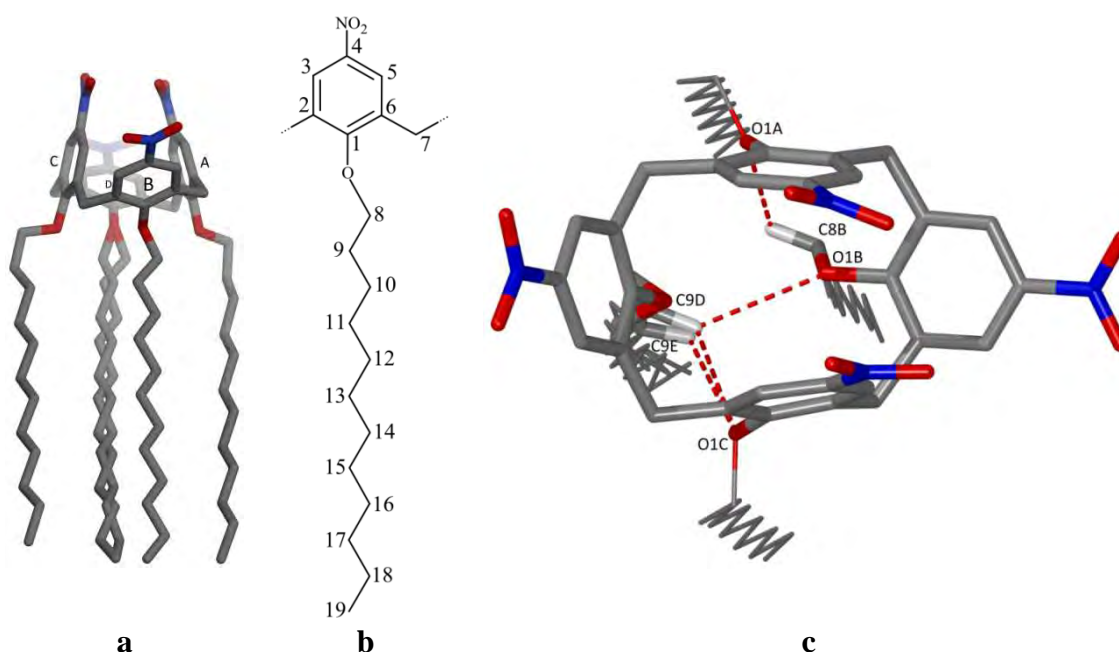

Fig. 111. $NO_2C[4]OC_{12}$ (cone): (a) asymmetric unit; (b) numbering scheme; (c) conformation stabilised by C–H⋯O intramolecular contacts.

Table 66. Crystal data and structure refinement for NO$_2$C[4]OC$_{12}$ (cone)

Molecular formula	C$_{76}$H$_{116}$N$_4$O$_{12}$
Formula weight	1277.73
Crystal system	Triclinic
Space group	$P\bar{1}$
Unit cell dimensions	a = 11.303(2) Å $\quad$ α = 71.294(6)°
	b = 17.751(2) Å $\quad$ β = 85.55(1)°
	c = 20.001(3) Å $\quad$ γ = 72.489(6)°
Volume	3624(1) Å^3
Z	2
Temperature	100.0(5)
Radiation and wavelength	Mo Kα radiation, λ = 0.71073 Å
Monochromator	graphite
Density (calculated)	1.171 Mg·m^{-3}
Absorption coefficient	0.08 mm^{-1}
F(000)	1392
Crystal size	0.15 × 0.18 × 0.20 mm
θ range for data collection	2.8–22.1°
Index ranges	-11 ≤ h ≤ 11, -18 ≤ k ≤ 18, -21 ≤ l ≤ 19
Reflections collected	41411
Independent reflections	8897 [R_{int} = 0.130]
Completeness	100.0 %
Absorption correction	None
Refinement method	Full-matrix least-squares on F^2
Weighting scheme	$[\sigma^2(F_o^2) + (0.0702P)^2 + 0.7535P]^{-1}$ *
Data / restraints / parameters	8897 / 20 / 932
Goodness-of-fit on F^2	1.03
Final R indices [$I > 2\sigma(I)$]	R = 0.061, wR = 0.138
R indices (all data)	R = 0.105, wR = 0.154
Extinction coefficient	Not refined
Largest diff. peak and hole	0.22 and -0.22 e·Å^{-3}

* $P = (F_o^2 + 2F_c^2)/3$

Dihedral angles between planes of each benzene ring and the mean plane of the four methylene groups and distances between distal C4 atoms are presented in Table 67.

Table 67. Calix[4]arene macrocyclic ring geometry for NO$_2$C[4]OC$_{12}$ (cone)

	∠(ring-to-CH$_2$-plane), °	Distal C4···C4 distances, Å	
A	75.27(8)	C4A···C4C	4.020(5)
B	140.67(8)		
C	79.80(9)	C4B···C4D	10.013(5)
D	145.43(9)		

The calix[4]arene conformation is stabilised by four C–H···O intramolecular contacts (Fig. 111c and Table 68) between H-atoms of the first and the second methylene

Table 68. Weak interactions in NO$_2$C[4]OC$_{12}$ (cone)

Hydrogen bonds

D–H⋯A	d(D–H), Å	d(H⋯A), Å	d(D⋯A), Å	∠D–H⋯A
C5C–H5C⋯O2D[1]	0.95	2.88	3.730(4)	150
C5C–H5C⋯O3D[1]	0.95	2.61	3.522(4)	162
C7B–H7B1⋯O2C[2]	0.99	2.63	3.558(4)	157
C7D–H7D2⋯O2A[3]	0.99	2.86	3.649(4)	138
C8A–H8A2⋯O2A[3]	0.99	2.37	3.250(4)	147
C8B–H8B1⋯O2B[4]	0.99	2.86	3.413(4)	117
C8B–H8B2⋯O1A	0.99	2.62	3.105(4)	110
C8C–H8C1⋯O3B[2]	0.99	2.61	3.294(4)	127
C9B–H9B2⋯O2B[4]	0.99	2.58	3.244(5)	124
C9D–H9D1⋯O1B	0.99	2.98	3.68(2)	128
C9D–H9D2⋯O1C	0.99	2.76	3.43(2)	125
C9E–H9E2⋯O1C	0.99	2.71	3.31(2)	119
C17C–H17E⋯O3A[5]	0.99	2.56	3.448(4)	149
C18D–H18D⋯O3A[5]	0.99	2.19	3.06(1)	145
C19A–H19B⋯O2A[6]	0.98	2.99	3.746(5)	136
C19B–H19E⋯O2C[6]	0.98	2.52	3.498(4)	174
C19B–H19E⋯O3C[6]	0.98	2.89	3.600(4)	130
C19C–H19G⋯O2C[5]	0.98	2.97	3.574(5)	121
C19C–H19H⋯O2B[5]	0.98	2.50	3.390(4)	151
C19C–H19I⋯O3A[5]	0.98	2.61	3.453(5)	144

Symmetry codes: (1) $-1 - x$, $1 - y$, $- z$; (2) $-1 - x$, $2 - y$, $- z$; (3) $- x$, $1 - y$, $- z$; (4) $- x$, $2 - y$, $- z$; (5) x, y, $1 + z$; (6) $1 + x$, y, $1 + z$.

π⋯π interactions

CgI⋯CgJ	d(CgI⋯CgJ)	α	β	γ	⊥(CgI⋯πJ)	⊥(CgJ⋯πI)
CgB⋯CgB[1]	4.713(5)	0	47	47	3.217(5)	3.217(5)
CgD⋯CgD[2]	6.205(5)	0	65	65	2.644(5)	2.644(5)

Symmetry codes: (1) $- x$, $2 - y$, $-z$; (2) $-1 - x$, $1 - y$, $- z$.

d(CgI⋯CgJ) – distance between ring centroids I and J (Å), α – dihedral angle between planes I and J; β – angle between CgI⋯CgJ vector and normal to plane I; γ – angle between CgI⋯CgJ vector and normal to plane J (°), ⊥(CgI⋯πJ) – perpendicular distance of CgI on ring J; ⊥(CgJ⋯πI) – perpendicular distance of CgJ on ring I (Å).

groups of the alkyl chains B, D and E and oxygen atoms of phenoxy moieties A, C and D.

In spite of elongation of the alkyl chains to twelve carbon atoms, the crystal structure of NO$_2$C[4]OC$_{12}$ is kindred with crystal structures of NO$_2$C[4]OC$_1$·CHCl$_3$, tetra-O-propylated *para*-nitrocalix[4]arenes[113–115] and NO$_2$C[4]OC$_8$·CHCl$_3$. NO$_2$C[4]OC$_{12}$ molecules in opposite spatial orientation form infinite chains (Fig. 112) due to π-π stacking interactions between the conjugated systems of benzene rings and nitro groups of the neighbouring calixarenes [ring B⋯ring B and ring D⋯ring D] with
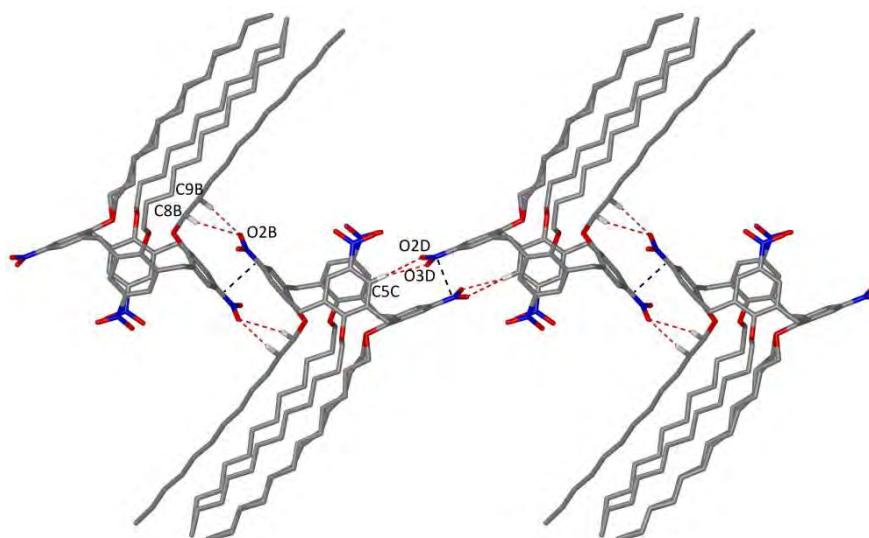
Fig. 112. NO$_2$C[4]OC$_{12}$ (cone): self-assembly in infinite chains along diagonal between a and *b* crystallographic axes due to π-π stacking interactions and C–H···O contacts.

additional stabilisation by C–H···O contacts (Table 68). The shortening of the distance between the interacting π-electronic systems of the rings D can be explained by stronger polarisation effect of C–H···O contacts (C5C···O3D and C5C···O2D).

Chains of calixarene molecules in NO$_2$C[4]OC$_{12}$ are joined by C–H···O binding (Fig. 113a and Table 68) between H-atoms of first methylene groups of alkyl substituents and oxygen atoms of the nitro groups at rings A and B and H-atoms of calixarene methylene bridges B and C and oxygen atoms of the nitro groups at rings C and A.

a   b

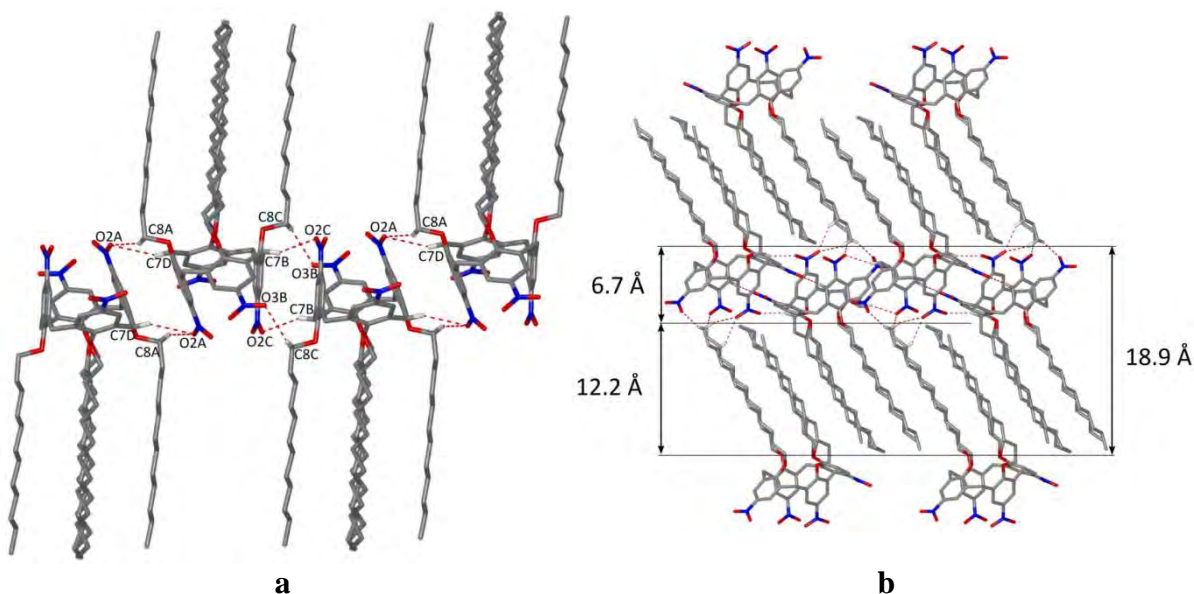**Fig. 113. NO$_2$C[4]OC$_{12}$ (cone): (a) self-assembly perpendicular to diagonal between a and *b* crystallographic axes due to C–H···O contacts; (b) packing diagram, view along the *a* crystallographic axis.**

137

The presence of long hydrophobic alkyl chains force a different self-assembly of $NO_2C[4]OC_{12}$ molecules, compared to the analogous molecules with shorter substituents. Infinite chains of the calixarene molecules, combined in direction perpendicular to diagonal between a and *b* crystallographic axes by C–H···O contacts, form classical for amphiphilic compounds bilayer motif with interdigitated alkyl chains (Fig. 113b). Hydrogen atoms of the last carbon atoms of alkyl chains are hydrogen donors in C–H···O contacts where the acceptors are oxygen atoms of nitro groups (Table 68). Additionally, they take part in weak van der Waals interactions between alkyl chains stabilising the bilayer formation. The thickness of aromatic and aliphatic layers are *ca.* 6.7 and 12.2 Å.

There are voids present between the calix[4]arene aromatic systems and aliphatic chains in the crystal structure of NO2C[4]OC₁₂ (Fig. 114). The volume of a single void equals *ca.* 14 Å^3 and is not large enough to accommodate a solvent molecule.
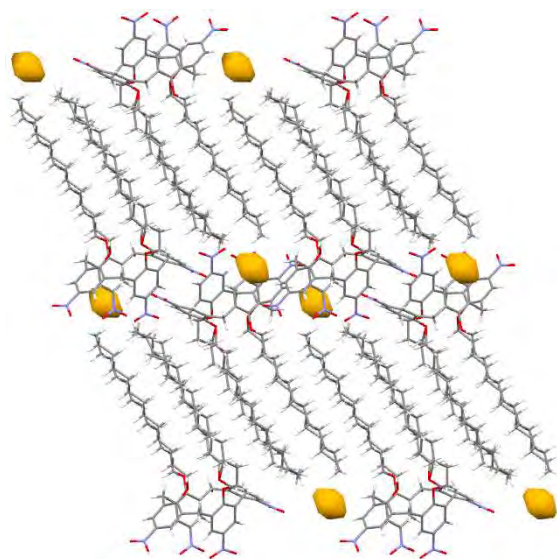
Fig. 114. Voids in crystal of $NO_2C[4]OC_{12}$ (cone).

4.3.4 Crystal structure of O-tetradecylated *para*-nitrocalix[4]arene (cone) chloroform monosolvate

O-Tetradecylated *para*-nitrocalix[4]arene-chloroform solvate with a stoichiometry 1:1 ($NO_2C[4]OC_{14} \cdot CHCl_3$) crystallises from methanol/chloroform mixture in the monoclinic crystallographic system and is isostructural with tBuC[4]OC₁₀, tBuC[4]OC₁₂ and tBuC[4]OC₁₄ chloroform monosolvates. Crystal data for the monosolvate are presented in Table 69. Carbon atom numbering scheme is shown in Fig. 115a. The asymmetric unit comprises one molecule of the host and one molecule of the guest.

Table 69. Crystal data and structure refinement for NO$_2$C[4]OC$_{14}$ (cone)·CHCl$_3$

Molecular formula	C$_{84}$H$_{132}$N$_4$O$_{12}$·CHCl$_3$
Formula weight	1509.30
Crystal system	Monoclinic
Space group	$P2_1/c$
Unit cell dimensions	a = 30.0091(7) Å
	b = 15.5077(4) Å β = 104.7983(7)°
	c = 18.5583(5) Å
Volume	8350.0(4) Å^3
Z	4
Temperature	100.0(5) K
Radiation and wavelength	Mo Kα radiation, λ = 0.71073 Å
Monochromator	graphite
Density (calculated)	1.201 Mg·m^{-3}
Absorption coefficient	0.17 mm^{-1}
F(000)	3272
Crystal size	0.15 × 0.30 × 0.40 mm
θ range for data collection	2.9–26.0°
Index ranges	-37 ≤ h ≤ 37, -18 ≤ k ≤ 19, -22 ≤ l ≤ 22
Reflections collected	73710
Independent reflections	15569 [R_{int} = 0.026]
Completeness	95.8 %
Absorption correction	None
Refinement method	Full-matrix least-squares on F^2
Weighting scheme	$[\sigma^2(F_o^2) + (0.032P)^2 + 20.0067P]^{-1}$ *
Data / restraints / parameters	15569 / 0 / 941
Goodness-of-fit on F^2	1.09
Final R indices [$I > 2\sigma(I)$]	R = 0.056, wR = 0.120
R indices (all data)	R = 0.070, wR = 0.127
Extinction coefficient	Not refined
Largest diff. peak and hole	0.70 and -0.66 e·Å^{-3}

* $P = (F_o^2 + 2F_c^2)/3$

The calix[4]arene assumes a pinched cone conformation (Fig. 115b). Dihedral angles between planes of each benzene ring and the mean plane of the four methylene groups and distances between distal C4 atoms are presented in Table 70.

Table 70. Calix[4]arene macrocyclic ring geometry for NO$_2$C[4]OC$_{14}$ (cone)·CHCl$_3$

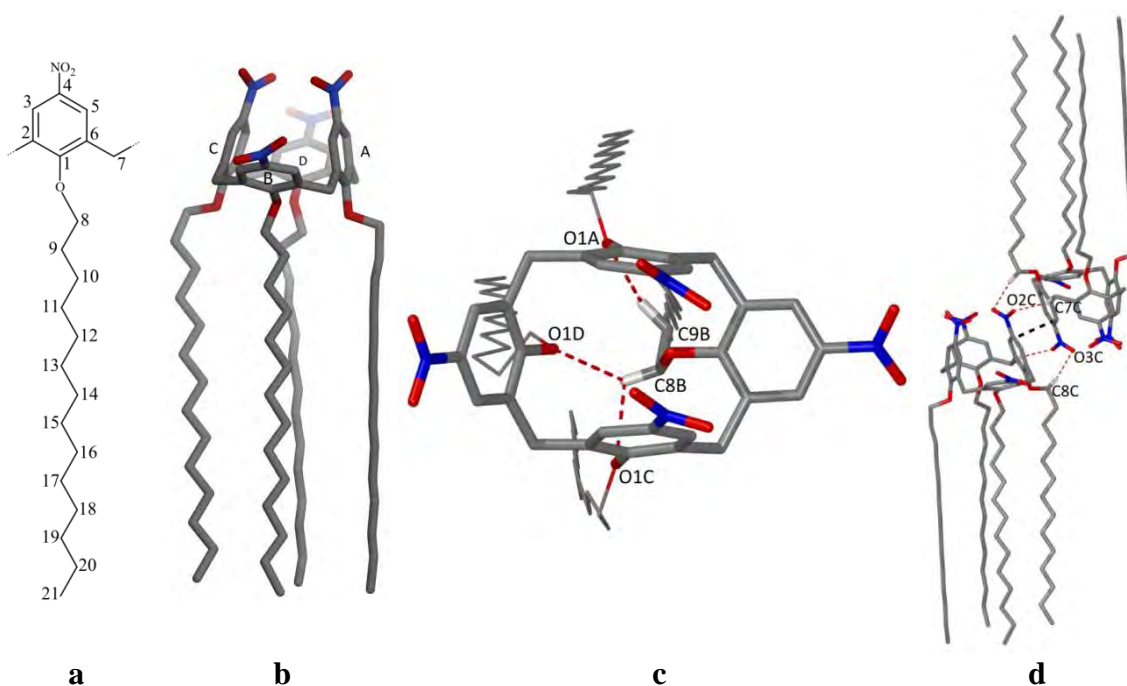|	∠(ring-to-CH$_2$-plane), °	Distal C4···C4 distances, Å	
A	80.32(5)	C4A···C4C	4.209(3)
B	153.63(3)		
C	75.85(5)	C4B···C4D	10.138(3)
D	142.67(5)		

Fig. 115. $NO_2C[4]OC_{14} \cdot CHCl_3$ **(cone): (a) numbering scheme; (b) molecule of the host; (c) conformation stabilised by C–H⋯O intramolecular contacts; (c) dimer formation.**

The conformation is stabilised by one bifurcated and one normal C–H⋯O hydrogen bond (Fig. 115c and Table 71) between H-atoms of the first and the second methylene groups of the chain B and oxygen atoms of phenoxy moieties A, C and D.

Contrary to $NO_2C[4]OC_1 \cdot CHCl_3$, tetra-O-propylated *para*-nitrocalix[4]-arenes,[113–115] $NO_2C[4]OC_8 \cdot CHCl_3$ and $NO_2C[4]OC_{12}$, π-π stacking interactions in $NO_2C[4]OC_{14} \cdot CHCl_3$ combine calix[4]arene molecules in centrosymmetric dimers (Fig. 115d). Distance between the planes of the interacting π-systems equals to 3.592(3) Å. π-π Stacking interaction is enhanced by four C–H⋯O contacts (two symmetrically independent) between H-atoms of calix[4]arene methylene bridge C [C7C⋯O2C] and the first methylene group of alkyl chain C [C8C⋯O3C] and oxygen atoms of nitro group of centrosymmetrically related ring C (Table 71).

Each calix[4]arene molecule is involved in C–H⋯O hydrogen binding with three molecules in opposite spatial orientation. When one of them additionally takes part in π-π stacking interactions in dimer, the other two participate in four C–H⋯O contacts between *meta*-H-atoms of benzene rings and oxygen atoms of nitro groups A and D, and one between calixarene methylene bridge D and oxygen atom of the nitro group C (Fig. 116a and Table 71). Self-assembly of $NO_2C[4]OC_{14}$ molecules in the same spatial orientation due to C–H⋯O binding between H-atoms of the first and the second methylene groups of alkyl chain C and oxygen atom of the nitro group B is shown in Fig. 116b.

15:

Table 71. Weak interactions in NO$_2$C[4]OC$_{14}$ (cone)·CHCl$_3$

Hydrogen bonds

D–H$\cdots A$	d(D–H), Å	d(H$\cdots A$), Å	d(D$\cdots A$), Å	$\angle D$–H$\cdots A$
C3B–H3B$\cdots$O3D[1]	0.95	2.68	3.187(3)	114
C5A–H5A$\cdots$O3D[1]	0.95	2.56	3.452(3)	156
C5B–H5B$\cdots$O2A[1]	0.95	2.41	3.103(3)	129
C5D–H5D$\cdots$O3A[2]	0.95	2.51	3.396(3)	156
C7C–H7C2$\cdots$O2C[3]	0.99	2.47	3.347(3)	147
C7D–H7D1$\cdots$O2C[2]	0.99	2.36	3.168(2)	138
C8B–H8B1$\cdots$O1C	0.99	2.55	3.029(2)	109
C8B–H8B1$\cdots$O1D	0.99	2.96	3.553(3)	119
C8C–H8C2$\cdots$O3B[4]	0.99	2.56	3.250(3)	127
C8C–H8C2$\cdots$O3C[3]	0.99	2.53	3.314(3)	136
C9B–H9B2$\cdots$O1A	0.99	2.93	3.674(3)	132
C9C–H9C1$\cdots$O3B[4]	0.99	2.76	3.164(3)	105
C1S–H1S$\cdots$O2A[2]	1.00	2.66	3.464(3)	137
C1S–H1S$\cdots$O3A[2]	1.00	2.69	3.498(3)	138
C1S–H1S$\cdots$O2D[5]	1.00	2.36	3.246(3)	147
C8D–H8D2$\cdots$Cl1	0.99	2.90	3.755(2)	145

Symmetry codes: (1) $1 - x$, $-0.5 + y$, $0.5 - z$; (2) $1 - x$, $0.5 + y$, $0.5 - z$; (3) $1 - x$, $- y$, $1 - z$; (4) x, $-0.5 - y$, $0.5 + z$; (5) $1 - x$, $1 - y$, $1 - z$.

Short N$\cdots$O contacts

N$\cdots$O	d(N$\cdots$O), Å	N$\cdots$O	d(N$\cdots$O), Å
N1A$\cdots$O3C	3.155(2)	N1D$\cdots$O2B[2]	3.063(3)
N1A$\cdots$O2D[1]	2.901(2)	N1D$\cdots$O3D[3]	3.007(2)
N1C$\cdots$O3A	3.122(2)		

Symmetry codes: (1) x, $0.5 - y$, $-0.5 + z$; (2) $1 - x$, $0.5 + y$, $0.5 - z$; (3) $1 - x$, $1 - y$, $1 - z$.

C–H$\cdots\pi$ interactions

C–H$\cdots$Cg	d(H$\cdots$Cg)	$\perp d$(H$\cdots\pi$)	d(C$\cdots$Cg)	$\angle$C–H$\cdots$Cg	$\angle$C–H$\cdots\pi$
C21A–H21B$\cdots$CgB[1]	3.50	2.96	4.331(3)	144	150
C21B–H21F$\cdots$CgB[1]	3.39	2.97	4.022(3)	125	97

Symmetry codes: (1) $- x$, $-y$, $-z$.

$\pi\cdots\pi$ interaction

CgI$\cdots$CgJ	d(CgI$\cdots$CgJ)	α	β	γ	$\perp$(CgI$\cdots\pi$J)	$\perp$(CgJ$\cdots\pi$I)
CgC$\cdots$CgC[1]	4.415(3)	0	36	36	3.586(3)	3.586(3)

Symmetry codes: (1) $1 - x$, $-y$, $1 - z$.

d(CgI$\cdots$CgJ) – distance between ring centroids I and J (Å), α – dihedral angle between planes I and J; β – angle between CgI$\cdots$CgJ vector and normal to plane I; γ – angle between CgI$\cdots$CgJ vector and normal to plane J (°), $\perp$(CgI$\cdots\pi$J) – perpendicular distance of CgI on ring J; $\perp$(CgJ$\cdots\pi$I) – perpendicular distance of CgJ on ring I (Å).

a

b
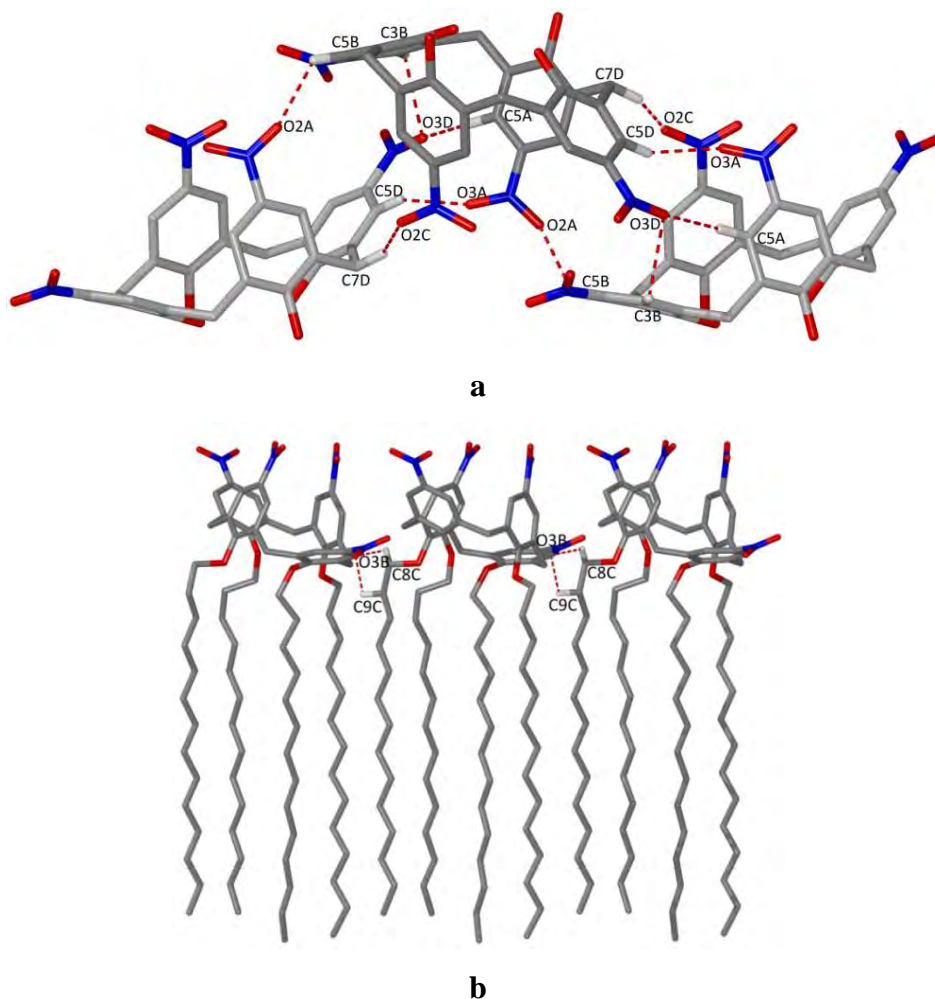
Fig. 116. NO$_2$C[4]OC$_{14}$·CHCl$_3$ (cone): (a) C–H···O hydrogen binding between the calix[4]arene molecules in opposite orientation. Alkyl substituents are omitted for clarity; (b) C–H···O hydrogen binding between the calix[4]arene molecules in the same orientation.

Molecules of NO$_2$C[4]OC$_{14}$ are assembled in bilayer shown in Fig. 117a. The thickness of aromatic and aliphatic regions are 9.2 and 19.8 Å, respectively. The bilayer structure is also stabilised by two C–H···π interactions between H-atoms of terminal carbons of chains A and B and aromatic ring B of neighbouring calix[4]arene (Fig. 117b).

There are short N···O contacts between the nitro groups in structure of NO$_2$C[4]OC$_{14}$·CHCl$_3$, which additionally stabilise the structure (Table 71).

Chloroform molecules are included in the voids between the calix[4]arene aromatic systems and aliphatic chains (Fig. 117a). Each guest molecule is a hydrogen donor in trifurcated C–H···O bonds to oxygen atoms O2A, O3A and O2D of the neighbouring molecules of NO$_2$C[4]OC$_{14}$ and a hydrogen acceptor in C8D–H8D2···Cl1 bond (Fig. 117c and Table 71).
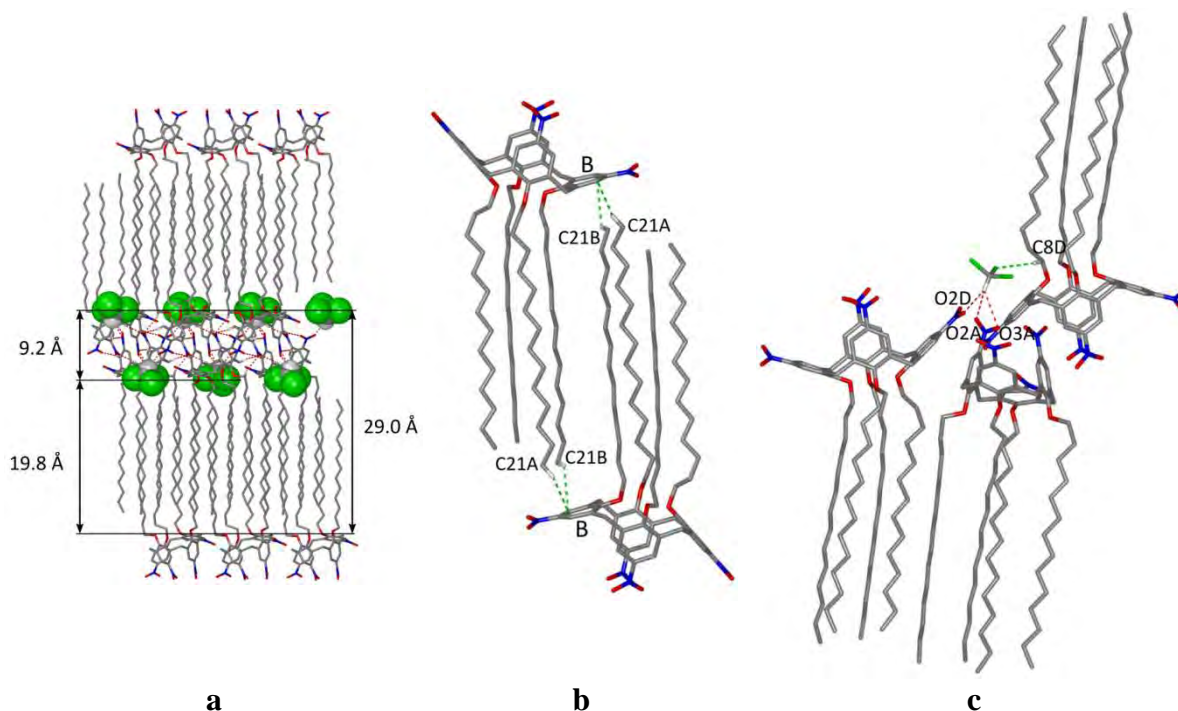
142

a	**b**	**c**

Fig. 117. NO$_2$C[4]OC$_{14}$·CHCl$_3$ (cone): (a) packing diagram, view along the *b* crystallographic axis. Chloroform molecules are shown in the spacefill mode; (b) C–H···π interactions; (c) chloroform inclusion.

4.3.5 Crystal structure of O-tetradecylated *para*-nitrocalix[4]arene (cone) chloroform disolvate

O-Tetradecylated *para*-nitrocalix[4]arene-chloroform solvate with stoichiometry 1:2 (NO$_2$C[4]OC$_{14}$·2CHCl$_3$) crystallises from methanol/chloroform mixture in the triclinic crystallographic system. Data collection was performed at 140 K. Below this temperature mosaicity start to increase up to 4.2° and crystal cracking is observed. Crystal data are presented in Table 72. Carbon atom numbering scheme is shown in Fig. 118a.

Table 72. Crystal data and structure refinement for NO$_2$C[4]OC$_{14}$ (cone)·2CHCl$_3$

Molecular formula	C$_{84}$H$_{132}$N$_4$O$_{12}$·2CHCl$_3$	
Formula weight	1628.67	
Crystal system	Triclinic	
Space group	$P\bar{1}$	
Unit cell dimensions	a = 12.5405(1) Å	α = 91.6215(8)°
	b = 13.4126(2) Å	β = 95.8869(6)°
	c = 27.3215(4) Å	γ = 102.0774(5)°
Volume	4464.2(1) Å^3	
Z	2	
Temperature	140.0(5) K	
Radiation and wavelength	Mo Kα radiation, λ = 0.71073 Å	
Monochromator	graphite	
Density (calculated)	1.212 Mg·m^{-3}	

Table 72. Continuation.

Absorption coefficient	0.25 mm^{-1}
$F(000)$	1752
Crystal size	0.15 × 0.21× 0.25 mm
θ range for data collection	1.6–26.7°
Index ranges	-15 ≤ h ≤ 15, -16 ≤ k ≤ 16, -34 ≤ l ≤ 34
Reflections collected	72134
Independent reflections	18720 [R_{int} = 0.076]
Completeness	99.0 %
Absorption correction	None
Refinement method	Full-matrix least-squares on F^2
Weighting scheme	$[\sigma^2(F_o^2) + (0.0847P)^2 + 2.3343P]^{-1}$ *
Data / restraints / parameters	18720 / 0 / 977
Goodness-of-fit on F^2	1.05
Final R indices [$I > 2\sigma(I)$]	R = 0.056, wR = 0.155
R indices (all data)	R = 0.067, wR = 0.163
Extinction coefficient	Not refined
Largest diff. peak and hole	0.55 and -0.62 e·Å^{-3}

* $P = (F_o^2 + 2F_c^2)/3$

The asymmetric unit comprises one host molecule and two guest molecules. The calix[4]arene assumes a pinched cone conformation shown in Fig. 118b.

Dihedral angles between planes of each benzene ring and the mean plane of the four methylene groups and distances between distal C4 atoms are presented in Table 73. The conformation is stabilised by two C–H···O contacts between H-atoms of the first
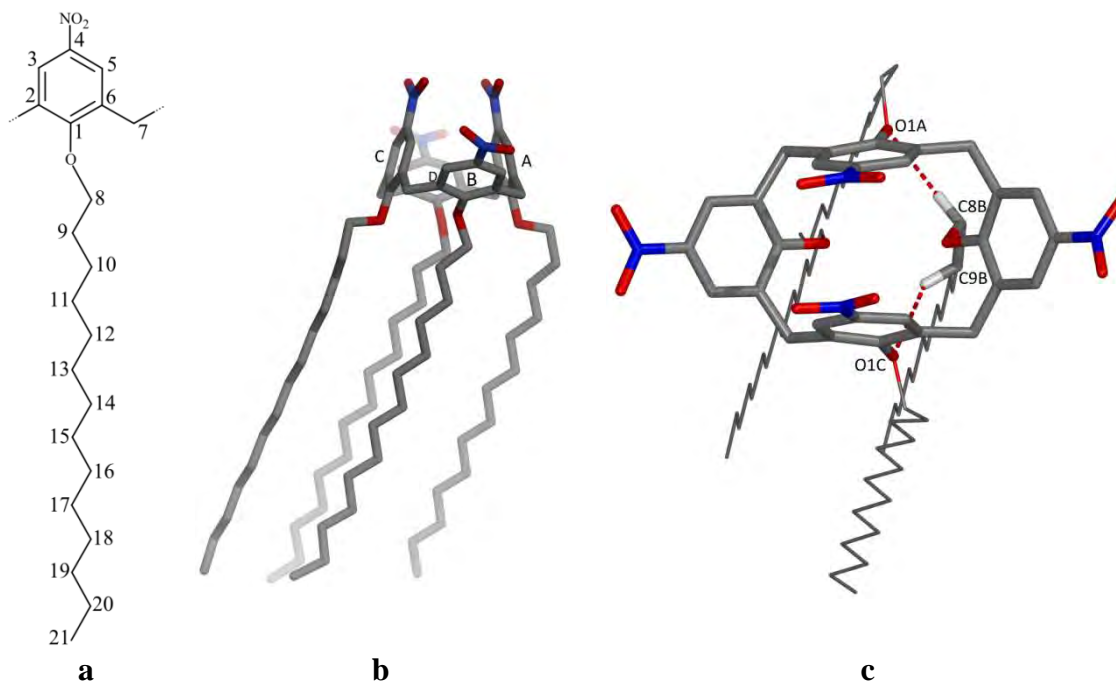

a   b   c

Fig. 118. NO$_2$C[4]OC$_{14}$ (cone)·2CHCl$_3$: (a) numbering scheme; (b) molecule of the host; (c) conformation stabilised by C–H···O intramolecular contacts.

Table 73. Calix[4]arene macrocyclic ring geometry for NO$_2$C[4]OC$_{14}$ (cone)·2CHCl$_3$

∠(ring-to-CH$_2$-plane), °		Distal C4···C4 distances, Å	
A	77.39(4)	C4A···C4C	4.020(2)
B	149.14(4)		
C	75.35(5)	C4B···C4D	10.046(2)
D	140.21(4)		

and the second methylene groups of the chain B and oxygen atoms of phenoxy moieties A and C (Fig. 118c and Table 74).

Calix[4]arene molecules in NO$_2$C[4]OC$_{14}$·2CHCl$_3$, similarly to NO$_2$C[4]OC$_{14}$· CHCl$_3$, form centrosymmetric dimers (Fig. 119a) due to π-π stacking interactions (ring A···ring A) enhanced by two C–H···O contacts between H-atom of the first methylene group of alkyl chain A and oxygen atom of nitro group at centrosymmetrically related ring A (C8A···O3A).
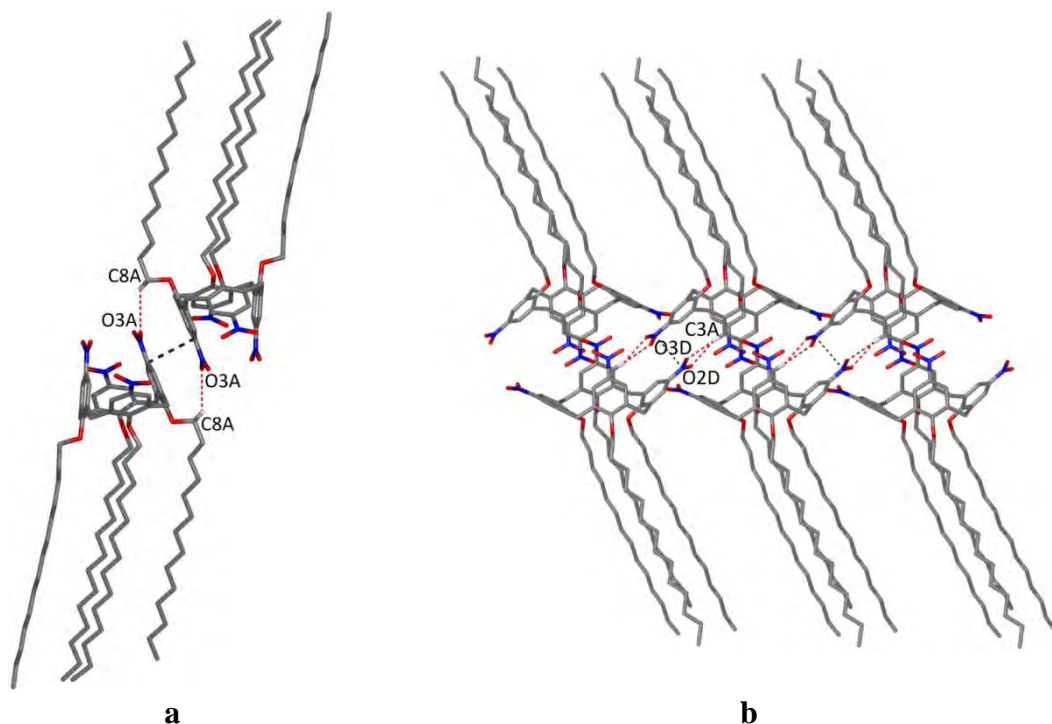
Fig. 119. NO$_2$C[4]OC$_{14}$ (cone)·2CHCl$_3$: (a) self-assembly of the dimers in ribbon, only enhanced by C–H···O hydrogen binding π-π stacking interactions are shown; (b) dimer formation.

Then the dimers are self-assembled in ribbons (Fig. 119b) also due to π-π stacking interactions (ring D···ring D) enhanced by two bifurcated C–H···O contacts between *meta*-H-atoms of the ring A and oxygen atoms of nitro group D of neighbouring calixarene (C3A···O2D and C3A···O3D). Fig. 120a represents C–H···O contacts in a half of the ribbon with calix[4]arene molecules in the same orientation, which (contacts) were omitted in Fig. 119a. These contacts can be separated into two

Table 74. Weak interactions in NO$_2$C[4]OC$_{14}$ (cone)·2CHCl$_3$

Hydrogen bonds

D–H···A	d(D–H), Å	d(H···A), Å	d(D···A), Å	∠D–H···A
C3A–H3A···O2D[1]	0.95	2.69	3.564(2)	153
C3A–H3A···O3D[1]	0.95	2.88	3.782(2)	158
C3B–H3B···O2D[2]	0.95	2.73	3.557(2)	146
C3D–H3D···O2B[3]	0.95	2.70	3.517(2)	144
C5B–H5B···O3C[4]	0.95	2.80	3.671(3)	152
C7A–H7A2···O2D[2]	0.99	2.86	3.741(2)	149
C7C–H7C2···O2B[3]	0.99	2.58	3.432(2)	146
C8A–H8A1···O3A[5]	0.99	2.97	3.417(2)	108
C8B–H8B2···O1A	0.99	2.44	3.271(2)	142
C9B–H9B1···O1C	0.99	2.58	3.370(2)	136
C1S–H1S···O2A	1.00	2.40	3.169(2)	134
C1S–H1S···O3C	1.00	2.42	3.050(2)	120
C1S–H1S···O3D[1]	1.00	2.54	3.274(3)	130
C2S–H2S···O2B	1.00	2.59	3.400(3)	138
C2S–H2S···O3B	1.00	2.61	3.253(3)	122
C2S–H2S···O3B[6]	1.00	2.65	3.441(3)	136
C7B–H7B1···Cl3[4]	0.99	2.72	3.649(2)	156
C8A–H8A1···Cl3[5]	0.99	2.87	3.603(2)	132
C20B–H20D···Cl3[7]	0.99	3.08	3.545(2)	110
C21A–H21B···Cl1[7]	0.98	2.86	3.543(3)	127
C21B–H21E···Cl3[7]	0.98	2.88	3.605(2)	132
C21D–H21K···Cl5[8]	0.98	2.93	3.462(3)	115

Symmetry codes: (1) 1 − x, 2 − y, − z; (2) 1 + x, y, z; (3) −1 + x, y, z; (4) 2 − x, 3 − y, −z; (5) 2 − x, 2 − y, −z; (6) 3 − x, 3 − y, −z; (7) x, y, 1 + z; (8) 2 − x, 3 − y, 1 − z.

C–H···π interactions

C–H···Cg	d(H···Cg)	⊥d(H···π)	d(C···Cg)	∠C–H···Cg	∠C–H···π
C21B–H21D···CgB[1]	3.76	2.95	4.397(3)	125	116
C21C–H21G···CgB[1]	3.15	3.13	3.915(3)	136	131

Symmetry codes: (1) 2 − x, 3 − y, 1 − z.

π···π interactions

CgI···CgJ	d(CgI···CgJ)	α	β	γ	⊥(CgI···πJ)	⊥(CgJ···πI)
CgA···CgA[1]	4.600(2)	0	42	42	3.396(2)	3.396(2)
CgD···CgD[2]	6.549(2)	0	67	67	2.603(2)	2.603(2)

Symmetry codes: (1) 2 − x, 2 − y, −z; (2) 1 − x, 2 − y, −z.

d(CgI···CgJ) – distance between ring centroids I and J (Å), α – dihedral angle between planes I and J; β – angle between CgI···CgJ vector and normal to plane I; γ – angle between CgI···CgJ vector and normal to plane J (°), ⊥(CgI···πJ) – perpendicular distance of CgI on ring J; ⊥(CgJ···πI) – perpendicular distance of CgJ on ring I (Å).

groups. The first one is realised between *meta*-H-atoms of rings B and D and oxygen atoms of nitro groups D and B of neighbouring calixarenes (C3B···O2D and C3D···O2B), then the second one between H-atoms of calix[4]arene methylene bridges and the same oxygen atoms of nitro groups D and B of neighbouring calixarenes (C7A···O2D and C7C···O2B).
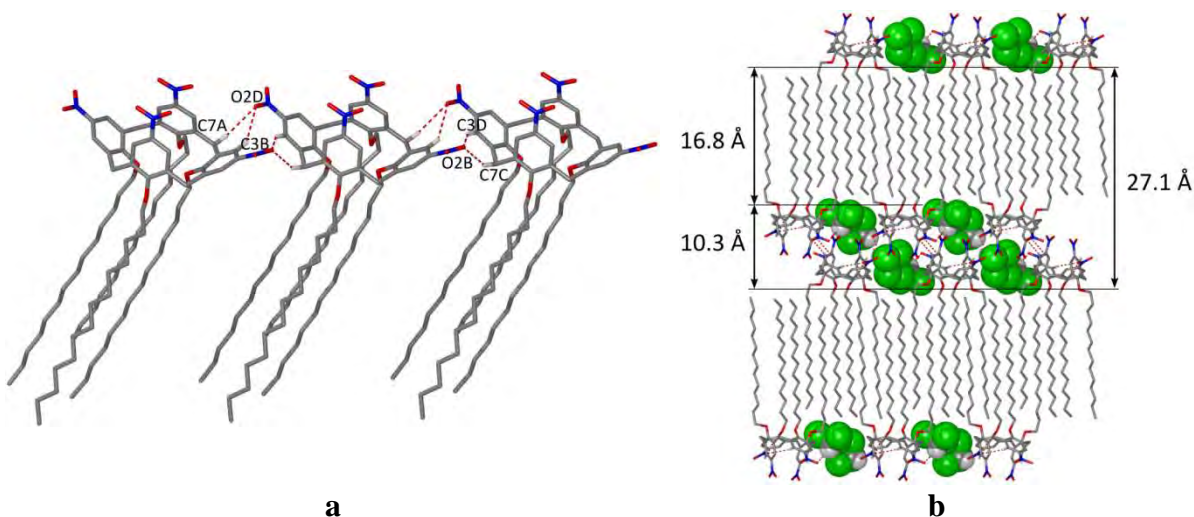

Fig. 120. $NO_2C[4]OC_{14}$ (cone)·$2CHCl_3$: (a) C–H···O contacts between the calix[4]arene molecules in the same orientation; (b) packing diagram, view along the *a* crystallographic axis, chloroform molecules are shown in the spacefill mode;.

The ribbons are joined by C–H···O contacts between *meta*-H-atoms of rings B and oxygen atoms of nitro groups of rings C of adjacent calix[4]arenes [C5B···O3C]. The resulting bilayer motif of self-assembling is shown in Fig. 120b. It is additionally stabilised by C–H···π interactions of two terminal carbon atoms, C21B and C21C, and benzene ring B of neighbouring calixarene.

The thickness of aromatic and aliphatic regions are equal to 10.3 and 16.8 Å, respectively.

There are two molecules of chloroform included in the crystal structure of $NO_2C[4]OC_{14}$·$2CHCl_3$. One solvent molecule is a hydrogen donor in trifurcated C–H···O contacts to oxygen atoms of the neighbouring molecules of $NO_2C[4]OC_{14}$ and a hydrogen acceptor in four C–H···Cl contacts (Fig. 121a). The second chloroform molecule also participates in trifurcated C–H···O bond to adjacent nitro groups but, in contrast to the first chloroform molecule, in only one C–H···Cl contact of 3.462(3) Å to terminal carbon atom C21D (Fig. 121b). Additionally one short Cl4···O2D contact of 3.041(2) Å is present between calixarene and chloroform molecules.
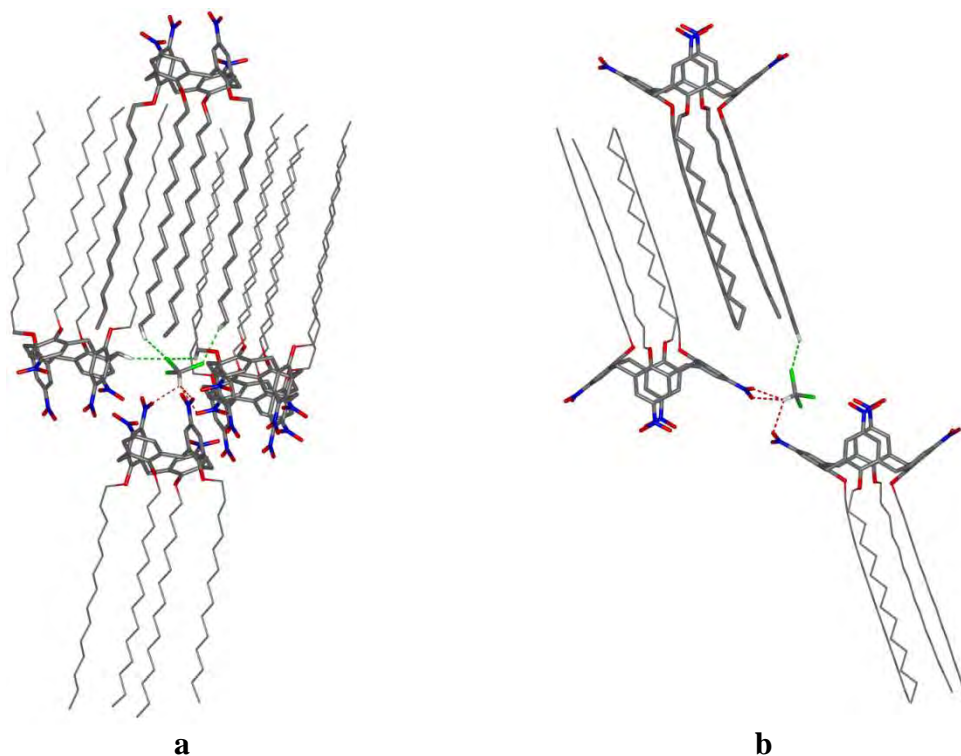
Fig. 121. NO$_2$C[4]OC$_{14}$ (cone)·2CHCl$_3$: (a) and (b) exo-complexation of chloroform molecules.

4.4 Crystal structures of O-alkylated *para-tert*-butylcalix[6]arenes

4.4.1 Crystal structure of O-propylated *para-tert*-butylcalix[6]arene chloroform disolvate

O-Propylated *para-tert*-butylcalix[6]arene crystallises from methanol/ chloroform mixture in the monoclinic crystallographic system as a calix[6]arene-chloroform solvate with stoichiometry 1:2 (tBuC[6]OC$_3$·2CHCl$_3$). Crystal data are presented in Table 75. There is no disorder in the crystal structure. The asymmetric unit comprises half of the calix[6]arene molecule and one molecule of chloroform. The molecule of the calix[6]arene assumes a centrosymmetric inverted double partial cone conformation (Fig. 122a).
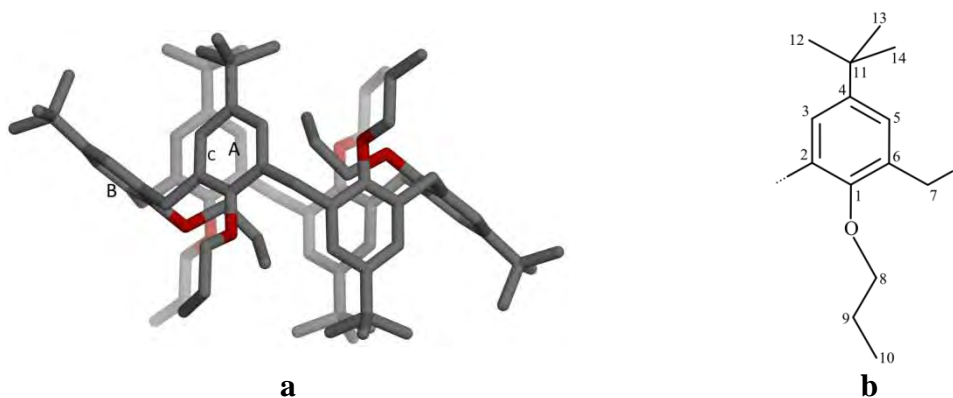

Fig. 122. tBuC[6]OC$_3$ (inverted double partial cone)·2CHCl$_3$: (a) molecule of the calix[6]arene; (b) numbering scheme.

Table 75. Crystal data and structure refinement for tBuC[6]OC$_3$·2CHCl$_3$

Molecular formula	C$_{84}$H$_{120}$O$_6$·2(CHCl$_3$)
Formula weight	1464.54
Crystal system	Monoclinic
Space group	$P2_1/c$
Unit cell dimensions	a = 14.8658(1) Å
	b = 16.6259(1) Å β = 118.1961(3)°
	c = 19.0468(2) Å
Volume	4148.94(6) Å^3
Z	2
Temperature	100.0(5)
Radiation and wavelength	Mo Kα radiation, λ = 0.71073 Å
Monochromator	graphite
Density (calculated)	1.172 Mg·m^{-3}
Absorption coefficient	0.26 mm^{-1}
F(000)	1576
Crystal size	0.17 × 0.22 × 0.24 mm
θ range for data collection	3.0–27.5°
Index ranges	-19 ≤ h ≤ 19, -21 ≤ k ≤ 21, -24 ≤ l ≤ 20
Reflections collected	70207
Independent reflections	9484 [R_{int} = 0.034]
Completeness	100 %
Absorption correction	None
Refinement method	Full-matrix least-squares on F^2
Weighting scheme	$[\sigma^2(F_o^2) + (0.0396P)^2 + 2.6142P]^{-1}$ *
Data / restraints / parameters	9484 / 0 / 454
Goodness-of-fit on F^2	1.06
Final R indices [$I > 2\sigma(I)$]	R = 0.039, wR = 0.094
R indices (all data)	R = 0.044, wR = 0.097
Extinction coefficient	Not refined
Largest diff. peak and hole	0.38 and -0.36 e·Å^{-3}

* $P = (F_o^2 + 2F_c^2)/3$

Carbon atom numbering scheme is shown in (Fig. 122b). Dihedral angles between planes of each benzene ring and the mean plane of the six methylene groups and distances between distal atoms C4 are presented in Table 76.

Table 76. Calix[4]arene macrocyclic ring geometry for tBuC[6]OC$_3$·2CHCl$_3$

	∠(ring-to-CH$_2$-plane), °	Distal C4···C4 distances, Å	
A	83.96(3)	C4A···C4A^1	10.329(2)
B	136.77(4)	C4B···C4B^1	13.366(2)
C	75.64(3)	C4C···C4C^1	8.829(2)

Symmetry codes: (1) –x, –y, 1 – z.
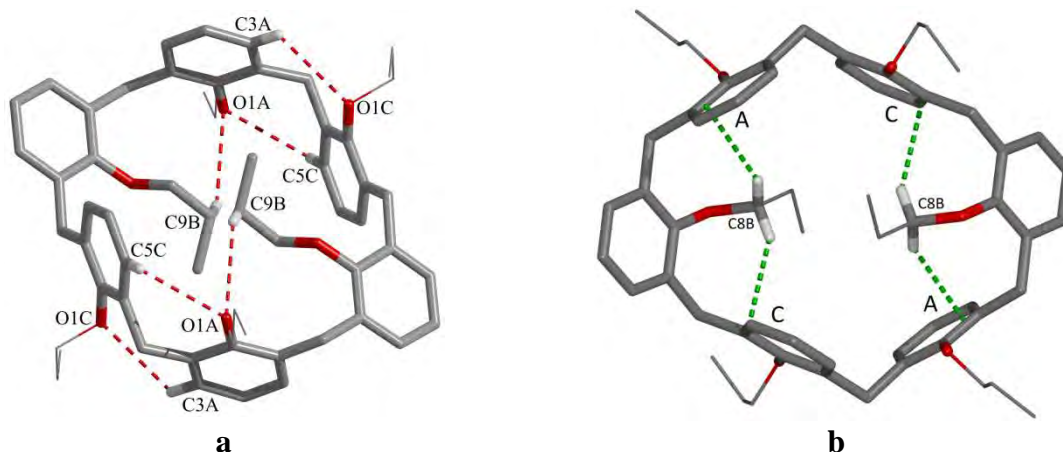
Fig. 123. tBuC[6]OC₃ (inverted double partial cone)·2CHCl₃: (a) conformation stabilised by intramolecular C–H···O; (b) C–H···π interactions, *tert*-butyl groups are omitted for clarity.

The calix[6]arene molecule conformation is stabilised by six intramolecular C–H···O bonds (Fig. 123a) and, similarly to tBuC[6]OC₁[119] and tBuC[6]OC₂,[120,121] by C–H···π interactions (Fig. 123b) between H-atoms of two alkyl chains, which close the calix[6]arene cavity from the oxygens' side, and proximal benzene rings A and C (Table 77).

Molecules of the calix[6]arene are self-assembled due to C–H···π interactions between H-atoms of *tert*-butyl groups and aromatic rings of adjacent calixarenes. The strongest C–H···π interaction is between H-atom of *tert*-butyl group at the ring B

Table 77. Weak interactions in tBuC[6]OC₃·2CHCl₃

Hydrogen bonds

D–H···A	d(D–H), Å	d(H···A), Å	d(D···A), Å	∠D–H···A
C3A–H3A···O1C[1]	0.95	2.78	3.316(2)	117
C9B–H9B1···O1A	0.99	2.92	3.643(2)	131
C5C–H5C···O1A[1]	0.95	2.78	3.282(2)	114
C7C–H7C2···Cl2[2]	0.99	2.95	3.763(2)	140
C10C–H10I···Cl3	0.98	3.06	3.796(2)	133
C13C–H13I···Cl3[3]	0.98	2.97	3.864(2)	153

Symmetry codes: (1) –x, –y, 1 – z; (2) –1 + x, 0.5 – y, –0.5 + z; (3) –x, –0.5 + y, 0.5 – z.

C–H···π interactions

C–H···Cg	d(H···Cg)	⊥d(H···π)	d(C···Cg)	∠C–H···Cg	∠C–H···π
C8B–H8B1···CgA	2.84	2.59	3.783(2)	159	135
C8B–H8B2···CgC	3.22	2.62	4.194(2)	168	133
C13B–H13E···CgA[1]	2.85	2.83	3.681(2)	144	139
C14A–H14C···CgC[2]	2.89	2.86	3.865(2)	179	171
C1S–H1S···CgB	2.43	2.43	3.375(2)	157	156

Symmetry codes: (1) 1 – x, –y, 1 – z; (2) –x, –0.5 + y, 0.5 – z.

16:

and π-electrons of the ring A, which results in the formation of infinite chains along the *a* crystallographic axis (Fig. 124a). Then the infinite chains are combined by weaker C–H⋯π interaction [between *tert*-butyl group at the ring A and π-electrons of the ring C] in three- dimensional framework (Fig. 124b). Two chloroform molecules are located in cavities between chains (Fig. 124c). Each guest molecule participates in C–H⋯π interaction with π-electrons of the ring B of the adjacent molecule of the host and C–H⋯Cl contact (Fig. 124d and Table 77). The closest Cl⋯Cl distance between two chloroform molecules within the cavity is equal to 3.9057(8) Å and it is notably more than sum of van der Waals radii[146] of two Cl atoms (3.50 Å).
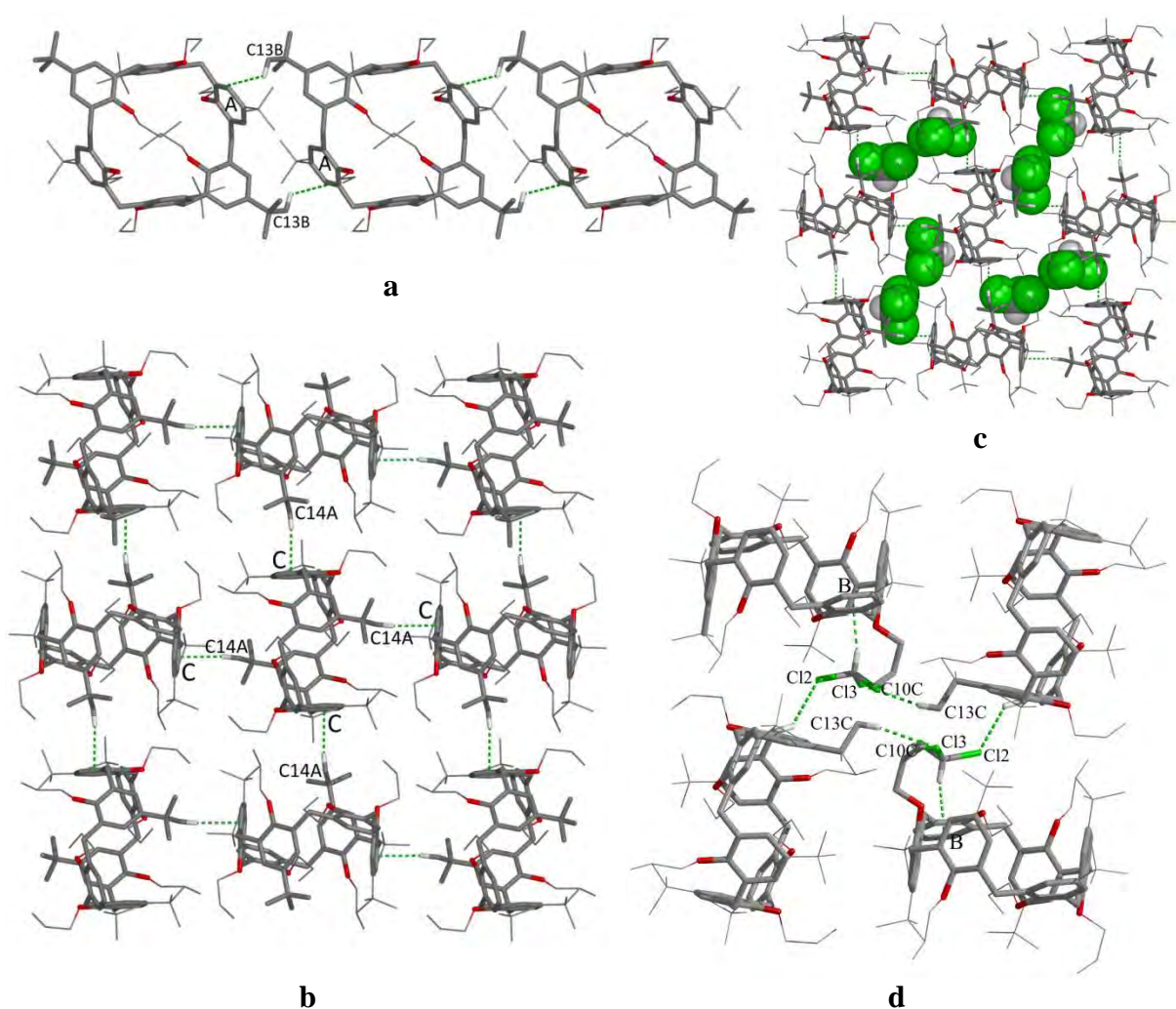
Fig. 124. tBuC[6]OC₃·2CHCl₃: **(a)** self-assembly of calix[6]arene molecules in infinite chains along the *a* crystallographic axis due to C–H⋯π interactions; **(b)** C–H⋯π interactions between chains, along the *a* crystallographic axis; **(c)** chloroform molecules shown in the spacefill mode located in cavities between chains; **(d)** bridging role of chloroform molecules.

16;

4.4.2 Crystal structure of O-butylated *para-tert*-butylcalix[6]arene chloroform monosolvate

O-Butylated *para-tert*-butylcalix[6]arene crystallises from methanol/chloroform mixture in the triclinic crystallographic system as a calix[6]arene-chloroform solvate with stoichiometry 1:1 (tBuC[6]OC$_4$·CHCl$_3$). Crystal data are presented in Table 78. The asymmetric unit of tBuC[6]OC$_4$·CHCl$_3$ comprises one molecule of calix[6]arene and one molecule of chloroform (Fig. 125a). The numbering scheme is presented in Fig. 125b. The *n*-butyl chain at the ring A is disordered over two positions on its whole

Table 78. Crystal data and structure refinement for tBuC[6]OC$_4$·CHCl$_3$

Molecular formula	C$_{90}$H$_{132}$O$_6$·CHCl$_3$
Formula weight	1429.32
Crystal system	Triclinic
Space group	$P\bar{1}$
Unit cell dimensions	a = 13.5948(4) Å α = 86.248(1)°
	b = 14.2051(4) Å β = 85.487(1)°
	c = 23.3836(9) Å γ = 72.975(2)°
Volume	4300.2(2) Å^3
Z	2
Temperature	100.0(5)
Radiation and wavelength	Mo Kα radiation, λ = 0.71073 Å
Monochromator	graphite
Density (calculated)	1.104 Mg·m^{-3}
Absorption coefficient	0.16 mm^{-1}
$F(000)$	1556
Crystal size	0.07 × 0.10 × 0.10 mm
θ range for data collection	3.0–19.8°
Index ranges	-12 $\leq h \leq$ 12, -13 $\leq k \leq$ 13, -22 $\leq l \leq$ 22
Reflections collected	42054
Independent reflections	7747 [R_{int} = 0.087]
Completeness	99.4 %
Absorption correction	None
Refinement method	Full-matrix least-squares on F^2
Weighting scheme	$[\sigma^2(F_o^2) + (0.1425P)^2 + 15.5147P]^{-1}$ *
Data / restraints / parameters	7747 / 338 / 1146
Goodness-of-fit on F^2	1.01
Final R indices [$I > 2\sigma(I)$]	R = 0.113, wR = 0.282
R indices (all data)	R = 0.149, wR = 0.204
Extinction coefficient	Not refined
Largest diff. peak and hole	0.63 and -0.79 e·Å^{-3}

* $P = (F_o^2 + 2F_c^2)/3$

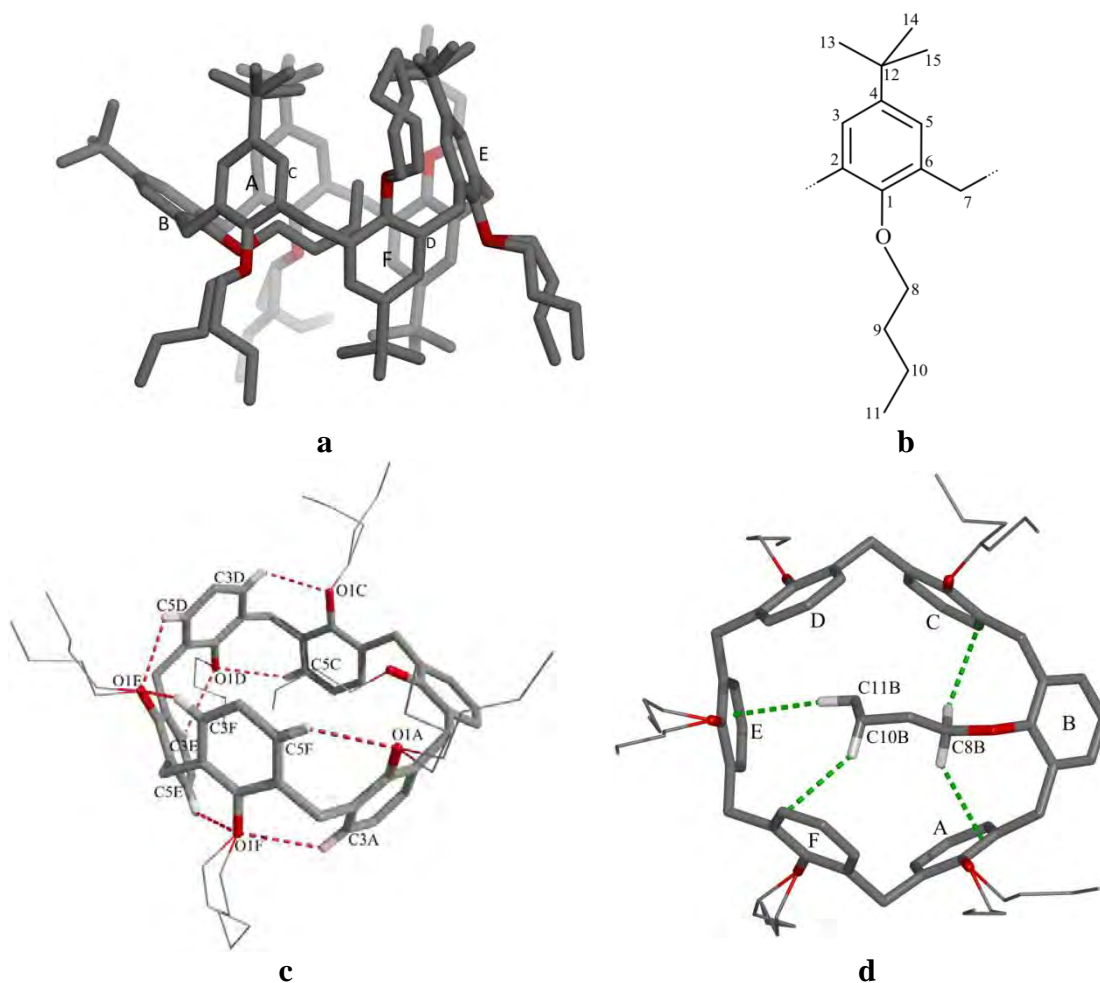**Fig. 125. tBuC[6]OC₄·CHCl₃: (a) molecule in 1,3-alterante conformation; (b) numbering scheme; (c) conformation stabilised by intramolecular C–H⋯O and (d) C–H⋯π interactions, _tert_-butyl groups are omitted for clarity.**

length with equal occupancy factors of 0.50. Three last methylene groups of _n_-butyl chain at the ring C and _n_-butyl chain at the ring E on its whole length are disordered over two positions with the same occupancy factors of 0.71 and 0.29. The three first methylene groups of _n_-butyl chain at the ring F are disordered over two positions with similar occupancy factors of 0.72 and 0.28.

The calix[6]arene macrocyclic ring adopts 1,3-alternate conformation, which is stabilised by eight C–H⋯O hydrogen contacts between H- and O-atoms of phenyl rings (Fig. 125c) and C–H⋯π interactions (Fig. 125d) between H-atoms of the first, the third and terminal carbon atoms and π-electrons of benzene rings A, C, E and F (Table 79).

Dihedral angles between planes of each benzene ring and the mean plane of the six methylene groups and distances between distal C4 atoms are presented in Table 80.

Two adjacent molecules of calix[6]arene form a centrosymmetric dimer as a result of π-π stacking interactions with the distance between planes of interacting

153

Table 79. Weak interactions in tBuC[6]OC$_4$·CHCl$_3$

Hydrogen bonds

D–H···A	d(D–H), Å	d(H···A), Å	d(D···A), Å	∠D–H···A
C3A–H3A···O1F	0.95	2.80	3.42(1)	124
C5C–H5C···O1D	0.95	3.03	3.53(1)	115
C3D–H3D···O1C	0.95	2.54	3.13(1)	121
C5D–H5D···O1E	0.95	2.70	3.29(1)	121
C3E–H3E···O1D	0.95	2.87	3.40(1)	117
C5E–H5E···O1F	0.95	2.89	3.50(1)	123
C3F–H3F···O1E	0.95	2.77	3.40(1)	124
C5F–H5F···O1A	0.95	2.76	3.36(1)	122
C15B–H15E···O1B	0.98	2.69	3.61(1)	156
C7D–H7D1···Cl2A[1]	0.99	3.08	3.71(2)	123
C7E–H7E2···Cl2B[2]	0.99	3.01	3.67(2)	125
C8E–H8E1···Cl2A[2]	0.99	3.10	3.98(2)	149
C9E–H9E2···Cl1A[1]	0.99	2.79	3.55(2)	134
C14E–H14O···Cl3[2]	0.98	3.07	3.62(2)	116
C15I–H15···Cl1A[2]	0.98	3.07	3.92(2)	146
C15I–H15Y···Cl3[3]	0.98	2.68	3.51(2)	142
C7F–H7F1···Cl2A	0.99	3.08	3.68(2)	121
C7F–H7F1···Cl2B	0.99	3.00	3.52(3)	114

Symmetry codes: (1) *x*, −1 + *y*, *z*; (2) −*x*, 2 − *y*, 1 − *z*; (3) 1 + *x*, −1 + *y*, *z*.

C–H···π interactions

C–H···Cg	d(H···Cg)	⊥d(H···π)	d(C···Cg)	∠C–H···Cg	∠C–H···π
C8B–H8B1···CgC	3.29	2.71	4.15(1)	146	132
C8B–H8B2···CgA	2.75	2.57	3.69(1)	161	142
C10B–H10C···CgF	2.90	2.87	3.81(1)	154	153
C11B–H11E···CgE	2.64	2.60	3.60(1)	165	176
C10C–H10F···CgC[3]	3.36	2.97	4.23(2)	148	125
C8D–H8D1···CgA[1]	3.32	3.11	4.02(1)	130	121
C9D–H9D2···CgA[1]	3.73	2.94	4.31(1)	120	153
C10E–H10J···CgE[4]	3.69	2.42	4.66(2)	166	126
C8F–H8F1···CgF[2]	3.51	3.00	4.35(2)	144	121
C9H–H9···CgC[3]	3.38	2.83	4.29(5)	155	171
C11H–H11V···CgC[3]	2.98	2.93	3.91(4)	159	165
C9I–H9I2···CgE[4]	3.42	2.73	4.25(3)	143	169
C8L–H8L2···CgF[2]	3.78	2.88	4.14(3)	105	145
C9L–H9L2···CgF[2]	3.69	2.92	4.39(6)	130	157
C1SA–H1SA···CgE[2]	3.00	2.36	3.86(2)	144	170

Symmetry codes: (1) *x*, −1 + *y*, *z*; (2) −*x*, 2 − *y*, 1 − *z*; (3) −*x*, 1 − *y*, −*z*; (4) − *x*, 1 − *y*, 1 − *z*.

π···π interaction

| CgI···CgJ	d(CgI···CgJ)	α	β	γ	⊥(CgI···πJ)	⊥(CgJ···πI)
CgB···CgB[1]	3.769(9)	0	22	22	3.496(9)	3.496(9)

Symmetry codes: (1) −*x*, 2 − *y*, −*z*.

d(CgI···CgJ) – distance between ring centroids I and J (Å), α – dihedral angle between planes I and J; β – angle between CgI···CgJ vector and normal to plane I; γ – angle between CgI···CgJ vector and normal to plane J (°), ⊥(CgI···πJ) – perpendicular distance of CgI on ring J; ⊥(CgJ···πI) – perpendicular distance of CgJ on ring I (Å).

Table 80. Calix[4]arene macrocyclic ring geometry for tBuC[6]OC$_4$·CHCl$_3$

∠(ring-to-CH$_2$-plane), °		Distal C4···C4 distances, Å	
A	74.7(2)	C4A···C4D	9.379
B	138.8(2)		
C	81.8(2)	C4B···C4E	10.289
D	-73.8(1)		
E	77.9(2)	C4C···C4F	9.173
F	-71.8(2)		

rings B equal to 3.494(9) Å. The π-π interactions are additionally stabilised by C–H···O contacts between *tert*-butyl groups and oxygen atoms of two adjacent phenoxy moieties B (Fig. 126).
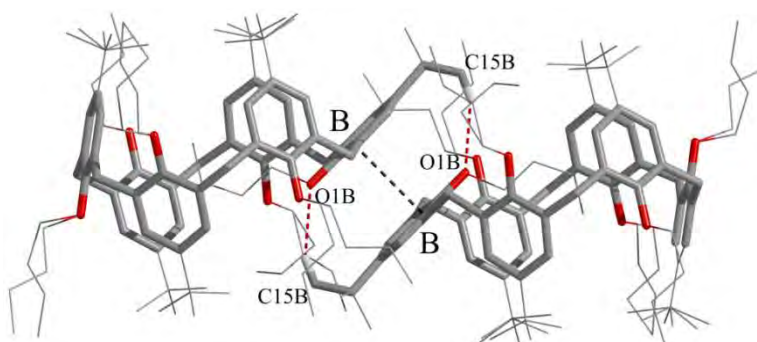
Fig. 126. Self-assembly of tBuC[6]OC$_4$·CHCl$_3$: dimerization via π-π stacking interaction.

Dimers participate in numerous C–H···π interactions (Table 79) mainly between H-atoms of disordered *n*-butyl chains (except *n*-butyl substituent at the ring B, which is ordered) and benzene rings of adjacent calixarenes as shown in Fig. 127. H-atoms of the first and the second methylene groups of ordered *n*-butyl chain at the ring D are involved in C–H···π interaction with the phenyl ring A [C8D···ring A, C9D···ring A]. H-atoms of the second, the third and terminal carbon atoms of disordered *n*-butyl chain at the ring C take part in C–H···π interactions with related by centre of inversion adjacent ring C [C9H···ring C′, C10C···ring C′ and C11H···ring C′]. Disordered *n*-butyl substituents at the ring E and related by centre of inversion adjacent benzene ring E participate in C–H···π interactions between H-atoms of the second and the third methylene groups and adjacent benzene ring E [C9I···ring E′ and C10E···ring E′]. *n*-Butyl chain at the ring F and related by centre of inversion adjacent ring F are in C–H···π interactions between H-atoms of the first and the second methylene groups and adjacent ring F [C8F···ring F′, C8L···ring F′ and C9L···ring F′]. As a result of π-π stacking and C–H···π interactions, molecules of the calix[6]arene are self-assembled in
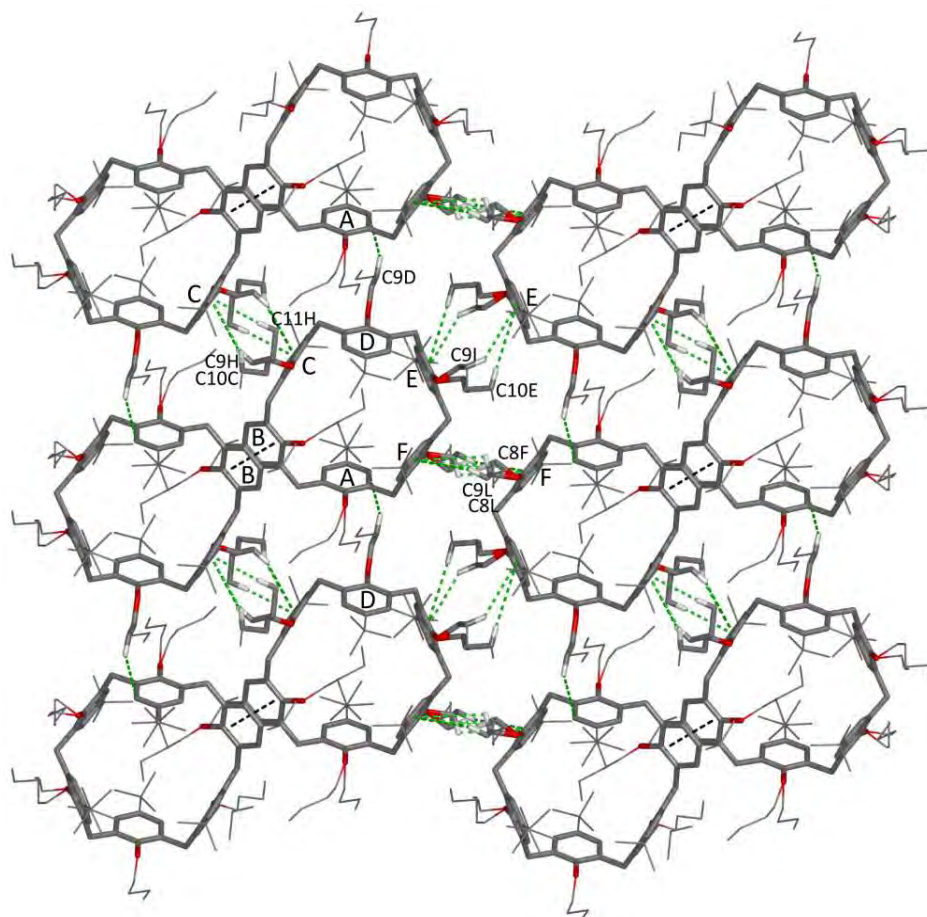
155

Fig. 127. Self-assembly of tBuC[6]OC$_4$·CHCl$_3$: layer formation due to C–H···π interactions, view along the *a* crystallographic axis.

layers which are extending parallel to the *bc* crystallographic plane (Fig. 128). Between layers only van der Waals interactions between hydrogen atoms of *tert*-butyl and *n*-butyl substituents occur.

Chloroform molecules are disordered in cavities located between layers over two positions with the occupancy factors of 0.62 and 0.38 (Fig. 128). The molecule **A** is involved in one C–H···π interaction with the ring E of one calix[6]arene molecule and
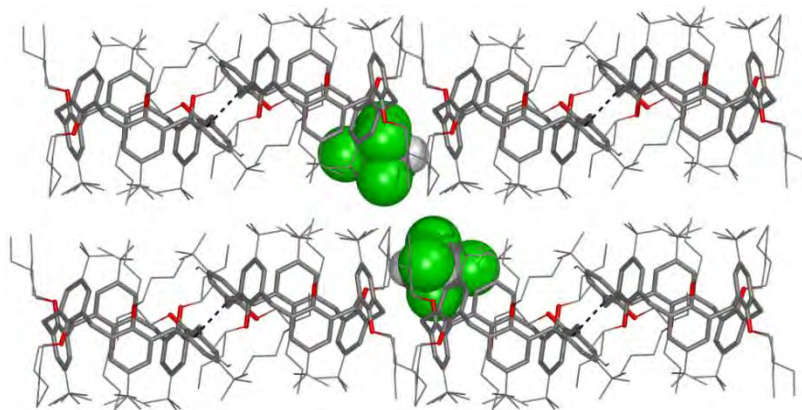

Fig. 128. Packing diagram of tBuC[6]OC$_4$·CHCl$_3$, view along the *b* crystallographic axis.

156

in C–H⋯Cl contacts with the same and three other adjacent calix[6]arene molecules (Fig. 129a and Table 79). The molecule **B** takes part C–H⋯Cl contacts only Fig. 129b and Table 79).
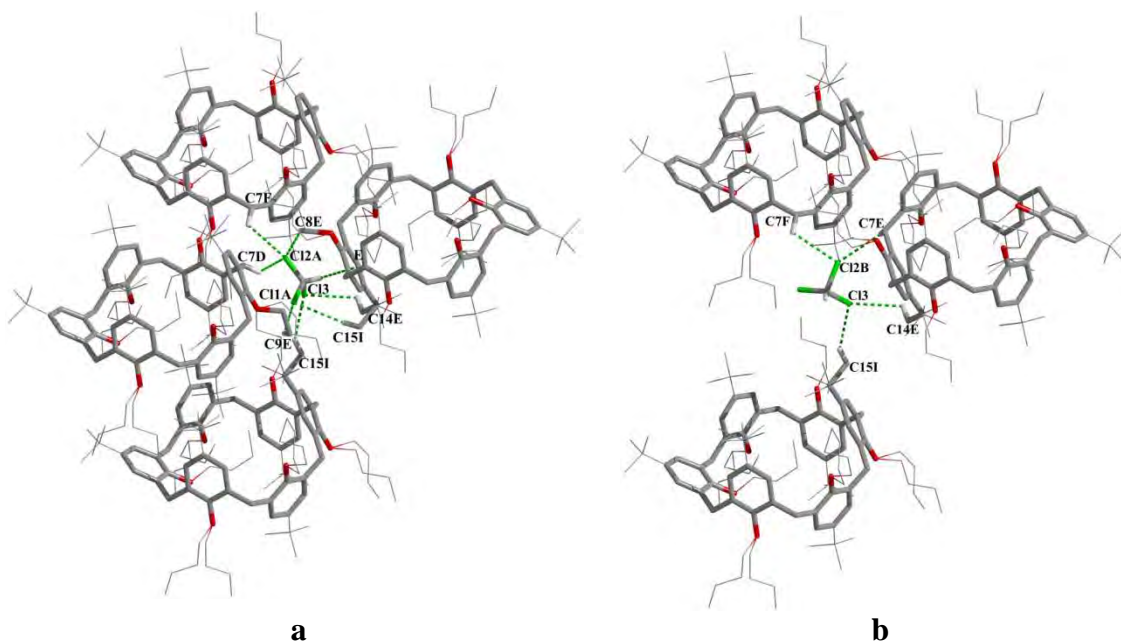

a   **b**

Fig. 129. tBuC[6]OC$_4$·CHCl$_3$: (a) packing diagram, view along the b crystallographic axis; (b) interaction of chloroform molecule A and (c) B with adjacent calix[6]arene molecules.

4.4.3 Crystal structure of O-hexylated *para-tert*-butylcalix[6]arene chloroform disolvate

O-Hexylated *para-tert*-butylcalix[6]arene crystallises from methanol/chloroform mixture in the monoclinic crystallographic system as a calix[6]arene-chloroform solvate with stoichiometry 1:2 (tBuC[6]OC$_6$·2CHCl$_3$). Crystal data are presented in Table 81 and the labelling scheme is shown in Fig. 130a. Similarly to tBuC[6]OC$_1$,[119]

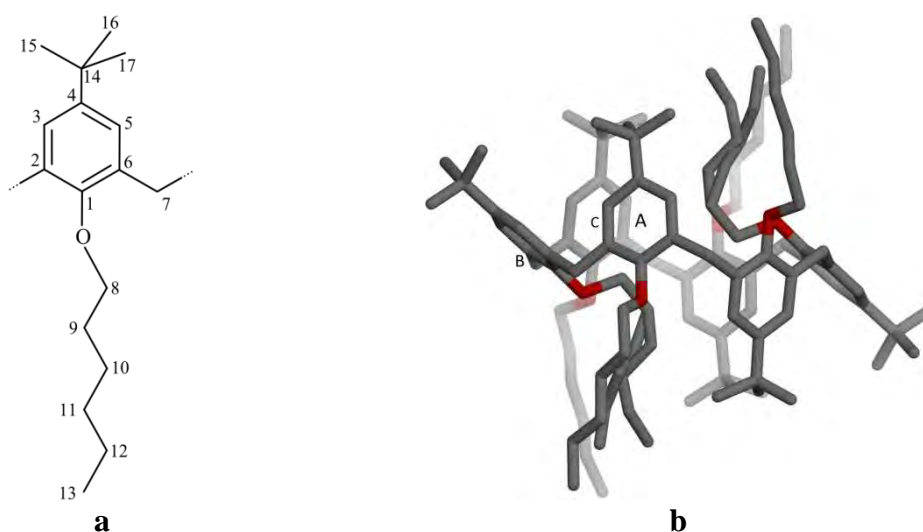**a**   **b**

Fig. 130. tBuC[6]OC$_6$·2CHCl$_3$: (a) numbering scheme; (b) molecule of the calix[6]arene.

177

Table 81. Crystal data and structure refinement for tBuC[6]OC$_6$·2CHCl$_3$

Molecular formula	C$_{102}$H$_{156}$O$_6$·2(CHCl$_3$)
Formula weight	1717.00
Crystal system	Monoclinic
Space group	C2/c
Unit cell dimensions	a = 14.1229(3) Å
	b = 26.0837(5) Å β = 90.395(1)°
	c = 27.5761(7) Å
Volume	10158.2(4) Å^3
Z	4
Temperature	100.0(5)
Radiation and wavelength	Mo Kα radiation, λ = 0.71073 Å
Monochromator	graphite
Density (calculated)	1.123 Mg·m^{-3}
Absorption coefficient	0.22 mm^{-1}
F(000)	3728
Crystal size	0.25 × 0.38 × 0.45 mm
θ range for data collection	3.0–27.5°
Index ranges	-18 ≤ h ≤ 18, -32 ≤ k ≤ 33, -35 ≤ l ≤ 35
Reflections collected	43590
Independent reflections	11415 [R_{int} = 0.023]
Completeness	98 %
Absorption correction	None
Refinement method	Full-matrix least-squares on F^2
Weighting scheme	$[\sigma^2(F_o^2) + (0.1029\,P)^2 + 37.2105\,P]^{-1}$ *
Data / restraints / parameters	11415 / 135 / 610
Goodness-of-fit on F^2	1.07
Final R indices [$I > 2\sigma(I)$]	R = 0.095, wR = 0.239
R indices (all data)	R = 0.111, wR = 0.250
Extinction coefficient	Not refined
Largest diff. peak and hole	1.30 and -0.93 e·Å^{-3}

* $P = (F_o^2 + 2F_c^2)/3$

tBuC[6]OC$_2$[120,121] and tBuC[6]OC$_3$·2CHCl$_3$, the asymmetric unit comprises half of the calix[6]arene molecule and one molecule of chloroform. The four last carbon atoms of n-hexyl chain at the ring B are disordered over two positions with occupancy factors of 0.69 and 0.31. The molecule of calix[6]arene assumes a centrosymmetric inverted double partial cone conformation (Fig. 130b) stabilised by intramolecular C–H···O hydrogen binding (Fig. 131a) and four C–H···π interactions (Fig. 131b) between H-atoms of first methylene groups of two alkyl chains at distal rings B, which close the calix[6]arene cavity from the oxygens' side, and proximal benzene rings A and C (Table 82). Dihedral angles between planes of each benzene ring and the mean plane of the six methylene groups and distances between distal atoms C4 are presented in Table 83.
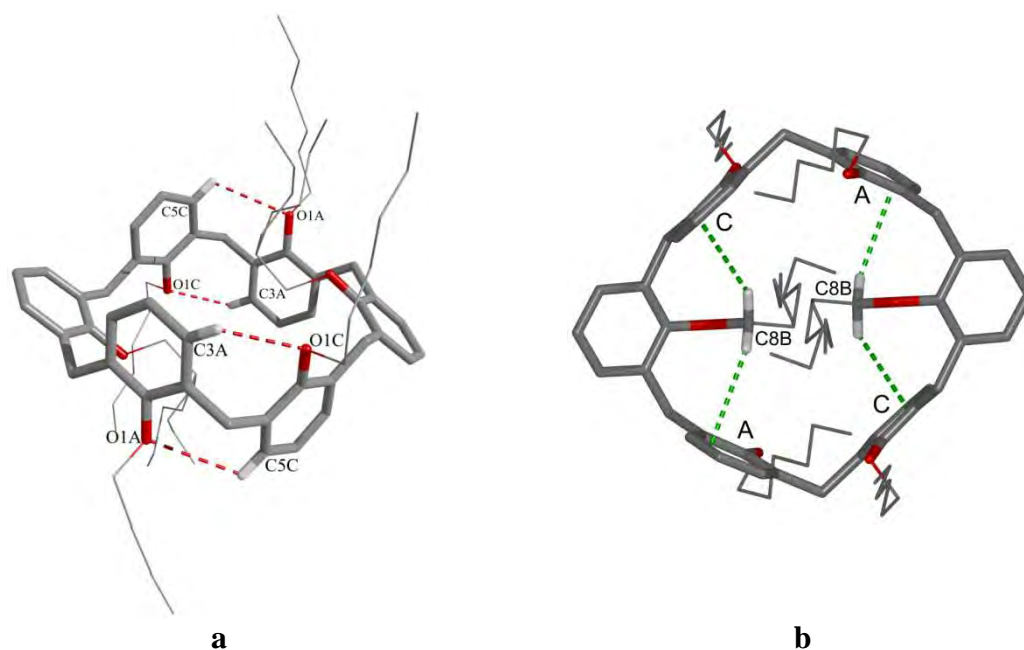
a	**b**

Fig. 131. tBuC[6]OC$_6$·2CHCl$_3$: (a) conformation stabilised by intramolecular C–H···O and (b) C–H···π interactions, *tert*-butyl groups are omitted for clarity.

Table 82. Weak interactions in tBuC[6]OC$_6$·CHCl$_3$

Hydrogen bonds

D–H···*A*	*d*(*D*–H), Å	*d*(H···*A*), Å	*d*(*D*···*A*), Å	∠*D*–H···*A*
C3A–H3A···O1C	0.95	2.62	3.167(3)	117
C5C–H5C···O1A	0.95	2.94	3.420(4)	112
C7A–H7A2···Cl2B[1]	0.99	2.80	3.506(5)	129
C7A–H7A2···Cl3A[1]	0.99	2.96	3.799(9)	143
C17C–H17G···Cl1B[2]	0.98	2.94	3.909(7)	172
C1SB–H1SB···Cl3A[3]	1.00	2.90	3.47(1)	117

Symmetry codes: (1) –0.5 + *x*, –0.5 + *y*, *z*; (2) –*x*, –*y*, 1 – *z*; (3) 1 – *x*, *y*, 0.5 – *z*.

C–H···π interactions

C–H···Cg	*d*(H···Cg)	⊥*d*(H···π)	*d*(C···Cg)	∠C–H···Cg	∠C–H···π
C8B–H8B1···CgA	3.14	2.83	4.015	149	127
C8B–H8B2···CgC	3.48	2.71	4.449	165	132
C9C–H9C2···CgA[1]	3.66	2.67	4.579(4)	156	122
C11A–H11B···CgB[2]	2.76	2.76	3.654(4)	151	153
C1SA–H1···CgA[3]	2.98	2.67	3.947(9)	163	149

Symmetry codes: (1) –0.5 + *x*, 0.5 + *y*, *z*; (2) –*x*, *y*, 0.5 – *z*; (3) 0.5 + *x*, 0.5 + *y*, *z*.

Table 83. Calix[4]arene macrocyclic ring geometry for tBuC[6]OC$_6$·2CHCl$_3$

	∠(ring-to-CH$_2$-plane), °	Distal C4···C4 distances, Å	
A	72.28(5)	C4A···C4A[1]	9.860(3)
B	133.95(7)	C4B···C4B[1]	13.068(3)
C	78.98(6)	C4C···C4C[1]	9.423(3)

Symmetry codes: (1) –*x*, –*y*, 1 – *z*.

179

Molecules of the calix[6]arene related by 2-axis symmetry take part in C–H···π interactions between hydrogen atoms of fourth methylene groups of hexyl substituents at rings A and π-electrons of adjacent rings B (Table 82), which results in infinite chains arrangement along the *c* crystallographic axis (Fig. 132a). The chains related by 2_1-axis symmetry are arranged by C–H···π interactions between H-atoms of second methylene groups of hexyl substituents at rings C and π-electrons of adjacent rings A (Table 82) in three-dimensional framework shown in Fig. 132b.
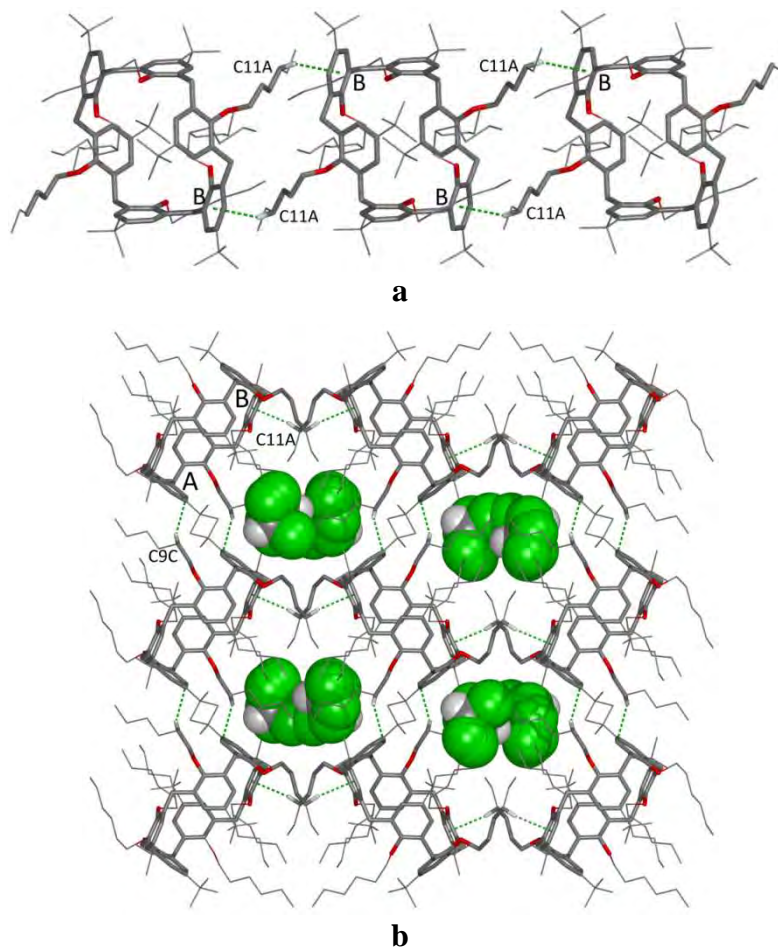

a

b

Fig. 132. tBuC[6]OC$_6$·2CHCl$_3$: (a) infinite chain of calix[6]arene molecules; (b) packing diagram, view along chains (the *c* crystallographic axis).

Within the framework discrete cavities are formed and each cavity contains two related by centre of symmetry chloroform molecules. Each of two chloroform molecules is disordered within the cavity over two positions (Fig. 133a) with equal occupancy factors of 0.50. Chloroform molecules interact with the neighbouring calixarene molecules as donors in C–H···π interactions and as acceptors in C–H···Cl hydrogen bonds (Fig. 133b and Table 82).

17:
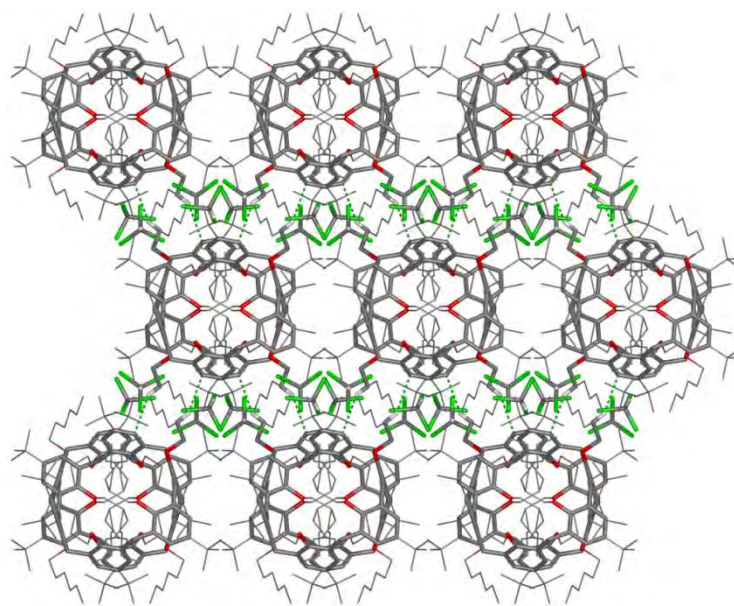
a
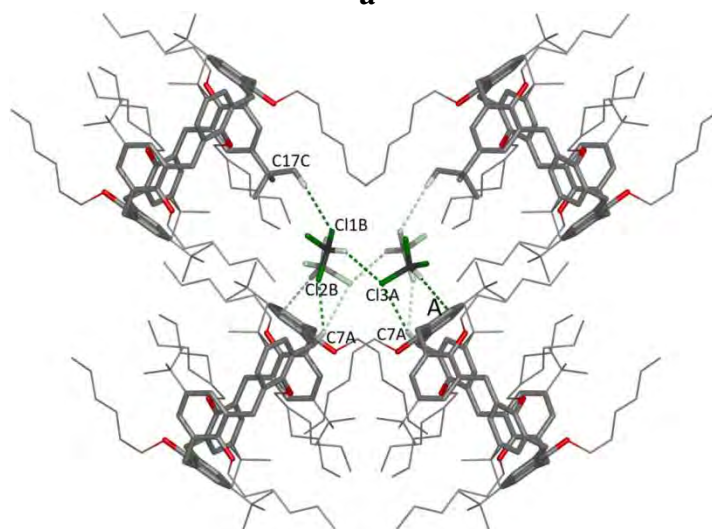
b

Fig. 133. tBuC[6]OC$_6$·2CHCl$_3$: (a); packing diagram, view along the *a* crystallographic axis; (b) inclusion of two chloroform molecules in the cavity between calix[6]arene molecules.

5   DISCUSSION

Fully O-alkylated calix[n]arenes are almost nonpolar when they are not substituted at the upper rim, or substituted by *tert*-butyl groups. On the other hand, nitration of O-alkylated at the *para*-position may cause a large dipole moment in the molecule. The dipole moment of calix[4]arene strongly depends on conformation of the macrocyclic ring. It is largest in the case of the cone conformation, medium for partial cone and close to zero for 1,2-alternate and 1,3-alternate cone conformations.[2] In the absence of such strong interactions as electrostatic ion-ion interactions and hydrogen bonding, the interactions between permanent dipoles can be an important driving force in molecular self-assembly of alkylated calixarenes. Therefore, self-assembly of pseudo-amphiphilic calix[n]arenes depends not only on the length of alkyl chains at the lower rim, but also on the type of substituents at the upper rim and conformation of calix[n]arene macrocyclic ring, and it would be appropriate here to separate the examined calix[4]arenes in groups according to four main conformations: cone, partial cone, 1,3-alternate and 1,2-alternate.

Calixarene molecules discussed here consist of two distinct parts: π-electron rich calix[n]arene macrocyclic ring and alkyl substituents. It is convenient to distinguish them in figures by colours *e.g.* aromatic part in blue and aliphatic ones in red. Self-assembling process of amphiphilic calix[n]arenes results in spatial separation of calixarene 'heads' and alkyl 'tails' into aromatic and aliphatic regions of crystal, respectively. Depending on spatial distribution of the regions, there are possible eight main types of organisation for discussed compounds shown in Fig. 134.
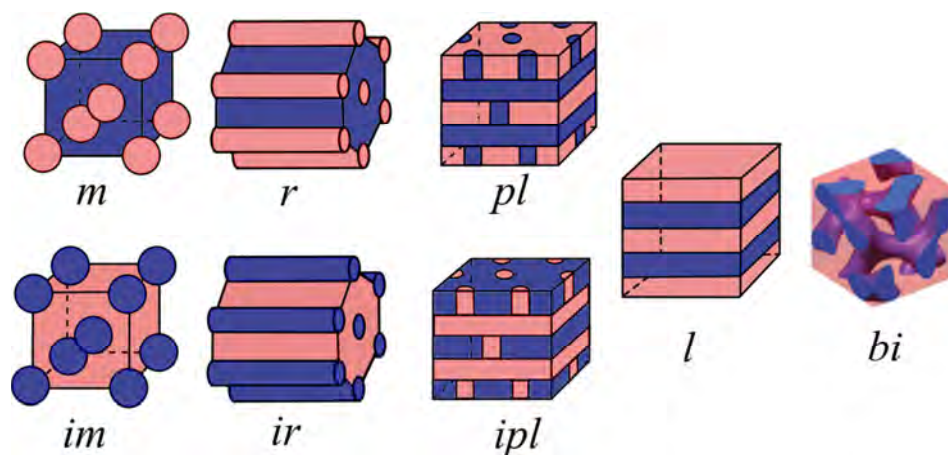

Fig. 134. Basic topologies: direct and inverted micelle (*m* and *im*), ribbon and inverted ribbon (*r* and *ir*), perforated layer and inverted perforated layer (*pl* and *ipl*), layer (*l*) and bicontinuous (*bi*).

161

5.1 Self-assembly of O-alkylated calix[4]arenes in cone conformation

5.1.1 Self-assembly of the non-substituted at the upper rim calix[4]arenes (cone)

O-Propylated HC[4]OC$_3$[94] and O-butylated HC[4]OC$_4$[95] calix[4]arenes reveal similar self-assembly (Fig. 135). In both cases, the neighbouring molecules of calix[4]-
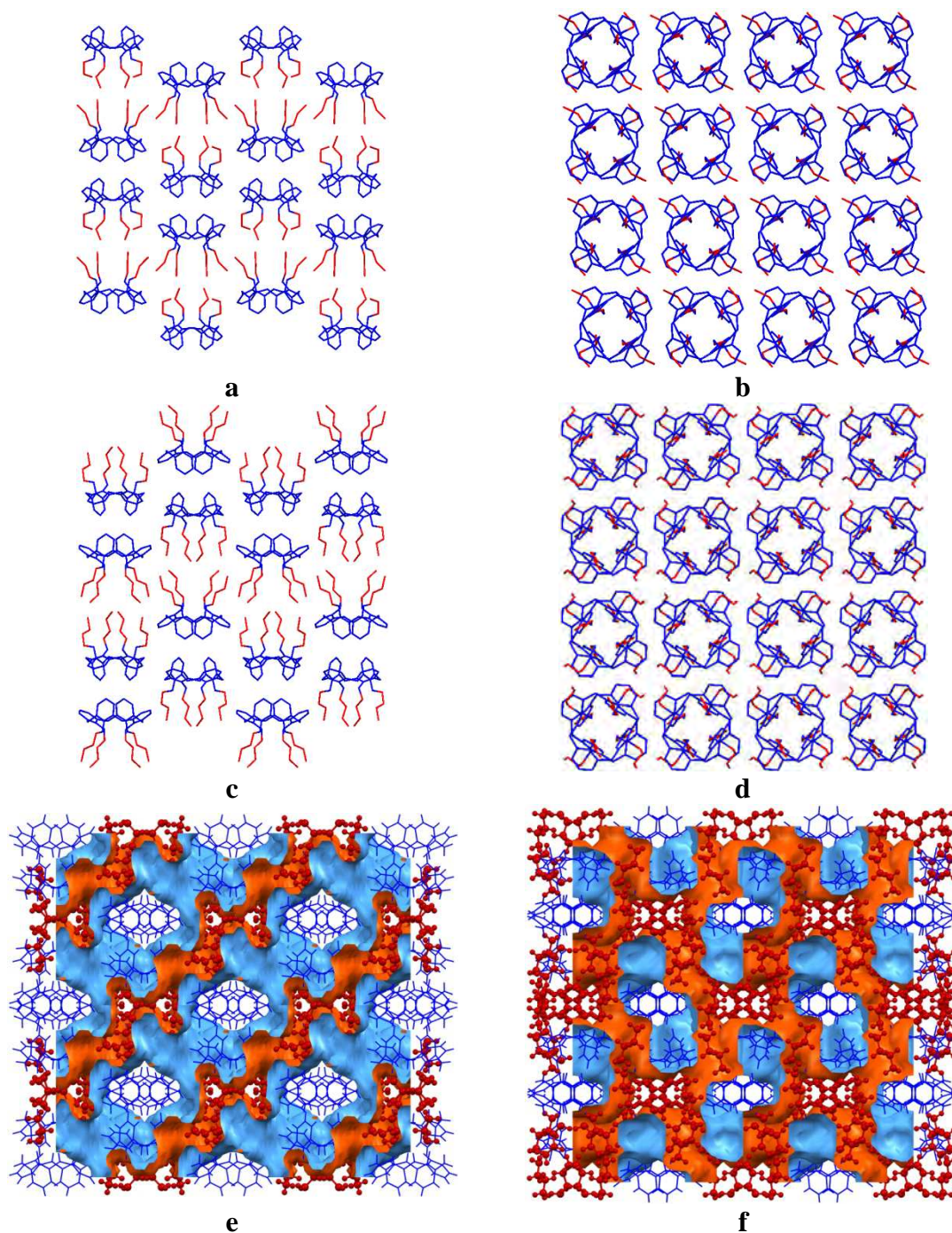
Fig. 135. Packing diagram comparison: (a) four adjacent columns of HC[4]OC$_3$[94] molecules; (b) packing diagram of HC[4]OC$_3$[94] along the *b* crystallographic axis; (c) four adjacent columns of HC[4]OC$_4$[95] molecules; (d) packing diagram of HC[4]OC$_4$[95] along the *c* crystallographic axis; (e) bicontinuous separation of aromatic and aliphatic regions in HC[4]OC$_3$[94] viewed along the *c* crystallographic axis; (f) bicontinuous separation of aromatic and aliphatic regions in HC[4]OC$_4$[95] viewed along the *b* crystallographic axis.

arenes are self-assembled in head-to-head and tail-to-tail mode shown in Fig. 135a and c, which are packed in columns along the alkyl chain direction (Fig. 135b and d). Differences in arrangement of adjacent columns result in complicate interpenetrating system of zigzag ribbons of aromatic and aliphatic regions in both HC[4]OC$_3$[94] and HC[4]OC$_4$[95] crystal structures (Fig. 135e and f).

Likewise HC[4]OC$_3$[94] and HC[4]OC$_4$,[95] molecules of HC[4]OC$_7$ also are organised in head-to-head and tail-to-tail mode (Fig. 136a). Nevertheless, the molecules are self-assembled in corrugated layers (Fig. 136b), which correlate with increasing hydrophobic-to-total volume ratio (Table 84).

In the case of longer alkyl substituents (11 and more carbon atoms in the chain) the arrangement of HC[4]OC$_n$ molecules is similar to 'real-amphiphiles': interactions

Table 84. Molecular hydrophobic-to-total volume ratio and structural topology for HC[4]OC$_n$ (cone).

Formula	Vol. ratio, %	Topology	Reference
HC[4]OC$_3$	38.2	*bi*	LAGQEQ[94]
HC[4]OC$_4$	44.5	*bi*	QADTIZ[95]
HC[4]OC$_7$	57.5	*l*	This work
HC[4]OC$_{11}$	67.6	*l*	This work
HC[4]OC$_{12}$	69.5	*l*	LALFUA[96]
HC[4]OC$_{12}$	69.5	*l*	LALFUA01[97]
HC[4]OC$_{14}$	72.5	*l**	FAGFEA[97]
HC[4]OC$_{16}$·5H$_2$O	75.1	*ipl*	FAGFOK[97]
HC[4]OC$_{18}$·2C$_6$H$_6$	77.2	*ipl*	KENHAN[98]
HC[4]OC$_{18}$·C$_6$H$_5$CH$_3$	77.2	*ipl*	KENHER[98]

*Alkyl chains do not interdigitate.

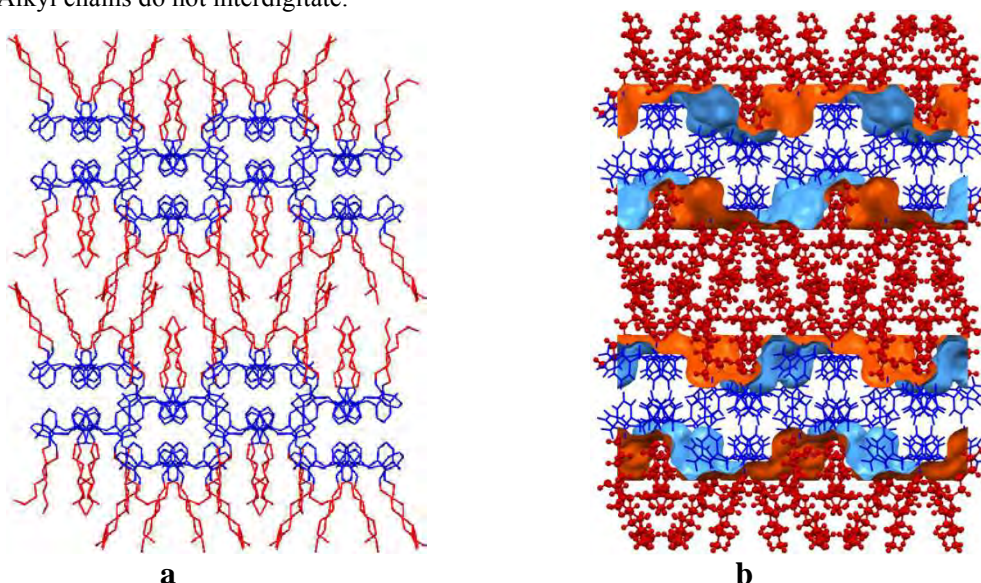a   b

Fig. 136. HC[4]OC$_7$: (a) packing viewed along the *b* crystallographic axis, H-atoms are omitted for clarity; (b) separated layers of aromatic and aliphatic regions viewed along the *b* crystallographic axis.

between long parallel alkyl chains dominate and control the solid state assembly. Thus, molecules of HC[4]OC$_{11}$ and two polymorphs of HC[4]OC$_{12}$[96,97] are self-assembled in easily recognisable bilayers with parallel alkyl chains (Fig. 137a-c). Both surfaces of the bilayer are covered by the calixarene head groups and form aromatic interlayer regions.

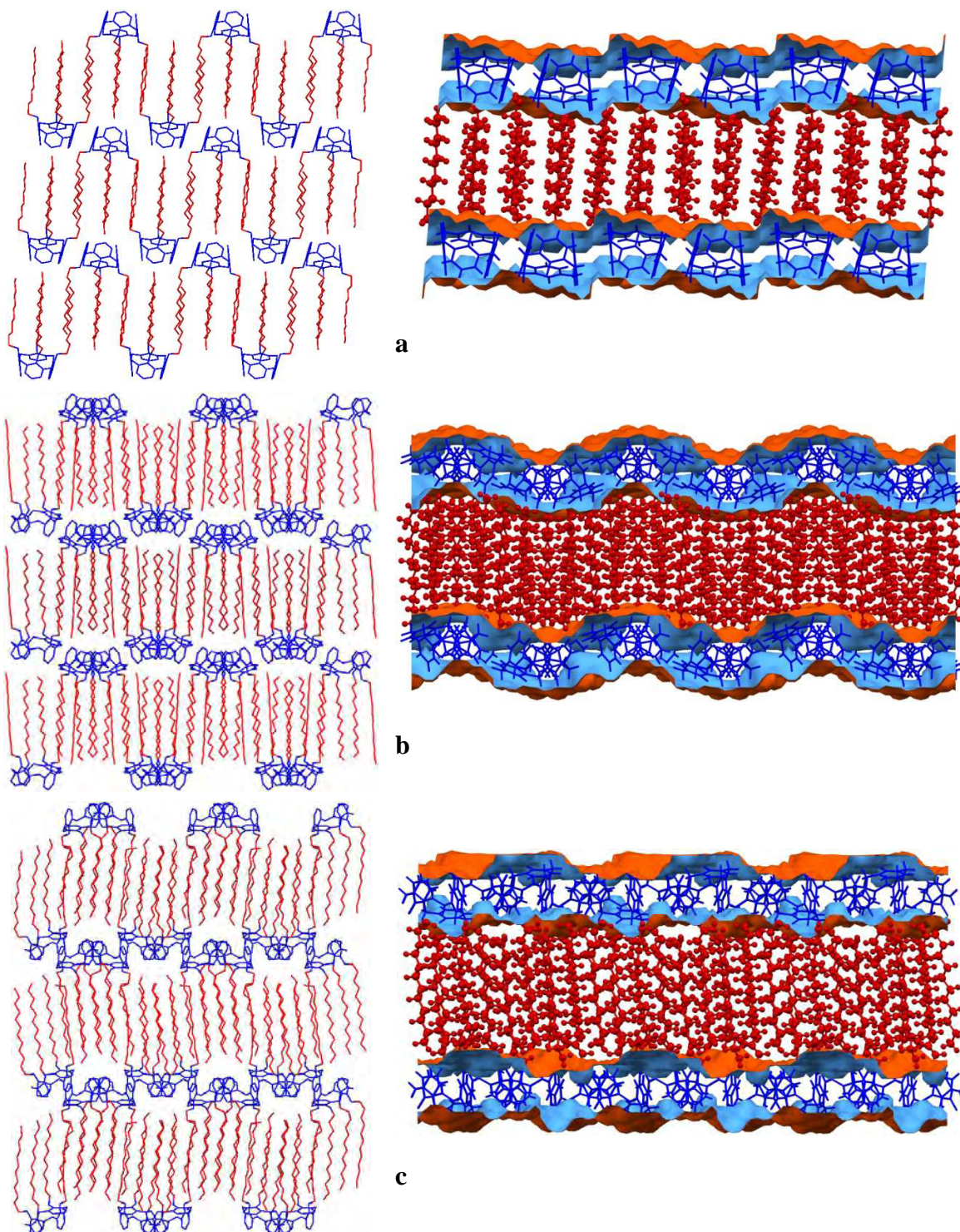**Fig. 137. Packing diagram and aromatic/aliphatic regions: (a) HC[4]OC$_{11}$, view along the *a* crystallographic axis; (b) HC[4]OC$_{12}$,[96] view along the *b* crystallographic axis; (c) HC[4]OC$_{12}$,[97] view along the *a* crystallographic axis.**

Surprisingly, the spatial arrangement of HC[4]OC$_{14}$[97] is distinctly different in comparison with other systems with a high number carbon atoms, as the molecules are packed without interdigitating alkyl chains (Fig. 138a). Such pattern of self-assembly is often observed for Langmuir-Blodgett films of surfactants with strong 'head-to-head' interactions (Y-type of the film).[147] Head-to-head orientation of calix[4]arene molecules in HC[4]OC$_{14}$[97] is amplified by π-π stacking interactions.

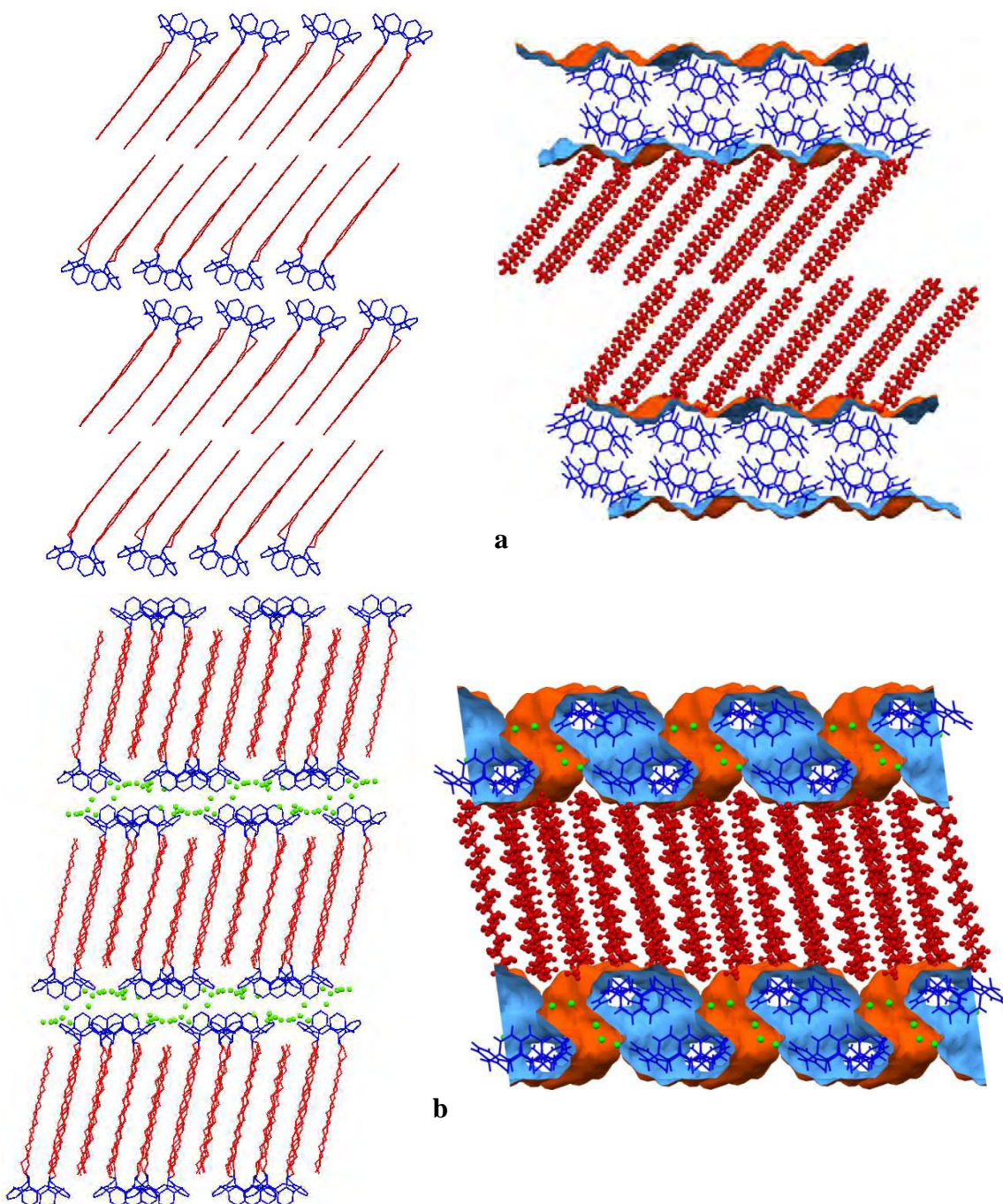**Fig. 138. Packing diagram and aromatic/aliphatic regions: (a) HC[4]OC$_{14}$,[97] view along the *a* crystallographic axis; (b) HC[4]OC$_{16}$ (cone)·nH$_2$O,[97] view along the *b* crystallographic axis.**

Molecules of HC[4]OC$_n$ with longer alkyl substituents (16 and 18 carbon atoms in the chain) are arranged in bilayer motif similar to that found for HC[4]OC$_{11}$ and HC[4]OC$_{12}$[96,97] (Fig. 138a). Voids formed between head groups are filled by solvent molecules. Packing diagram for HC[4]OC$_{16}$ molecules is show in Fig. 138b.

Benzene (Fig. 139a) and toluene (Fig. 139b) solvates of HC[4]OC$_{18}$[98] show very close unit cells parameters a, b and c but different angles and symmetry. This can be explained by different inclination of alkyl chains to the plane defined by macrocyclic rings.
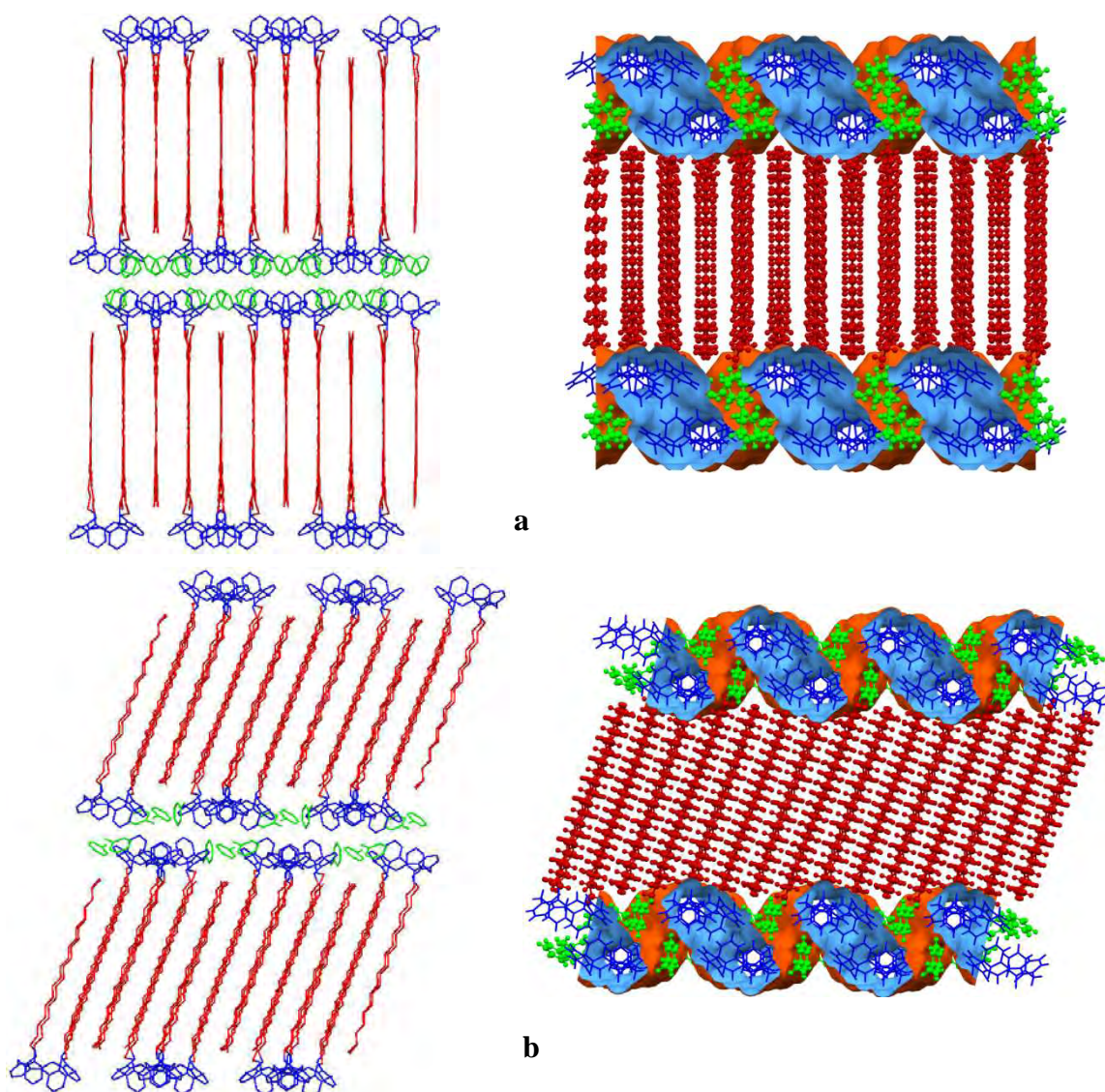

Fig. 139. Packing diagram and aromatic/aliphatic regions: (a) HC[4]OC$_{18}$·2benzene[97] clathrate, view along the c crystallographic axis ; (d) HC[4]OC$_{18}$·toluene[97] clathrate, view along the b crystallographic axis.

5.1.2 Self-assembly of O-alkylated *para-tert*-butyl-calix[4]arenes (cone)

At a first glance $tBuC[4]OC_n$ molecules should be less 'amphiphilic' than $HC[4]OC_n$ ones. Nevertheless, the *tert*-butyl-groups can act as an extension of *n*-alkyl substituents of the molecule located above the molecule under consideration and increase hydrophobic-to-total volume ratio for all *tert*-butyl-derivatives (Table 85). This results in 'amphiphile-like' self-assembly even in the case of short *n*-alkyl substituents. Thus, $tBuC[4]OC_3$ molecules are arranged in parallel columns, similar to these found for $HC[4]OC_3$,[94] and $HC[4]OC_4$,[95] with *tert*-butyl groups directed towards *n*-propyl ones. Next, columns are self-assembled in a way that spatial coherence of location of aliphatic and aromatic parts in the structure results in honeycomb-like pattern, where phenyl rings form a rigid channel type matrix [with the wall thickness of 4.9 Å and diameter of channels of 8.1 Å] and channels are formed by *tert*-butyl groups and disordered flexible propyl chains (Fig. 140a). The walls are penetrated by *tert*-butyl- and *n*-propyl substituents resulting in bicontinuous structure.

Table 85. Molecular hydrophobic-to-total volume ratio and structural topology for $tBuC[4]OC_n$ (cone).

Formula	Vol. ratio, %	Topology	Reference
$tBuC[4]OC_3$	60.3	*bi*	This work
$tBuC[4]OC_3 \cdot CH_3CN$	60.3	*ipl*	GIYTEN[108]
$tBuC[4]OC_4$	63.2	*bi*	This work
$tBuC[4]OC_4 \cdot 4CHCl_3 \cdot 2H_2O$	63.2	*bi*	FOVRIS[110]
$tBuC[4]OC_5$	65.7	*ipl*	DAYKIY[111]
$tBuC[4]OC_6$	67.8	*ir*	This work
$tBuC[4]OC_9$	73.0	*ipl*	This work
$tBuC[4]OC_{10} \cdot CHCl_3$	74.4	*ir*	This work
$tBuC[4]OC_{11}$	75.6	*ipl*	This work
$tBuC[4]OC_{12} \cdot CHCl_3$	76.7	*ir*	This work
$tBuC[4]OC_{14} \cdot CHCl_3$	78.7	*ir*	This work

Presence of acetonitrile molecules in the crystal structure of $tBuC[4]OC_3 \cdot CH_3CN$[108] changes the packing from hexagonal to layered and topology of the surface between aromatic and aliphatic regions changes from bicontinuous to inverted perforated layers (Fig. 140b).

Elongation of *n*-alkyl substituents at the lower rim by one CH_2-group results in isostructural to $tBuC[4]OC_3$ hexagonal arrangement of $tBuC[4]OC_4$ molecules (Fig. 140c). Thickness of aromatic wall is the same but the channel diameter is slightly larger compared to $tBuC[4]OC_3$ simply because of longer aliphatic substituents.

167
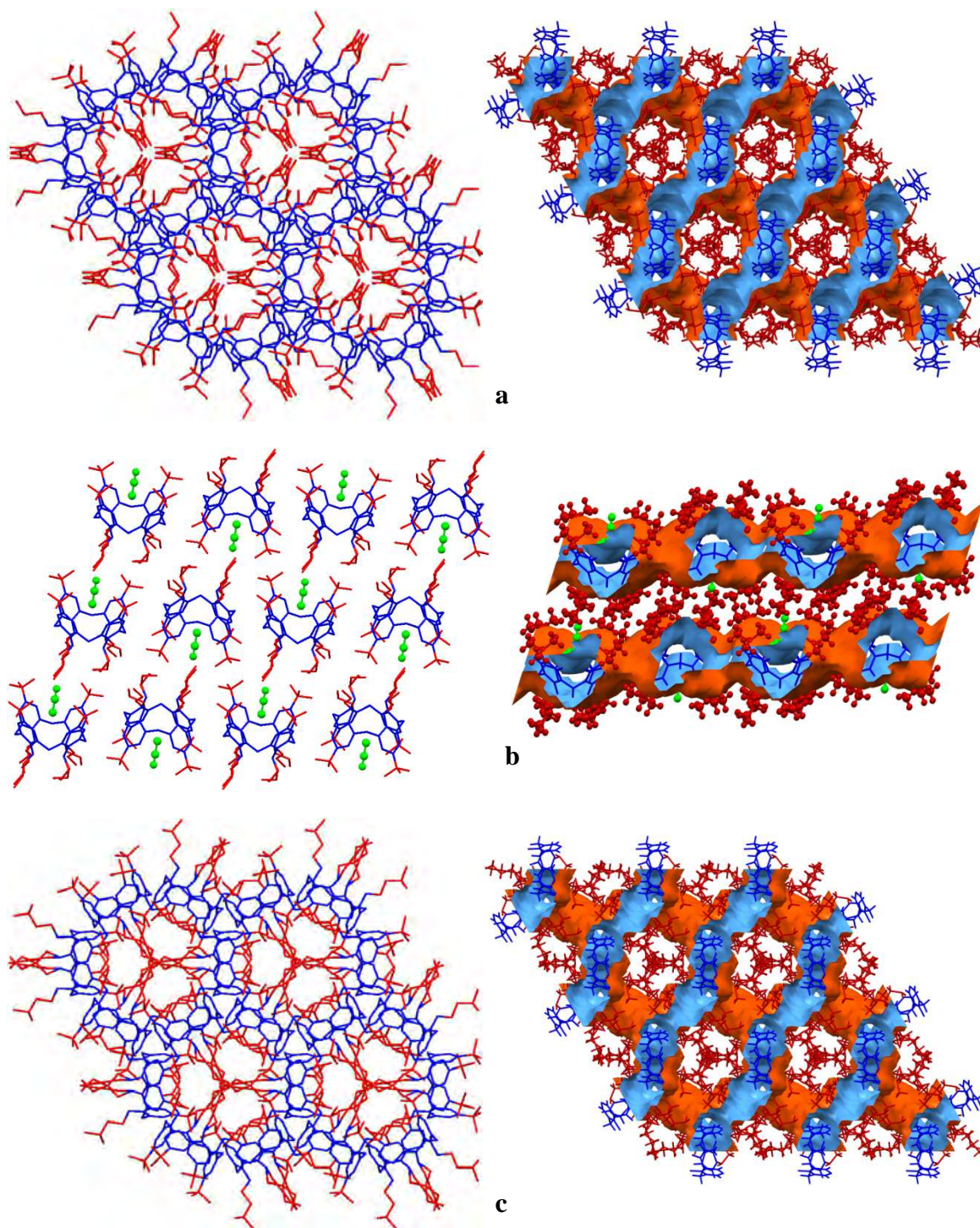
Fig. 140. Packing diagram and aromatic/aliphatic regions: (a) tBuC[4]OC₃, view along the *c* crystallographic axis; (b) tBuC[4]OC₃·CH₃CN,[108] view along the *a* crystallographic axis; (c) tBuC[4]OC₄, view along the *c* crystallographic axis.

Similarly to tBuC[4]OC₃, the spatial coherence of column arrangement resulting in hexagonal self-assembly of tBuC[4]OC₄ molecules is destroyed in presence of solvent molecules (mixture of water and chloroform) and crystal packing (Fig. 141) changes to inverted perforated layers.

168

a	**b**

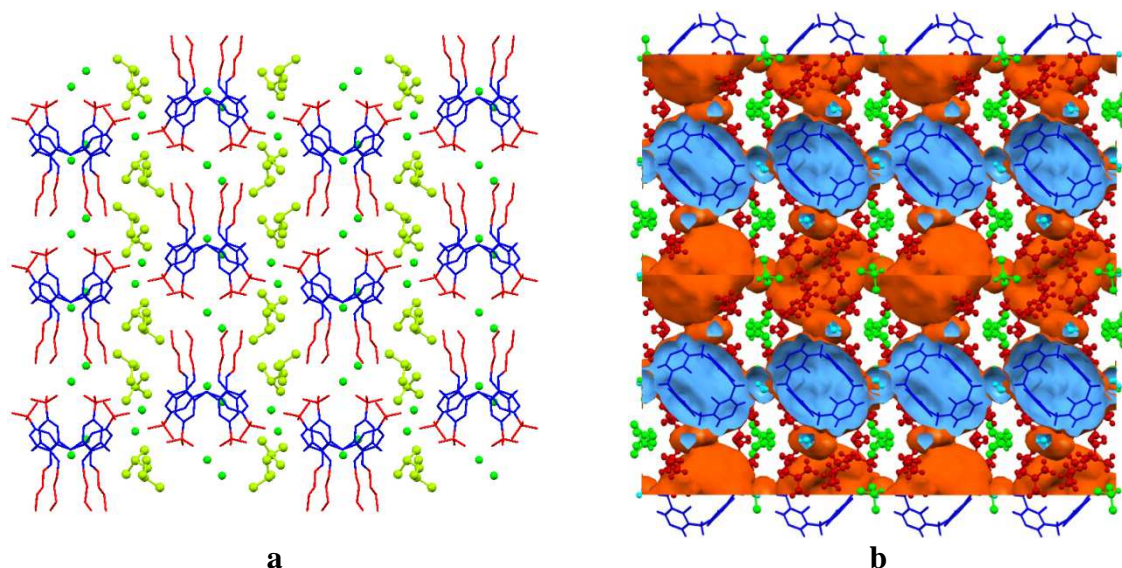**Fig. 141. tBuC[4]OC$_4$·4CHCl$_3$·H$_2$O:[110] (a)** columnar arrangement of calix[4]arene molecules, packing diagram along the *a* crystallographic axis; **(b)** single calix[4]arene bowls are bound by water molecules in bicontinuous organisation of aromatic and aliphatic regions, view along the *b* crystallographic axis.

Similarly to previously discussed calixarenes, molecules of tBuC[4]OC$_5$ are oriented in a *tert*-butyl-to-*n*-pentyl and are self-assembled in columns with different spatial alignment along the alkyl chains, which results in inverted perforated layer topology (Fig. 142).

a	**b**
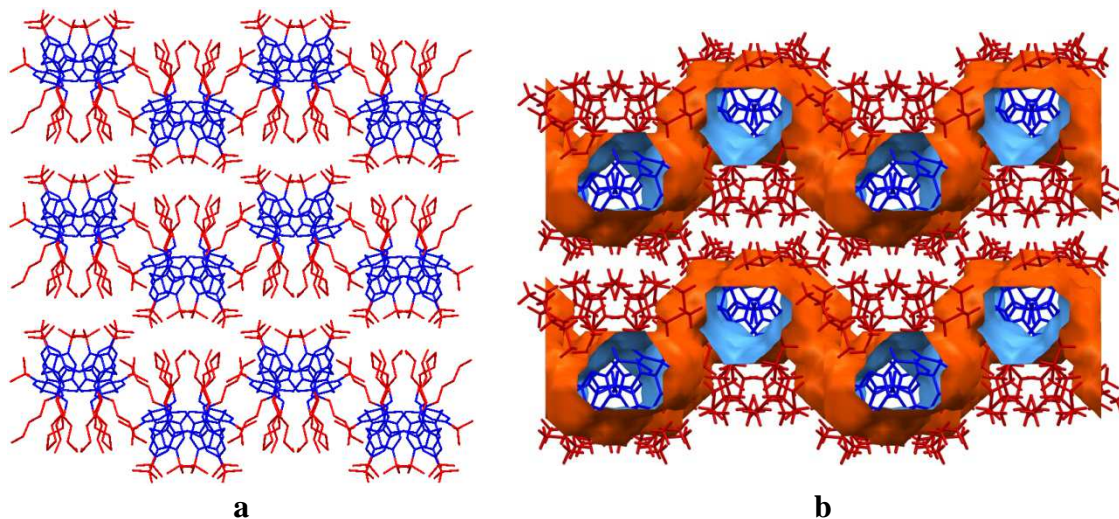
Fig. 142. tBuC[4]OC$_5$, view along the diagonal between a and *c* crystallographic axes: (a) packing diagram reveals columnar arrangement of calix[4]arene molecules; **(b)** inverted perforated layer organisation of aromatic and aliphatic regions.

Elongation of *n*-alkyl substituent to six carbon atoms in tBuC[4]OC$_6$ leads to change of the topology from inverted perforated layers to inverted ribbons formed by calix[4]arene macrocyclic moieties are located in aliphatic matrix formed by both *n*-alkyl substituents and *tert*-butyl groups (Fig. 143).

169

a

b

Fig. 143. tBuC[4]OC$_6$, view along the *a* crystallographic axis: (a) packing diagram; (b) inverted ribbon organisation of aromatic ribbons in aliphatic matrix.

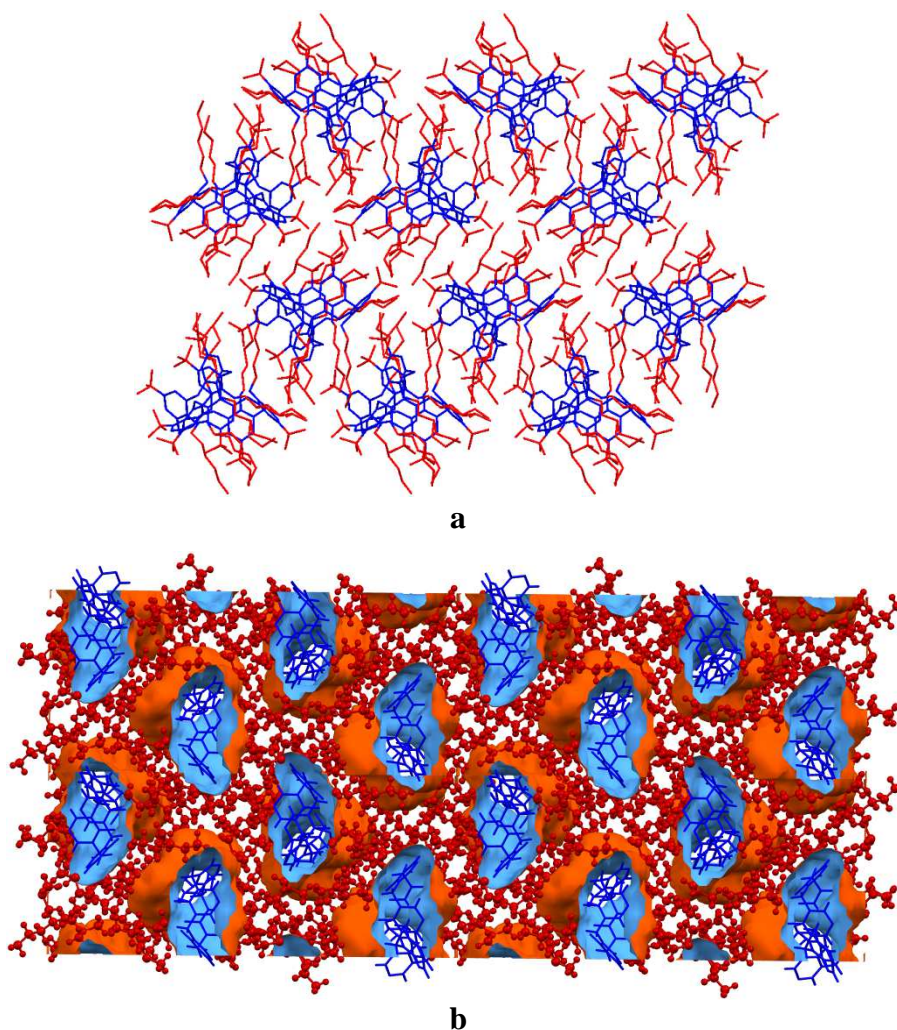Compounds tBuC[4]OC$_9$ and tBuC[4]OC$_{10}$·CHCl$_3$ crystallise in the same crystallographic space group *P*2$_1$/*c* but with different arrangement modes. tBuC[4]OC$_9$ molecules are self-assembled in corrugated layers where *n*-nonyl substituents form almost flat domains with 'bulges' of *tert*-butyl groups (Fig. 144a). tBuC[4]OC$_{10}$ molecules are arranged in bilayers with *n*-decyl chains being interdigitated inside bilayer and *tert*-butyl groups located on outer surface of the bilayer (Fig. 144b).

Further elongation of *n*-alkyl substituents causes tBuC[4]OC$_{11}$ to be isostructural with tBuC[4]OC$_9$, while tBuC[4]OC$_{12}$·CHCl$_3$ and tBuC[4]OC$_{14}$·CHCl$_3$ are isostructural with tBuC[4]OC$_{10}$·CHCl$_3$. This suggests the existence of two homological series of tBuC[4]OC$_n$ for $n \geq 9$. Crystal with odd n are probably isostructural with tBuC[4]OC$_9$, while these with even n should rather form solvent clathrates isostructural with tBuC[4]OC$_{10}$·CHCl$_3$. Such type of odd-even behaviour is well known in organic chemistry.
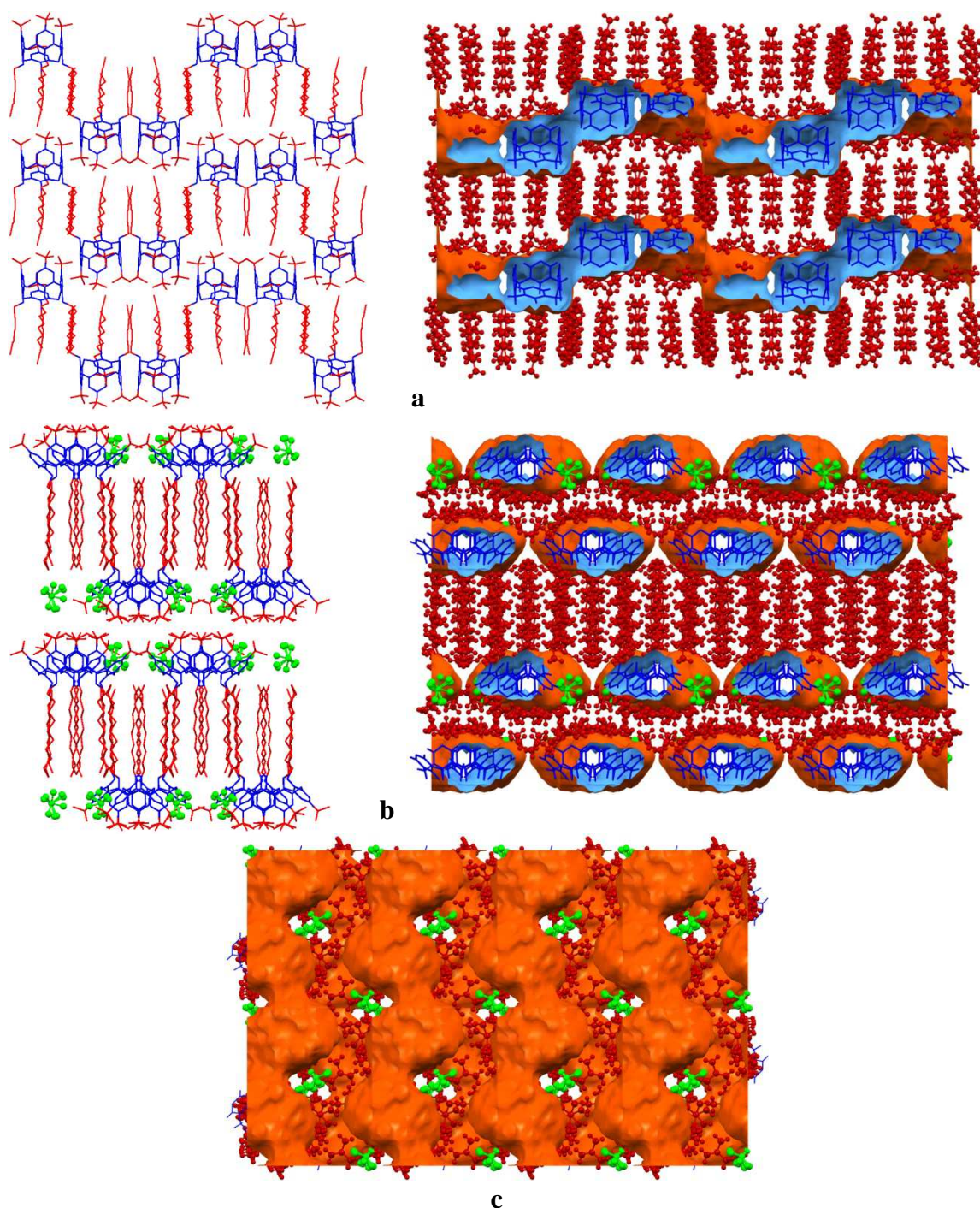
Fig. 144. Packing diagram and aromatic/aliphatic regions: (a) tBuC[4]OC$_9$, view along the *c* crystallographic axis; (b) tBuC[4]OC$_{10}$·CHCl$_3$, view along the *c* crystallographic axis; (c) tBuC[4]OC$_{10}$·CHCl$_3$, zigzag aromatic ribbons separated by aliphatic *tert*-butyl groups and chloroform molecules, view along the *a* crystallographic axis.

Aromatic regions in crystal structures with odd *n* are folded which leads to changes in thickness of aliphatic regions. Alkyl substituents penetrate the aromatic corrugated layers. In the case of crystal structures with even *n*, calix[4]arene macrocyclic rings are arranged in zigzag ribbons (Fig. 144c) in aliphatic matrix formed by *n*-alkyl and *tert*-butyl substituents.

171

5.1.3 Self-assembly of O-alkylated *para*-nitro-calix[4]arenes (cone)

Para-nitro O-alkylated calix[4]arenes in the cone conformation are expected to be more amphiphilic compared to HC[4]OC$_n$ (cone) and tBuC[4]OC$_n$ (cone) due to both the presence of considerable dipole moment on the 'head' and lower hydrophobic-to-total volume ratio.

Aromatic-aliphatic domain analysis reveal, that in the case of NO$_2$C[4]OC$_2$ ·CHCl$_3$ (cone)[112] crystal structure even such short alkyl substituent as ethyl are combined in domains in aromatic matrix formed by *para*-nitro calix[4]arene moieties (Fig. 145a).
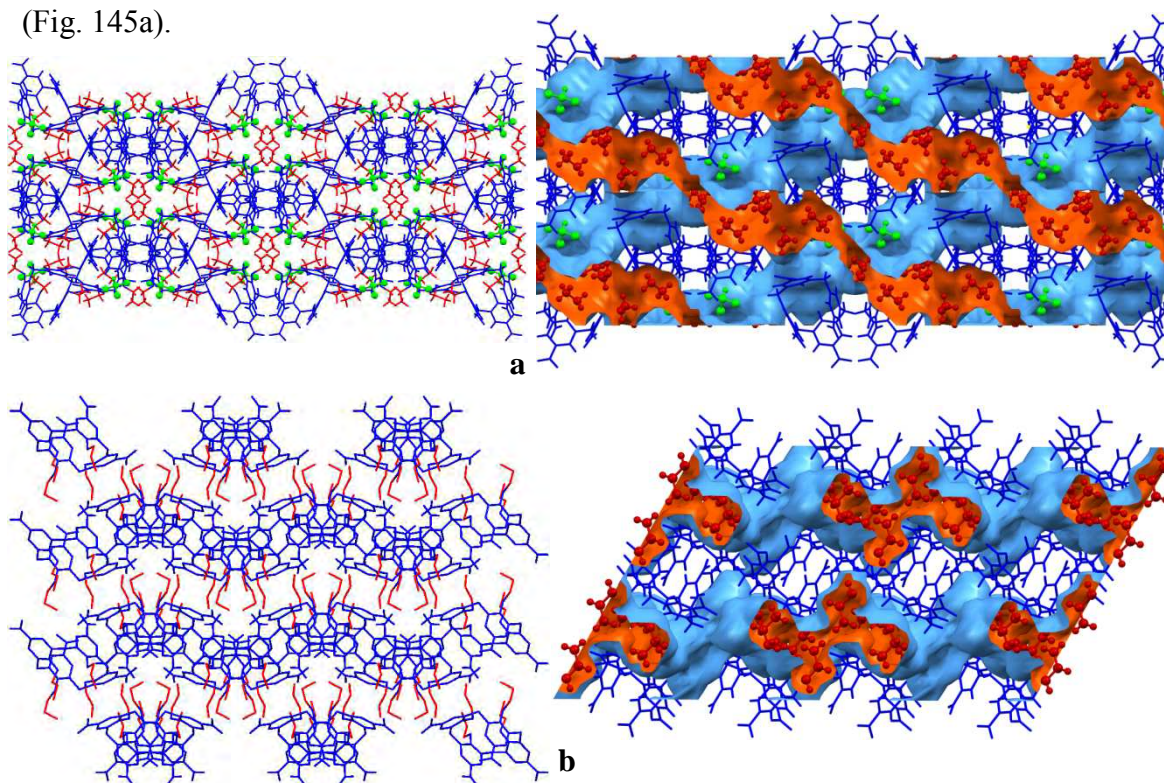
Fig. 145. Packing diagram and aromatic/aliphatic regions: (a) NO$_2$C[4]OC$_2$·CHCl$_3$,[112] view along the *c* crystallographic axis; (b) NO$_2$C[4]OC$_3$ (cone),[115] view along the *b* crystallographic axis.

In solvent-free NO$_2$C[4]OC$_3$,[115] C–H···O contacts are stronger than interactions between permanent dipoles and NO$_2$C[4]OC$_3$ molecules are self-assembled in corrugated layers, where propyl substituents form distinct layers between these formed by calix[4]arene macrocyclic rings (Fig. 145b).

The presence of solvent molecules in all known crystal structures of NO$_2$C[4]OC$_3$ solvates results in self-assembling of more polar *n*-propyl derivatives in infinite chains in the 'up-down' mode (Fig. 146a-c) due to significant dipole moment. Different arrangement of the chains in crystal structures of NO$_2$C[4]OC$_3$ (cone)·*Solv*,[113]

NO$_2$C[4]OC$_3$·CH$_2$Cl$_2$[114] and NO$_2$C[4]OC$_3$·0.5THF[115] leads to different unit cell symmetry and parameters but similar bicontinuous topology.
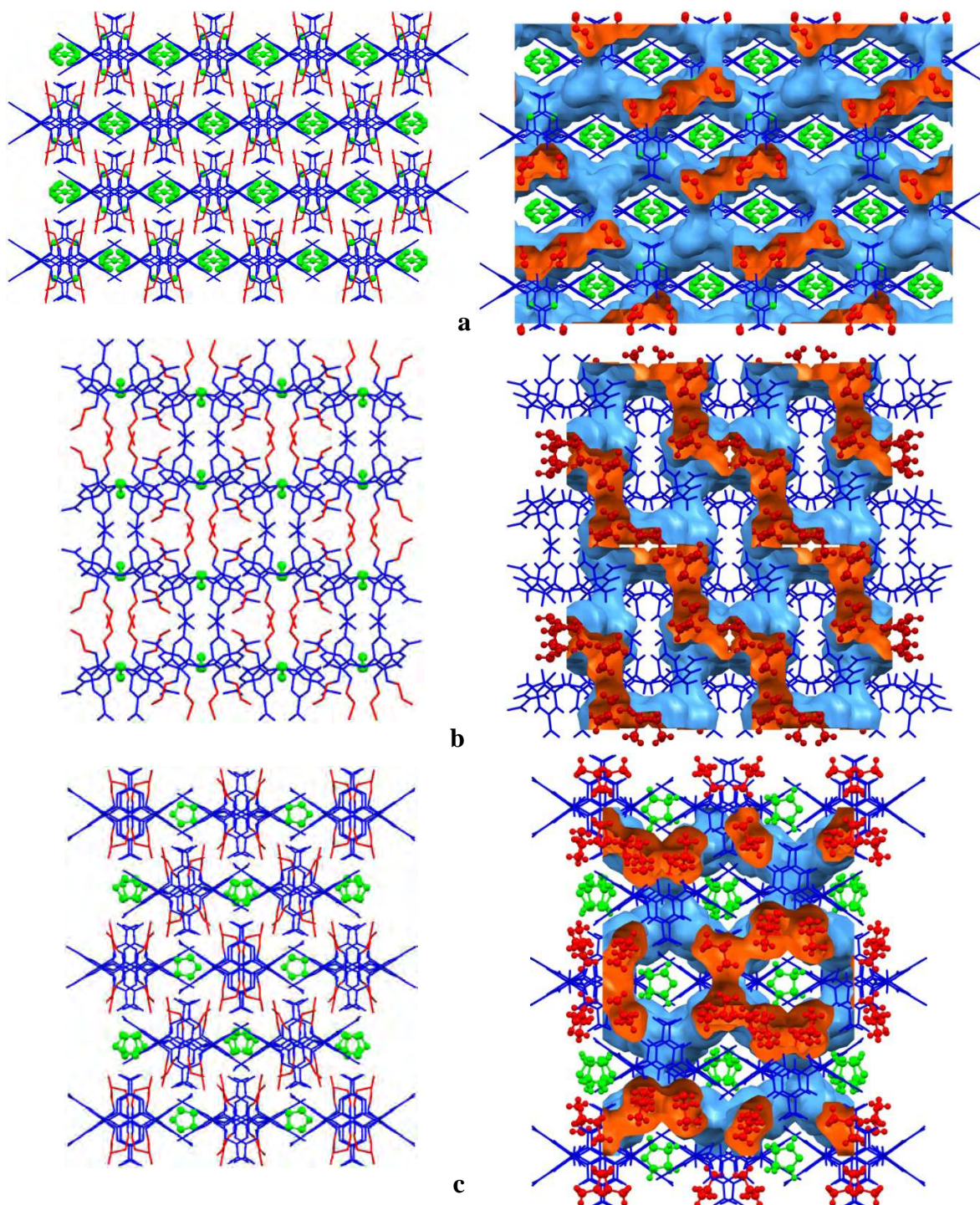
Fig. 146. Packing diagram and aromatic/aliphatic regions: (a) NO$_2$C[4]OC$_3$·*Solv*,[113] view along the *c* crystallographic axis; (b) NO$_2$C[4]OC$_3$·CH$_2$Cl$_2$,[114] view along the *c* crystallographic axis; (c) NO$_2$C[4]OC$_3$·0.5THF,[115] view along the *c* crystallographic axis.

Molecules of NO$_2$C[4]OC$_4$ in acetone clathrate[116] are assembled in different way than the propyl derivatives described above, but resulting topology is similar, *i.e.* bicontinuous (Fig. 147a). Further elongation of *n*-alkyl substituents leads to increased

173

hydrophobic-to-total volume ratio (Table 86) and, contrary to solvent-free $NO_2C[4]OC_3$,[115] the solvent-free $NO_2C[4]OC_5$[117] reveals bicontinuous topology (Fig. 147b).
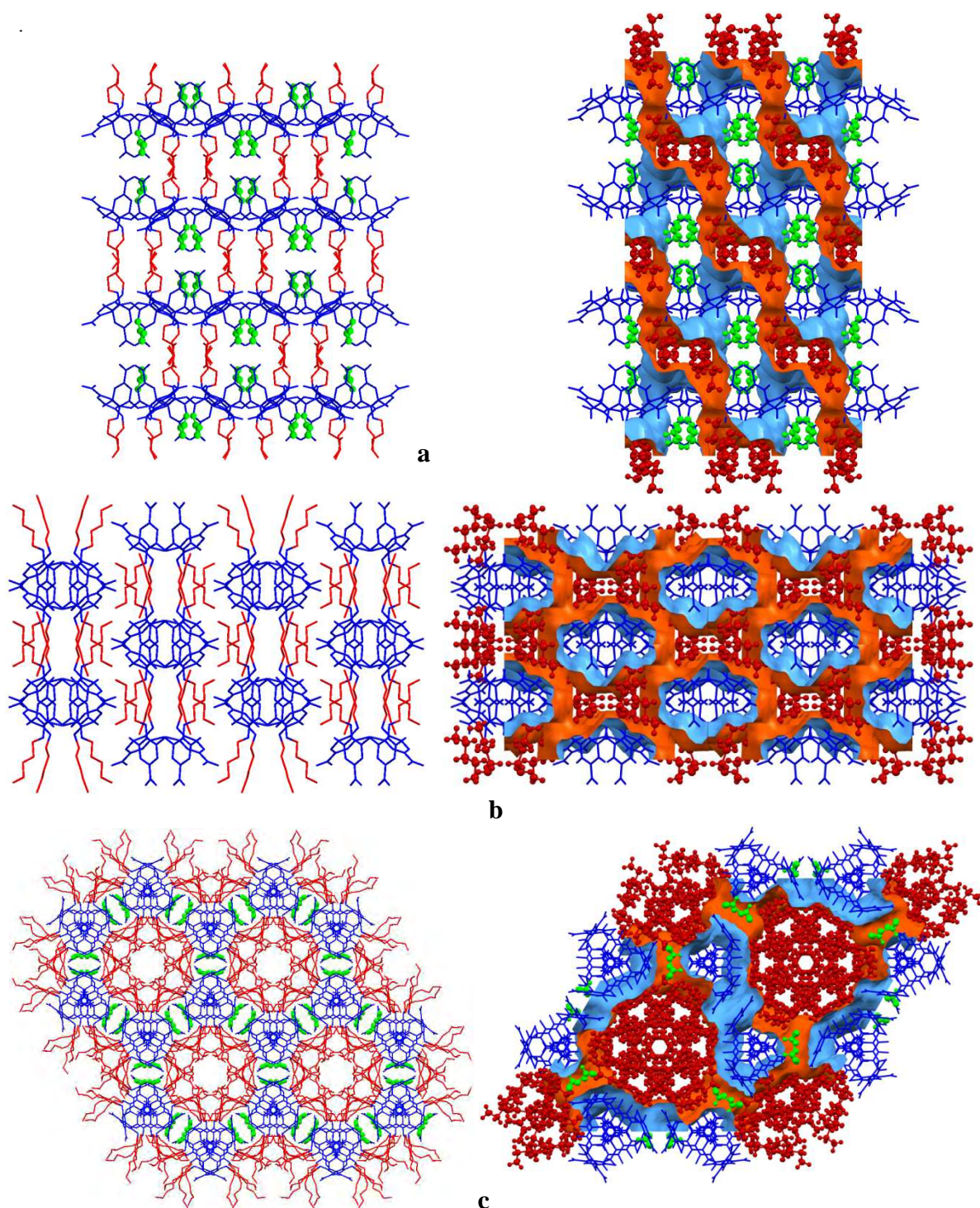
Fig. 147. Packing diagram and aromatic/aliphatic regions: (a) $NO_2C[4]OC_4 \cdot (CH_3)_2CO$,[116] view along the *a* crystallographic axis; (b) $NO_2C[4]OC_5$,[117] view along the *c* crystallographic axis; (c) $NO_2C[4]OC_8 \cdot CHCl_3$, view along $\bar{3}$ axis.

Surprisingly, molecules of $NO_2C[4]OC_8$, as with *n*-propylated *para*-nitro calix[4]arene, self-assemble in infinite chains. Spatial coherence in placement of alkyl

174

groups results in relatively rigid channel type aromatic matrix with hexagonal distribution of channels formed by strongly disordered flexible alkyl chains (Fig. 147c). The aromatic regions are penetrated by chloroform molecules and topology of aromatic/aliphatic surface is bicontinuous.

Molecules of $NO_2C[4]OC_n$ with long alkyl chains ($n = 12$, 14) reveal bilayer structure typical for amphiphilic compounds. $NO_2C[4]OC_{12}$ crystallises from $CHCl_3/CH_3OH$ mixture without inclusion of solvent molecules (Fig. 148). In the same conditions, $NO_2C[4]OC_{14}$ forms two chloroform clathrates with stoichiometry 1:1 and 1:2 (Fig. 149a and b, respectively) where solvent molecules are located in voids between aromatic and aliphatic regions.
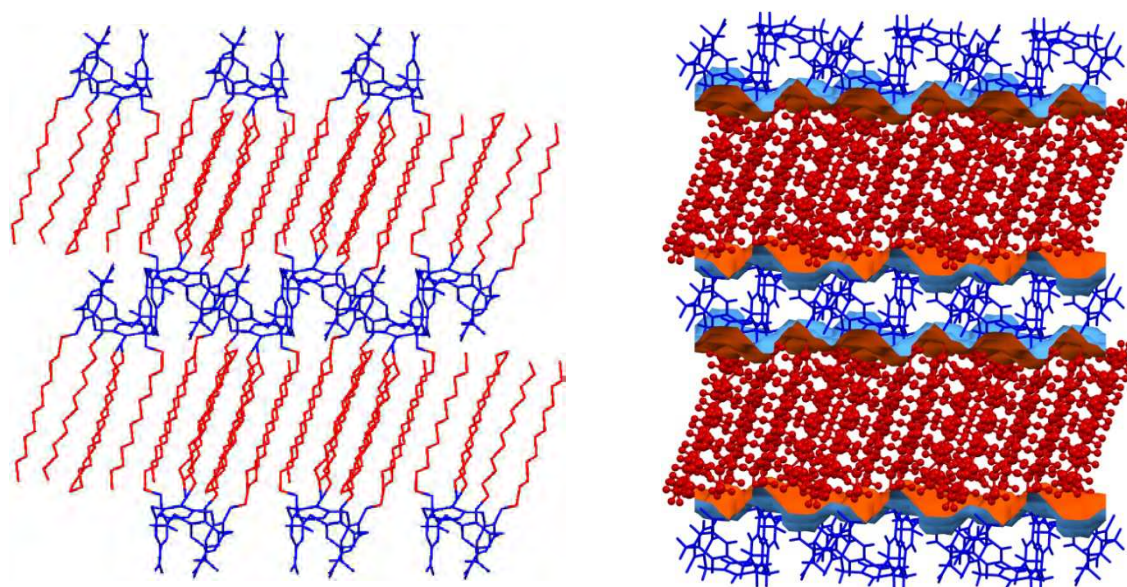
Fig. 148. Packing diagram and aromatic/aliphatic regions for $NO_2C[4]OC_{12}$, view along the *b* crystallographic axis.

Table 86. Molecular hydrophobic-to-total volume ratio and structural topology for $NO_2C[4]OC_n$ (cone).

Formula	Vol. ratio, %	Topology	Reference
$NO_2C[4]OC_2 \cdot CHCl_3$	25.7	*bi*	YOKKAL[112]
$NO_2C[4]OC_3$	33.0	*pl*	SINJIJ[115]
$NO_2C[4]OC_3 \cdot CH_2Cl_2$	33.0	*bi*	HEVYUC[114]
$NO_2C[4]OC_3 \cdot 0.5THF$	33.0	*bi*	MIPVUD[115]
$NO_2C[4]OC_3 \cdot Solv$	33.0	*bi*	SASRAF01[113]
$NO_2C[4]OC_4 \cdot (CH_3)_2CO$	39.0	*bi*	WORZOS[116]
$NO_2C[4]OC_5$	44.0	*bi*	KATGOC[117]
$NO_2C[4]OC_8 \cdot CHCl_3$	55.1	*bi*	This work
$NO_2C[4]OC_{12}$	64.4	*l*	This work
$NO_2C[4]OC_{14} \cdot CHCl_3$	67.8	*l*	This work
$NO_2C[4]OC_{14} \cdot 2CHCl_3$	67.8	*l*	This work

175
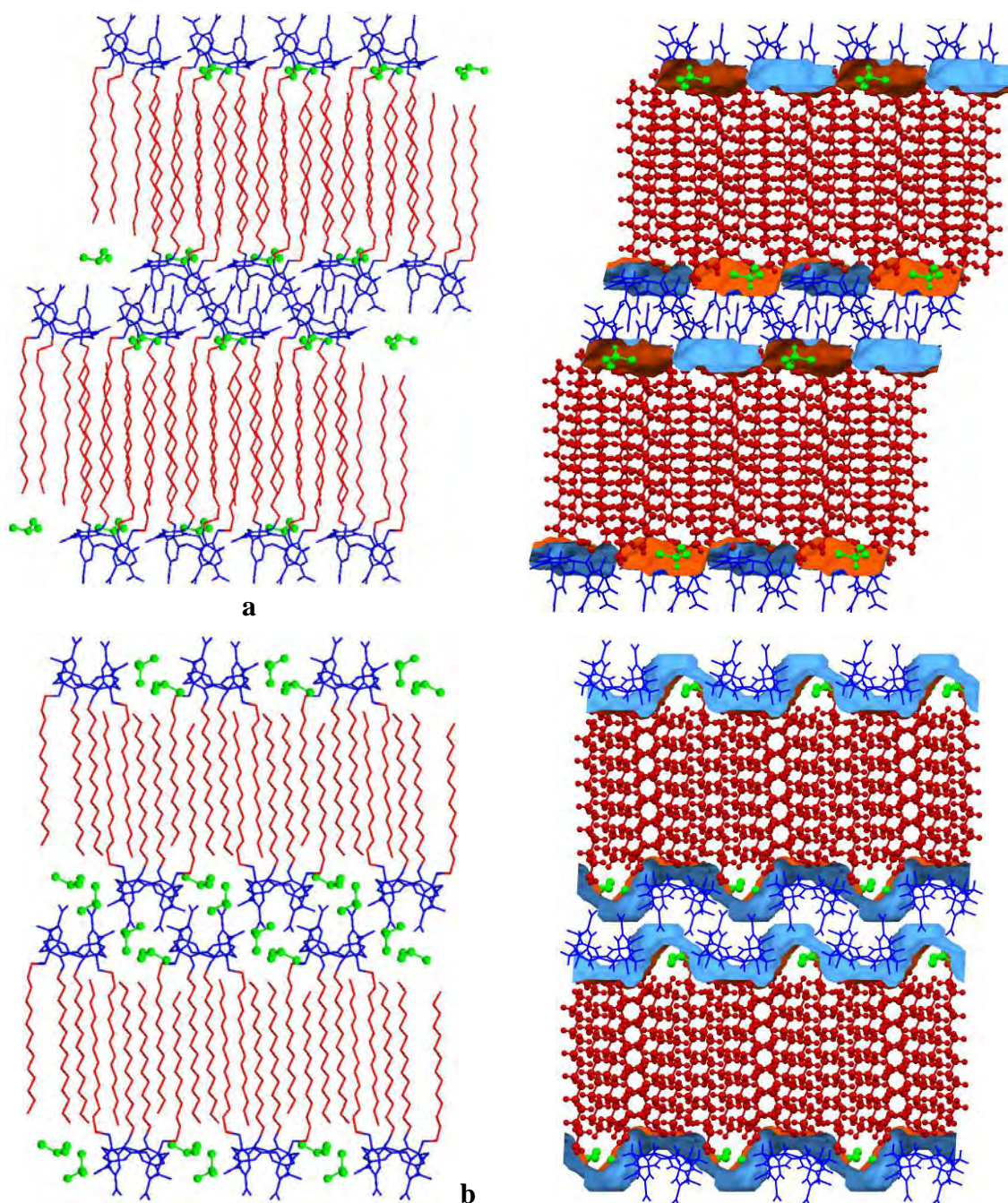
Fig. 149. Packing diagram and aromatic/aliphatic regions: (a) NO$_2$C[4]OC$_{14}$·CHCl$_3$, view along the *b* crystallographic axis; (b) NO$_2$C[4]OC$_{14}$·2CHCl$_3$, view along the *a* crystallographic axis.

5.2 Self-assembly of O-alkylated calix[4]arenes in a partial cone conformation

Only one crystal structure of HC[4]OC$_n$ (*n* = 3) calix[4]arene in a partial cone conformation is known.[93] Even if the molecules are not oriented in head-to-head or tail-to-tail mode, they are arranged in columns along the *c* crystallographic axis like the molecules in the cone conformations and similarly reveal bicontinuous topology of aromatic and aliphatic regions in the crystal (Fig. 150). Change in conformation also results in decreasing of crystal symmetry and decreasing the unit cell volume by factor of 4.

Fig. 150. HC[4]OC$_3$:[93] (a) packing diagram along the *c* crystallographic axis; **(b)** aromatic and aliphatic regions, view along the *b* crystallographic axis.

For all O-alkylated *para-tert*-butyl-calix[4]arenes in partial cone conformation, the hydrophobic contribution in total volume of the molecule is larger compared to the unsubstituted calix[4]arenes (Table 87) which suggest the inverted topology occurrence.

Table 87. Molecular hydrophobic-to-total volume ratio and structural topology for XC[4]OC$_n$ (partial cone).

Formula	Vol. ratio, %	Topology	Reference
HC[4]OC$_3$	38.2	*bi*	LAGQEQ02[93]
tBuC[4]OC$_1$	52.9	*ipl*	KEVXUE[80]
tBuC[4]OC$_1$·THF	52.9	*ipl*	CIQDUC[106]
tBuC[4]OC$_1$·0.5CH$_2$Cl$_2$	52.9	*ipl*	HISQOQ[107]
tBuC[4]OC$_1$·0.125CHCl$_3$	52.9	*ipl*	This work
tBuC[4]OC$_2$	56.9	*ipl*	This work
tBuC[4]OC$_3$·0.5THF	60.3	*ipl*	POQHAF[105]
tBuC[4]OC$_3$·0.5CHCl$_3$	60.3	*ipl*	This work
tBuC[4]OC$_4$	63.2	*ipl*	This work
tBuC[4]OC$_5$	65.7	*ipl*	This work
tBuC[4]OC$_6$	67.8	*ipl*	This work
tBuC[4]OC$_7$	69.8	*ipl*	This work
tBuC[4]OC$_8$	71.5	*ipl*	This work
NO$_2$C[4]OC$_1$·DMF	16.6	*r*	EQUSIS[134]
NO$_2$C[4]OC$_1$·CHCl$_3$	16.6	*r*	This work
NO$_2$C[4]OC$_2$·2CHCl$_3$	25.7	*r*	YOKKEP[112]
NO$_2$C[4]OC$_3$	33.0	*pl*	SINJIJ01[113]

Crystals of solvent-free tBuC[4]OC$_1$[80] and its clathrates with THF,[106] CH$_2$Cl$_2$[107] and CHCl$_3$ are isostructural. In all these structures, there are two types of layers (Fig. 151a) with different density of molecular packing: without voids and with cavities between tBuC[4]OC$_1$ molecules, in which solvent molecules can be included. In terms

of aromatic and aliphatic regions, calix[4]arene macrocyclic rings of both crystallographically independent molecules form corrugated layers parallel to the *bc* crystallographic plane. The layers are penetrated by *tert*-butyl and methyl groups (Fig. 151b).
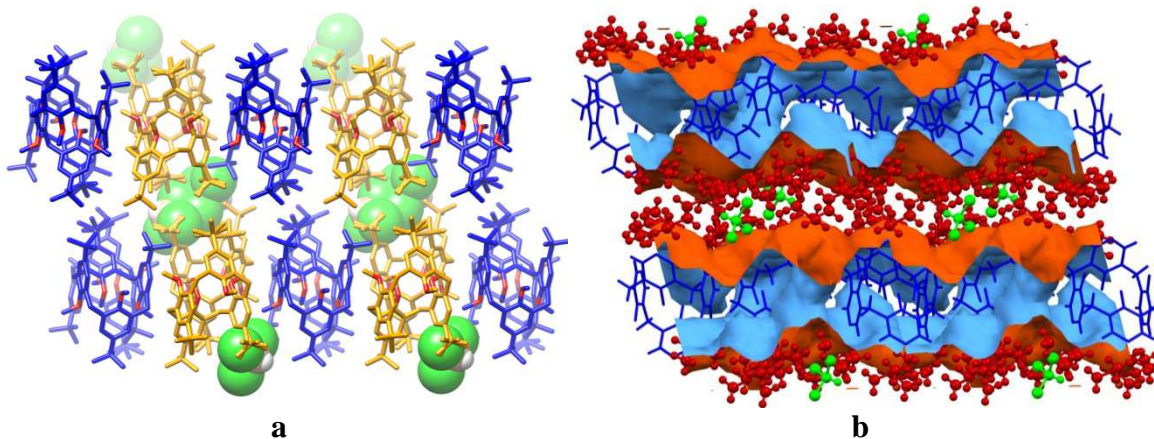
Fig. 151. tBuC[4]OC$_1$·0.125CHCl$_3$: (a) two types of layers, with and without solvent; (b) aromatic and aliphatic regions in the structure, view along the *b* crystallographic axis.

Elongation of the *n*-alkyl substituents results in self-assembly of tBuC[4]OC$_2$ molecules in layers. *tert*-Butyl and ethyl substituents are perpendicular to the layer (Fig. 152a) except the inverted phenyl ring, where the ethyl substituent is built in the aromatic regions (Fig. 152b).
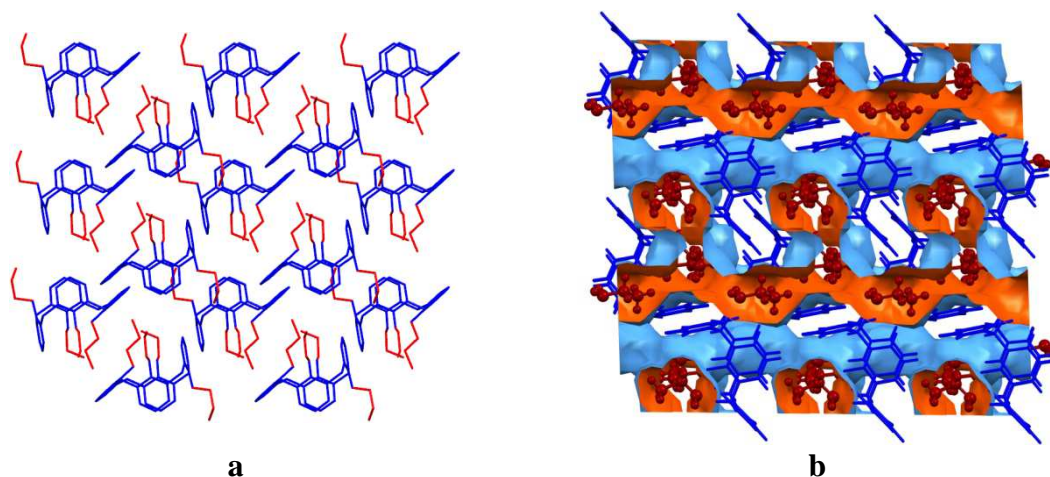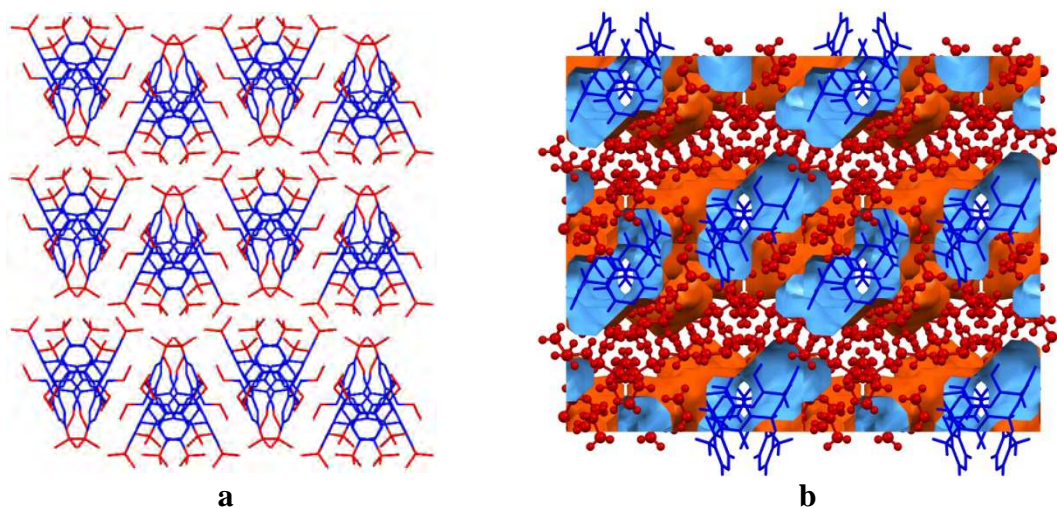

Fig. 152. tBuC[4]OC$_2$: (a) packing diagram, view along the *c* crystallographic axis; (b) aromatic and aliphatic regions, view along the *b* crystallographic axis.

The crystals of tBuC[4]OC$_3$·0.5THF[105] and tBuC[4]OC$_3$·0.5CHCl$_3$ are isostructural. tBuC[4]OC$_3$ molecules are self-assembled in layers. The aromatic regions form flat layers penetrated by alkyl substituents (Fig. 153a), so the topology of both THF and CHCl$_3$ solvates is inverted perforated layer (Table 87).

178

Contrary to tBuC[4]OC$_3$ clathrates, crystals of tBuC[4]OC$_4$ do not contain any solvent (Fig. 153b). The unit cell parameters and the space group are different, but the calixarene molecules are self-assembled in layers and the topology is the same as for tBuC[4]OC$_3$ clathrates (inverted perforated layer, Table 87).

Fig. 153. Packing diagram and aromatic/aliphatic regions: (a) tBuC[4]OC$_3$·0.5CHCl$_3$, view along the *b* crystallographic axis; (b) tBuC[4]OC$_4$, view along the *c* crystallographic axis.

Molecules of tBuC[4]OC$_5$ and tBuC[4]OC$_6$ are self-assembled in layers similarly to tBuC[4]OC$_3$ clathrates (Fig. 154). Despite the same space groups and almost identical unit cell parameters, crystals of tBuC[4]OC$_5$ and tBuC[4]OC$_6$ are not isostructural. In tBuC[4]OC$_5$ a double layer is formed with the interlayer space filled

179
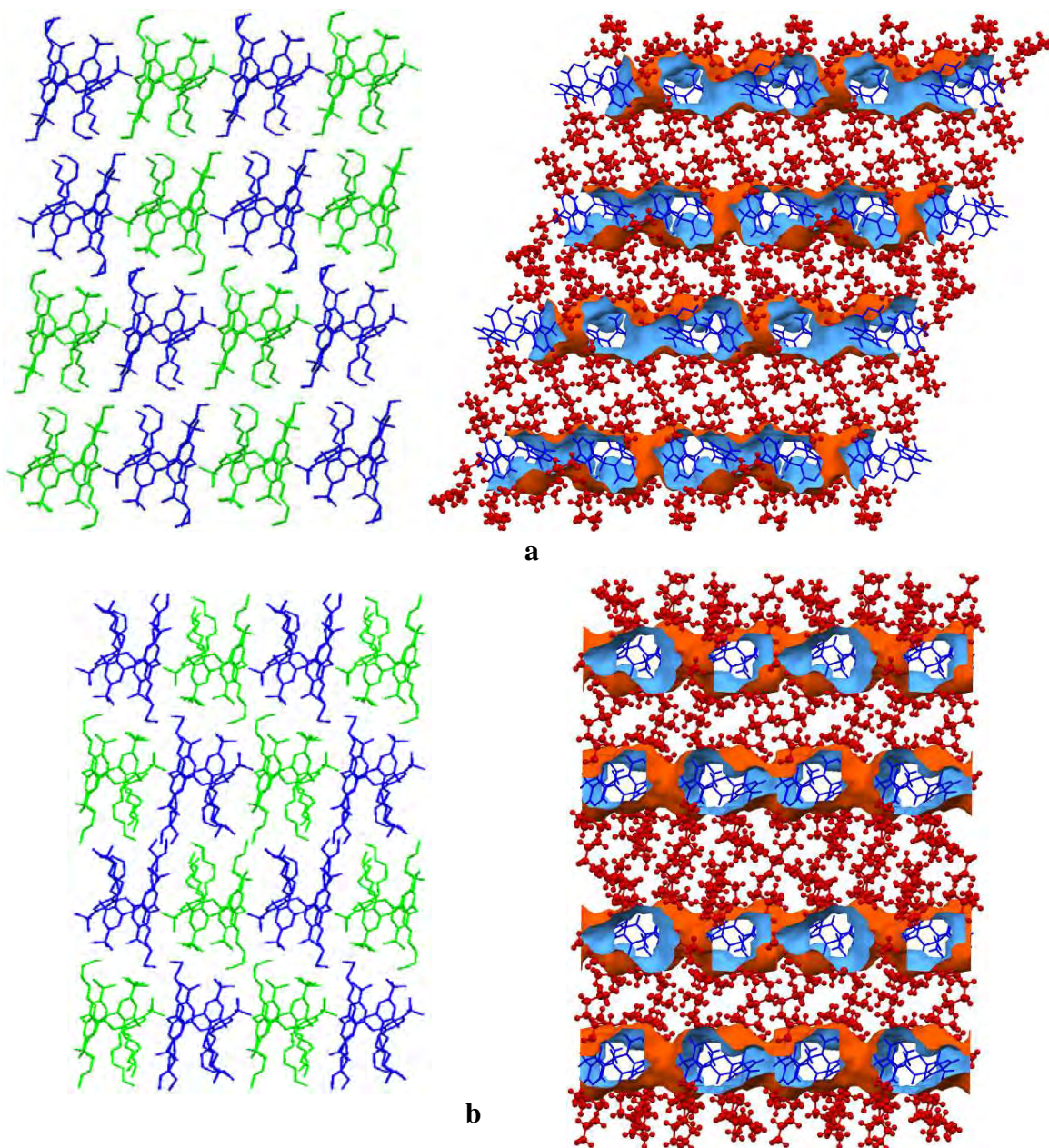
Fig. 154. Packing diagram and aromatic/aliphatic regions: (a) tBuC[4]OC$_5$, view along the
a crystallographic axis; (b) tBuC[4]OC$_6$, view along the a crystallographic axis.

with alkyl substituents. The second double layer is shifted by one calix[4]arene. In tBuC[4]OC$_6$ every second layer is shifted by one calixarene. In both structures the layer arrangement is 'head-to-head' and topology is inverted perforated layer (Table 87).

Contrary to tBuC[4]OC$_5$ and tBuC[4]OC$_6$, crystals of tBuC[4]OC$_7$ and tBuC[4]OC$_8$ are isostructural. n-Alkyl substituents in tBuC[4]OC$_7$ are strongly disordered (Fig. 155a), whereas they are quite ordered in tBuC[4]OC$_8$ (Fig. 155b). Both structures are layer-type structures similar to tBuC[4]OC$_3$ (partial cone) clathrates and reveal inverted perforated layer topology (Table 87). All calix[4]arene molecules in the layer are in the same spatial orientation.
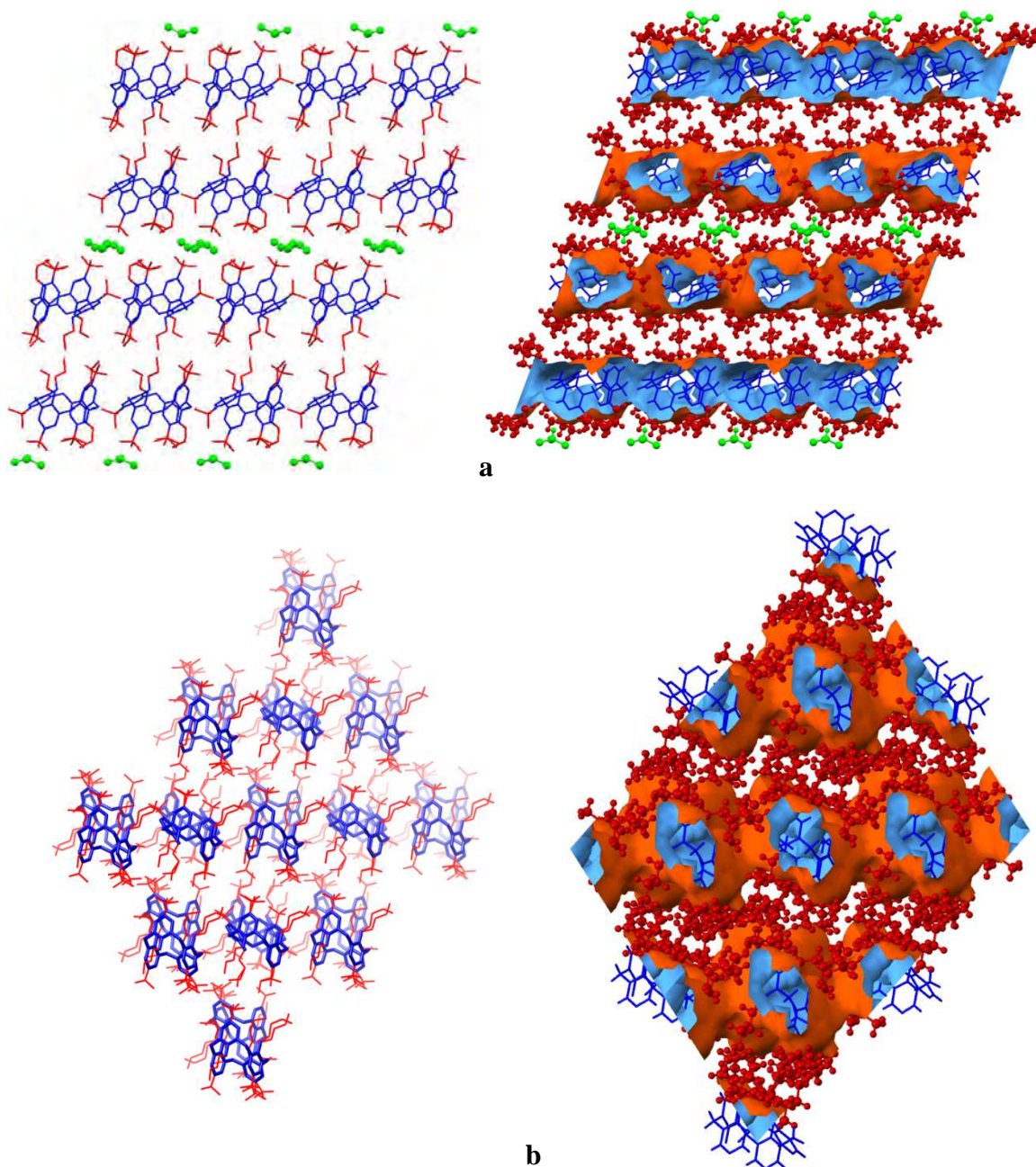
180
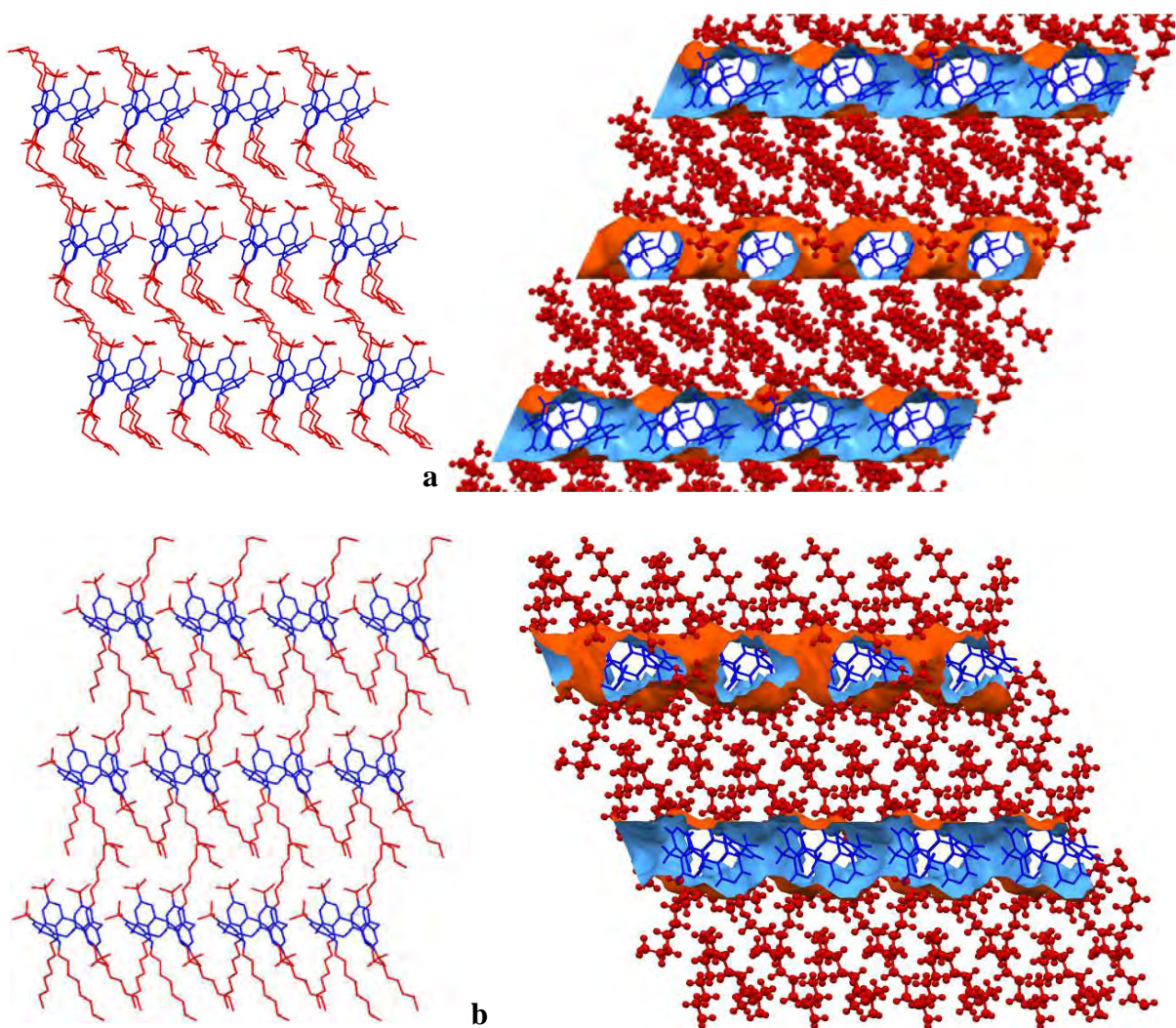
Fig. 155. Packing diagram and aromatic/aliphatic regions: (a) tBuC[4]OC$_7$, view along the *a* crystallographic axis; (b) tBuC[4]OC$_8$, view along the *a* crystallographic axis.

All known O-alkylated *para*-nitro-calix[4]arenes in a partial cone conformation show direct topology due to low hydrophobic contribution in molecular structure (Table 87). Crystals of NO$_2$C[4]OC$_1$·DMF[134] and NO$_2$C[4]OC$_1$ ·CHCl$_3$ are isostructural. There are voids in both crystals, where solvent molecules are located. Surface between aromatic and aliphatic regions form infinite zigzag ribbons in aromatic matrix along the *b–c* crystallographic direction (Fig. 156a).

Both NO$_2$C[4]OC$_2$·2CHCl$_3$[112] and NO$_2$C[4]OC$_3$[113] crystallise in the same space group *P*2$_1$/*c* but they are not isostructural. The clathrate[112] reveal similar topology as clathrates of methyl derivatives (Fig. 156b). Chloroform molecules are located in voids present in the crystal. In the case of propyl derivative, the volume of hydrophobic *n*-alkyl substituents is large enough (Table 87) to force changes in molecular self-assembly to corrugated layers and topology to perforated layers parallel to the *bc* crystallographic plane (Fig. 156c).

181
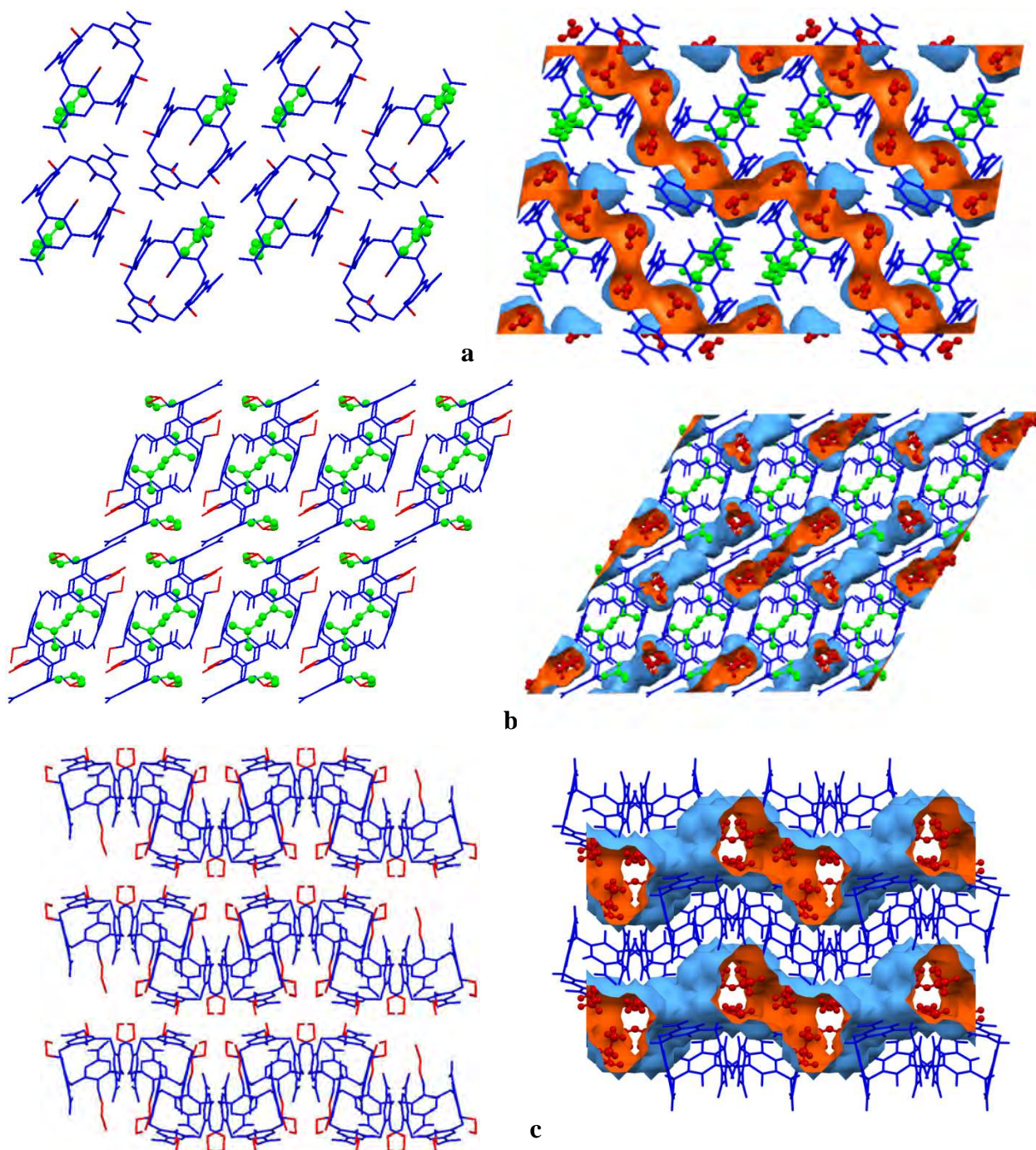
Fig. 156. Packing diagram and aromatic/aliphatic regions: (a) NO₂C[4]OC₁·DMF,[134] view along the a crystallographic direction; (b) NO₂C[4]OC₂·2CHCl₃,[112] view along the *b* crystallographic axis; (c) NO₂C[4]OC₃,[113] view along the *b* crystallographic axis.

5.3 Self-assembly of O-alkylated calix[4]arenes in 1,2- or 1,3-alternate conformations

There are only six known crystal structures of tetra-O-alkylated calix[4]arenes in 1,2- or 1,3-alternate conformations.

tBuC[4]OC₂ molecules in crystal structure of tBuC[4]OC₂·2CH₂Cl₂ (1,2-alternate)[58] are self-assembled in strongly corrugated layers parallel to the *bc*

crystallographic plane (Fig. 157a) with layered topology (Table 88). Surface of the layer is covered in equal density with *tert*-butyl and *n*-alkyl substituents due to 1,2-alternate conformation of calix[4]arene macrocyclic ring.

Elongation of alkyl substituents by one methylene group changes the topology of tBuC[4]OC$_3$ (1,2-alternate)[109] structure to inverted columnar, where zigzag aromatic ribbons are located in aliphatic matrix along the *b–c* crystallographic direction (Fig. 157b).

Fig. 157. Packing diagram and aromatic/aliphatic regions: (a) tBuC[4]OC$_2$ (1,2-alternate) ·2CH$_2$Cl$_2$,[58] view along the *c* crystallographic axis; (b) tBuC[4]OC$_3$ (1,2-alternate),[109] view along the *b-c* direction.

Table 88. Molecular hydrophobic-to-total volume ratio and structural topology for tBuC[4]OC$_n$ (1,2-alternate).

Formula	Vol. ratio, %	Topology	Reference
tBuC[4]OC$_2$·2CH$_2$Cl$_2$	56.9	*l*	VIVDUZ[58]
tBuC[4]OC$_3$	60.3	*ir*	KARNUN01[109]

Similarly to HC[4]OC$_3$ (cone) and HC[4]OC$_3$ (partial cone),[93] molecules of HC[4]OC$_3$ (1,3-alternate)[92] are arranged exactly one above the other in columns along the *b* crystallographic axis which, however, results in layered topology (Fig. 158a).

tBuC[4]OC$_3$ molecules in the 1,3-alternate conformation (like tBuC[4]OC$_3$ (1,2-alternate)) are self-assembled to corrugated layers parallel to the *ac* crystallographic

183
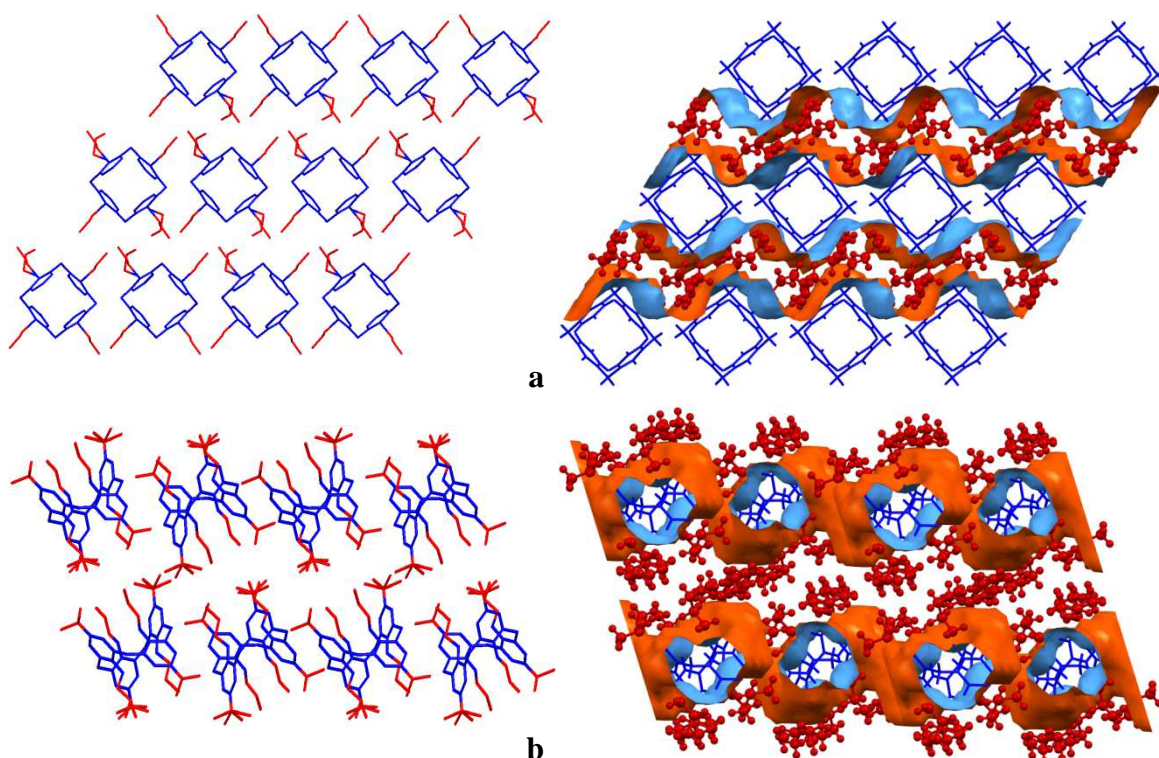
Fig. 158. Packing diagram and aromatic/aliphatic regions: (a) HC[4]OC$_3$ (1,3-alternate),[92] view along the *b* crystallographic axis; tBuC[4]OC$_3$ (1,3-alternate),[92] view along the *b* crystallographic axis.

plane. However, the presence of four large hydrophobic *tert*-butyl substituents (Table 89) and the different calixarene conformation lead to inverted perforated layers of aromatic regions shown in Fig. 158b.

Table 89. Molecular hydrophobic-to-total volume ratio and structural topology for XC[4]OC$_n$ (1,3-alternate).

Formula	Vol. ratio, %	Topology	Reference
HC[4]OC$_3$	38.2	*l*	LAGQEQ01[92]
tBuC[4]OC$_3$	60.3	*ipl*	KARNUN[92]
tBuC[4]OC$_8$	71.5	*ipl*	This work
NO$_2$C[4]OC$_3$·CH$_3$OH	33.0	*r*	SASRAF[113]

tBuC[4]OC$_8$ (1,3-alternate) molecules crystallise in a different space group than tBuC[4]OC$_3$ (1,3-alternate).[92] Nevertheless, close values of unit cell parameters a and *c* result in similar self-assembly in layers parallel to the *ac* crystallographic plane and inverted perforated layer topology (Fig. 159a). Elongation of unit cell parameter *b* corresponds to much longer *n*-alkyl substituents in the case of tBuC[4]OC$_8$ (1,3-alternate).

There is only one known crystal structure of *para*-nitro-tetra-O-alkylated calix[4]arene in the 1,3-alternate conformations: NO$_2$C[4]OC$_3$·CH$_3$OH (1,3-
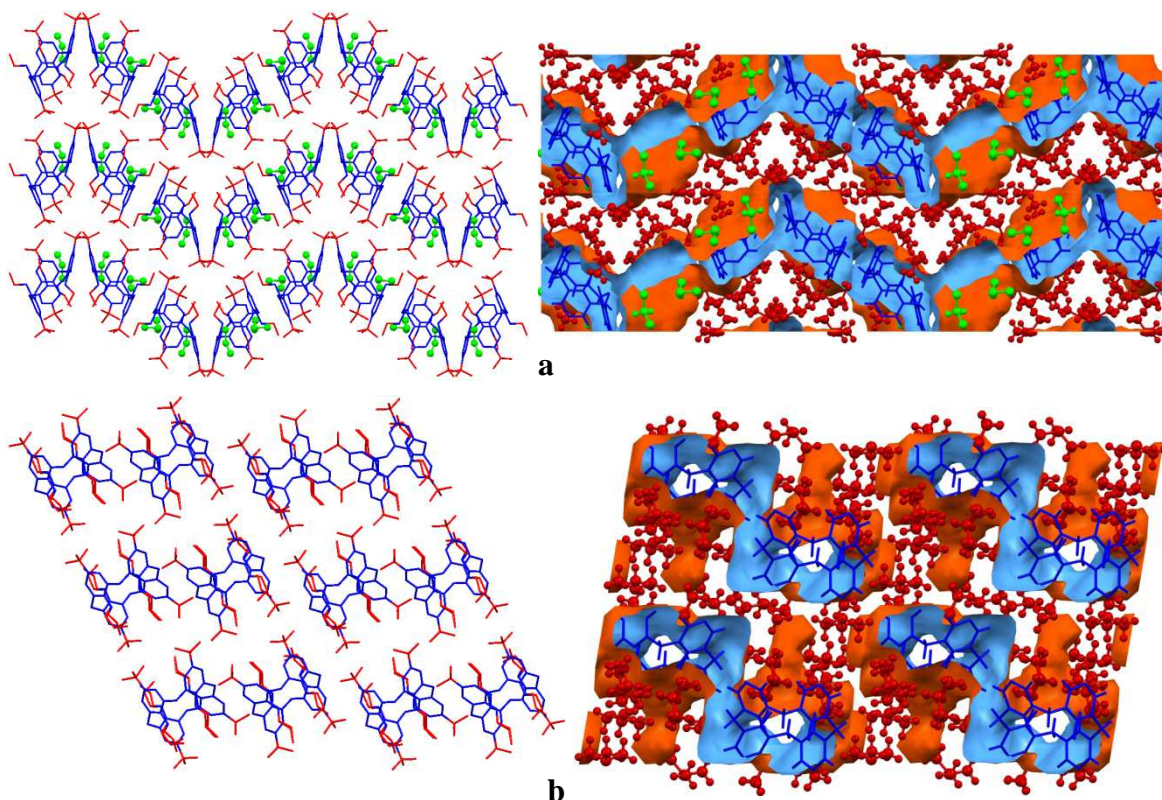
184
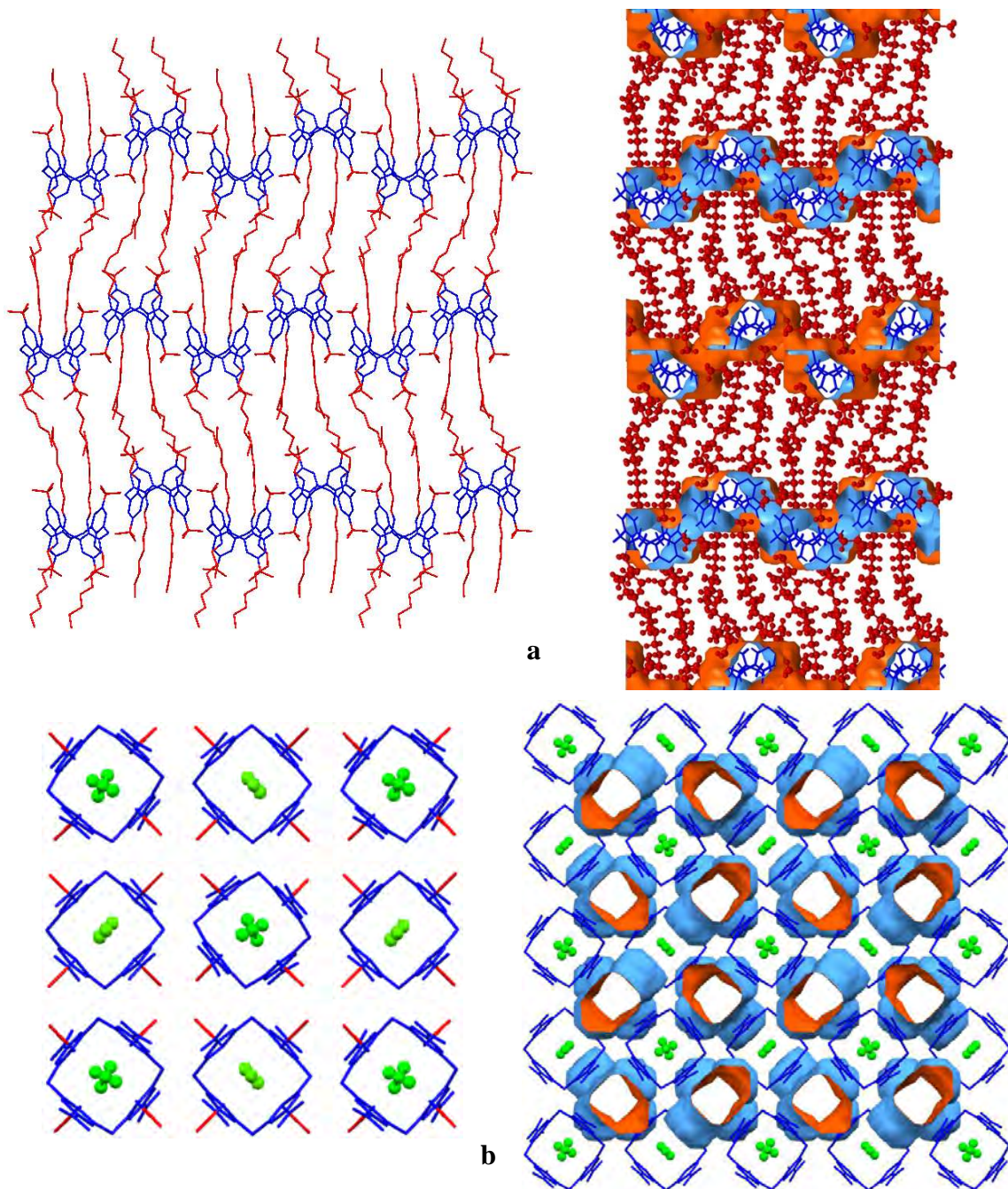
Fig. 159. Packing diagram and aromatic/aliphatic regions: (a) tBuC[4]OC$_8$ (1,3-alternate), view along the *a* crystallographic axis; (b) NO$_2$C[4]OC$_3$·CH$_3$OH (1,3-alternate),[113] view along the *c* crystallographic axis, *n*-alkyl substituents in' channels' are omitted for clarity.

alternate).[113] Likewise HC[4]OC$_3$ (cone), HC[4]OC$_3$ (partial cone)[93] and HC[4]OC$_3$ (1,3-alternate),[92] molecules of NO$_2$C[4]OC$_3$ (1,3-alternate) are arranged in columns (Fig. 159b) with different alignment along the *c* crystallographic axis but resulting topology is ribbon.

5.4   Self-assembly of O-alkylated calix[6]arenes

The peculiarity of O-alkylated calix[6]arene is full or partial self-inclusion of alkyl chain(s) within the macrocyclic ring. This results in inverted perforated layer topology for layered structures and the 'inverted micelle' is in fact an aromatic torus (not a sphere or an ellipsoid) with alkyl substituents inside and outside the calix[6]arene cavity.

HC[6]OC$_{18}$[118] (inverted double partial cone) is the only one known crystal structures of non-substituted at the *para*-positions fully O-alkylated calix[6]arene. Van der Waals interactions between long octadecyl substituents dominate the crystal structure and result in layered self-assembly parallel to the *ab* crystallographic plane (Fig. 160). First methylene groups of two distal alkyl substituents are partially included into calix[6]arene cavity which initiates inverted perforated layers topology (Table 90).

| a | b |
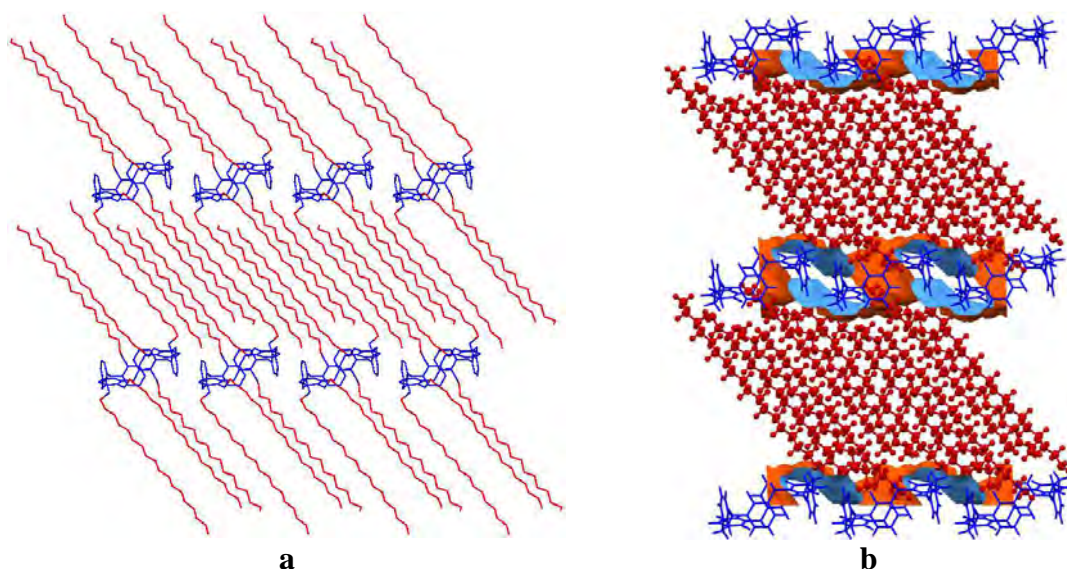
Fig. 160. HC[6]OC$_{18}$:[118] **(a) packing diagram and (b) aromatic and aliphatic regions, view along the *a* crystallographic axis.**

Table 90. Molecular hydrophobic-to-total volume ratio and structural topology for XC[6]OC$_n$.

Formula	Vol. ratio, %	Topology	Reference
HC[6]OC$_{18}$	77.2	*ipl*	ADOGIK[118]
tBuC[6]OC$_1$	52.9	*im*	UFOGOM[119]
tBuC[6]OC$_2$	56.9	*ir*	RALQIE[120]
tBuC[6]OC$_2$·benzophenone	56.9	*ipl*	RALQEA[121]
tBuC[6]OC$_3$·2CHCl$_3$	60.3	*im*	This work
tBuC[6]OC$_4$·CHCl$_3$	63.2	*ipl*	This work
tBuC[6]OC$_6$·2CHCl$_3$	67.9	*im*	This work

186

Molecules of fully O-alkylated *para-tert*-butyl-calix[6]arenes usually assume centrosymmetric inverted double partial cone conformation (except tBuC[6]OC$_4$·CHCl$_3$, which adopts 1,3-alternate one). Alternating orientation of phenyl moieties make them similar to calix[4]arene analogues in partial cone conformation. Nevertheless, due to high flexibility and the absence of strong interactions, even small changes in chain length or solvent presence cause different self-assembly of the calix[6]arene molecules (Table 90).

Crystal packing of tBuC[6]OC$_1$[104] can be described as an arrangement of isolated aromatic tori in alkyl matrix (Fig. 161a) and then the topology is inverted micelle (*im*).
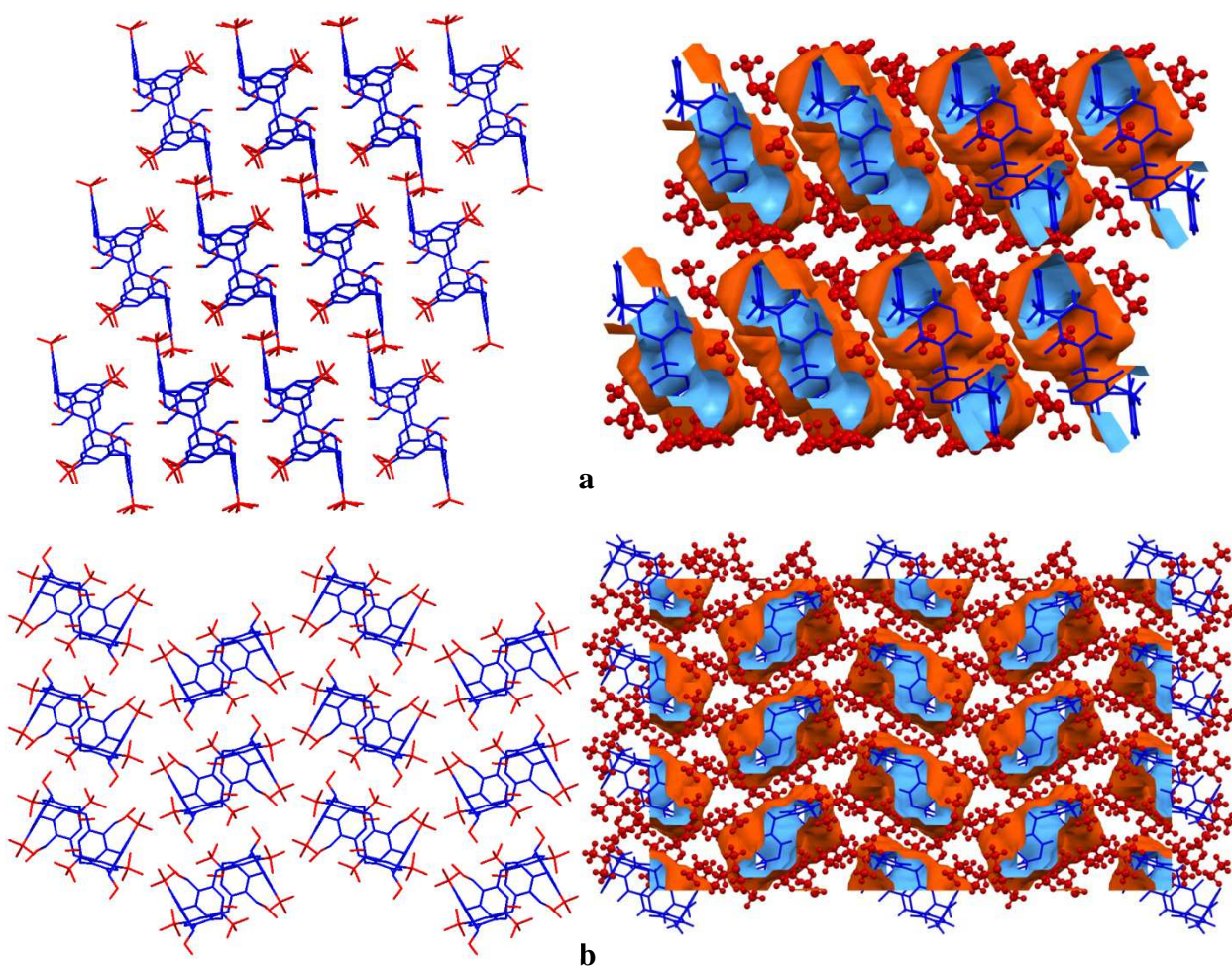
Fig. 161. Packing diagram and aromatic/aliphatic regions: (a) tBuC[6]OC$_1$,[119] view along the (*a-b*) crystallographic direction; (b) tBuC[6]OC$_2$,[120] view along the *a* crystallographic axis.

Molecules of tBuC[6]OC$_2$[120] are organized in ribbons along the *a* crystallographic axis with inverted ribbon topology (Fig. 161b).

Presence of benzophenone molecules[121] induces self-assembly of tBuC[6]OC$_2$ molecules in perforated layers (Fig. 162).

187
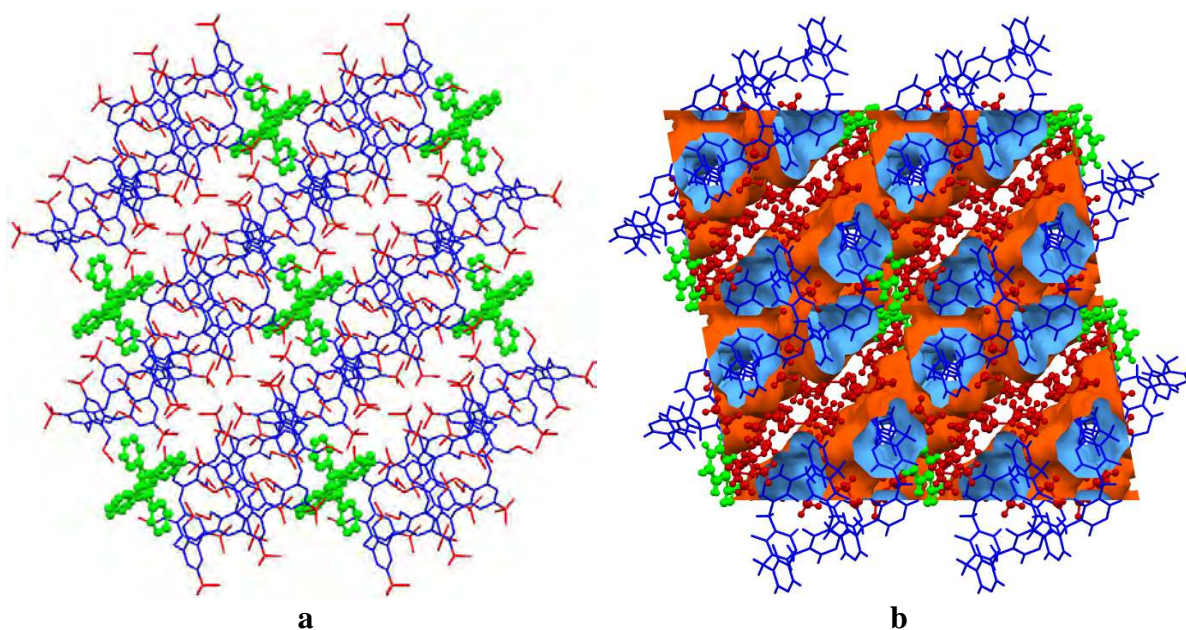
Fig. 162. tBuC[6]OC$_2$ benzophenone clathrate:[121] (a) packing diagram and (b) aromatic and aliphatic regions, view along the *b* crystallographic axis.

Further elongation of alkyl substituents up to 3 carbon atoms and presence of chloroform in tBuC[6]OC$_3$·2CHCl$_3$ surprisingly brakes the layers and inverted micelle topology is observed (Fig. 163).
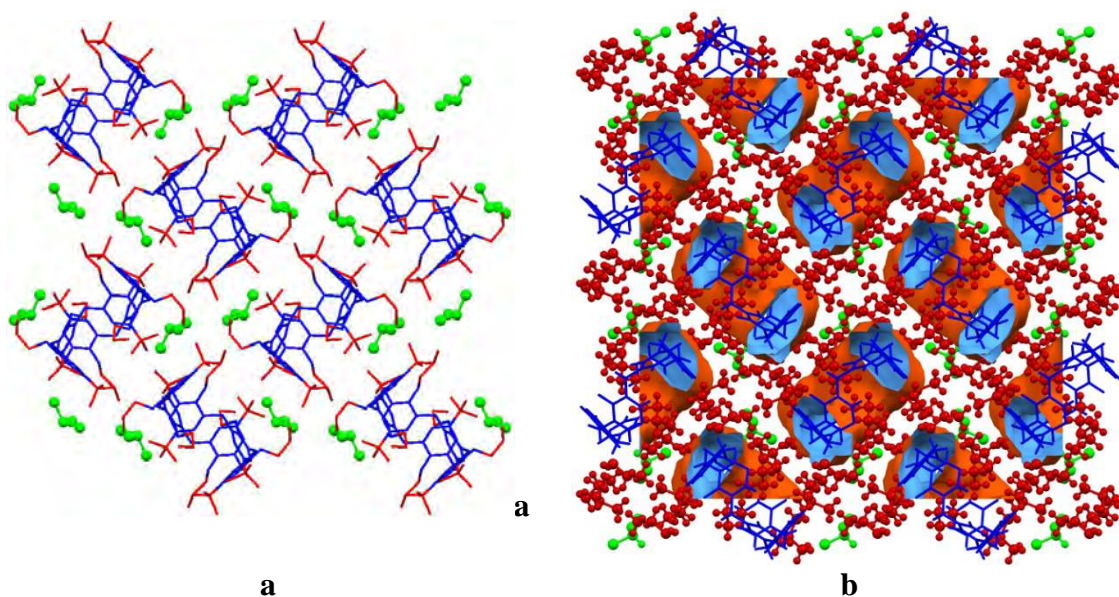
Fig. 163. tBuC[6]OC3·2CHCl$_3$: (a) packing diagram and (b) aromatic/aliphatic regions, view along the a crystallographic axis;

Molecules of tBuC[6]OC$_4$ assume 1,3-alternate conformation which leads to widespread net of C–H···π interactions and inverted perforated layer(s) formation (Fig. 164a).

188

Finally, combination of 6 carbon atoms in alkyl substituents and inclusion of two chloroform molecules in tBuC[6]OC$_6$·2CHCl$_3$ again results in inverted micelle topology (Fig. 164b).
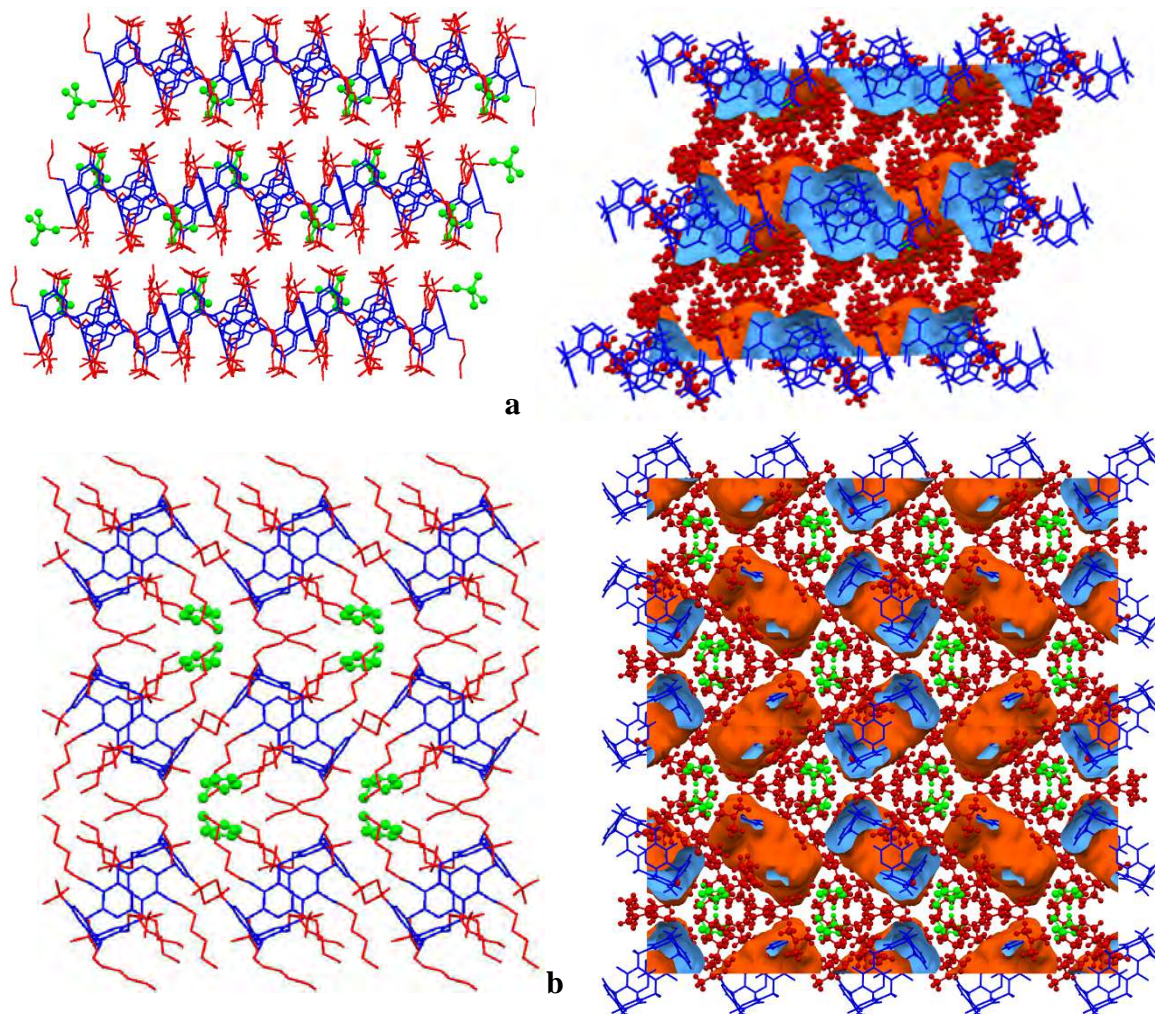
Fig. 164. Packing diagram and aromatic/aliphatic regions: (a) tBuC[6]OC$_4$·CHCl$_3$, view along the *c* crystallographic axis; (b) tBuC[6]OC$_6$·2CHCl$_3$, view along the *a* crystallographic axis.

5.5 Structure type - hydrophobic-to-total volume ratio correlation

Hydrophobic-to-total volume ratio and type of topology for all discussed in this thesis O-alkylated calixarenes was collected in Table 91. It might be expected for amphiphilic compound to present diagonal distribution of the data in the table. The lowest volume ratio is for tetra-O-methylated *para*-nitro-calix[4]arene (16.6%) and the highest one for tetra-O-tetradecylated *para-tert*-butylcalix[4]arene (78.7%). For the data available the hydrophobic-to-total volume ratios at ranges 0–10% and 80–100% are not presented (Table 91).

Table 91. Molecular hydrophobic-to-total volume ratios and number of structures with the same topology.

Vol. ratio, %	*m* or *r*	*pl*	*bi* or *l*	*ipl*	*ir* or *im*
0-10					
10-20	2				
20-30	1		1		
30-40	1	2	7		
40-50			2		
50-60			3	6	2
60-70			9	10	4
70-80			1	8	3
80-90					
90-100					

Topologies: direct micelle (*m*), ribbon (*r*), perforated layer (*pl*), layer (*l*), bicontinuous (*bi*), inverted perforated layer (*ipl*), inverted ribbons (*ir*) and inverted micelle (*im*).

It should be noticed that for volume ratio range 40–50% (crystal structures of HC[4]OC$_4$ and NO$_2$C[4]OC$_5$ in the cone conformation) bicontinuous topology is observed. For the lower or the higher volume ratios, different topologies occur: ribbons, perforated layers, bicontinuous and layers for the volume range of 20–40% and bicontinuous, layers, inverted perforated layers, inverted ribbons and inverted micelles. The reason of these deviations from the main trend is a greater importance of weak intermolecular interactions in the solid state in comparison with liquid phase. In other words, weak interactions, such as C–H⋯O hydrogen bonding, C–H⋯π interactions, π-π stacking interactions and van der Waals interactions between hydrogen atoms of adjacent long alkyl chains ($n \geq 9$) might overbalance the minimisation of hydrophobic-to-hydrophilic contacts, especially in solid state, where thermal motions are reduced.

5.6   Analysis of conformation of calix[4]arene macrocyclic ring

One of the possible ways of numerical description of calix[4]arene conformation is a measure of the distances between centroids of distal phenyl rings *d* (Table 92). Each calix[4]arene has one pair of *d* values between two pairs of distal rings. It is more convenient to analyse the difference (Δd) of the *d* values for each ring rather than the individual *d* values. Values of Δd as function of alkyl chain length (*n*) are shown in Fig. 165. The plot shows that Δd values for O-alkylated calix[4]arenes in 1,2- or 1,3-alternate conformation are close to 0, while for calix[4]arenes in partial cone

Table 92. Distances between centroids of distal phenyl rings of calix[4]arenes

Formula	d_1, Å	d_2, Å	Reference
HC[4]OC$_n$ (cone)			
HC[4]OC$_3$	4.97 5.05	7.69 7.60	LAGQEQ[94]
HC[4]OC$_4$	4.74	7.76	QADTIZ[95]
HC[4]OC$_7$	4.78 5.23	7.69 7.49	This work
HC[4]OC$_{11}$	4.64	7.73	This work
HC[4]OC$_{12}$	4.53 4.52 4.60 4.56	7.84 7.73 7.75 7.82	LALFUA01[97]
HC[4]OC$_{12}$	4.70	7.70	LALFUA[96]
HC[4]OC$_{14}$	5.61 5.50	7.34 7.42	FAGFEA[97]
HC[4]OC$_{16}$·5H$_2$O	4.67 4.79	7.78 7.81	FAGFOK[97]
HC[4]OC$_{18}$·2C$_6$H$_6$	4.69	7.78	KENHAN[98]
HC[4]OC$_{18}$·C$_6$H$_5$CH$_3$	4.78	7.69	KENHER[98]
tBuC[4]OC$_n$ (cone)			
tBuC[4]OC$_3$	5.47	7.32	This work
tBuC[4]OC$_3$·CH$_3$CN	6.55	6.60	GIYTEN[108]
tBuC[4]OC$_4$	5.59	7.33	This work
tBuC[4]OC$_4$·4CHCl$_3$·2H$_2$O	5.49	7.40	FOVRIS[110]
tBuC[4]OC$_5$	5.33	7.50	DAYKIY[111]
tBuC[4]OC$_6$	5.56 5.28	7.33 7.49	This work
tBuC[4]OC$_9$	5.47	7.29	This work
tBuC[4]OC$_{10}$·CHCl$_3$	5.32	7.47	This work
tBuC[4]OC$_{11}$	5.47	7.29	This work
tBuC[4]OC$_{12}$·CHCl$_3$	5.35	7.47	This work
tBuC[4]OC$_{14}$·CHCl$_3$	5.37	7.47	This work
NO$_2$C[4]OC$_n$ (cone)			
NO$_2$C[4]OC$_2$·CHCl$_3$	4.68	7.82	YOKKAL[112]
NO$_2$C[4]OC$_3$	4.77	7.87	SINJIJ[115]
NO$_2$C[4]OC$_3$·CH$_2$Cl$_2$	4.74	7.76	HEVYUC[114]
NO$_2$C[4]OC$_3$·0.5THF	4.95 4.80 5.15	7.73 7.79 7.69	MIPVUD[115]
NO$_2$C[4]OC$_3$·*Solv*	4.95	7.71	SASRAF01[113]
NO$_2$C[4]OC$_4$·(CH$_3$)$_2$CO	4.64	7.92	WORZOS[116]
NO$_2$C[4]OC$_5$	4.93	7.69	KATGOC[117]
NO$_2$C[4]OC$_8$·CHCl$_3$	4.55	7.74	This work
NO$_2$C[4]OC$_{12}$	4.57	7.79	This work
NO$_2$C[4]OC$_{14}$·CHCl$_3$	4.76	7.81	This work
NO$_2$C[4]OC$_{14}$·2CHCl$_3$	4.61	7.79	This work

Formula	d_1, Å	d_2, Å	Reference
XC[4]OC$_n$ (partial cone)			
HC[4]OC$_3$	4.95	6.86	LAGQEQ02[93]
tBuC[4]OC$_1$	5.51	6.82	KEVXUE[80]
	5.53	6.84	
tBuC[4]OC$_1$·THF	5.51	6.82	CIQDUC[106]
	5.54	6.86	
tBuC[4]OC$_1$·0.5CH$_2$Cl$_2$	5.54	6.82	HISQOQ[107]
	5.49	6.82	
tBuC[4]OC$_1$·0.125CHCl$_3$	5.49	6.81	This work
	5.48	6.84	
tBuC[4]OC$_2$	5.47	6.89	This work
tBuC[4]OC$_3$·0.5THF	5.62	6.82	POQHAF[105]
tBuC[4]OC$_3$·0.5CHCl$_3$	5.63	6.83	This work
tBuC[4]OC$_4$	5.45	6.88	This work
	5.47	6.82	
tBuC[4]OC$_5$	5.62	6.82	This work
	5.68	6.84	
tBuC[4]OC$_6$	5.57	6.83	This work
	5.65	6.87	
tBuC[4]OC$_7$	5.55	6.80	This work
tBuC[4]OC$_8$	5.59	6.91	This work
NO$_2$C[4]OC$_1$·DMF	5.76	6.79	EQUSIS[134]
NO$_2$C[4]OC$_1$·CHCl$_3$	5.66	6.85	This work
NO$_2$C[4]OC$_2$·2CHCl$_3$	5.16	6.93	YOKKEP[112]
NO$_2$C[4]OC$_3$	5.02	6.97	SINJIJ01[113]
XC[4]OC$_n$ (1,2-alternate)			
tBuC[4]OC$_2$·2CH$_2$Cl$_2$	6.75	6.84	VIVDUZ[58]
tBuC[4]OC$_3$	6.82	6.83	KARNUN01[109]
XC[4]OC$_n$ (1,3-alternate)			
HC[4]OC$_3$	4.86	4.88	LAGQEQ01[92]
tBuC[4]OC$_3$	6.10	6.14	KARNUN[92]
tBuC[4]OC$_8$	5.92	6.05	This work
	5.88	6.10	
NO$_2$C[4]OC$_3$·CH$_3$OH	5.56	5.56	SASRAF[113]
	5.45	5.60	

conformation vary from 1.03 to 1.95 Å, and for calix[4]arenes in cone conformation change from 1.73 to 3.26 Å.
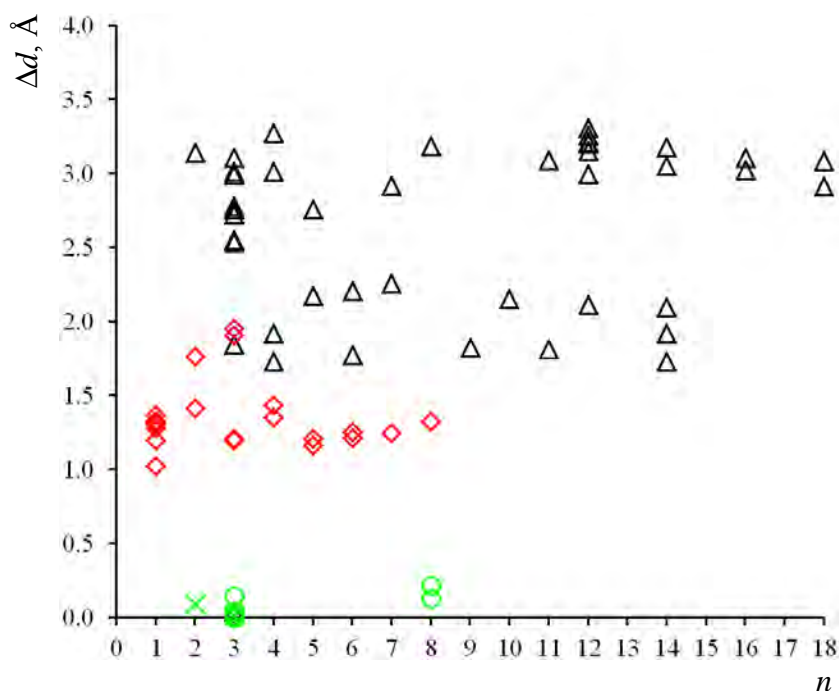
Fig. 165. Plot of Δ*d* values as a function of number of carbon atoms in alkyl substituents (*n*) for all discussed calix[4]arenes in cone (△), partial cone (◇), 1,2-alternate (×) and 1,3-alternate (○) conformations.

The plot of Δ*d* values for calix[4]arenes in cone conformation only is shown in Fig. 166. It is interesting that Δ*d* values for $HC[4]OC_n$ (△) and $NO_2C[4]OC_n$ (△) lie in the same region with arithmetic mean value *ca.* 3.0 Å. Data for *n* = 14 correspond to $HC[4]OC_{14}$[97] and are exception but self-assembly of this calix[4]arene in the solid state is also different.

In the case of $tBuC[4]OC_n$ (△), Δ*d* range is narrower. There is a difference between two homologous series (even/odd number of carbon atoms in *n*-alkyl substituent) induced by presence of $CHCl_3$ molecules included in the voids between the calix[4]arene macrocyclic rings and adjacent alkyl chains. Arithmetic mean value of Δ*d* for $tBuC[4]OC_n$ with odd *n* = 9, 11, equals 1.82 Å, whereas for deformed macrocyclic rings of calix[4]arenes with even *n* = 10, 12, 14, this value is 2.12 Å. Data with *n* = 3 and Δ*d* ≈ 0 correspond to acetonitrile molecule inclusion into calix[4]arene cavity in $tBuC[4]OC_3 \cdot CH_3CN$.[108]

It should be noted that for both non-substituted and *para*-nitro-calix[4]arenes, a wide distinguish of Δ*d* values for low *n* rapidly narrows for *n* ≥ 8 (Fig. 166).
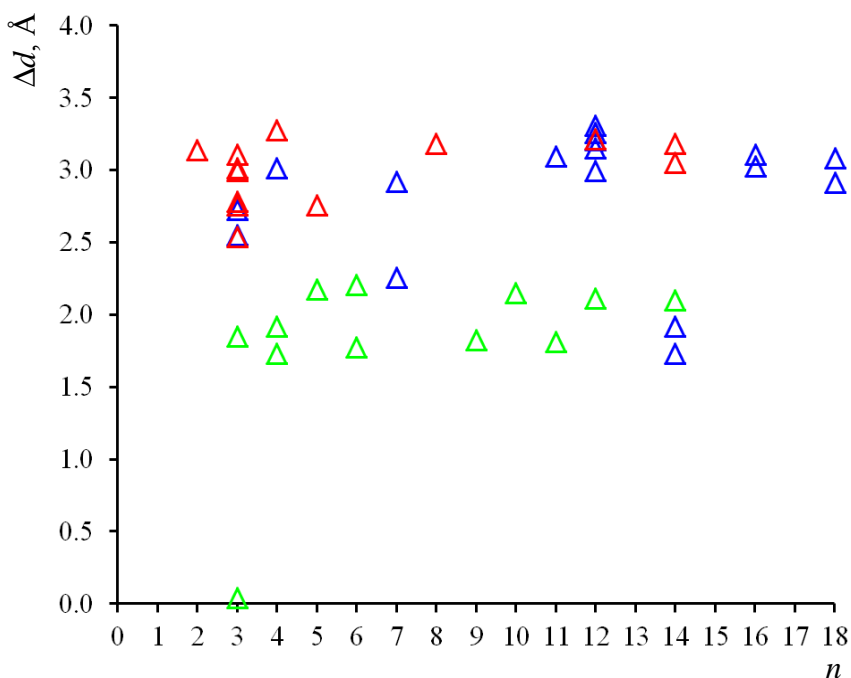
Fig. 166. Plot of Δ*d* values as a function of number of carbon atoms in alkyl substituents for calix[4]arene in cone conformation: HC[4]OC$_n$ (△), tBuC[4]OC$_n$ (△) and NO$_2$C[4]OC$_n$ (△).

All tBuC[4]OC$_n$ in partial cone conformation reveal similar layered self-assembly which results in close Δ*d* values (Fig. 167, ◇). Structure of the layer in the case of calix[4]arenes with *n* = 1, 2 and 4 differs from other calix[4]arenes in the homologous series and it is reflected in larger Δ*d* values.

Δ*d* Value for *para*-nitro-calix[4]arene homologous series (Fig. 167, ◇) varies in a wider range than for *para-tert*-butyl ones.
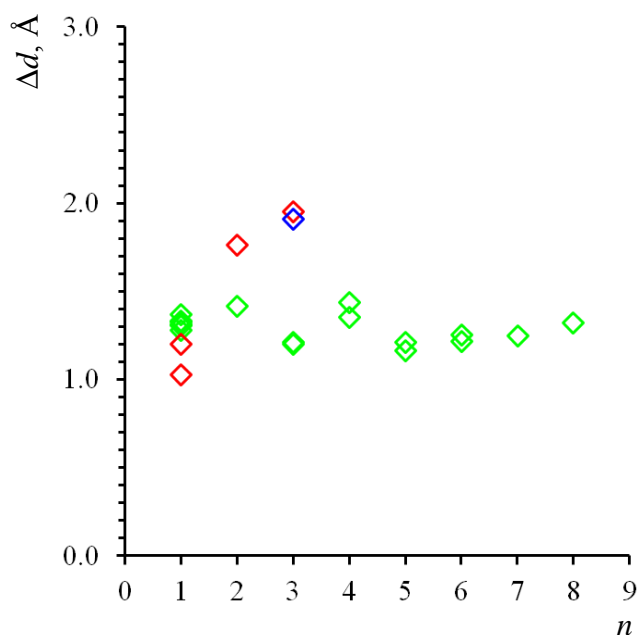

Fig. 167. Plot of Δ*d* as a function of alkyl chain length for calix[4]arenes in partial cone conformations: HC[4]OC$_n$ (◇), tBuC[4]OC$_n$ (◇) and NO$_2$C[4]OC$_n$ (◇).

194

Contrary to the calix[4]arenes in cone conformation, arithmetic mean values of Δd for $NO_2C[4]OC_n$ and $tBuC[4]OC_n$ are much closer [1.49 and 1.29 Å, respectively].

There is only one known non-substituted tetra-O-alkylated calix[4]arene[77] and similarly to the calix[4]arenes in cone conformation, its conformation is similar to *para*-nitro derivatives (Fig. 167, ◆).

1,2- and 1,3-alternate conformations of calix[4]arene macrocyclic rings are independent of alkyl chain length and their Δd values are close to 0 (Fig. 168).
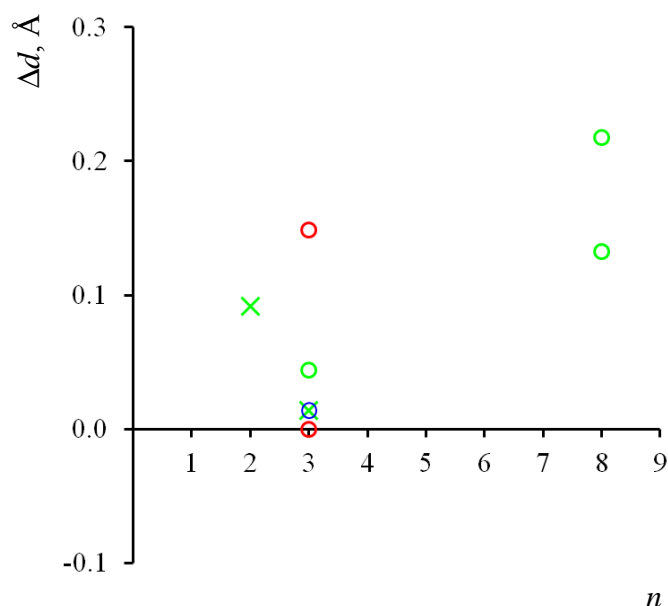
Fig. 168. Plot of Δd as a function of alkyl chain length for calix[4]arenes in 1,2- alternate conformations, tBuC[4]OC$_n$ (×); and 1,3-alternate conformations: HC[4]OC$_n$ (O), tBuC[4]OC$_n$ (o) and NO$_2$C[4]OC$_n$ (o).

Another way of presenting conformational analysis of the calix[4]arene rings is two-dimensional plot of d values for each calix[4]arene. Distances d_1 and d_2 are selected in such a way that d_1 is always smaller than d_2. Plot of d_2 as a function of d_1 for all discussed calix[4]arenes is shown in Fig. 169. The four regions in the plot correspond to four main calix[4]arene conformations: cone, partial cone and 1,2- and 1,3-alternate.

Further analysis of the region corresponding to the calix[4]arenes in cone conformation (Fig. 170) reveals that conformations of *para*-nitro-derivatives are the most pinched, conformation of *para-tert*-butyl derivatives are the least pinched ones and conformation of non-substituted calix[4]arene macrocyclic ring may vary in a wide range. The structure with $d_1 \approx d_2$ corresponds to tBuC[4]OC$_3$·CH$_3$CN[108] crystal structure (GIYTEN) where almost ideal cone conformation is induced by inclusion of acetonitrile molecule into the macrocyclic cavity. This is the only inclusion complex among all the crystal structures analysed in this thesis, so it should be omitted from the statistical analysis.

195
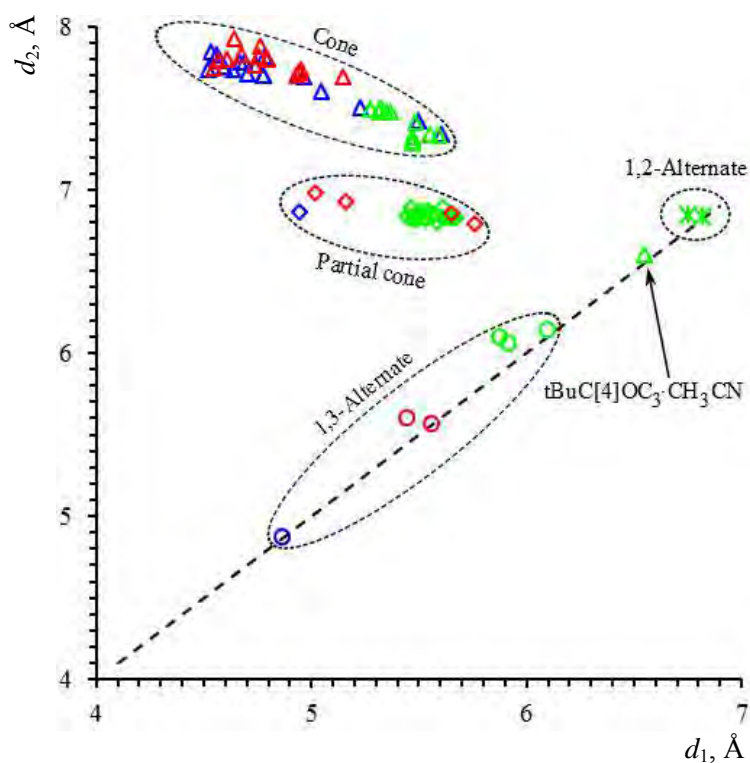
Fig. 169. Plot of d_2 as a function of d_1 for all discussed calix[4]arenes.
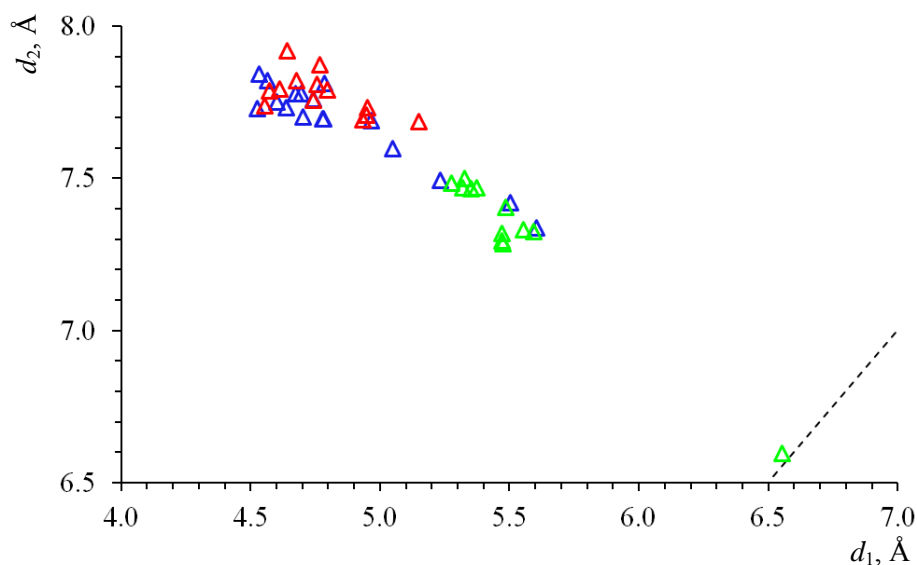
Fig. 170. Plot of d_2 as a function of d_1 for calix[4]arenes in cone conformation: HC[4]OC$_n$ (△), tBuC[4]OC$_n$ (△) and NO$_2$C[4]OC$_n$ (△).

Partial cone conformation of *para-tert*-butyl derivatives is very similar for all known examples for which crystal structures were determined, whereas partial cone conformations of *para*-nitro-derivatives change in a wide range: the smallest difference between d_1 and d_2 distances corresponds to tetra-O-methylated derivative and the largest to tetra-O-propylated one (Fig. 171). For calix[4]arenes in partial cone conformations, d_1 parameter corresponds to distance between parallel phenyl rings and d_2 to antiparallel

196

ones. It should be noted here, that d_2 changes in a small range of max. 0.172 Å, whereas d_1 changes in a wider range max 0.814 Å. This means that the distance between antiparallel phenyl rings changes slightly, whereas distance between parallel rings may change significantly.
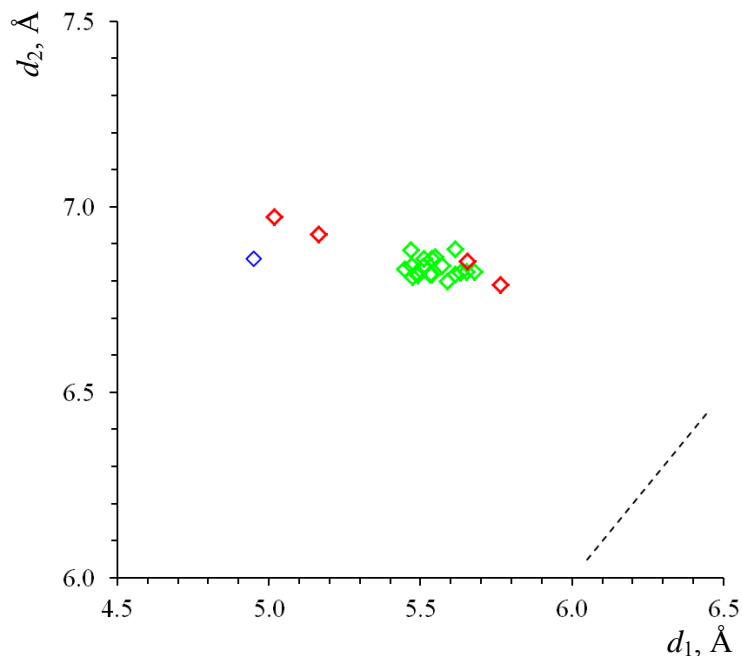
Fig. 171. Plot of d_2 as a function of d_1 for calix[4]arenes in partial cone conformations: HC[4]OC$_n$ (◇), tBuC[4]OC$_n$ (◇) and NO$_2$C[4]OC$_n$ (◇).

Tetra-O-alkylated calix[4]arenes in 1,2- and 1,3-alternate conformations are the most symmetrical in terms of differences in distances d_1 and d_2 (Fig. 172). d Values for
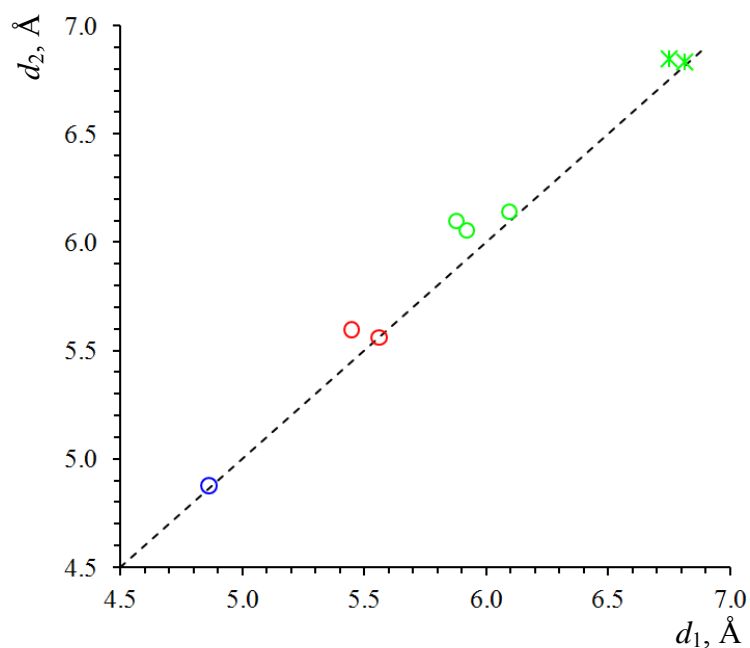
Fig. 172. Plot of d_2 as a function of d_1 for calix[4]arenes in 1,2- alternate conformations, tBuC[4]OC$_n$ (✳); and 1,3-alternate conformations: HC[4]OC$_n$ (O), tBuC[4]OC$_n$ (O) and NO$_2$C[4]OC$_n$ (O).

197

1,3-alternate conformation increase when a size of substituent in *para*-position of calix[4]arene rings increase: H– < NO_2– < tBu–. 1,2-Alternate conformation of *para-tert*-butyl calix[4]arene macrocyclic ring results in the largest d_1 and d_2 distances for distal antiparallel phenyl rings (Fig. 172, ✳).

Analysis of d distances of all discussed calix[4]arenes shows four conformational regions (Fig. 169). Histogram of Δd values reveals four peaks (Fig. 173a) at 0.2, 1.4, 2.0 and 3.2 Å, corresponding to four the most probable values of Δd.

a

b
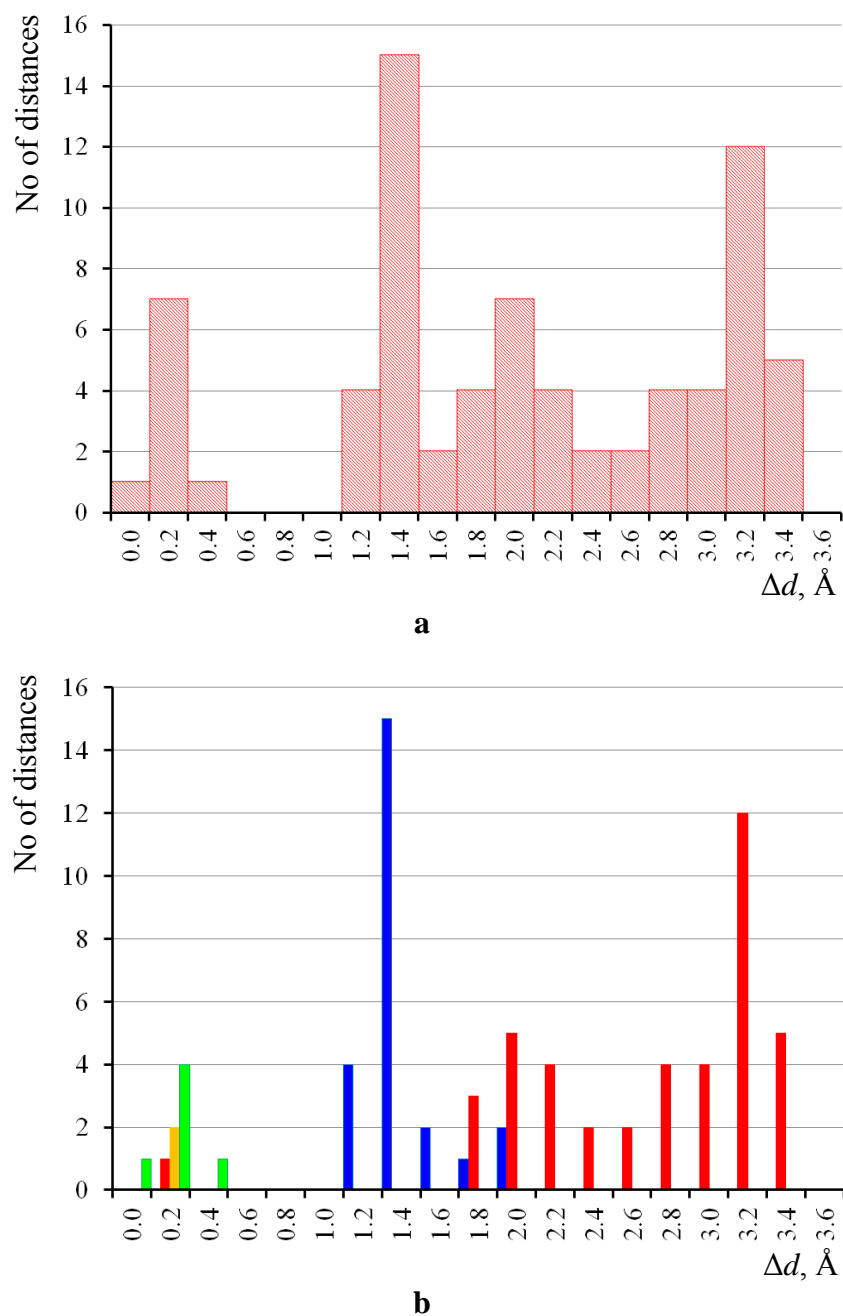
Fig. 173. Histogram of difference in distances between centroids: (a) all discussed calix[4]arenes; (b) separated in four groups for cone (■), partial cone (■), 1,2- (■) and 1,3-alternate (■) conformations.

198

The first peak at 0.2 Å corresponds to seven (Fig. 173b) calix[4]arene macrocyclic rings with the lowest Δd: two tBuC[4]OC$_n$ calix[4]arenes in 1,2-alternate conformation, four calix[4]arenes in 1,3-alternate conformation and tBuC[4]OC$_3$·CH$_3$CN[108] (cone).

The second peak at 1.4 Å (Fig. 173b) represents calix[4]arene in partial cone conformation with large substituents at *para*-position (all tBuC[4]OC$_n$ (partial cone)) or with guest molecules partially included into calix[4]arene cavity (NO$_2$C[4]OC$_1$ (partial cone) inclusion complexes with DMF[134] and CHCl$_3$).

The third peak (Fig. 173b) corresponds to less flattened calix[4]arenes: all known tBuC[4]OC$_n$ (cone), NO$_2$C[4]OC$_2$·2CHCl$_3$[112] (partial cone), NO$_2$C[4]OC$_3$[113] (partial cone) and HC[4]OC$_3$ (partial cone).

Last, the fourth peak (Fig. 173b) corresponds to the most pinched calix[4]arenes in cone conformations: all known HC[4]OC$_n$ (cone) and all known NO$_2$C[4]OC$_n$ (cone).

200

6   CONCLUSIONS

Hydrophobic-to-total volume ratio analysis reveals that self-assembly of all discussed fully O-alkylated calix[n]arenes (n = 4, 6) in molecular crystals mimic microstructures observed in surfactant assemblies and block copolymers.[148] Therefore, in the solid state fully O-alkylated calix[n]arenes can be treated as amphiphilic compounds.

Amphiphilic behaviour at such small differences between hydrophobic and hydrophilic parts of molecule reveals that molecular crystals of discussed calixarenes are closer to block copolymers than solutions of non-polymeric surfactants.

Hydrophobic-to-total volume ratio takes into account both nature and size of substituents at the calixarene macrocyclic ring. Substituents at oxygen atoms and at the *para*-positions change the volume ratio and bring specific intermolecular interactions (C–H$\cdots$O, C–H$\cdots$$\pi$, π-π stacking, interactions between long alkyl chains) in self-assembly of molecules in crystals.

Bicontinuous topology is typical for crystal structures of the calix[4]arenes in the cone conformations with short alkyl substituents: HC[4]OC$_n$ (n = 3-4), tBuC[4]OC$_n$ (n = 3-4) and NO$_2$C[4]OC$_n$ (n = 2-8). There are two exceptions. Formation of inclusion complex with acetonitrile molecule changes conformation of tBuC[4]OC$_3$ molecule in comparison with homologues which results in *ipl* topology in the crystal structure. In the case of NO$_2$C[4]OC$_3$, topology in the crystal structure is changed to *pl* due to the absence of solvent.

Elongation of the alkyl chains results in *l* topology of HC[4]OC$_n$ and NO$_2$C[4]OC$_n$, whereas two different homologous series of tBuC[4]OC$_n$ are observed. The crystal structure topology is *ipl* for odd n values and *ir* for the even ones.

Conformation of calix[4]arene macrocyclic ring defines the effective shape of the amphiphile and spatial arrangement of substituents around of the calix[4]arene core. Change in conformation might cause change of the self-assembling motif. While topology of HC[4]OC$_3$ in partial cone conformation is the same as for the cone one (*bi*), the partial cone conformation of tBuC[4]OC$_n$ calixarenes contributes to layered crystal structures with *ipl* topology. This was observed even for tBuC[4]OC$_1$, where volume ratio equals to 52.9%, whereas in the case of tBuC[4]OC$_n$ cone calixarenes *ipl* topology occurs firstly for tBuC[4]OC$_5$ with its volume ratio 65.7%.

In the case of $NO_2C[4]OC_2$ calixarene, partial cone conformation causes formation of *r* topology *versus bi* for the cone.

Generally, topologies in crystal structures of fully O-alkylated calix[4]arenes in 1,2- and 1,3-alternate conformations differ from those in the cone and partial cone conformations. Crystal structures of $tBuC[4]OC_3$ and $tBuC[4]OC_8$ in 1,3-alternate conformation are the exception: they remind crystal structures of corresponding analogues in partial cone conformation.

Fully O-alkylated calix[4]arenes, contrary to mono- and di-O-alkylated, do not include alkyl chains into calix[4]arene bowl. The calix[6]arenes have large cavities which can easily include one or two of its own alkyl chains. This self-inclusion contributes to formation of perforated layers topologies and even 'inverted micelles' in the form of torus.

Conformations of calix[4]arenes in the cone, partial cone and 1,2-alternate conformation are stabilised by C–H···O contacts between oxygen atoms of phenoxy moiety and H-atoms of the first and the second methylene groups of two distal alkoxy groups. Conformations of fully O-alkylated calix[6]arene are stabilised by self-inclusion of alkyl chain(s) and by C–H···O contacts between H-atoms in *meta*-positions of calix[6]arene phenyls and oxygen atoms of the adjacent phenoxy moieties.

It should be noted that for each of the most numerous groups of discussed calix[4]arenes [$HC[4]OC_n$ (cone), $NO_2C[4]OC_n$ (cone), $tBuC[4]OC_n$ (cone) and $tBuC[4]OC_n$ (partial cone)] noticeable differences in conformations for short alkyl substituents rapidly decrease with elongation of the substituents. For $tBuC[4]OC_n$ (cone) due to two homologous series for odd and even number of carbon atoms in chains, are observed.

Amphiphilic calix[n]arenes discussed in this thesis often form inclusion compounds with solvent molecules. Nevertheless, there are only four inclusion complexes, $tBuC[4]OC_3$ (cone)·CH_3CN,[108] $NO_2C[4]OC_1$·DMF,[134] $NO_2C[4]OC_1$·$CHCl_3$ and $NO_2C[4]OC_3$·CH_3OH,[113] where solvent molecules are included into calix[4]arene cavity. For the rest of the cases, the guest molecules are located in cavities between molecules of the host forming clathrate compounds. Presence of guest molecule is mainly guided by C–H···O, C–H···Cl and C–H···π interactions between host and guest molecules and additionally stabilises the crystal structure.

Hydrophobic-to-total volume ratio analysis looks to be a very promising tool for understanding and design of crystals with desired structural topology. Nevertheless,

202

presence of solvent molecules is an important factor in the calix[n]arenes assembly but its role is so far not clear from point of view of aliphatic/aromatic surface analysis. One of the possible approach is to treat solvent molecules as a third component in addition to aliphatic and aromatic regions in the crystal.

The question of self-assembly of calix[n]arenes with the volume ration lower than 10% (with one and two short alkyl chains) and larger than 80% remains to be investigated.

204

7   SUMMARY

Hydrophobic effect plays a key role in living organisms: protein folding, ligand-protein and protein-protein binding, micelle and membrane formation *etc*. It is widely applied in surfactant and block copolymer chemistry for rational design of supramolecular assemblies and molecular recognition in, *e.g.* drug delivery and sensing. However, in the field of crystal engineering, spatial unpredictability of the hydrophobic effect is still an open question.

The aim of this work is to show that even apparently non-polar O-alkylated calix[4]arenes and calix[6]arenes in molecular crystals mimic microstructures observed in surfactant assemblies and block copolymers. As good model compounds three classes of O-alkylated calix[n]arenes (n = 4, 6) have been chosen: non-substituted at the upper rim (possible C–H···π and π-π stacking interactions), substituted at *para*-positions with *tert*-butyl groups (possibility for π-π stacking interactions are blocked), and substituted at *para*-positions with nitro groups calix[n]arenes (more polar molecules with additional possibility for C–H···O hydrogen bonding). Self-assembly of such calixarenes in twenty seven crystal structures were analysed in this thesis.

Structural analysis of investigated compounds and thirty five their analogues from Cambridge Structural Database show localisation of aliphatic and aromatic regions in crystals. Topological analysis of the surface between these regions reveals that topology of crystal structure depends on relationship between volumes of aromatic and aliphatic parts of molecules.

Crystal structures of fully O-alkylated calix[4]arenes in the cone conformation with short alkyl chains [HC[4]OC$_n$ (n = 3,4), tBuC[4]OC$_n$ (n = 3,4) and NO$_2$C[4]OC$_n$ (n = 2–8)] reveals *bicontinuous* topology. For crystal structures of HC[4]OC$_n$ (n = 7–14) and NO$_2$C[4]OC$_n$, (n = 12–14), the *layered* topology is proper. For tBuC[4]OC$_n$ with number of carbon atoms in the alkyl chains larger than 4, two homologous series are observed: the *inverted perforated layers* topology has been found for odd n (5,9 and 11) and the *inverted ribbons* topology for even n (6–14).

Changes in calix[4]arene conformation may be followed by changes in the topology. Thus, tBuC[4]OC$_n$ (partial cone) (n = 1–8) is the largest group of the calix[4]arenes which adopts other than the cone conformation. Crystal structures of all tBuC[4]OC$_n$ (partial cone) show the *inverted perforated layers* topology.

In the case of calix[6]arenes, only 7 structures are known so far. The resulting topology strongly depends on both presence of solvent molecules in the structure and calix[6]arene conformation. The only one common feature for all the known structures is self-inclusion of methyl or methylene group(s) into calix[6]arene cavity.

Apparently non-polar fully O-alkylated calix[4]arenes and calix[6]arenes reveal amphiphilic behaviour in the solid state. Hydrophobic-to-total volume analysis is a powerful tool for understanding the crystal chemistry of amphiphilic compounds and provides the possibility of rational design of crystals with 0-, 1-, 2- or 3-dimensonal distribution of domains of desired nature, which is important in designing, *e.g.* organic semiconductors.

8 REFERENCES

1. Southall, N. T.; Dill, K. A.; Haymet, A. D. J. A View of the Hydrophobic Effect. *J. Phys. Chem. B* (2002), *106*, 521–533.

2. Gutsche, D. C. *Calixarenes: An Introduction*; 2nd ed.; Royal Society of Chemistry, 2008.

3. Shinkai, S.; Mori, S.; Koreishi, H.; Tsubaki, T.; Manabe, O. Hexasulfonated calix[6]arene Derivatives: A New Class of Catalysts, Surfactants, and Host Molecules. *J. Am. Chem. Soc.* (1986), *108*, 2409–2416.

4. Helttunen, K.; Shahgaldian, P. Self-Assembly of Amphiphilic Calixarenes and Resorcinarenes in Water. *New J. Chem.* (2010), *34*, 2704.

5. Wattebled, L. *Oligomeric Surfactants as Novel Type of Amphiphiles: Structure - Property Relationships and Behaviour with Additives*; PhD Thesis, Potsdam University, 2006.

6. Basilio, N.; Francisco, V.; Garcia-Rio, L. Aggregation of *para*-Sulfonatocalixarene-Based Amphiphiles and Supra-Amphiphiles. *Int J Mol Sci* (2013), *14*, 3140–3157.

7. Perret, F.; Tauran, Y.; Suwinska, K.; Kim, B.; Chassain-Nely, C.; Boulet, M.; Coleman, A. W. Molecular Recognition and Transport of Active Pharmaceutical Ingredients on Anionic Calix[4]arene-Capped Silver Nanoparticles. *J. Chem.* (2012), *2013*.

8. Ramírez, F. de M.; Tosheva, T.; Tashev, E.; García-Villafaña, E.; Shenkov, S.; Varbanov, S. Synthesis of a *para-tert*-octylcalix[4]arene Fitted with Phosphinoyl Pendant Arms and Its Complexation Properties towards F-Elements. *Polyhedron* (2013), *56*, 123–133.

9. Lee, M.; Lee, S.-J.; Jiang, L.-H. Stimuli-Responsive Supramolecular Nanocapsules from Amphiphilic Calixarene Assembly. *J. Am. Chem. Soc.* (2004), *126*, 12724–12725.

10. Kellermann, M.; Bauer, W.; Hirsch, A.; Schade, B.; Ludwig, K.; Böttcher, C. The First Account of a Structurally Persistent Micelle. *Angew. Chem. Int. Ed.* (2004), *43*, 2959–2962.

11. Strobel, M.; Kita-Tokarczyk, K.; Taubert, A.; Vebert, C.; Heiney, P. A.; Chami, M.; Meier, W. Self-Assembly of Amphiphilic Calix[4]arenes in Aqueous Solution. *Adv. Funct. Mater.* (2006), *16*, 252–259.

12. Kim, H. J.; Lee, M. H.; Mutihac, L.; Vicens, J.; Kim, J. S. Host–guest Sensing by Calixarenes on the Surfaces. *Chem. Soc. Rev.* (2012), *41*, 1173–1190.

13. Hartley, G. S. *Aqueous Solutions of Paraffin-Chain Salts*; Hermann et Cie, 1936.

14. Vos, J. G.; Forster, R. J.; Keyes, T. E. *Interfacial Supramolecular Assemblies*; John Wiley and Sons, 2003.

15. Rosen, M. J. *Surfactants and Interfacial Phenomena*; John Wiley and Sons, 2004.

16. Brickenkamp, C. S. Polyhedral Clathrate Hydrates. XVII. Structure of the Low Melting Hydrate of N-Propylamine: A Novel Clathration Framework. *J. Chem. Phys.* (1973), *58*, 5284.

17. Janeda, S.; Mootz, D. Lower Hydrates of Aliphatic Primary Amines. New Studies of Formation and Structure. *Z. Naturforsch., B: Chem. Sci.* (1998), *53*, 1197.

18. Frank, H. S.; Evans, M. W. Free Volume and Entropy in Condensed Systems III. Entropy in Binary Liquid Mixtures; Partial Molal Entropy in Dilute Solutions;

Structure and Thermodynamics in Aqueous Electrolytes. *J. Chem. Phys.* (1945), *13*, 507.

19. Yamaguchi, T.; Matsuoka, T.; Koda, S. Mode-Coupling Study on the Dynamics of Hydrophobic Hydration. *J. Chem. Phys.* (2004), *120*, 7590.

20. Rusanov, A. I.; Shchekin, A. K.; Kuni, F. M. Thermodynamic and Kinetic Theory of Ionic Micellar Systems: 1. Work of Aggregation. *Colloid J.* (2009), *71*, 816–825.

21. Rusanov, A. I.; Shchekin, A. K.; Kuni, F. M. Thermodynamic and Kinetic Theory of Ionic Micellar Systems: 2. Statistical-Thermodynamic Relations. *Colloid J.* (2009), *71*, 826–834.

22. Israelachvili, J. N. *Intermolecular and Surface Forces, Second Edition: With Applications to Colloidal and Biological Systems*; 2nd ed.; Academic Press, 1992.

23. Parrot-Lopez, H.; Perret, F.; Bertino-Ghera, B. Les Cyclodextrines Amphiphiles et Leurs Applications. Élaboration de Nanoparticules de Cyclodextrines Amphiphiles Pour Des Applications Biomédicales. *Ann Pharm Fr* (2010), *68*, 12–26.

24. Jardetzky, O.; Finucane, M. D.; Division, N. A. T. O. S. A. *Dynamics, Structure, and Function of Biological Macromolecules*; IOS Press, 2001.

25. Alberts, B. *Essential Cell Biology*; Taylor & Francis, 1998.

26. Norde, W. *Colloids and Interfaces in Life Sciences*; CRC Press, 2003.

27. Blandamer, M. J.; Cullis, P. M.; Soldi, L. G.; Engberts, J. B. F. N.; Kacperska, A.; Van Os, N. M.; Subha, M. C. S. Thermodynamics of Micellar Systems: Comparison of Mass Action and Phase Equilibrium Models for the Calculation of Standard Gibbs Energies of Micelle Formation. *Adv. Colloid Interface Sci.* (1995), *58*, 171–209.

28. Kallay, N.; Glusac, T.; Preocanin, T.; Cop, A. Standard States and Equilibrium in Ionic Micellar Systems. *Colloids Surf., A* (2009), *347*, 76–80.

29. Spencer, N. D.; Moore, J. H. *Encyclopedia of Chemical Physics and Physical Chemistry*; Taylor & Francis, 2001.

30. McNaught, D. A. D.; Wilkinson, A. *IUPAC Compendium of Chemical Terminology*; 2nd Revised edition.; WileyBlackwell, 1997.

31. Singh, S. Phase Transitions in Liquid Crystals. *Phys. Rep.* (2000), *324*, 107–269.

32. Schick, M. J. *Nonionic Surfactants*; CRC Press, 1987.

33. Atwood, J. L.; Steed, J. W. *Encyclopedia of Supramolecular Chemistry*; CRC Press, 2004.

34. Kitaigorodsky, A. I. *Molecular Crystals and Molecules*; 1st ed.; Academic Press Inc, 1973.

35. Bernstein, J. *Polymorphism in Molecular Crystals*; Oxford University Press US, 2008.

36. Xu, Z.; Kiang, Y.-H.; Lee, S.; Lobkovsky, E. B.; Emmott, N. Hydrophilic-to-Hydrophobic Volume Ratios as Structural Determinant in Small-Length Scale Amphiphilic Crystalline Systems: Silver Salts of Phenylacetylene Nitriles with Pendant Oligo(ethylene Oxide) Chains. *J. Am. Chem. Soc.* (2000), *122*, 8376–8391.

37. Xu, Z.; Lee, S.; Lobkovsky, E. B.; Kiang, Y.-H. Structure Rationalization and Topology Prediction of Two-Distinct-Component Organic Crystals: The Role of Volume Fraction and Interface Topology. *J. Am. Chem. Soc.* (2002), *124*, 121–135.

38. Mallik, A. B.; Lee, S.; Tran, L.; Lobkovsky, E. B. Crystal Topology Prediction in Alternating Amphiphiles: Aromatic Polyethers and the Role of Volume Fraction. *Cryst. Growth Des.* (2003), *3*, 467–473.

39. Mallik, A. B.; Lee, S.; Lobkovsky, E. B. Three Trigonal Coordination Extended Solids with Gyroid and Lamellar Topologies. *Cryst. Growth Des.* (2005), *5*, 609–616.

40. Lee, S.; Mallik, A. B.; Xu, Z.; Lobkovsky, E. B.; Tran, L. Small Amphiphilic Organics, Coordination Extended Solids, and Constant Curvature Structures†. *Acc. Chem. Res.* (2005), *38*, 251–261.

41. Desiraju, G. R.; Steiner, T. *The Weak Hydrogen Bond: In Structural Chemistry and Biology*; Oxford University Press, 2001.

42. Jeffrey, G. A.; Saenger, W. *Hydrogen Bonding in Biological Structures*; Springer-Verlag, 1991.

43. Malone, J. F.; Murray, C. M.; Charlton, M. H.; Docherty, R.; Lavery, A. J. X-H⋯π (phenyl) Interactions Theoretical and Crystallographic Observations. *J. Chem. Soc., Faraday Trans.* (1997), *93*, 3429–3436.

44. Thalladi, V. R.; Weiss, H.-C.; Bläser, D.; Boese, R.; Nangia, A.; Desiraju, G. R. C−H⋯F Interactions in the Crystal Structures of Some Fluorobenzenes. *J. Am. Chem. Soc.* (1998), *120*, 8702–8710.

45. Aakeröy, C. B.; Evans, T. A.; Seddon, K. R.; Pálinkó, I. The C–H⋯Cl Hydrogen Bond: Does It Exist? *New J. Chem.* 1999, *23*, 145–152.

46. Jetti, R. K. R.; Boese, R.; Thakur, T. S.; Vangala, V. R.; Desiraju, G. R. Proton Transfer and N(+)–HS(−) Hydrogen Bonds in the Crystal Structure of 4-Aminothiophenol. *Chem. Commun.* (2004), 2526–2527.

47. Braga, D.; Grepioni, F.; Biradha, K.; Desiraju, G. R. Agostic Interactions in Organometallic Compounds. A Cambridge Structural Database Study. *J. Chem. Soc., Dalton Trans.* (1996), 3925.

48. Steiner, T. The Hydrogen Bond in the Solid State. *Angew. Chem. Int. Ed.* (2002), *41*, 48–76.

49. Desiraju, G. R. The C-H⋯O and Other Weak Hydrogen Bonds. From Crystal Engineering to Virtual Screening. In; Bangalore, 2006.

50. Gavezzotti, A. *Molecular Aggregation: Structure Analysis and Molecular Simulation of Crystals and Liquids*; Oxford University Press, USA, 2007.

51. Nishio, M.; Umezawa, Y.; Honda, K.; Tsuboyama, S.; Suezawa, H. CH/π Hydrogen Bonds in Organic and Organometallic Chemistry. *CrystEngComm* (2009), *11*, 1757–1788.

52. Tsuzuki, S.; Honda, K.; Uchimaru, T.; Mikami, M.; Fujii, A. Magnitude and Directionality of the Interaction Energy of the Aliphatic CH/π Interaction: Significant Difference from Hydrogen Bond. *J. Phys. Chem. A* 2006, *110*, 10163–10168.

53. Tsuzuki, S. CH/π Interactions. *Annu. Rep. Prog. Chem., Sect. C: Phys. Chem.* (2012), *108*, 69–95.

54. Hunter, C. A.; Singh, J.; Thornton, J. M. π-π Interactions: The Geometry and Energetics of Phenylalanine-Phenylalanine Interactions in Proteins. *J. Mol. Biol.* (1991), *218*, 837–846.

55. Plevin, M. J.; Bryce, D. L.; Boisbouvier, J. Direct Detection of CH/π Interactions in Proteins. *Nat Chem* (2010), *2*, 466–471.

56. Daszkiewicz, M. Importance of ON Interaction between Nitro Groups in Crystals. *CrystEngComm* (2013), *15*, 10427–10430.

57. Gutsche, C. D.; Dhawan, B.; Levine, J. A.; Hyun No, K.; Bauer, L. J. Calixarenes 9 : Conformational Isomers of the Ethers and Esters of calix[4]arenes. *Tetrahedron* (1983), *39*, 409–426.

58. Groenen, L. C.; Van Loon, J. D.; Verboom, W.; Harkema, S.; Casnati, A.; Ungaro, R.; Pochini, A.; Ugozzoli, F.; Reinhoudt, D. N. The 1,2-Alternate Conformation of calix[4]arenes: A Rare Conformation? Dynamic 1H NMR Studies of Flexible Tetraalkylated calix[4]arenes. *J. Am. Chem. Soc.* (1991), *113*, 2385–2392.

59. Kanamathareddy, S.; Gutsche, C. D. Synthesis and Conformational Properties of calix[6]arenes Bridged on the Lower Rim: Self-Anchored Rotaxanes. *J. Am. Chem. Soc.* (1993), *115*, 6572–6579.

60. Ugozzoli, F.; Andreetti, G. D. Symbolic Representation of the Molecular Conformation of Calixarenes. *J Incl Phenom Macrocycl Chem* (1992), *13*, 337–348.

61. Wolfgong, W. J.; Talafuse, L. K.; Smith, J. M.; Adams, M. J.; Adeogba, F.; Valenzuela, M.; Rodriguez, E.; Contreras, K.; Carter, D. M.; Bacchus, A.; McGuffey, A. R.; Bott, S. G. The Influence of Solvent of Crystallization upon the Solid-State Conformation of calix[6]arenes'. *Supramol. Chem.* (1996), *7*, 67.

62. Vicens, J.; Harrowfield, J. M.; Baklouti, L. *Calixarenes in the Nanoworld*; Springer, 2007.

63. Allen, F. H. The Cambridge Structural Database: A Quarter of a Million Crystal Structures and Rising. *Acta Crystallogr B Struct Sci* (2002), *58*, 380–388.

64. Ungaro, R.; Pochini, A.; Andreetti, G. D.; Sangermano, V. Molecular Inclusion in Functionalized Macrocycles. Part 8. The Crystal and Molecular Structure of calix[4]arene from Phenol and Its (1 : 1) and (3 : 1) Acetone Clathrates. *J. Chem. Soc., Perkin Trans. 2* (1984), 1979–1985.

65. Harrowfield, J. M.; Richmond, W. R.; Sobolev, A. N.; White, A. H. Alkylammonium Cation Interactions with Calixarene Anions. Part 2. Structural Characterisation of a Salt of 2:3 Cation: Calixarene Stoichiometry. *J. Chem. Soc., Perkin Trans. 2* (1994), 5–9.

66. Asfari, Z.; Bilyk, A.; Dunlop, J. W. C.; Hall, A. K.; Harrowfield, J. M.; Hosseini, M. W.; Skelton, B. W.; White, A. H. Subtleties with Sulfur: Calixarenes as Uranophiles13. *Angew. Chem. Int. Ed.* (2001), *40*, 721–723.

67. Atwood, J. L.; Barbour, L. J.; Jerga, A. Storage of Methane and Freon by Interstitial van Der Waals Confinement. *Science* (2002), *296*, 2367–2369.

68. Brouwer, D. H.; Moudrakovski, I. L.; Udachin, K. A.; Enright, G. D.; Ripmeester, J. A. Guest Loading and Multiple Phases in Single Crystals of the van Der Waals Host P- Tert-Butylcalix[4]arene. *Cryst. Growth Des.* (2008), *8*, 1878–1885.

69. Udachin, K. A.; Enright, G. D.; Brown, P. O.; Ripmeester, J. A. Pseudopolymorphism in the P-Tert-butylcalix[4]arene-N-Butylamine System: Directing the Structural Motifs. *Chem. Commun.* (2002), 2162–2163.

70. Pojarova, M.; Ananchenko, G. S.; Udachin, K. A.; Perret, F.; Coleman, A. W.; Ripmeester, J. A. α-C=O Provides Access to the Cavity in Acyl calix[4]arenes: A Comparative Study of Crystal Structures. *New J. Chem.* (2007), *31*, 871–878.

71. Ananchenko, G. S.; Udachin, K. A.; Coleman, A. W.; Polovyanenko, D. N.; Bagryanskaya, E. G.; Ripmeester, J. A. Crystalline Inclusion Complex of a Calixarene with a Nitroxide. *Chem. Commun.* (2008), 223–225.

72. Ananchenko, G. S.; Udachin, K. A.; Pojarova, M.; Dubes, A.; Ripmeester, J. A.; Jebors, S.; Coleman, A. W. Van Der Waals Nanocapsular Complexes of Amphiphilic Calixarenes. *Cryst. Growth Des.* (2006), *6*, 2141–2148.

73. Ramon, G.; Coleman, A. W.; Nassimbeni, L. R. Inclusion of Terpenes by *para*-Acyl Calix[4]arenes. *Cryst. Growth Des.* (2006), *6*, 132–136.

74. Shahgaldian, P.; Coleman, A. W.; Rather, B.; Zaworotko, M. J. Double Molecular Encapsulation of Tetrahydrofuran by an Amphiphilic Calix[4]arene. *J Incl Phenom Macrocycl Chem* (2005), *52*, 241–245.

75. Suwinska, K.; Leśniewska, B.; Wszelaka-Rylik, M.; Straver, L.; Jebors, S.; Coleman, A. W. A Dodecameric Self-Assembled calix[4]arene Aggregate with Two Types of Cavities. *Chem. Commun.* (2011), *47*, 8766–8768.

76. Marsh, R. E.; Clemente, D. A. A Survey of Crystal Structures Published in the J. Am. Chem. Soc.. *Inorg. Chim. Acta* (2007), *360*, 4017–4024.

77. Dalgarno, S. J.; Atwood, J. L.; Raston, C. L. Sulfonatocalixarenes: Molecular Capsule and " Russian Doll" Arrays to Structures Mimicking Viral Geometry. *Chem. Commun.* (2006), 4567.

78. Hanna, T. A.; Liu, L.; Angeles-Boza, A. M.; Kou, X.; Gutsche, C. D.; Ejsmont, K.; Watson, W. H.; Zakharov, L. N.; Incarvito, C. D.; Rheingold, A. L. Synthesis, Structures, and Conformational Characteristics of Calixarene Monoanions and Dianions. *J. Am. Chem. Soc.* (2003), *125*, 6228–6238.

79. Maharaj, F.; Craig, D.; Scudder, M.; Bishop, R.; Kumar, N. Crystallographic and Inclusion Properties of Some Diacetylated Calix[4]arenes. *J Incl Phenom Macrocycl Chem* (2006), *55*, 315–324.

80. Grootenhuis, P. D. J.; Kollman, P. A.; Groenen, L. C.; Reinhoudt, D. N.; van Hummel, G. J.; Ugozzoli, F.; Andreetti, G. D. Computational Study of the Structural, Energetic, and Acid-Base Properties of calix[4]arenes. *J. Am. Chem. Soc.* (1990), *112*, 4165–4176.

81. Kennedy, S.; Dalgarno, S. J. Modulation of Nanotube Packing through the Controlled Self-Assembly of tris-*para*-carboxylatocalix[4]arenes. *Chem. Commun.* (2009), 5275–5277.

82. Pakhomova, S.; Ondracek, J.; Vindys, M.; Stibor, I. Crystal Structure of 25,27-Dipropoxy-26,28-dihydroxycalix[4]arene, $C_{34}H_{36}O_4$. *Z. Kristallogr.-New Cryst. Struct.* *212*, 459–460.

83. Kuz'mina, L.; Sadikov, G.; Howard, J.; Shokova, É.; Kovalev, V. Molecular and Crystal Structures of calix[4]arene 1,3-di-n-Propyl Ether. *Crystallogr. Rep.* (2003), *48*, 233–238.

84. Janiak, C. A Critical Account on π-π Stacking in Metal Complexes with Aromatic Nitrogen-Containing Ligands. *J. Chem. Soc., Dalton Trans.* (2000), 3885–3896.

85. Perret, F.; Lazar, A. N.; Shkurenko, O.; Suwinska, K.; Dupont, N.; Navaza, A.; Coleman, A. W. Geometrical and Inclusion Considerations in the Formation of Hexagonal Nanotubes of calix[4]arene di-Methoxycarbonyl Methyl Ester and Acid. *CrystEngComm* (2006), *8*, 890–894.

86. Lazar, A. N.; Dupont, N.; Navaza, A.; Coleman, A. W. Helical Aquatubes of calix[4]arene di-Methoxycarboxylic Acid. *Chem. Commun.* (2006), 1076–1078.

87. Coles, S. J.; Hall, C. W.; Hursthouse, M. B. 2,4-Dihydroxy-1,3-bis(methoxycarbonylmethoxy)calix[4]arene and 1,3-bis(ethoxycarbonylmethoxy)-2,4-dihydroxycalix[4]arene Chloroform Solvate. *Acta Crystallogr C Cryst Struct Commun* (2001), *58*, o29–o31.

88. Guillon, J.; Leger, J.-M.; Dapremont, C.; Denis, L. A.; Sonnet, P.; Massip, S.; Jarry, C. First Synthesis of 1,3-Alternate 25,27-Dialkyloxy-5,17-diarylcalix[4]arenes-Crown-6 as New Cesium Selective Extractants by Suzuki Cross-Coupling Reaction. *Supramol. Chem.* (2004), *16*, 319.

89. Stumpf, S.; Goretzki, G.; Gloe, K.; Gloe, K.; Seichte, W.; Weber, E.; Bats, J. W. Solution and X-Ray Crystal Structures of the Di- and Tetra-Allyl Ether of *tert*-butylcalix[4]arene. *J Incl Phenom Macrocycl Chem* (2003), *45*, 225–233.

90. Bo, Z.; Li, Y.-Z.; Xiao-Feng, L.; Guo-Yuan, L. Crystal Structure of 25, 27-Dioctyloxy-26, 28-Dihydroxy calix[4]arene. *J. Chem. Crystallogr.* (2005), *35*, 281–284.

91. Patra, S.; Suresh, E.; Paul, P. Functionalized calix[4]arene as an Ionophore: Synthesis, Crystal Structures and Complexation Study with Na^{+} and K^{+} Ions. *Polyhedron* (2007), *26*, 4971–4980.

92. Sýkora, J.; Budka, J.; Lhoták, P.; Stibor, I.; Císařová, I. Two Structural Types of 1,3-Alternate tetrapropoxycalix[4]arene Derivatives in the Solid State. *Org. Biomol. Chem.* (2005), *3*, 2572.

93. Tabatabai, M.; Schollmeyer, D.; Ritter, H. LAGQEQ02, CSD Code. *Private Communication* (2011).

94. Bolte, M.; Sakhaii, P. LAGQEQ, CSD Code. *Private Communication* (2004).

95. Evans, D. R.; Huang, M.; Fettinger, J. C.; Williams, T. L. Synthesis and Characterization of Diametrically Substituted Tetra-O-*n*-butylcalix[4]arene Ligands and Their Chelated Complexes of Titanium, Molybdenum, and Palladium. *Inorg. Chem.* (2002), *41*, 5986–6000.

96. Shahgaldian, P.; Coleman, A. W.; Kuduva, S. S.; Zaworotko, M. J. Amphiphilic Behavior of an Apparently Non-Polar Calixarene. *Chem. Commun.* (2005), 1968–1970.

97. Martin, A. D.; Sobolev, A. N.; Raston, C. L. Mapping out the Diversity of Interplay of O-Alkylated calix[4]arenes. *CrystEngComm* (2010), *12*, 2666.

98. Clark, T. E.; Makha, M.; Raston, C. L.; Sobolev, A. N. Supersized Bilayers Based on an O-Alkyl Substituted calix[4]arene. *CrystEngComm* (2006), *8*, 707.

99. Matvieiev, Y.; Boyko, V.; Podoprigorina, A.; Kalchenko, V. Preparative Synthesis of *para-tert*-butylcalix[4]arene Monoalkyl Ethers. *J Incl Phenom Macrocycl Chem* (2008), *61*, 89–92.

100. Gradiner, M. G.; Koutsantonis, G. A.; Lawrence, S. M.; Nichols, P. J.; Raston, C. L. Endo-, Exo-Cavity Hydride Isomerism for an Aluminium Complex of Dimetallated 1,3-Dimethyl Ether P-Tert-butylcalix[4]arene. *Chem. Commun.* (1996), 2035–2036.

101. Bugge, K. E.; Verboom, W.; Reinhoudt, D. N.; Harkema, S. Ethanol Complex of 1,3-Diethoxy-P-Tert-butylcalix[4]arene. *Acta Crystallogr C Cryst Struct Commun* (1992), *48*, 1848–1851.

102. Asfari, Z.; Bilyk, A.; Bond, C.; Harrowfield, J. M.; Koutsantonis, G. A.; Lengkeek, N.; Mocerino, M.; Skelton, B. W.; Sobolev, A. N.; Strano, S.; Vicens, J.; White, A. H. Factors Influencing Solvent Adduct Formation by Calixarenes in the Solid State. *Org. Biomol. Chem.* (2004), *2*, 387–396.

103. Arena, G.; Contino, A.; Longo, E.; Spoto, G.; Arduini, A.; Pochini, A.; Secchi, A.; Massera, C.; Ugozzoli, F. An Integrated Approach to the Study of the Recognition of Guests Containing CH3 and CH2 Acidic Groups by Differently Rigidified Cone *para-tert*-butylcalix[4]arene derivatives. *New J. Chem.* (2004), *28*, 56.

104. Arduini, A.; Nachtigall, F. F.; Pochini, A.; Secchi, A.; Ugozzoli, F. Calix[4]Arene Cavitands: A Solid State Study on the Interactions of Their Aromatic Cavity with Neutral Organic Guests Characterised by Acid CH$_3$ or CH$_2$ Groups. *Supramol. Chem.* (2000), *12*, 273.

105. Gruber, T.; Peukert, M.; Schindler, D.; Seichter, W.; Weber, E.; Bombicz, P. Crystalline Inclusion Compounds of Lower Rim Propyl Substituted calix[4]arenes Featuring Different Number and Positions of the Modifying Groups. *J Incl Phenom Macrocycl Chem* (2008), *62*, 311–324.

106. Fischer, C.; Gruber, T.; Seichter, W.; Weber, E. 5,11,17,23-tetra-*tert*-Butyl-25,26,27,28-tetramethoxycalix[4]arene Tetrahydrofuran Solvate. *Acta Crystallogr E Struct Rep Online* (2007), *63*, o4572–o4573.

107. Fischer, C.; Gruber, T.; Seichter, W.; Schindler, D.; Weber, E. 5,11,17,23-Tetra-*tert*-Butyl-25,26,27,28-tetramethoxycalix[4]arene Dichloromethane Hemisolvate. *Acta Crystallogr E Struct Rep Online* (2008), *64*, o673–o673.

108. Verboom, W.; Struck, O.; Reinhoudt, D. N.; van Duynhoven, J. P. M.; Van Hummel, G. J.; Harkema, S.; Udachin, K. A.; Ripmeester, J. A. *Gazz.Chi.Ital.* (1997), *127*, 727–730.

109. Lhotak, P.; Bila, A.; Budka, J.; Pojarova, M.; Stibor, I. Simple Synthesis of calix[4]arenes in a 1,2-Alternate Conformation. *Chem. Commun.* (2008), 1662–1664.

110. Li, Z.; Yuan, D.; Xi, H.; Sun, X. 25,26,27,28-Tetrabutoxy-5,11,17,23-Tetra-*tert*-butylcalix[4]arene Chloroform Tetrasolvate Dihydrate. *Acta Crystallogr E Struct Rep Online* (2009), *65*, o1697–o1697.

111. Brusko, V.; Böhmer, V.; Bolte, M. 5,11,17,23-Tetra-*tert*-Butyl-25,26,27,28-tetrapentoxycalix[4]arene. *Acta Crystallogr E Struct Rep Online* (2005), *61*, o4272–o4273.

112. Kunsági-Máté, S.; Csók, Z.; Tuzi, A.; Kollár, L. Permittivity-Dependent Entropy Driven Complexation Ability of Cone and Paco Tetranitro-calix[4]arene toward *para*-Substituted Phenols. *J. Phys. Chem. B* (2008), *112*, 11743–11749.

113. Kenis, P. J. A.; Noordman, O. F. J.; Houbrechts, S.; van Hummel, G. J.; Harkema, S.; van Veggel, F. C. J. M.; Clays, K.; Engbersen, J. F. J.; Persoons, A.; van Hulst, N. F.; Reinhoudt, D. N. Second-Order Nonlinear Optical Properties of the Four Tetranitrotetrapropoxycalix[4]arene Conformers. *J. Am. Chem. Soc.* (1998), *120*, 7875–7883.

114. Kelderman, E.; Derhaeg, L.; Verboom, W.; Engbersen, J. F. J.; Harkema, S.; Persoons, A.; Reinhoudt, D. N. Calix[4]arenes as Molecules for Second Order Nonlinear Optics. *Supramol. Chem.* (1993), *2*, 183.

115. Klimentová, J.; Vojtísek, P.; Sklenárová, M. Symmetrically Tetrasubstituted P-nitrocalix[4]arenes: Synthesis, Spectra and Crystal Structures. *J. Mol. Struct.* (2007), *871*, 33–41.

116. Lu, G.; Song, W.; Wan, X. Crystal Structure of the Molecular Inclusion Complex Tetra-*para*-Nitro-Tetra-O-Butyl calix[4]arene with Acetone (1:2). *J. Chem. Crystallogr.* (2000), *30*, 185–188.

117. Vysotsky, M. O.; Böhmer, V.; Bru Roig, M.; Bolte, M. 5,11,17,23-Tetranitro-25,26,27,28-tetrapentyloxycalix[4]arene. *Acta Crystallogr E Struct Rep Online* (2005), *61*, o3526–o3528.

118. Clark, T. E.; Makha, M.; McKinnon, J. J.; Sobolev, A. N.; Spackman, M. A.; Raston, C. L. Variable Temperature Hirshfeld Surface Analysis of Interdigitated calix[6]arene Bearing O-Alkyl C18 Linear Chains. *CrystEngComm* (2007), *9*, 566.

119. Tsue, H.; Ishibashi, K.; Tokita, S.; Takahashi, H.; Matsui, K.; Tamura, R. Azacalix[6]arene Hexamethyl Ether: Synthesis, Structure, and Selective Uptake of Carbon Dioxide in the Solid State. *Chem. Eur. J.* (2008), *14*, 6125–6134.

120. Zhang, Y.; Coppens, P. RALQIE, CSD Code. *Private Communication* (2001).

121. Zhang, Y.; Coppens, P. RALQEA, CSD Code. *Private Communication* (2001).

122. Koner, A. L.; Schatz, J.; Nau, W. M.; Pischel, U. Selective Sensing of Citrate by a Supramolecular 1,8-Naphthalimide/Calix[4]arene Assembly via Complexation-Modulated p*K*a Shifts in a Ternary Complex. *J. Org. Chem.* (2007), *72*, 3889–3895.

123. Becherer, M. S.; Schade, B.; Böttcher, C.; Hirsch, A. Supramolecular Assembly of Self-Labeled Amphicalixarenes. *Chem. Eur. J.* (2009), *15*, 1637–1648.

124. Genorio, B.; He, T.; Meden, A.; Polanc, S.; Jamnik, J.; Tour, J. M. Synthesis and Self-Assembly of Thio Derivatives of Calix[4]arene on Noble Metal Surfaces. *Langmuir* (2008), *24*, 11523–11532.

125. Li, H.; Qu, F. Synthesis of CdTe Quantum Dots in Sol−Gel-Derived Composite Silica Spheres Coated with Calix[4]arene as Luminescent Probes for Pesticides. *Chem. Mater.* (2007), *19*, 4148–4154.

126. De Haas, H.; de Fattler, U. Loading Of A Camptothecin Drug Into Colloidal Nanoparticles. WO2005063210 (A2), July 14, 2005.

127. Pojarova, M.; Ananchenko, G. S.; Udachin, K. A.; Daroszewska, M.; Perret, F.; Coleman, A. W.; Ripmeester, J. A. Solid Lipid Nanoparticles of *para*-Hexanoyl Calix[4]arene as a Controlling Agent in the Photochemistry of a Sunscreen Blocker. *Chem. Mater.* (2006), *18*, 5817–5819.

128. Wang, Y.-X.; Guo, D.-S.; Cao, Y.; Liu, Y. Phosphatase-Responsive Amphiphilic Calixarene Assembly. *RSC Adv.* (2013).

129. Richardson, T.; Greenwood, M. B.; Davis, F.; Stirling, C. J. M. Pyroelectric Molecular Baskets: Temperature-Dependent Polarization from Substituted Calix[8]arene Langmuir-Blodgett Films. *Langmuir* (1995), *11*, 4623–4625.

130. Park, H. S.; Lin, Q.; Hamilton, A. D. Protein Surface Recognition by Synthetic Receptors: A Route to Novel Submicromolar Inhibitors for A-Chymotrypsin. *J. Am. Chem. Soc.* (1999), *121*, 8–13.

131. Zadmard, R.; Arendt, M.; Schrader, T. Multipoint Recognition of Basic Proteins at a Membrane Model. *J. Am. Chem. Soc.* (2004), *126*, 7752–7753.

132. Shahgaldian, P.; Sciotti, M. A.; Pieles, U. Amino-Substituted Amphiphilic Calixarenes: Self-Assembly and Interactions with DNA. *Langmuir* (2008), *24*, 8522–8526.

133. Zadmard, R.; Schrader, T. DNA Recognition with Large Calixarene Dimers. *Angew. Chem.* (2006), *118*, 2769–2772.

134. Kumar, S.; Varadarajan, R.; Chawla, H. M.; Hundal, G.; Hundal, M. S. Preparation of P-Nitrocalix[n]arene Methyl Ethers via Ipso-Nitration and Crystal Structure of Tetramethoxytetra-*para*-nitrocalix[4]arene. *Tetrahedron* (2004), *60*, 1001–1005.

135. Nonius. *COLLECT*; Nonius BV: Delft, The Netherlands, 1998.

136. Carter, C. W.; Sweet, R. M. *Methods in Enzymology, Volume 276: Macromolecular Crystallography, Part A*; 1st ed.; Academic Press, 1997.

137. Mackay, S.; Gilmore, C. J.; Edwards, C.; Tremayne, M.; Stuart, N.; Shankland, K. *maXus*; University of Glasgow, Scotland, UK, Nonius BV, Delft, The Netherlands and MacScience Co Ltd., Yokochama, Japan, 1998.

138. Agilent. *CrysAlis Pro*; Agilent Technologies: Yarnton, Oxfordshire, England, 2011.

139. Sheldrick, G. M. *SHELX97: Program for Crystal Structure Analysis*; University of Göttingen, Germany, 1997.

140. Bürgi, H.-B.; Capelli, S. C. Getting More out of Crystal-Structure Analyses. *Helvetica Chimica Acta* (2003), *86*, 1625–1640.

141. Marsh, R. E. Some Thoughts on Choosing the Correct Space Group. *Acta Crystallogr., Sect. B: Struct. Sci* (1995), *51*, 897–907.
142. Farrugia, L. J. WinGX Suite for Small-Molecule Single-Crystal Crystallography. *J Appl Crystallogr* (1999), *32*, 837–838.
143. Brandenburg, K. *DIAMOND*; Crystal Impact GbR: Bonn, Germany, 1999.
144. Pettersen, E. F.; Goddard, T. D.; Huang, C. C.; Couch, G. S.; Greenblatt, D. M.; Meng, E. C.; Ferrin, T. E. UCSF Chimera – a Visualization System for Exploratory Research and Analysis. *J Comput Chem* (2004), *25*, 1605–1612.
145. Molinspiration Cheminformatics: Slovensky Grob, Slovak Republic, 2013.
146. Bondi, A. Van Der Waals Volumes and Radii. *J. Phys. Chem.* (1964), *68*, 441–451.
147. Nalwa, H. S. *Handbook of Surfaces and Interfaces of Materials, Five-Volume Set*; Academic Press, 2001.
148. Holmberg, K. *Surfactants and Polymers in Aqueous Solution*; John Wiley & Sons: Chichester [etc.], 2003.